12-2013

Seismic Site Coefficient Model and Improved Design Response Spectra Based on Conditions in South Carolina

Shimelies Aboye
Clemson University, saboye@g.clemson.edu

SEISMIC SITE COEFFICIENT MODEL AND IMPROVED DESIGN RESPONSE SPECTRA BASED ON CONDITIONS IN SOUTH CAROLINA

A Dissertation
Presented to
the Graduate School of
Clemson University

In Partial Fulfillment
of the Requirements for the Degree of
Doctor of Philosophy
Civil Engineering

---

by
Shimelies Ahmed Aboye
December 2013

Accepted by:
Dr. Ronald D. Andrus, Committee Chair
Dr. Nadarajah Ravichandran
Dr. C. Hsein Juang
Dr. WeiChiang Pang

This research was supported by the South Carolina Department of Transportation (SCDOT) and the Federal Highway Administration (FHWA) under SCDOT project No. 686. The views and conclusions contained in this dissertation are those of the author and should not be interpreted as necessarily representing the official policies, either expressed or implied, of SCDOT or FHWA.

ABSTRACT

A new seismic site coefficient model is developed in this dissertation from the results of over 60,000 total stress, one-dimensional equivalent linear and nonlinear ground response simulations assuming conditions in South Carolina. Computed site coefficients (F) are plotted versus average shear wave velocity in the top 30 m (V_{S30}) and grouped by location, spectral acceleration ($S_{outcrop}$) and spectral period. Locations considered in the Coastal Plain include Aiken, Charleston, Columbia, Florence, Lake Marion, Myrtle Beach, and the South Carolina side of Savannah. Locations considered in the Piedmont include Columbia, Greenville, Greenwood, and Rock Hill. In all the plots of V_{S30} versus F, the following three distinct trends can be seen—(1) an increasing trend in F as V_{S30} increases from a low value; (2) a zone of peak values of F, depending on $S_{outcrop}$; and (3) a decreasing trend in F as V_{S30} increases beyond the zone of peak F values.

Development of the mathematical site coefficient model begins by estimating the peak coefficient (F_P) and the corresponding average shear wave velocity (V_{S30P}) for each V_{S30}-F plot. Next, the values of F_P and V_{S30P} are studied to determine the most significant influencing variables. Variables found to be most influential are $S_{outcrop}$, mean predominant period of the outcrop ground motion (T_m), average shear wave velocity in the top 100 m (V_{S100}), and depth to top of soft rock ($H_{B\text{-}C}$) or hard rock (H_{HR}). Then, regression analysis is applied to the values of F_P and V_{S30P}. Finally, assuming the best-fit values of F_P and V_{S30P}, median relationships for the plotted site coefficients are expressed

by a linear relationship for lower values of V_{S30} and a linear or exponential relationship for higher values of V_{S30}.

The amount of variability within the plotted site coefficients is characterized by 95% upper bound and 5% lower bound relationships. The 95% upper bounds are, on average, 42% higher than the median relationships; and the 5% low bounds are, on average, 36% lower than the median relationships.

Computed site coefficients for the Coastal Plain are found to be greater in Myrtle Beach, followed by Savannah, Charleston, Florence, Columbia, Lake Marion and Aiken. More closely matching values of T_m and T_{100} may explain the higher site coefficients in Myrtle Beach and Savannah.

Computed site coefficients for periods of 0.0, 0.2 and 1.0 s (designated as F_{PGA}, F_a, and F_v, respectively) are compared with the 1994 National Hazard Reduction Program (NEHRP) F_a and F_v values, which are commonly assumed in current seismic design codes. Significant differences are found between the computed site coefficients and the NERHP values, particularly for Site Class D and E, and where the top of rock is at shallow depths.

The computed F_{PGA}, F_a and F_v median relationships are recommended for South Carolina because they are: (1) based on regional conditions; (2) continuous with V_{S30}, (3) considers depth to rock, and (4) consider the frequency (or period) content of the outcrop motion. If it is desired to design with more conservatism than the median relationships

provide, the median coefficients can be increased by 40% to obtain values corresponding to the 95% upper bound.

Because the proposed seismic site coefficient model is based on a very broad range of soil/rock conditions, much of it can be directly applied to other areas of the world. Specific variables needed to apply the model are: V_{S30}, V_{S100}, $H_{B\text{-}C}$ or H_{HR}, $S_{outcrop}$, and T_m. The first three variables characterize the site. The latter two variables characterize the design rock motion. It is important to remember that the soft- or hard-rock site coefficients selected should correspond to the $S_{outcrop}$ values available for the area. A relationship to estimate T_m based on H_{HR} and site-to-source distance is suggested for areas influenced by the Charleston Seismic Hazard Zone. This T_m relationship may not be applicable for other areas.

Finally, the simplified procedure for constructing acceleration design response spectrum (ADRS), sometimes called the three-point ADRS method, is shown to be generally adequate when $V_{S30} > 200$ m/s. However, when $V_{S30} \leq 200$ m/s, significant spectral peaks may occur at periods greater than 1.0 s. For this reason, it is recommended that a multi-point ADRS be plotted with the three-point ADRS to check if long-period accelerations are under predicted. Site coefficients for long periods (1.6 and 3.0 s) are included in the proposed model for constructing multi-point ADRS. The objective of the multi-point ADRS is not to replace the building code philosophy, but to present an option for the designer to make sure that longer period accelerations are not under-predicted by the three-point ADRS.

DEDICATION

This dissertation is dedicated to my primary school teacher Abayneh Moges.

ACKNOWLEDGMENTS

I would like to express my sincere gratitude to my advisor Dr. Ronald Andrus for his continuous support and professional guidance. His well-organized insights and mentoring have enabled me to achieve my desired academic and research objectives. His consistently positive and encouraging personality has helped me to overcome some difficult moments during my stay in Clemson. I am humbled and honored to have had the opportunity to work with him and be a student in his classes. I hope that my future career will reflect the professional integrity and ethics I learned from him.

I would like to thank Dr. Nadarajah Ravichandran for his kind support and advice during my PhD study. I have benefited from his technical insights, reviews, and suggestions on my research and the SCDOT project.

I am very grateful to Dr. WeiChiang Pang for giving me technical support with the statistical analysis, and for his time to review my dissertation. I would also like to thank Dr. C. Hsein Juang for his time to review my dissertation.

I am grateful to my friend Akhter Hossain, for his gracious company during my years of study at Clemson. I would also like to thank Ariful Haque for his active collaboration on the SCDOT project.

This research was supported by SCDOT. I would like to express my appreciation for the valuable assistance I received from SCDOT. I am thankful to Nicholas Harman of the SCDOT for his time to review my papers and this dissertation. I would also like to

thank the Aniket Shrikhande family for providing me the Aniket Shrikhande Memorial Fellowship.

Finally, I wish to acknowledge the support and love I received from all my family members.

TABLE OF CONTENTS

Table of contents (Continued)

Page

Table of contents (Continued)

Page

Table of contents (Continued)

Page

LIST OF TABLES

List of Tables (Continued)

Table Page

List of Tables (Continued)

Table Page

List of Tables (Continued)

Table Page

LIST OF FIGURES

List of Figures (Continued)

Figure Page

List of Figures (Continued)

Figure Page

List of Figures (Continued)

Figure Page

List of Figures (Continued)

Figure Page

List of Figures (Continued)

Figure Page

List of Figures (Continued)

Figure Page

List of Figures (Continued)

Figure Page

CHAPTER ONE

INTRODUCTION

1.1 Background

Local site conditions can greatly influence ground surface motions and structural damage caused by earthquakes (Kramer 1996). Two earthquakes that emphasized the influence of local site conditions on site amplification and had a major impact on seismic building codes were the 1985 Michoacán, Mexico, and the 1989 Loma Prieta, California, earthquakes (Idriss 1990; Borcherdt 1994). Conditions of importance include the travel path geology, the underlying basin structure, the thicknesses of soil layers, the small-strain stiffness and material damping of each layer, the variation of stiffness and material damping with shearing strain amplitude of each layer, and the site topography.

Presented in Figure 1.1 is a schematic of earthquake motion propagation from source to site. The rupture at the fault initiates stress waves that propagate through the earth to the bedrock beneath the soil layers, and finally through soil layers to reach the ground surface. The rupture mechanism and wave passage effects through rock are modeled in general seismic hazard analysis studies (e.g., U.S. Geological Survey hazard maps), which provide ground motion parameters at the top of soft or hard rock. Site response analysis mainly deals with ground motion propagation from the bedrock through the soil layers.

Several investigators have noted the particular significance of small-strain stiffness represented by shear modulus or shear wave velocity on dynamic behavior (Idriss 1990; Borcherdt 1994; Boore et al. 1994; Joyner et al. 1994). Because a complete characterization of small-strain shear wave velocity (V_s) to bedrock and a site-specific ground response analysis are often not economically feasible, the average V_s in the top 30 m (V_{S30}) has been adopted for seismic site classification (Borcherdt 1994; Seed et al. 1994; Dobry et al. 2000). The value of V_{S30} is computed by:

$$V_{S30} = \frac{30}{\sum_{i=1}^{m} \frac{H_i}{V_{si}}} \tag{1.1}$$

where H_i is the thickness in meters of layer i; V_{si} is the shear wave velocity in m/s of layer i; and m is the number of layers in the top 30 m.

Profiles with V_{S30} > 1,500 m/s, 760 < V_{S30} ≤ 1,500 m/s, 360 < V_{S30} ≤ 760 m/s, 180 < V_{S30} ≤ 360 m/s and V_{S30} ≤ 180 m/s correspond to site classes designated as A, B, C, D and E, respectively, assuming no special condition (e.g., peats, highly organic clays, very high plasticity clays, very thick soft/medium stiff clay) that are designated as Site Class F. These site classes are often referred to as the National Hazard Reduction Program (NEHRP) site classes after the program study where they were first introduced (BSSC 1995).

One of the outputs of ground response analysis is the site acceleration response spectrum, which is a plot of the maximum spectral acceleration responses of a series of single degree-of-freedom systems, typically with 5% damping, for a given base motion.

From the site response spectrum and the input rock outcrop response spectrum, the site coefficient (F) is calculated by:

$$F = \frac{S_{site}}{S_{outcrop}} \tag{1.2}$$

where S_{site} is the site spectral acceleration at a selected period; and $S_{outcrop}$ is the soft-rock outcrop spectral acceleration at the same period.

The site coefficients for short-period or 0.2 s (F_a) and long-period or 1.0 s (F_v) adopted in the American Society of Civil Engineers Standard ASCE 7-10 (ASCE 2010), the International Building Code (ICC 2012), and the AASHTO guide (AASHTO 2011) first appeared in the 1994 NEHRP provisions (BSSC 1995). Values of F_a and F_v at small levels of shaking (peak ground accelerations $\approx$ 0.1 g) were derived from empirical investigations using strong motion data recorded in the San Francisco Bay area during the 1989 Loma Prieta earthquake (Borcherdt 1994; Joyner et al. 1994). At stronger levels of shaking, values of F_a and F_v were derived from the results of one-dimensional equivalent linear and nonlinear site response analyses assuming western U.S. geologic and seismic general conditions (Seed et al. 1994; Dobry et al. 2000). These site factors are herein referred to as the NEHRP F_a and F_v values.

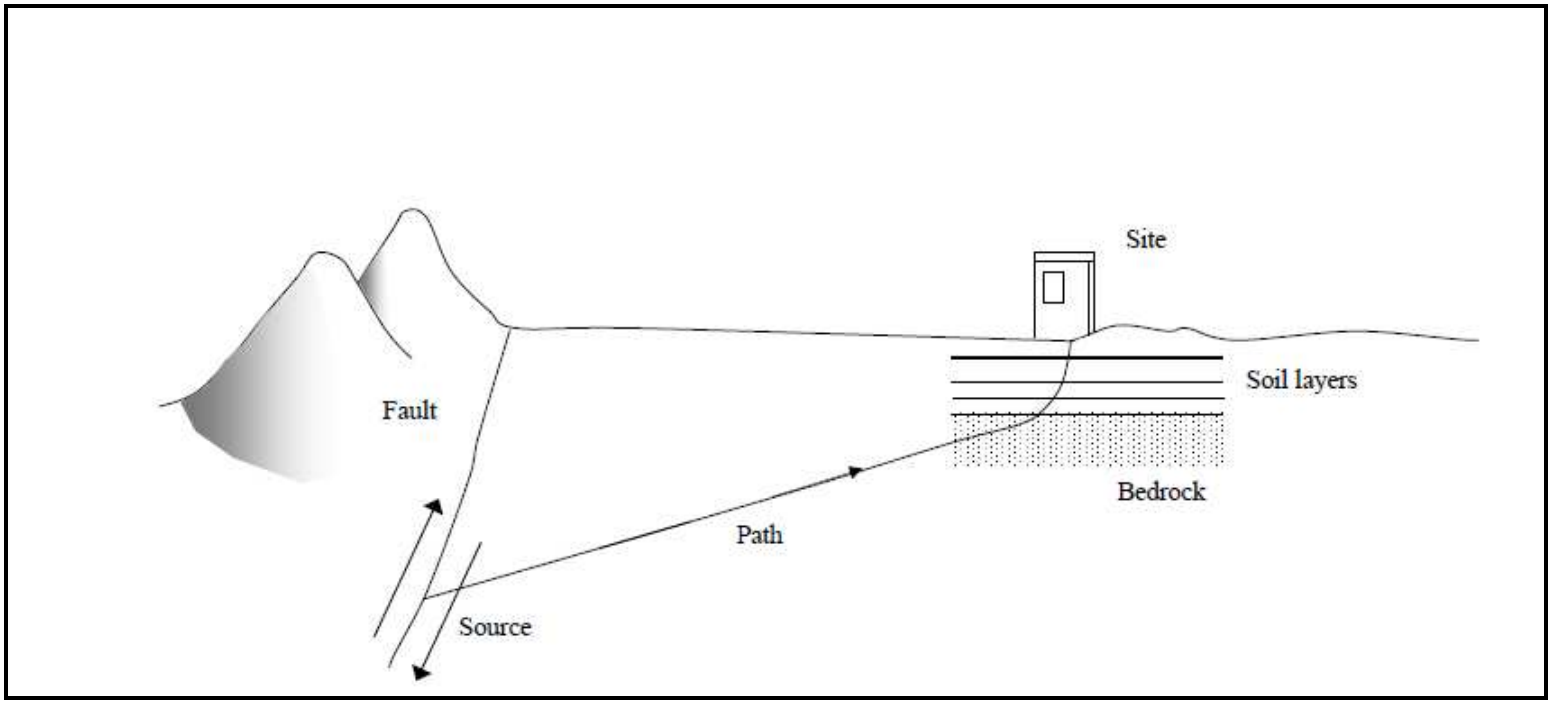

Figure1.1 Schematic ground motion propagation from source to site (after Kramer, 1996).

1.2 Problem Statement

The problem statement of this dissertation is conceived from the concerns highlighted by a number of investigators regarding the NEHRP F_a and F_v values as well as the recommended site-class based procedure. Some of these concerns include: (1) the appropriateness of using the 1994 values for soil conditions different from the Western United States; (2) the appropriateness of using a single value for an entire site class, regardless of variations in stiffness within a site class; and (3) the appropriateness of using a single value that is independent of the depth to top of rock.

Several studies using non-Loma Prieta strong motion data sets have provided F_a and F_v values that are somewhat different from the NEHRP F_a and F_v values. Borcherdt (2002) obtained F_a and F_v values that are slightly greater based on amplifications observed during the 1994 Northridge, California earthquake. Stewart et al. (2003) and Choi and Stewart (2005) also obtained slightly higher F_a and F_v values using various California earthquakes. Park and Hashash (2004) showed that the NEHRP F_a and F_v values may be over-conservative at short periods and unconservative at long periods for thick soil deposits. Silva et al. (2000) obtained significantly higher F_a and F_v for C and D site classes, and lower F_a and F_v for E site class using point-source model stochastic ground motions. Most recently, Baska and Tang (2011) presented response spectra from the February 2011 Christchurch, New Zealand earthquake that greatly exceeded design response spectra based on NEHRP F_a and F_v, especially at long periods. Crouse (2011) indicated that the NEHRP F_a and F_v and the commonly used procedure for constructing

design response spectra may not always capture long period acceleration response greater than 2.0 s.

In South Carolina, studies have shown that the NEHRP F_a and F_v can be unconservative (Hwang et al. 1997; Power et al. 1998; Lester and Chapman 2005; Chapman et al. 2006). Lester and Chapman (2005) obtained peak spectral accelerations in Columbia that significantly exceeded values predicted by the NEHRP values, especially at spectral periods around 1.0 s. Chapman et al. (2006) presented results of a ground response study for conditions in Charleston where F_a and F_v exceeded the NEHRP factors. Engineers at SCDOT have also observed unconservative predictions with design response spectra using NEHRP F_a and F_v, compared to the results of site-specific ground response analysis. Thus, updated seismic site factors are needed for South Carolina, and other parts of the world.

1.3 Objectives

The objectives of this dissertation are:

1. To derive new generalized mathematical models of $F_{PGA,}$ F_a and F_v, as well as site coefficients at other periods based on conditions typical of South Carolina. Conditions typical of Aiken, Charleston, Columbia, Florence, Lake Marion, Myrtle Beach, and the South Carolina side of Savannah (Georgia) are considered in the Coastal Plain. In the Piedmont, conditions typical of Columbia, Greenville, Greenwood and Rock hill areas are considered. The site coefficients are derived as a function of amplitude, V_{S30} (or stiffness of the soil in top 30 m), mean-predominant period of the base motion (T_m), and fundamental period of the soil in top 100 m (T_{100}). Computed values of F are plotted versus V_{S30} and grouped by amplitude and period. For the plotted V_{S30}-F data pairs, median, 95% upper bound and 5% lower bound curves are constructed. The derived site coefficients are compared with the NEHRP F_a and F_v values and previous studies.
2. To identify conditions where the commonly used (and sometimes called 3-point) simplified procedure for constructing acceleration design response spectra may not be appropriate, and to recommend modifications to the procedure where needed.
3. To investigate the effect of depth to soft rock ($H_{B\text{-}C}$) and depth to hard rock (H_{HR}) on the derived models, and to recommend adjustment coefficients. The effect of $H_{B\text{-}C}$ is investigated by assuming hypothetical $H_{B\text{-}C}$ values of 1.5, 5, 10, 20, 30, 50, 100, and >100 m. The effect of H_{HR} is investigated by considering geologic information in

Aiken, Charleston, Columbia, Florence, Lake Marion, Myrtle Beach, and Savannah areas.

4. To investigate the effect of duration of earthquake motion on predicted surface acceleration, and to recommend adjustment coefficients. The effect of duration of earthquake motion is quantified by considering earthquake moment magnitude (M_w) of 5, 6, 7, and 8.

1.4 Dissertation Outline

Chapter 2 presents a literature review of notable earthquakes that prompted seismic site response (or site amplification) studies, and the results of those studies. Also presented in Chapter 2 is the procedure for one-dimensional site response analysis, which includes equivalent linear frequency domain and non-linear time domain analyses.

Discussed in Chapter 3 is a ground response study performed for the Charleston area (Aboye et al. 2011, 2013b). The contribution of this chapter is a continuous V_{S30}- and amplitude-dependent seismic site coefficient model. Representative soil/rock conditions, deaggregated seismic hazard parameters, generated time histories, and recommended site coefficients for the Charleston area are presented. The adequacy of the 3-point procedure of constructing ADRS curves is checked for short- and long-period amplification cases, and a practical recommendation is suggested. The effect of geologic realistic and hard-rock models on seismic response is also discussed in this Chapter 3.

In Chapter 4, the site coefficient model developed for the Charleston area in Chapter 3 is extended to the South Carolina Coastal Plain. Soil/rock, geologic and seismic conditions representative of sites in Aiken, Columbia, Florence, Lake Marion, Myrtle Beach, and Savannah are considered. Additional proxy variables not considered in Chapter 3 are identified. The site coefficient model recommended in Chapter 4 is a function of V_{S30}, amplitude, T_m, T_{100}, $H_{B\text{-}C}$, and H_{HR}.

Chapter 5 presents the results of ground response analysis based on conditions in the South Carolina Piedmont (SCP). Soil/rock and geologic conditions typical of locations in Columbia, Greenville, Greenwood, and Rock Hill are considered. Effects of multiple earthquake sources, matching target frequencies, and rock model are analyzed. The recommended site coefficient model for the SCP is compared with the model recommended in Chapter 4 for the SCCP.

Presented in Chapter 6 are tabulated maximum median site coefficients within a seismic site class computed from the generalized models developed in Chapters 4 and 5. Also presented in Chapter 6 is a discussion on the site coefficients and the acceleration design response spectra (ADRS) procedure based on the South Carolina Department of Transportation Geotechnical Design Manual (SCDOT-GDM).

Presented in Chapter 7 are the conclusions and pertinent contributions of this dissertation, and the recommendations for future study.

CHAPTER TWO

LITERATURE REVIEW

2.1 Introduction

The significance of local site conditions on ground surface motions and structural damage caused by earthquakes has been known for many years (Kramer 1996). Using damage to structures data from the 1906 San Francisco earthquake, Lawson (1908) recognized that ground motion intensity can be correlated with local geology. Using microseismic data, Gutenberg (1927) related amplification coefficients with subsurface conditions. Strong motion records from the 1940 El Centro earthquake showed the damaging effects of long-period ground motions on structures far from the epicenter (Kramer 1996). Since these early observations, the influence of local conditions has been illustrated in earthquakes around the world (e.g., 1933 Long Beach, 1957 San Francisco, 1967 Caracas, 1985 Mexico City, 1989 Loma Prieta, and 1994 Northridge).

Presented in this chapter are: (1) a review of notable earthquakes that emphasized the influence of local site condition on shaking intensity, (2) a brief overview of site specific seismic response analysis, and (3) a review of previous seismic site response studies.

2.2 Review of Selected Significant Earthquakes

2.2.1 The 1906 San Francisco Earthquake

As reported by Lawson (1908), the San Francisco earthquake occurred on April 18, 1906. It ranks as one of the most significant historic earthquakes, particularly with its large horizontal displacements and great rupture length. The rupture occurred from the San Andreas Fault, and extended as far as 80 kilometers inland from the fault trace. The intensity of this earthquake was estimated to be VII to IX on the Modified Mercalli Intensity (MMI) scale. The earthquake was felt from southern Oregon to south of Los Angeles and inland as far as central Nevada. This earthquake took the lives of 700 people, and caused fire in the San Francisco area.

Lawson (1908) reported that damage to buildings from the 1906 San Francisco earthquake was strongly related to both the design and construction of the structure, and the local geology. Structures situated on soft sedimentary soils sustained stronger shaking compared to nearby rock sites.

2.2.2 The 1933 Long Beach Earthquake

Based on Heck and Neumann (1933), the 1933 Long Beach, California, earthquake occurred along the Newport-Inglewood fault. Its intensity was estimated to be VIII on the MMI scale, and had a moment magnitude (M_w) of 6.4. Although it is a moderate earthquake in terms of magnitude, it caused serious damage to weak masonry structures on land fill from Los Angeles south to Laguna Beach. Most of the damage was

reported to occur on landfills, deep water-soaked alluvium or sand, and poorly designed buildings. Property damage was estimated to be $40 million, and 115 people were killed.

2.2.3 The 1957 San Francisco Earthquake

As reported by Seed and Idriss (1969), the 1957 San Francisco earthquake (also called Lake Merced earthquake) occurred on March 22, 1957. The epicenter was located on the San Andreas Fault near Lake Merced, South of San Fransisco. It had an M_w of 5.3, and caused injuries to 40 people and property damage on the order of $1 million.

Presented in Figure 2.1 are four strong motion records from the 1957 San Francisco earthquake. These records were made on 80- and 100 m- thick unconsolidated soils and two rock sites. The recordings indicate a considerable difference in spectral acceleration depending on the soil/rock conditions. The surface spectral acceleration on the rock sites (marked by (a) in Figure 2.1) was high at the short-period; and low at long-period. This demonstrates the attenuation of long-period (high frequency) amplitudes in stiff soils. For the soil sites (marked by (b) and (c) in Figure 2.1), the surface spectral acceleration was low at short-period, and high at long-period. This demonstrates the amplification of long-period amplitudes in soft soils.

2.2.4 The 1967 Caracas Earthquake

Seed and Idriss (1982) studied damage that occurred during an earthquake with M_w = 6.6 that occurred near the coast of Venezuela, on July 29, 1967. The damage was estimated to be 240 deaths and $100 million property loss. Seed and Idriss (1982)

showed that the damage was most severe in: (1) three- to five-story buildings founded on 30 to 50 m thick soil, (2) five- to nine-story buildings founded on 50 to 70 m thick soil, and (3) 10-plus story building founded on 100 m-plus thick soil. The selective nature of the damage highlights the influence of matching resonance frequencies between the building structures and the underlying soil columns.

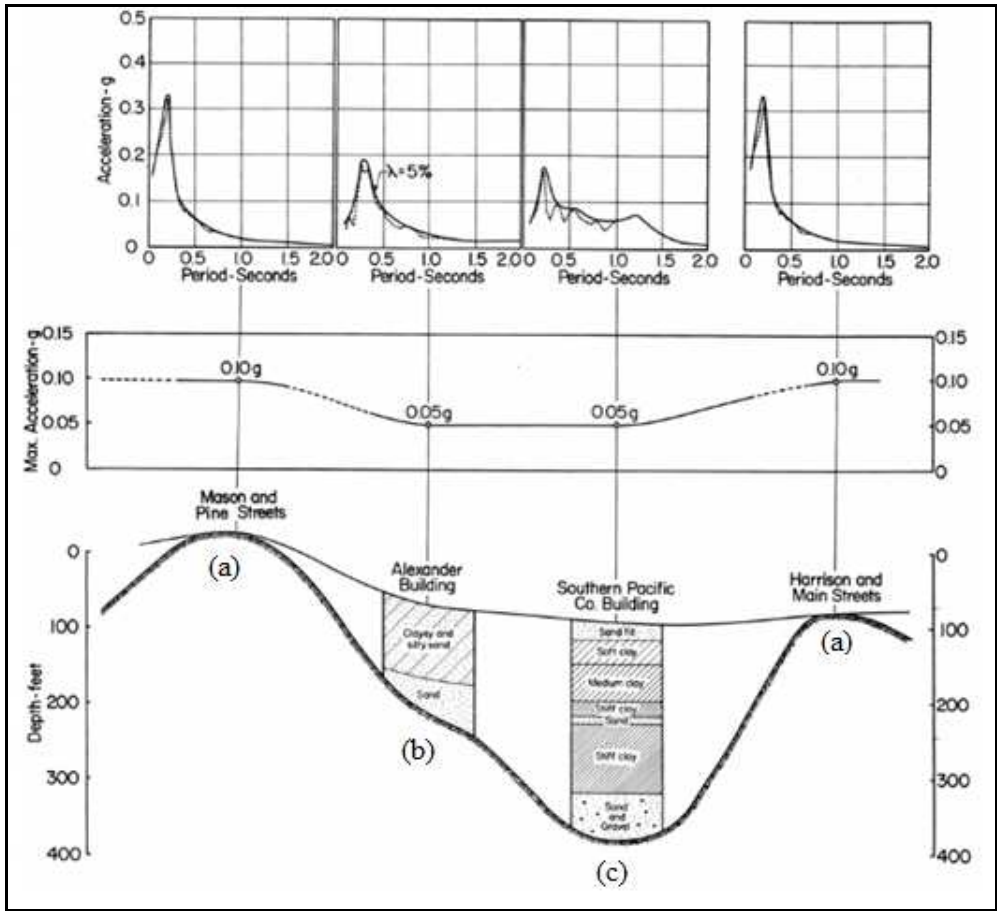

Figure 2.1 Comparison of recorded response spectra from the 1957 San Francisco Earthquake (Seed and Idriss 1969).

2.2.5 The 1985 Mexico City Earthquake

According to Seed et al. (1988), the M_w = 8.1 Michoacán, Mexico City, earthquake occurred on September 19, 1985. It occurred from subduction movement along the Pacific Coast of Mexico. Damage was moderate near the epicenter and significant some 350 km away in Mexico City. Complete collapse of 7- to 22-story buildings, death toll of 10,000 people, and property damage of $6 billion were reported.

Presented in Figure 2.2 are recorded spectral accelerations at one rock and two soft soil sites with depth to the hard rock of 0, 37 and 58 m, respectively. The rock site consisted of a V_s = 500 m/s material; and the soil sites consisted of clayey material with V_s = 75-80 m/s. Based on Seed et al. (1988), short-period amplitudes were significantly amplified at the 37-m thick clayey site compared to the 58-m thick clayey site and the rock site. For example, the *PGA* at the 37-m thick clayey site was about five-times the *PGA* at the rock site. Also noted from Figure 2.2 is the long-period amplification (particularly at T > 3.0 s) at the 58-m thick clayey site compared to the 37-m thick clayey site and the rock site.

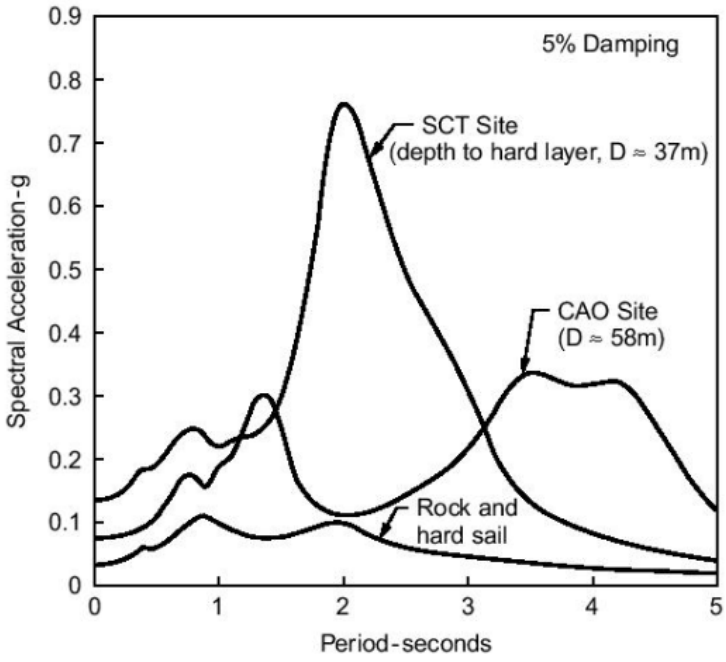

Figure 2.2 Recorded spectral acceleration from the 1985 Mexico City earthquake (Seed et al. 1988).

2.2.6 The 1989 Loma Prieta Earthquake

As reported by Seed et al. (1994), the M_w = 7.1 Loma Prieta earthquake occurred on October 17, 1989 in the Santa Cruz Mountains of California, about 100 km south of San Fransisco. The death toll was reported to be 62; 5,000 housing units were destroyed and the estimate of total property damage was $5.6 billion. On the MMI scale, the shaking in the epicentral region was VIII, and IX in San Fransisco and Oakland. This selective shaking demonstrated the dependence of earthquake damage on site-to-source distance.

Presented in Figure 2.3 are plots of spectral acceleration at Yerba Buena Station (YB) and Treasure Island recording stations (TI). The YB station represented a rock outcrop with V_s = 980 m/s, while the TI station represented a 14-m-thick loose sand underlain by 17 m of bay mud. The site-to-source distances of the two stations were practically the same. However, the *PGA* and peak spectral acceleration (*PSA*) were recorded to be different. The YB station had 0.05 and 0.17 g *PGA* and *PSA*, respectively. The corresponding values at the TI station were 0.15 and 0.75. The amplification at the TI station was 2 to 3 times at the short-period, and 5 to 6 times at long-period (Seed et al. 1994). Thus, the difference in amplification emphasized the significance of local site condition during the Loma Prieta earthquake.

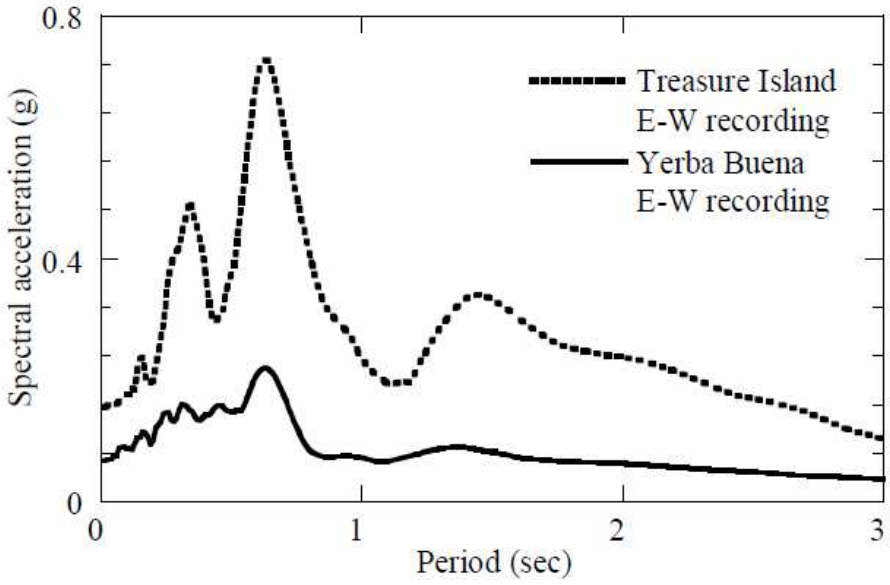

Figure 2.3 Recorded spectral acceleration from the 1989 Loma Prieta Earthquake (after Seed et al. 1994).

2.2.7 The 1994 Northridge Earthquake

As summarized by Somerville (2003), the M_w = 6.7 Northridge earthquake occurred on January 17, 1994 in the Santa Susana Mountains bordering the San Fernando Valley, California. Because of the proximity of the epicenter to the densely populated parts of Los Angeles metro area, the effect from this quake is recorded to be the most costly in United States history. Fifty-seven people were killed, 9,000 were injured, and 20,000 people were temporarily displaced. The damage was magnified by physical coefficients, such as ground water depth and depth of colluvium and alluvial deposits.

Damage was most severe on channel fills in alluvial deposits. Exceptionally high ground motion (*PGA* = 1.82 g) were recorded at the Tarzana Station located about 6 km from the epicenter. The recorded *PGA* was 0.3 to 1.3 g at a distance of 10 km; and 0.9 g and at a distance of 30 km. The Northridge earthquake showed that near fault ground motions produce long-period pulses and permanent displacements, which was not recognized in the lateral force provisions in the then-existing building codes (Somerville 2003).

2.2.8 The 1995 Kobe Earthquake

According to Bachman (1995), the M_w = 6.9 Kobe earthquake occurred on January 17, 1995 in Japan. It is one of the most devastating earthquakes that had hit Japan. This earthquake took the lives of 5,500 people, injured 26,000 people, heavily damaged over 100,000 buildings, and caused a property loss of about $200 billion. Kobe was built on very loose uncompacted soil which is highly susceptible to earthquake-

induced liquefaction. Accelerations at these loose sites were increased by two to three times compared to rock sites.

2.3 Site Specific Seismic Response Analysis

Site specific ground response analysis takes into account the rupture mechanism at the earthquake source, the propagation of seismic waves from the earthquake source to the top of the bedrock, and the modification of the seismic waves as they reach the ground surface (Park and Hashash 2004). The primary objective of seismic site response analysis is predicting ground surface acceleration. The steps needed to predict ground surface acceleration are: accurate characterization of a soil rock/model, selection of candidate base motions, realistic representation of soil nonlinear response, and computational programs (Silva et al. 2000, Rodriguez-Marek et al. 2001).

Characterization of idealized soil/rock model requires geophysical and geotechnical investigation, laboratory and field testing. Laboratory and field tests may be designed to calibrate the parameters needed for constitutive relationships of soil dynamic behavior. Most of these relationships require small-strain shear wave velocity, and shear modulus reduction and damping ratio versus shearing strain curves. Such characterization has been generally adopted by the engineering community for conducting site response analysis (Crouse and McGuire 1996).

Selection of candidate ground motions requires an appropriate set of recorded or synthetic rock motions consistent with the seismic hazard at the site. This stage requires

an interaction with seismologist (Seed et al. 1994, Borcherdt 1994, Joyner and Boore 2000, Lester and Chapman 2005).

Numerical programs such as SHAKE2000, D-MOD2000, DEEPSOIL, STRATA, and FLAC have been widely used to propagate the candidate motions vertically through the idealized soil/rock profiles to predict ground surface acceleration. These programs use equivalent linear, nonlinear or both formulations to solve for the wave propagation equation (Hashash and Park 2001, Ordóñez 2011, Matasović and Ordóñez 2011)

Because the formulations and underlying assumptions of equivalent linear and nonlinear site response approaches are different, some differences in the results from the two formulations are expected (Park and Hashash 2004). As summarized by (Kramer (1996), the advantages of the equivalent linear formulation are: (1) it can be efficient when the input motion can be characterized by small number of terms in Fourier series; and (2) it needs less number of parameters and has reduced computational time cost. The limitations related with the equivalent linear method are: (1) it can result in high amplification due to a coincidence of the strong component of the input motion with one of the natural frequencies of the soil, (2) it can filter out high frequency components of the input motion, and underestimate surface ground motion at long periods, and (3) it can lead to an overdamped system when the peak shear strain is much larger than the remainder of shear strains, and to an underdamped system when the peak shear strain is nearly uniform.

Based on Matasović (1993) and Hashash and Park (2001), the nonlinear approach can be formulated in terms of effective stresses to allow modeling of the generation, redistribution and dissipation of pore pressure during and after an earthquake. However, it requires a reliable constitutive model representation, and the parameters needed to describe such models are not as well established as those of the equivalent linear method.

2.4 Review of Seismic Site Response Studies

Previous seismic site response studies can be grouped into two categories: (1) those using empirical procedures that are based on recorded ground motion data, and (2) numerical simulations that are based on measured/idealized properties. The empirical studies are important and useful in that they can be used to understand seismic site response in general, and to validate results obtained from numerical simulations. However, empirical procedures have limited applicability. Because (1) not all places have recorded time histories during past earthquake events (e.g., eastern U.S), and (2) in places where there are recordings, the time histories may not cover the range of all amplitudes needed for seismic design (e.g., 1989 Loma Prieta earthquake). Numerical simulations, on the other hand, can be applied to all situations where measured or estimated inputs are available. The objective of this section is to review selected empirical and numerical site response studies in chronological order.

2.4.1 Empirical Studies

Seed et al. (1976) used recordings made at rock, stiff soil, deep cohesionless soil, and soft to medium clay sites from the 1969 San Francisco earthquake to compute normalized plots of spectral acceleration, as presented in Figure 2.4. Surface spectral accelerations at these sites were normalized with respect to *PGA* at rock site (PGA_{rock}). It can be seen from Figure 2.4 that spectral accelerations are greatly amplified in deep and soft soil sites when the spectral period (T) > 0.6 s.

Presented in Figure 2.5 are relationships of *PGA* on soft-soil sites ($PGA_{soft\ soils}$) compared to PGA_{rock}. It can be seen that values of $PGA_{soft\ soils}$ were lower than PGA_{rock} at higher amplitudes (PGA_{rock} > 0.2 g). At smaller amplitudes (PGA_{rock} < 0.2 g), however, the difference was not significant.

Idriss (1990) used data from the 1985 Mexico City and California earthquakes to study the relationship between PGA_{rock} and $PGA_{soft\ soils}$. Idriss (1990) showed that at smaller and moderate amplitudes (PGA_{rock} < 0.4 g), $PGA_{soft\ soils}$ were likely to be higher than PGA_{rock}, as shown in Figure 2.6. The 1985 Mexico City and the 1989 Loma Prieta data plotted on Figure 2.6 confirm the observation. At higher amplitudes ($PGA_{rock} \geq 0.4$ g), PGA_{rock} was found that was higher than $PGA_{soft\ soils}$. This deamplification is related to damping and nonlinearity in soft soils at high amplitudes.

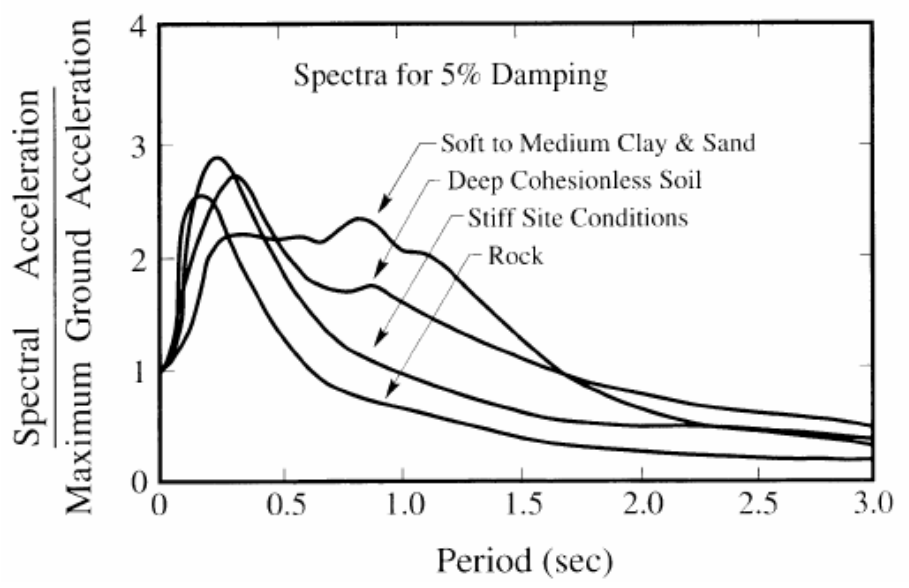

Figure 2.4 Normalized spectral acceleration plots (after Seed et al. 1976).

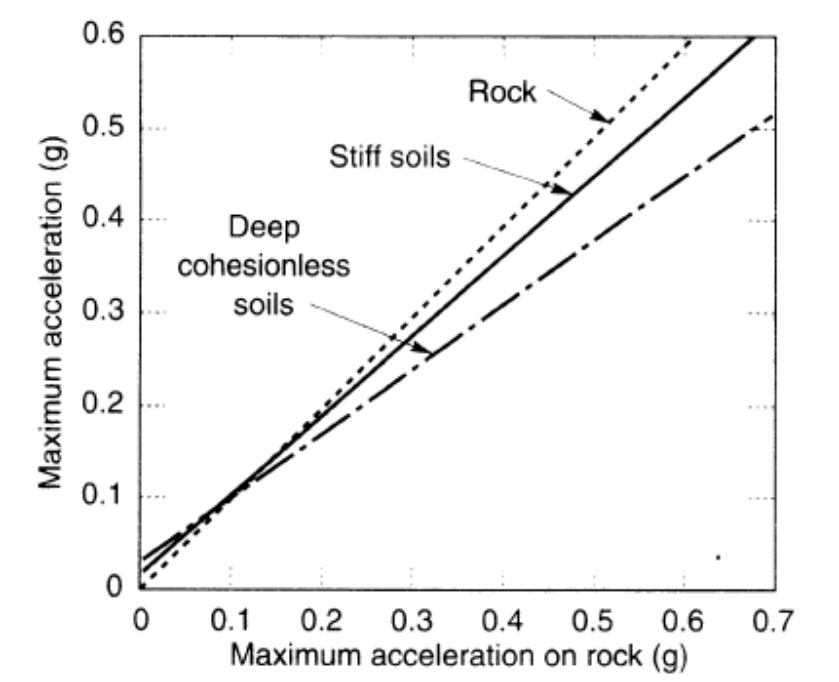

Figure 2.5 Comparison of $PGA_{soft\ soils}$ with PGA_{rock} (after Seed et al. 1976).

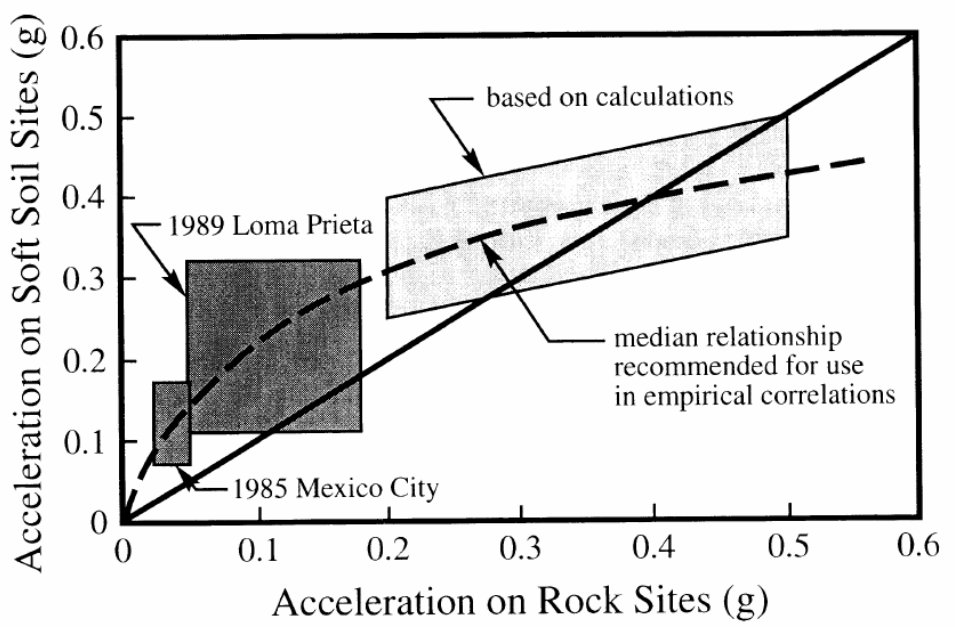

Figure 2.6 Comparison of $PGA_{soft\ soils}$ with PGA_{rock} (after Idriss 1990).

Borcherdt (1994) used 35 strong-motion recordings from the 1989 Loma Prieta earthquake to compute empirical relationship of seismic site coefficients as a function of V_{S30} and amplitude. The site coefficients were computed as a ratio of recorded Fourier amplitude spectra at soil sites to Fourier amplitude spectra at rock sites. Short-period (F_a) and mid-period (F_v) site coefficients were defined at T = 0.2 and 1.0 s, respectively. F_a and F_v were computed as arithmetic averages over a short-period band (0.1-0.5s) and a mid-period band (0.4-2.0 s), respectively. The reference rock site used in Borcherdt (1994) was characterized by V_{S30} = 795 m/s.

Crouse and McGuire (1996) analyzed data from 16 California earthquakes that occurred between 1933 and 1992 to derive site coefficients as a function of NEHRP site classes. The site coefficients were derived as ratios of spectral acceleration in NEHRP E,

D and C sites to spectral acceleration in NEHRP B site. F_a and F_v were defined at T = 0.3 and 1.0 s, respectively. F_v was computed as an arithmetic average of site coefficients at T = 1.0, 2.0, and 3.0 s. The reference rock was characterized by V_{S30} = 1,500 m/s.

Harmsen (1997) derived V_{S30} dependent site coefficients for short-period (≈0.17-0.5 s) and long-period (≈0.5-2 s) using main shock data in the San Fernando Valley and Los Angeles basin areas. The site coefficients were computed as ratios of recorded Fourier amplitude spectra at soil sites to Fourier amplitude spectra at rock sites. The reference rock site was characterized by V_{S30} between 1,140 and 1,370 m/s. The Harmsen (1997) site coefficients were amplitude independent.

Dobry et al. (2000) used 47 strong-motion recording data from the 1994 Northridge earthquake to compute site coefficients as a function of NEHRP site classes. The site coefficients were computed as a ratio of soil to rock response spectra. The definition and derivation of F_a and F_v were similar to Borcherdt (1994), except they used response spectra acceleration instead of Fourier amplitude acceleration. A V_{S30} = 1,500 m/s material was used as a reference rock site.

Rodriguez-Marek et al. (2001) derived attenuation relationships using the 1989 Loma Prieta and 1994 Northridge earthquake data. For each earthquake data set, site coefficients were computed as a ratio of recorded spectral acceleration at Site Class C and D to Site Class B. The site classification used in Rodriguez-Marek et al. (2001) was different from the NEHRP site classification system. The authors used soil and rock stiffness, and depth to rock as a means to classify sites. F_a and F_v were defined as

averages over period ranges (T = 0.1-0.5 s for F_a, and 0.4-2.0 s for F_v), and at discrete periods of 0.3 and 1.0 s for F_a and F_v, respectively.

Joyner and Boore (2000) estimated F_a and F_v values as a function of V_{S30}, pseudo spectral velocity and site-to-source distance. F_a and F_v were defined at discrete periods of 0.2 and 1.0 s, respectively. The V_{S30} of the reference rock site was 1068 m/s.

Steidl (2000) computed site coefficients at 0.3, 1.0, 3.0 s, and *PGA* by normalizing spectral accelerations obtained from recordings in Southern California. The site coefficients were derived as a function of V_{S30}. A V_{S30} = 1,054 m/s material was used as the reference rock site. Field (2000) also computed site coefficients based on a reference site with V_{S30} = 760 m/s.

Borcherdt (2002) analyzed data from 127 strong-motion recordings of the Northridge earthquake. The definition and derivation of F_a and F_v were similar to the earlier work by Borcherdt (1994). Measured and estimated V_{S30} values were used as a proxy for the regression analysis. The reference rock site was underlain by granite and metamorphic rock with V_{S30} = 850 m/s.

Stewart et al. (2003) computed F_a and F_v values by normalizing spectral acceleration from recordings by spectral accelerations obtained from the Abrahamson and Silva (1997) attenuation relationships. Sites were classified based on surficial geology, age, depositional environment, material composition, and V_{S30}. F_a and F_v were computed at discrete periods of 0.3 and 1.0 s. Two reference sites were used: (1) a V_{S30} = 520 m/s

rock site, and (2) a shallow soil site (< 20 m soil thickness) underlain by V_s = 620 m/s rock.

Choi and Stewart (2005) derived amplitude- and V_{S30}-dependent amplification coefficients by normalizing recorded surface spectral accelerations by reference site spectral accelerations. Compared to Stewart et al. (2003), Choi and Stewart (2005) used more attenuation relationships, and added the rupture directivity effects into their study. Nonlinearity was observed to be higher in NEHRP Site Class E, and decreases as V_{S30} increases. F_a and F_v were defined at discrete periods of 0.3 and 1.0 s, respectively. The reference rock site V_{S30} was regressed as a function of spectral period, T. For most values of T, V_{S30} of the reference sites range from 530 to 660 m/s.

2.4.2 Numerical Simulations

Silva et al. (2000) used parametric site response analyses to compute F_a and $F_{v.}$ Silva et al. (2000) used idealized V_s profiles representative of the NEHRP Site Classes C, D, and E. For Site Classes C and D, soil profile depths were arbitrary varied from 30 to 340 m, and two sets of shear modulus reduction (G/G_{max}) and damping (D) versus shearing strain amplitudes (γ) were used. For Site Class E, soil profile depths were arbitrarily varied from 30 to 200 m, and one set of G/G_{max} and D versus γ was used. F_a and F_v were computed at discrete periods of 0.3 s and 1.0 s, respectively. Silva et al. (2000) also computed F_a and F_v values as averages over a short-period range (0.1-0.5 s) and a long-period range (0.4-2.0s) for direct comparison with site coefficients in the

NEHRP Provisions. The discrete period F_a and F_v were found to be 1 to 1.25 times larger than F_a and F_v computed based on averages over the period ranges.

Hashash and Park (2001) used nonlinear one-dimensional site response analyses to compute site coefficients for deep unconsolidated deposits of the Mississippi Embayment over the New Madrid Seismic zone. *Vs* profiles considered range from 100 to 1000 m. The study used a modified hyperbolic model with extended Masing criteria to represent the soil-hysteretic behavior under seismic loading. Long-period amplification (F_v) was noted to be as large as 5 in deep soil deposits. The study highlighted the need to account for depth-dependent seismic site coefficients.

Chapman et al. (2006) performed ground response analyses on near-surface materials in Charleston, South Carolina. V_s profiles were compiled from measurements at 52 locations in the vicinity of Charleston. Point source synthetic ground motions were used in the study. The study highlighted the importance of impedance contrast between the Mesozoic basement and Cretaceous sediments, and the shallow impedance contrast between the Quaternary and Tertiary sediments. Site coefficients were computed at discrete periods of 0.2 and 1 s, for rock accelerations of 0.1, 0.3, and 0.5 g.

Lester and Chapman (2006) examined seismic response of four sites located in Columbia, South Carolina, using one-dimensional equivalent linear algorithm. The sites represent thin Coastal Plain sediments overlying V_s = 3,500 m/s Mesozoic\Paleozoic crystalline rock. The study highlighted the shortcomings of the NEHRP procedure in accounting for large impedance contrast between the soil and the crystalline rock,

particularly at depth less than 30 m. The authors recommended future studies to look for parameters accounting for the effect of depth to bedrock and near-surface impedance ratio.

Andrus et al. (2006) examined seismic site response of seven soil/rock profiles in Charleston, South Carolina using equivalent linear program. The soil/rock profiles were 806 m deep, and were characterized by different Quaternary thicknesses. Point source synthetic ground motions were used in the study. Andrus et al. (2006) showed that peak spectral acceleration generally increases with increasing Quaternary thickness.

Fairbanks et al. (2008) studied the relationship between damage during the 1886 Charleston earthquake and building dynamic height. The study used the soil/rock profiles in Andrus et al. (2006), and equivalent linear seismic site response analysis. The study found that in addition to thickness of the Quaternary sediments, the Marl and deeper soil/weak rock layers also contribute greatly to ground response in Charleston. The study showed that damage was independent (or only slightly dependent) on building height for the structures shaken by the 1886 Charleston earthquakes.

2.4.3 The 1997 NEHRP Provisions

The 1997 NEHRP site coefficients for the short- and long-period ranges, F_a and F_v were developed after a consensus made during a 1992 national workshop. F_a and F_v were defined as spectral acceleration ratios averaged over period ranges of 0.1-0.5 s and 0.4-2.0 s, respectively. The values computed at 0.1 g amplitude were based on empirical studies by Borcherdt (1994) and Seed et al. (1994). Values at higher amplitudes were

based on numerical simulations by Dobry et al. (1994) and Seed et al. (1994). The workshop resulted in (1) the table of the NEHRP values as presently being used in the U.S. Seismic code provisions (ASCE 2010; BSSC 2010; AASHTO 2011, ICC 2012), and (2) modifications of the NEHRP D-E boundary from 200 to 180 m/s and the B-C boundary from 700 to 760 m/s (Dobry et al. 2000).

Presented in Figure 2.7a is the original V_{S30}-F_a data presented by Borcherdt (1994). The data was obtained from the 1989 Loma Prieta earthquake and was presented in a log-log scale. Displayed in Figure 2.7b is the data in Figure 2.7a re-plotted on a linear scale. The NEHRP recommended F_a value for $PGA_{B\text{-}C}$ = 0.01 g is also plotted in Figures 2.7a and 2.7b. The NEHRP F_a suggests that maximum amplification occur in Site Class E. However, from Figure 2.7b, it can be clearly seen that maximum amplification occurs in Site Class D. The log-log plotting appears to have seemingly minimized the scatter in the data, and therefore might have influenced the selection of the recommended F_a value.

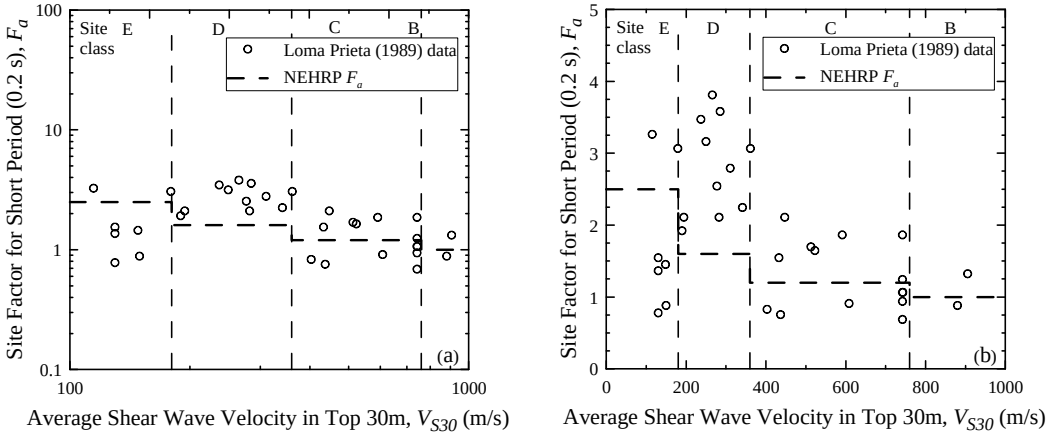

Figure 2.7 Loma Prieta (1989) data plotted in (a) log-log scale (as it was originally presented), (b) linear scale.

2.5 Summary

Presented in Tables 2.1-2.3 are the short-period amplification coefficients computed by the different investigators for the NEHRP Site Classes C, D and E, respectively, and for the range of $PGA_{outcrop}$ between 0.1 to 0.5 g. Long-period amplification coefficients (F_v) obtained by the same investigators are presented in Tables 2.4-2.6. Compared to the NEHRP (1997) values, Silva et al (2000), Rodriguez-Marek et al. (2001), and Borcherdt (2002) obtained larger values F_a for Site Classes C and D. For Site Class E, Silva et al. (2000) obtained significantly lower F_a values. Regarding F_v, Silva et al (2000) and Rodriguez-Marek et al. (2001) obtained lower values for C, D and E site classes, respectively.

Table 2.1 Summary of short-period amplification coefficient (F_a) reported by previous studies for NEHRP Site Class C.

Study	$PGA_{outcrop}$ (g)				
	0.1	0.2	0.3	0.4	0.5
Borcherdt (1994)	1.26	1.18	1.07	0.97	--
Crouse & McGuire (1996)	1.30	1.30	1.30	1.30	--
NEHRP (1997)*	1.20	1.20	1.40	1.00	1.00
Harmsen (1997)	1.30	--	--	--	--
Dobry et al. (2000)	1.36	--	--	--	--
Silva et al. (2000)	1.80	1.70	1.60	1.60	1.40
Steidl (2000)	1.10	--	--	--	--
Field (2000)	1.25	--	--	--	--
Joyner & Boore (2000)	1.23	1.16	1.10	1.04	0.99
Rodriguez-Marek et al. (2001)	1.46	1.31	1.23	1.17	--
Borcherdt (2002)	1.62	1.54	1.46	1.38	1.29
Stewart et al. (2003)	1.31	1.23	1.19	1.16	1.14
Choi & Stewart (2005)	1.36	1.29	1.24	1.22	1.20

*Values recommended in current design codes and guidelines.

Table 2.2 Summary of short-period amplification coefficient (F_a) reported by previous studies for NEHRP Site Class D.

Study	$PGA_{outcrop}$ (g)				
	0.1	0.2	0.3	0.4	0.5
Borcherdt (1994)	1.57	1.38	1.13	0.94	--
Crouse & McGuire (1996)	1.60	1.50	1.40	1.30	--
NEHRP (1997)*	1.60	1.40	1.20	1.10	1.00
Harmsen (1997)	1.80	--	--	--	--
Dobry et al. (2000)	1.46	--	--	--	--
Silva et al. (2000) soil model	1.70	1.30	1.00	0.90	0.75
Steidl (2000)	1.20	--	--	--	--
Field (2000)	1.60	--	--	--	--
Joyner & Boore (2000)	1.51	1.35	1.20	1.07	0.98
Rodriguez-Marek et al. (2001)	1.81	1.61	1.50	1.42	--
Borcherdt (2002)	2.06	1.88	1.71	1.54	1.36
Stewart et al. (2003)	1.63	1.58	1.56	1.54	1.52
Choi & Stewart (2005)	1.81	1.47	1.27	1.19	1.13

*Values recommended in current design codes and guidelines.

Table 2.3 Summary of short-period amplification coefficient (F_a) reported by previous studies for NEHRP Site Class E.

Study	$PGA_{outcrop}$ (g)				
	0.1	0.2	0.3	0.4	0.5
Borcherdt (1994)	1.98	1.62	1.21	0.91	--
Crouse & McGuire (1996)	2.10	1.90	1.80	1.70	--
NEHRP (1997)*	2.50	1.70	1.20	0.90	0.90
Harmsen (1997)	--	--	--	--	--
Dobry et al. (2000)	--	--	--	--	--
Silva et al. (2000) soil model	1.30	0.80	0.60	0.50	0.42
Steidl (2000)	--	--	--	--	--
Field (2000)	--	--	--	--	--
Joyner & Boore (2000)	--	--	--	--	--
Rodriguez-Marek et al. (2001)	--	--	--	--	--
Stewart et al. (2003)	2.10	1.64	1.36	1.21	1.07
Choi & Stewart (2005)	2.24	1.60	1.28	1.12	1.02

*Values recommended in current design codes and guidelines.

Table 2.4 Summary of long-period amplification coefficient (F_v) reported by previous studies for NEHRP Site Class C.

Study	$PGA_{outcrop}$ (g)				
	0.1	0.2	0.3	0.4	0.5
Borcherdt (1994)	1.54	1.49	1.43	1.35	--
Crouse & McGuire (1996)	1.70	1.70	1.70	1.70	--
NEHRP (1997)*	1.70	1.70	1.50	1.40	1.30
Harmsen (1997)	1.50	--	--	--	--
Dobry et al. (2000)	1.37	--	--	--	--
Silva et al. (2000)	1.80	1.80	1.80	1.90	1.90
Steidl (2000)	1.25	--	--	--	--
Field (2000)	1.50	--	--	--	--
Joyner & Boore (2000)	1.80	1.80	1.80	1.80	1.80
Rodriguez-Marek et al. (2001)	1.32	1.28	1.25	1.24	--
Stewart et al. (2003)	1.80	1.75	1.74	1.72	1.70
Choi & Stewart (2005)	1.62	1.56	1.54	1.52	1.51

*Values recommended in current design codes and guidelines.

Table 2.5 Summary of long-period amplification coefficient (F_v) reported by previous studies for NEHRP Site Class D.

Study	$PGA_{outcrop}$ (g)				
	0.1	0.2	0.3	0.4	0.5
Borcherdt (1994)	2.29	2.16	1.98	1.79	--
Crouse & McGuire (1996)	2.00	2.00	1.90	1.90	--
NEHRP (1997)*	2.40	1.80	1.80	1.60	1.50
Harmsen (1997)	2.30	--	--	--	--
Dobry et al. (2000)	1.61	--	--	--	--
Silva et al. (2000)	2.60	2.40	2.40	2.10	2.00
Steidl (2000)	1.70	--	--	--	--
Field (2000)	2.60	--	--	--	--
Joyner & Boore (2000)	3.20	3.20	3.20	3.20	3.20
Rodriguez-Marek et al. (2001)	2.04	1.94	1.89	1.85	--
Stewart et al. (2003)	2.39	2.35	2.34	2.33	2.32
Choi & Stewart (2005)	2.60	2.14	1.92	1.74	1.66

*Values recommended in current design codes and guidelines.

Table 2.6 Summary of long-period amplification coefficient (F_v) reported by previous studies for NEHRP Site Class E.

Study	$PGA_{outcrop}$ (g)				
	0.1	0.2	0.3	0.4	0.5
Borcherdt (1994)	3.51	3.21	2.81	2.41	--
Crouse & McGuire (1996)	2.90	2.70	2.60	2.60	--
NEHRP (1997)*	3.50	3.20	2.80	2.40	2.4
Harmsen (1997)	--	--	--	--	--
Dobry et al. (2000)	--	--	--	--	--
Silva et al. (2000)	3.30	2.70	2.10	1.85	1.50
Steidl (2000)	--	--	--	--	--
Field (2000)	--	--	--	--	--
Joyner & Boore (2000)	--	--	--	--	--
Rodriguez -Marek et al. (2001)	--	--	--	--	--
Stewart et al. (2003)	3.50	2.60	2.20	1.90	1.70
Choi & Stewart (2005)	3.60	2.63	2.16	1.90	1.70

*Value recommended in design codes and guidelines.

CHAPTER THREE

SEISMIC SITE COEFFICIENTS AND DESIGN RESPONSE SPECTRA BASED ON CONDITIONS IN CHARLESTON, SOUTH CAROLINA[1]

3.1 Introduction

The Charleston area, as displayed in Figure 3.1, is located within the lower part of the Atlantic Coastal Plain physiographic province. Gridlines in Figure 3.1 represent 7.5-minute quadrangle boundaries. Major rivers flowing through the area into the Atlantic Ocean include the Ashley, the Cooper, the Stono and the Wando. The subsurface geology consists of ocean-ward thickening Cretaceous and younger sediments down to depths of 700-1000 m (Chapman and Talwani 2002). Near-surface sediments are typically unconsolidated Quaternary deposits ranging from beach/barrier island sand to estuarine sand and clay to fluvial sand and silt (McCartan et al. 1984; Weems et al. 1993). Exposures of Tertiary sediments exist in limited areas along the stream banks in the northwest part of Figure 3.1. Tertiary and Cretaceous sediments are compacted, but weakly lithified. Beneath the Tertiary and Cretaceous sediments are hard Mesozoic/Paleozoic basement rock.

[1] A similar version of this chapter was accepted in June 2013 for publication in EERI's *Earthquake Spectra*; Aboye, S.A., Andrus, R.D., Ravichandran, N., Bhuiyan, A.H., and Harman, N., 2013. "Seismic Site Factors for Constructing Response Spectra Based on Conditions in Charleston, South Carolina."

With moment magnitude of ~7.0, the Charleston earthquake of August 31, 1886 is the largest historic earthquake to have occurred in the southeastern United States (Bollinger 1977). The epicentral area was located near Summerville, Ladson and Middleton Place. Displayed in Figure 3.1 is the Woodstock fault zone as delineated by Durá-Gómez and Talwani (2009), which is the likely source of the 1886 Charleston earthquake. Shaking was felt as far as Boston, Massachusetts; Havana, Cuba; Bermuda; and Iowa City, Iowa (Dutton 1889). Côté (2006) estimated 124 deaths were caused by the earthquake. From paleoliquefaction investigations, Talwani and Schaeffer (2001) estimated the recurrence rate for 1886-like earthquakes to be about 500 years.

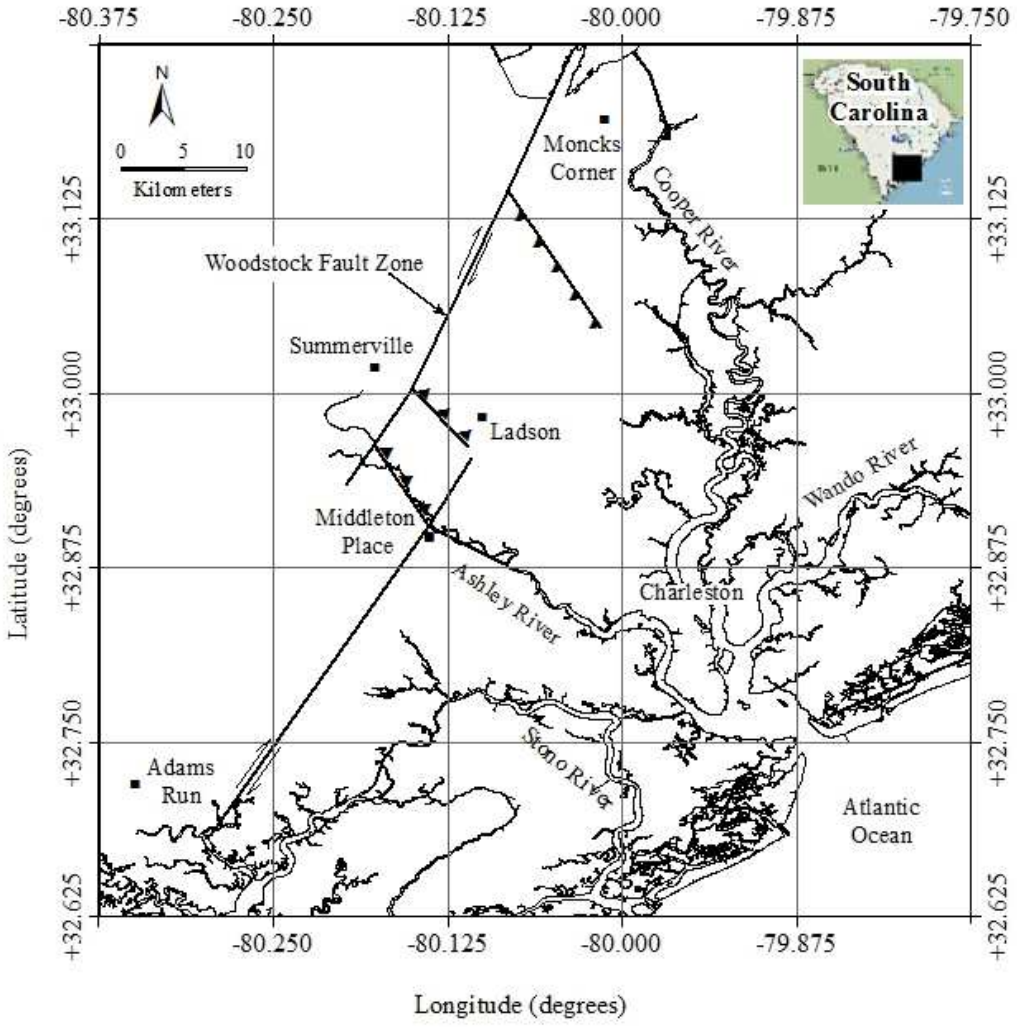

Figure 3.1 Map of the Charleston area showing the Woodstock fault zone as delineated in Durá-Gómez and Talwani (2009).

3.2 Dynamic Soil\rock model

The stress-strain path of a material during strong earthquake loading is complex and made up of several continuous hysteresis loops, which depends on stiffness, damping, and other properties of the material. Small-strain shear modulus (G_{max}) and V_s are directly related by

$$G_{\max} = \frac{\gamma_T V_s^2}{g} \tag{3.1}$$

where γ_T is the total unit weight of the material; and g is the acceleration due to gravity. Typically, when evaluating ground response for non-critical structures, V_s is measured in situ and the variations of normalized shear modulus (G/G_{max}) and material damping ratio (D) with shearing strain amplitude are estimated using generic relationships (e.g., Stokoe et al. 2004; Zhang et al. 2005, 2008).

In this chapter, fifty-six V_s profiles are used to represent the variations of small-strain soil/rock stiffnesses in the Charleston area. Presented in Figure 3.2a are twenty-eight V_s profiles that extend to a soft-rock (V_s = 700 m/s) half space at a depth of 137 m. Tabulated V_s values for the reference profile are given in Table 3.1. Above the depth of 80 m, values of V_s are taken from the statistical study by Andrus et al. (2006) based on compiled in situ measurements conducted by different investigators during the years of 1998-2004. Most of the V_s measurements were made by the seismic cone penetration test method. Some were conducted by the seismic downhole, spectral-analysis-of-surface-waves, suspension logger and seismic refraction methods. Above the depth of 10 m, the

V_s value of 190 m/s is the average for the 100,000-year-old Wando Formation. Between the depths of 10 and 80 m, the values of V_s ranging from 400 to 530 m/s are averages of measurements from the Tertiary-age sediments. Between the depths of 80 and 137 m, the values of V_s are averages of measurements made at one location by the suspension logger method for the South Carolina Department of Transportation (SCDOT) in 2006.

The V_s profiles plotted in Figure 3.2a are created to represent the range of likely variations in thickness of the Quaternary and V_s of the Quaternary and Tertiary within the Charleston area. Quaternary thicknesses are assumed to be 0, 10, 20 and 30 m. Variations in V_s are included by applying ±1, -2 and -3 standard deviations of ln(V_s) to the reference profile above the half space. The standard deviation (σ) of ln(V_s) is used because V_s data typically follow lognormal distributions. As given in Table 3.1, the average values of σ of ln(V_s) are 0.32 for the Wando, and 0.14 to 0.31 for the Tertiary-age sediments.

The other twenty-eight V_s profiles are plotted in Figure 3.2b and are considered to investigate spectral response differences that result from propagating hard-rock outcrop motions from a depth of 806 m versus propagating soft-rock outcrop motions from a depth of 137 m in Charleston. The V_s profiles presented in Figures 3.2a and 3.2b are identical in the top 137 m. Below 137 m in Figure 3.2b, commonly assumed values of V_s for Charleston are used (Andrus et al. 2006).

Displayed in Figure 3.3 are the V_s profiles shown in Figure 3.2a grouped by NEHRP site classes. Also plotted is the reference V_s profile which has a V_{S30} of 295 m/s. The number of V_s profiles corresponding to the NEHRP site classes E, D and C is 12, 13

and 3, respectively. The lognormal mean V_{S30} value of the generated V_s profiles is computed to be 208 m/s.

Table 3.1 Reference soil/soft rock profile with top of half space at a depth of 137 m (modified from Andrus et al. 2006).

Layer number(s)	Layer thickness (m)	Total unit weight (kN/m³)	Shear wave velocity, V_s (m/s)	Standard deviation of ln(V_s) (m/s)	Plasticity index, *PI* (%)	Mean effective stress, σ_m' (kPa)	Geologic age
1-3	1	18.2	190	0.32	15	15	Quaternary (Wando formation)
4-10	1	18.2	190	0.32	15	50	
11-25	1	18.5	400	0.312	50	220	Tertiary
26-37	1	18.5	435	0.191			
38-41	5	18.9	530	0.197	15	600	Tertiary
42-44	6	18.9	660	0.169			
45-49	6	18.9	630	0.262			
50-52	3.5	19.6	380	0.262	15	1400	Tertiary
53	2.5	19.6	640	0.139			
54	Half space	22.5	760				Tertiary and older

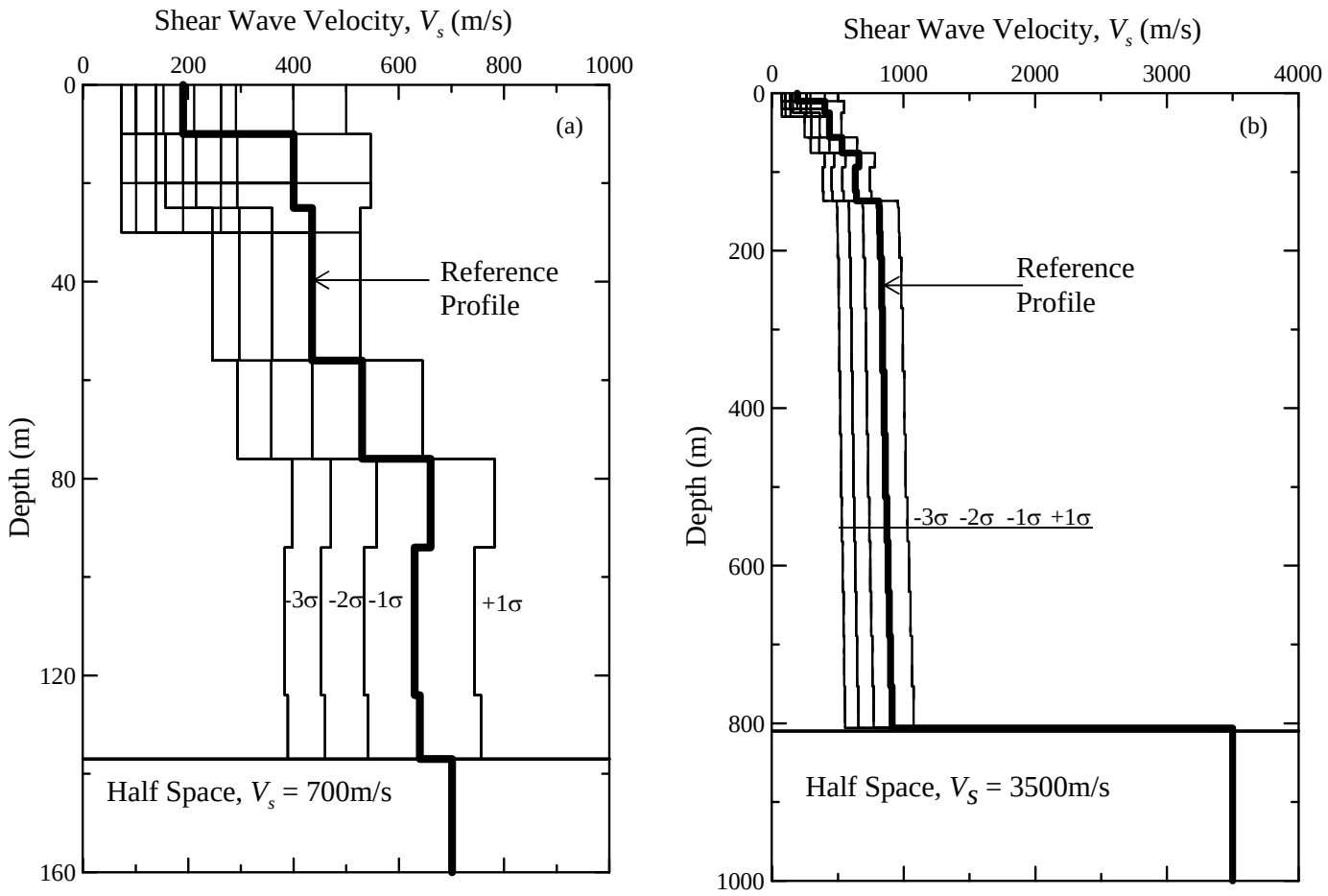

Figure 3.2 Shear wave velocity profiles considered for (a) the soft-rock outcropping condition, and (b) the hard-rock outcropping condition.

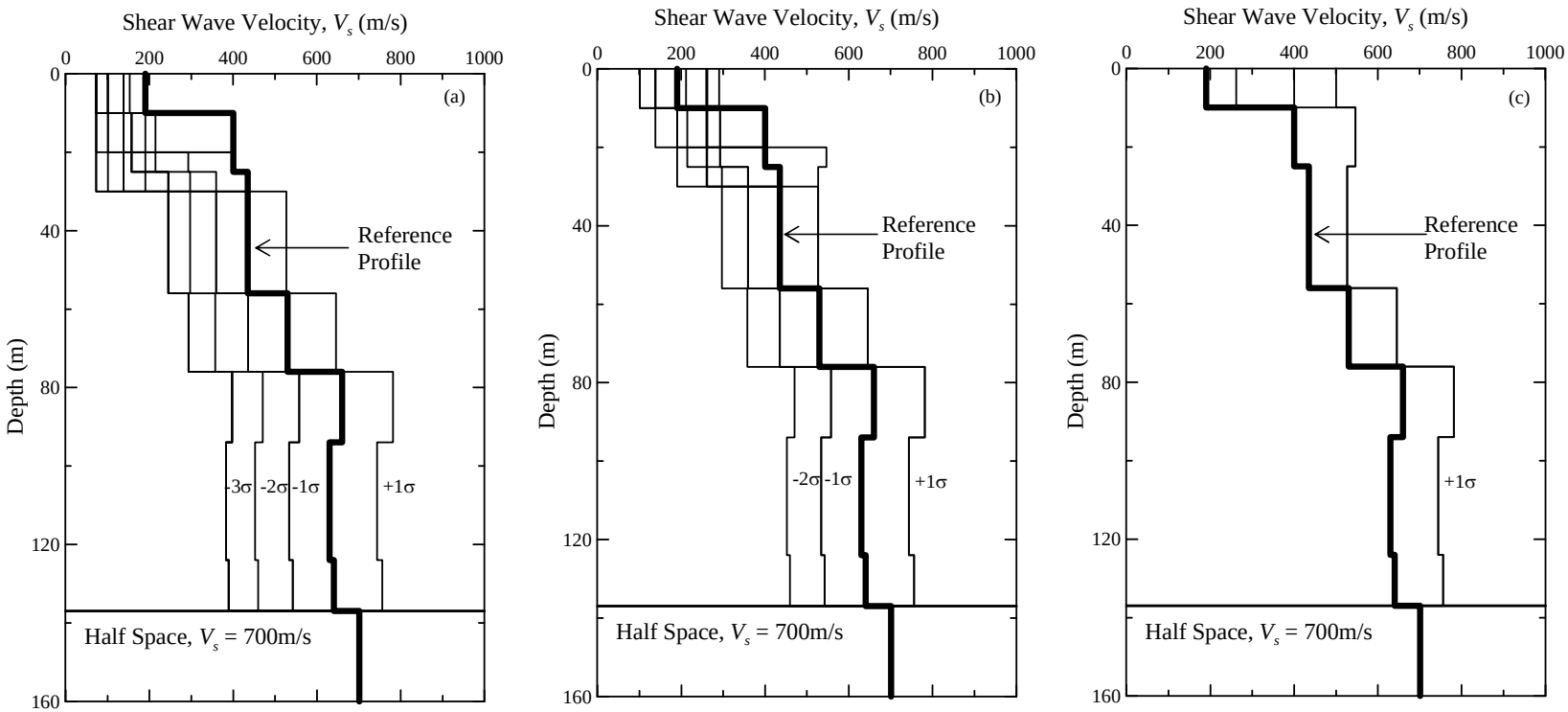

Figure 3.3 V_s profiles grouped by *NEHRP* site class (a) E, (b) D, and (c)

The Zhang et al. (2005, 2008) relationships that expressed variations of G/G_{max} and D with shearing strain amplitude (γ) in terms of geologic age, mean effective confining pressure, and soil plasticity index are used. Sample G/G_{max}-γ and D-γ relationships for Tertiary deposits with mean effective confining stresses of 220 kPa (depth ≈ 24 m) and 1400 kPa (depth ≈ 130 m) are displayed in Figure 3.4. Also displayed are the ±1σ G/G_{max}-γ and D-γ relationships. For the half space with V_{S30} = 700 m/s, purely linear relationships of G/G_{max}-γ and D-γ are assumed. This is done by entering G/G_{max} = 1 and D = 0.5% for all γ values. A value of D = 0.5% is taken to be representative for soft rock in the South Carolina Coastal Plain (SCDOT 2008).

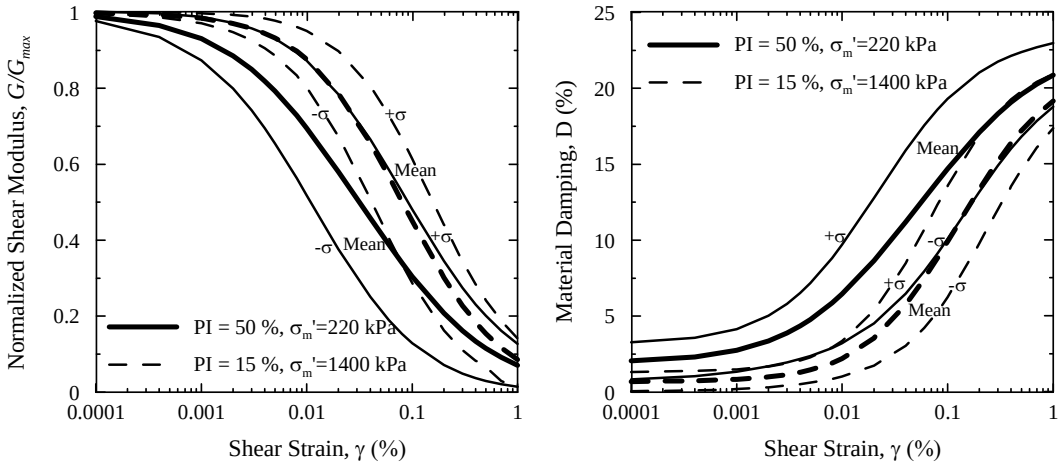

Figure 3.4 Sample G/G_{max}-γ and D-γ relationships (Zhang et al. 2005, 2008).

3.3 Input Motions

A computer program called Scenario_PC was used to simulate outcrop motions, because actual strong motion records are not available for the Charleston area. Scenario_PC was developed by Chapman (2006) for seismic hazard analysis in South Carolina. The program generates acceleration time histories based on a point-source stochastic model (Atkinson and Boore 1995). Necessary inputs for Scenario_PC include: (1) rock model; (2) earthquake moment magnitude; (3) site-to-source distance; and (4) return period.

Chapman and Talwani (2002) defined two rock models for South Carolina in program Scenario_PC. The first model is referred to as the geologic realistic condition and consists of a very thick, outcropping soft rock (V_s = 700 m/s) layer over hard rock. The thickness of the soft rock layer is equal to the thickness of Tertiary and Cretaceous sediments (e.g., 700-1000 m in the Charleston area). The second model is referred to as the hard-rock outcropping condition, which consists of 250 m of weathered hard rock (V_s = 2,500 m/s) underlain by a half space of unweathered hard rock (V_s = 3,500 m/s). Scenario_PC uses a B-C amplification function to transfer the hard-rock motions to geologic realistic soft-rock motions (Chapman 2006). The two main advantages of performing ground response analysis based on the geologic realistic condition are (1) the input V_s profiles need only to extend to about 137 m in Charleston, and (2) the computed site coefficients can be directly applied to the USGS B-C rock accelerations to construct the design response spectra.

Deaggregation analyses of the seismic hazard at six oscillator frequencies (0, 0.5, 1, 2, 3.33, 5 Hz) are performed for the centers of the twenty-four 7.5-minute quadrangles shown in Figure 3.1 using the 2002 USGS deaggregation program (https://geohazards.usgs.gov/deaggint/2002/index.php; accessed March 26, 2010). The return periods considered are 10% and 2% probabilities of exceedance in 50 years (or return periods of 475 and 2475 years, respectively). These return periods are referred to in SCDOT (2008) as the Functional Evaluation Earthquake (FEE) and the Safety Evaluation Earthquake (SEE), respectively. For a given quadrangle and return period, the predominant moment magnitude (M_w) and modal site-to-source distance (R) are found to be practically the same for all of the six spectral periods. The observation agrees with Chapman (2006) and SCDOT (2008). For the entire study area and both return periods, the deaggregated data suggest that the hazard at all spectral periods is dominated by events with M_w between 7.2 and 7.4, and R between 6 and 36 km.

Presented in Figure 3.5 are sample synthetic input motions generated for the center of the Charleston quadrangle and three other neighboring quadrangles (i.e., Johns Island, North Charleston and Fort Moultrie) for the FEE and SEE conditions. The synthetic motions are generated to match with the uniform hazard spectra points. Displayed in Figure 3.6 are the respective response spectra plots for the motion shown in Figure 3.5. It can be seen that the relative differences in period contents between the SEE and FEE motions are small, and periods at which peak accelerations occur are about 0.15s.

Because one of the objectives of this study is to provide site coefficients that are comparable with the NEHRP coefficients, the peak ground acceleration at the soft-rock outcrop surface ($PGA_{B\text{-}C}$) of the motions need to match with the range provided in the NEHRP. This is achieved by scaling the $PGA_{B\text{-}C}$ of the motions to match with the NEHRP $PGA_{B\text{-}C}$. Even though this step removes the association between the scaled time histories and the stated probability of exceedance (P_E) values, it is acceptable because it does not bring an additional bias to the response predicted. This is confirmed by a sensitivity analysis performed using the FEE motion and a scaled SEE motion. The scaled SEE motion predicts the same surface spectral accelerations as the FEE motion. This is an expected observation, because the seismic hazard is dominated by a single earthquake source. Park et al. (2012) suggested that such arbitrary scaling may be used when the seismic hazard is dominated by a single earthquake source zone.

Twelve sites, two return periods, and six $PGA_{B\text{-}C}$ scaling values lead to a total of 144 acceleration time histories that are used as input soft-rock outcrop motions. The soft-rock motions are applied at the half space located at a depth of 137 m in Figure 3.2a.

For the analysis involving the deeper V_s profiles presented in Figure 3.2b, twenty-four acceleration time histories representing the hard-rock outcropping condition are used and applied at the hard-rock half space located at a depth of 806 m in Figure 3.2b. Sample hard-rock acceleration time histories are presented in Figure 3.7. Displayed in Figure 3.8 are the respective response spectra plots for the motion shown in Figure 3.7. It

can be seen that the relative differences in period contents between the SEE and FEE motions are small, and periods at which peak accelerations occur are about 0.9s.

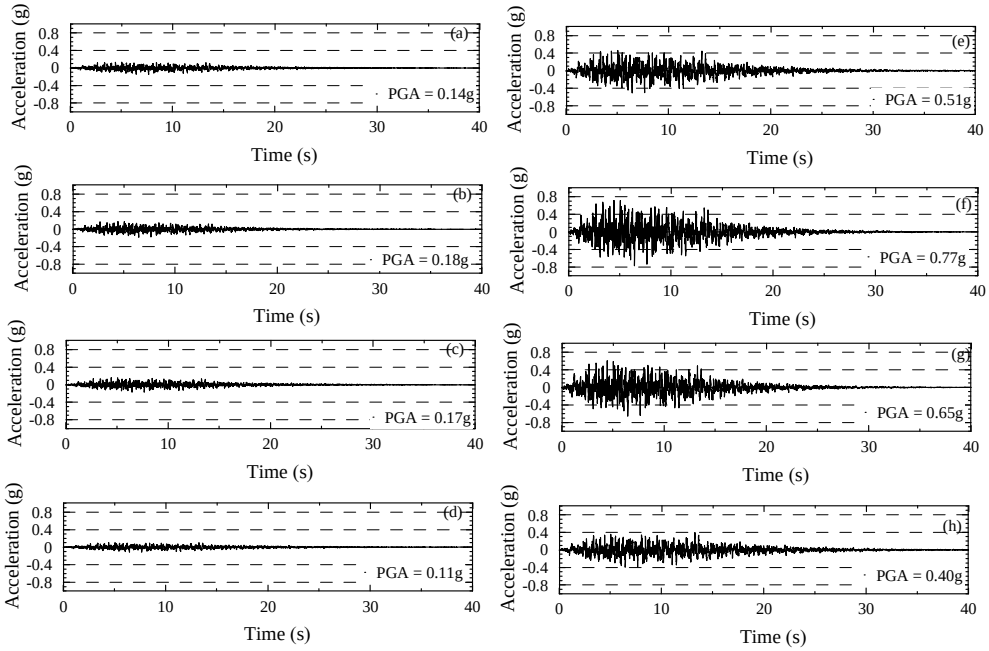

Figure 3.5 Sample synthetic soft-rock outcrop motions generated by Scenario_PC for (a-d) 10% and (e-h) 2% probability of exceedance in 50 years.

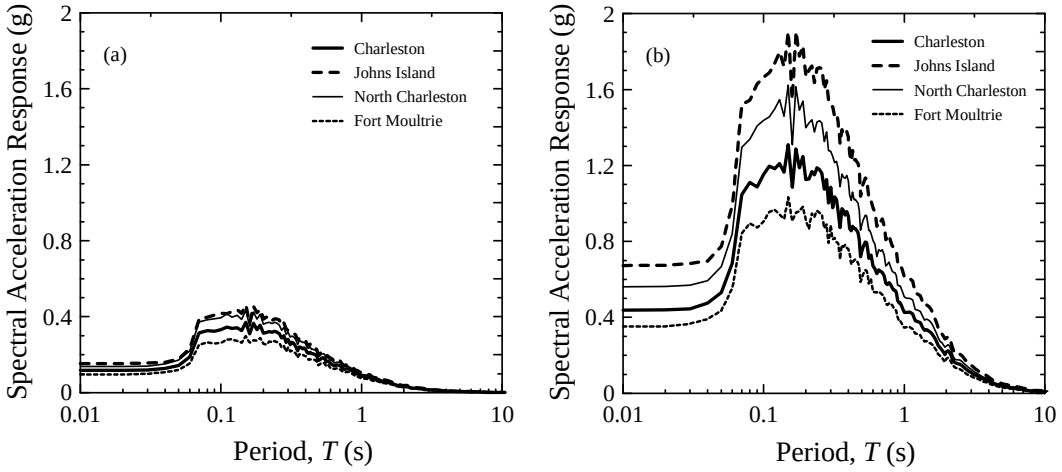

Figure 3.6 Response spectra of soft-rock outcrop ground motions for (a) 10% and (b) 2% probability of exceedance in 50 years for the time histories shown in Figure 3.5.

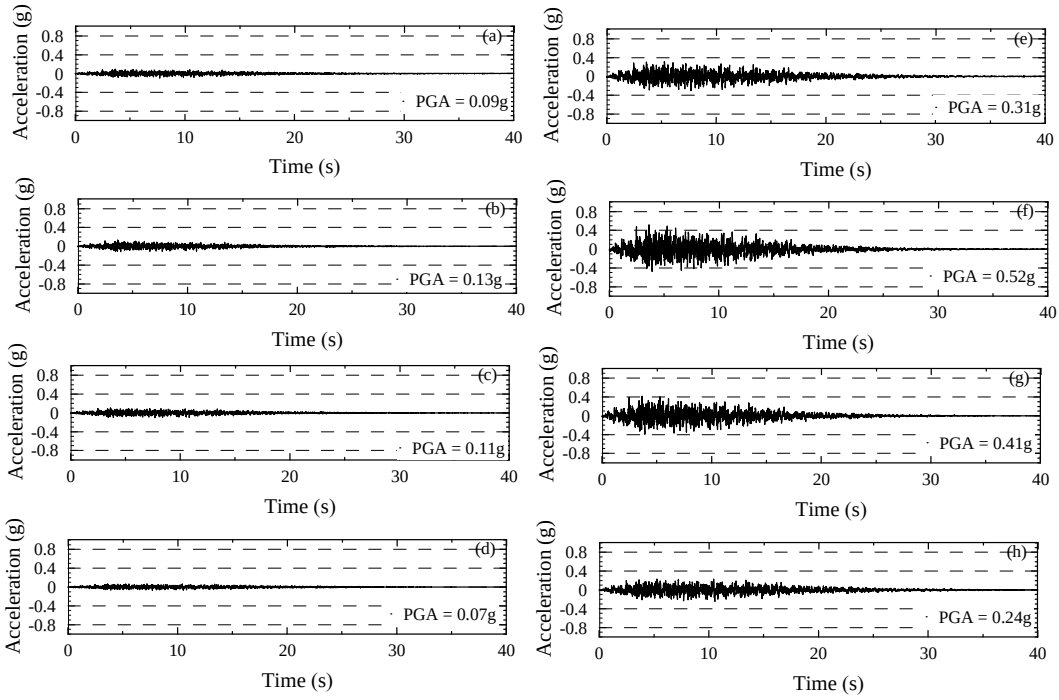

Figure 3.7 Sample synthetic hard-rock outcrop motions generated by Scenario_PC for (a-d) 10% and (e-h) 2% probability of exceedance in 50 years.

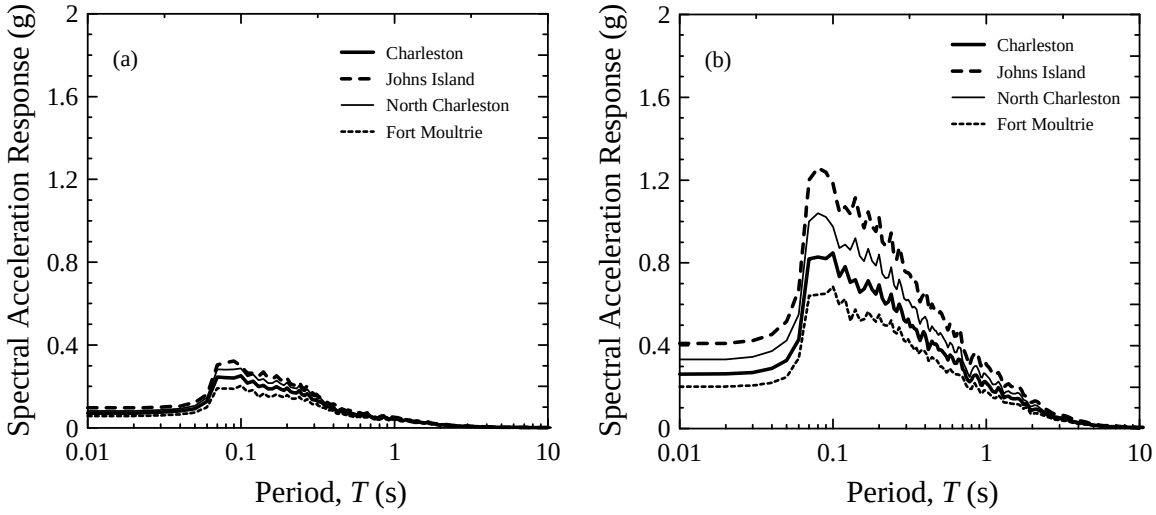

Figure 3.8 Response spectra of hard-rock outcrop ground motions for (a) 10% and (b) 2% probability of exceedance in 50 years for the time histories shown in Figure 3.7.

3.4 Ground Response Analysis

The computer programs SHAKE2000 (Ordóñez 2011) and D-MOD2000 (Matasović and Ordóñez 2011) are used to perform one-dimensional, total stress ground response analysis. The one-dimensionality assumption is taken to be valid for three reasons. First, due to subsequent refractions by the soil layers, stress waves propagate from the earthquake focus to the earth's surface in a nearly vertical path, especially close to the surface. Second, much of the Charleston area is flat within the source-to-site distance range, with ground surface elevations less than about 15 m above mean sea level. Third, soil properties generally vary more rapidly in the vertical direction than in the horizontal direction making the vertical soil/rock column more important. The stated justifications for one-dimensional analysis do not take into account topography of the bedrock or earthquake directivity effects, which are not well established for the Charleston area. Thus, one-dimensional analysis is considered adequate.

SHAKE2000 is based on the original SHAKE program by Schnabel et al. (1972) and uses the equivalent linear method of modeling the nonlinear response of a one dimensional horizontally layered soil profile to vertically propagating shear waves. Although a nonlinear formulation is preferred for modeling nonlinear systems, SHAKE2000 is considered adequate when computed peak ground acceleration is less than 0.4 g and computed values of γ are less than 2% (Kramer and Paulsen 2004). The advantage of SHAKE2000 is that it takes much less computation time and has less input needs than computer programs based on a nonlinear formulation.

D-MOD2000 is an enhanced version of D-MOD (Matasović 1993) and uses a nonlinear formulation where the stress-strain hysteretic response of soil is modeled by a degraded backbone curve generated by unloading-reloading rules developed by Masing and extended by Pyke (1979). Because this type of formulation considers only hysteretic damping, an external viscous damping formulation is incorporated in the form of Rayleigh damping. This requires an initial calibration step for D-MOD2000 to obtain suitable values of the viscous damping (ξ) and an odd integer (n) related to the modes at which target damping is matched. The calibration involves running D-MOD2000 at a low input value of $PGA_{B\text{-}C}$ and adjusting ξ and n until the response spectrum from D-MOD2000 matches the response spectrum from SHAKE2000. At low loading, the hysteretic damping is insignificant because the material behaves linearly even with non-linear material model. The ξ and n that produces the best match between spectra are then used in running D-MOD2000 at the desired high $PGA_{B\text{-}C}$ level (Bhuiyan et al. 2013).

Non-linear time domain analysis also requires special attention to layer thicknesses. Subdividing of major layers is often done by requiring a minimum fundamental frequency of 15-25 Hz for sublayers, because higher frequencies contain a relatively small amount of energy in an earthquake loading (Schnabel et al. 1972). The fundamental frequency of a layer is computed by $V_s/4h$, where h is the thickness of the sublayer.

For this study, SHAKE2000 is used when $PGA_{B\text{-}C} \leq 0.3$ g; and D-MOD2000 is used when $PGA_{B\text{-}C} > 0.3$ g. Values of ξ and n for use in D-MOD2000 are determined by

running both programs mostly with $PGA_{B\text{-}C}$ = 0.1 g. The best frequency calibration pairs are obtained to be either (ξ = 0.75, n = 7); (ξ = 0.5, n = 7); or (ξ = 0.5, n = 5). The criterion of layer frequency $\geq$ 25 Hz is shown to be sufficient to ensure ‘‘layer-independent’’ results, based on analyses performed assuming cutoff frequencies of 15, 20 and 25 Hz. Thus, sublayer thicknesses could not exceed $V_s/100$.

3.5 Results

Average values of F are computed for six spectral period ranges (T): $\leq$ 0.01, 0.01-0.4, 0.41-0.8, 0.81-1.2, 1.21-2.0 and 2.01-4.0 s, respectively based on the geologic realistic, soft-rock condition. These ranges are referred to by their middle range periods. The respective site coefficients are denoted as $F_{PGA,}$ $F_{0.2}$ (or F_a), $F_{0.6}$, F_1 (or F_v), $F_{1.6}$ and $F_{3.0}$. Presented in Figures 3.9-3.11 are computed $F_{PGA,}$ F_a and F_v values, respectively, plotted versus V_{S30}. Each data point is determined by averaging average values from twelve simulations involving twelve different time-histories. The data plotted in Figures 3.9-3.11 are results of over 9,000 SHAKE simulations and 4,500 D-MOD simulations.

Averaging values of F over a spectral period range is consistent with the development of the NEHRP F_a and F_v recommended values. It should be noted, however, that the NEHRP F_a and F_v were determined assuming the spectral period ranges of 0.1-0.5 s and 0.4-2.0 s, respectively (Borchedt 1994). Narrower period ranges allow for better predictions of spectral accelerations, because the periods at which spectral peaks occur can vary greatly from site to site and can exceed 1.0 s.

The plotted V_{S30}-F data pairs exhibit three general features--(1) an increasing trend in F as V_{S30} increases from a very low value; (2) a zone of peak F values, depending on $S_{outcrop}$; and (3) a decreasing trend in F as V_{S30} increases beyond the zone of peak F values. Similar general features can be observed in data reported by other investigators (Silva et al. 2000; Chapman et al. 2006; Fairbanks et al. 2008) and are supported by vibration theory, where V_{S30} is an index for site period. These three general features are assumed in developing mathematical models of F.

When V_{S30} is less than the estimated V_{S30} corresponding to the peak F value (V_{S30P}), the median F curves plotted in Figures 3.9-3.11 can be expressed by the following linear relationship:

$$F = \left(\frac{F_P}{V_{S30P}} \right) V_{S30} \qquad \text{for all values } T \text{ and } V_{S30} < V_{S30P} \tag{3.2}$$

where F_P is the estimated peak F value. F_P and V_{S30P} are calculated by:

$$F_p = x_1 S_{outcrop} + x_2 \tag{3.3a}$$

$$V_{S30P} = x_3 S_{outcrop} + x_4 \tag{3.3b}$$

where x_1, x_2, x_3 *and* x_4 are regression coefficients given in Table 3.2.

When $V_{S30} \geq V_{S30P}$, the median F curves plotted in Figures 3.9-3.11 can be expressed by the following linear or exponential relationships:

$$F = \frac{(F_P - 1)(760 - V_{S30})}{760 - V_{S30P}} + 1 \qquad \text{for } T < 0.2 \text{ s and } V_{S30} \geq V_{S30P} \tag{3.4a}$$

$$F = a + b\, e^{cV_{S30}} \qquad \text{for } T \geq 0.2 \text{ s and } V_{S30} \geq V_{S30P} \tag{3.4b}$$

where a is a regression coefficient given in Table 3.2; and b and c are regression coefficients calculated from:

$$b = \frac{1 - a}{e^{760c}} \tag{3.5}$$

$$c = \frac{\ln\left(\frac{1 - a}{F_p - a}\right)}{760 - V_{S30P}} \tag{3.6}$$

Table 3.2 Regression coefficients for estimating site coefficients.

Spectral period, T (s)	$S_{outcrop}$	x_1 (g^{-1})	x_2	x_3 (g^{-1}. m/s)	x_4 (m/s)	a	$Z_{0.95}$	$Z_{0.05}$
0.0	*PGA*	-1.88	1.99	359	142	-	1.38	0.64
0.2	S_s	-0.83	2.05	105	176	0.65	1.48	0.63
0.6	$S_{0.6}$	-3.53	3.09	207	156	0.85	1.40	0.70
1.0	S_1	-4.16	3.76	127	154	0.90	1.40	0.68
1.6	$S_{1.6}$	-5.36	3.86	198	121	0.97	1.40	0.68
3.0	$S_{3.0}$	-8.20	2.80	394	80	0.99	1.30	0.65

Equations 3.2 and 3.4 are derived to satisfy three conditions. First, Equations 3.2 and 3.4 provide the same F values at V_{S30P}. Second, Equation 3.2 assumes $F = 0$ when $V_{S30} = 0$ m/s. This assumption agrees with the fact that material with zero stiffness cannot support shear waves and, for this reason, F should be zero regardless of $S_{outcrop}$. Third, Equation 3.4 satisfies the condition that $F = 1.0$ when $V_{S30} = 760$ m/s, which is the assumed reference soft-rock outcrop site used in the NEHRP provisions.

The development of Equations 3.2 and 3.4 involved a two-step procedure. First, median curves are derived based on residual analysis of the individual subset of data in Figures 3.9-3.11. The appropriateness of the median curves is checked by studying residuals. The residual, ε, is defined here as F of the plotted data divided by F of the median curve. Presented in Figures 3.12a and 3.12b, are probability plots of the residuals assuming normal and lognormal distributions, respectively. The coefficient of determination (r^2) associated with Figures 3.12a and 3.12b are 0.97 and 0.99, respectively. The higher value of r^2 obtained in Figure 3.12b indicates that ε follows lognormal distribution better than normal distribution. Presented in Figures 3.13 and 3.14 are sample plots V_{S30}-ε, and lognormal probability distribution functions of ε, respectively. It can be seen from Figures 3.13 and 3.14 that the computed median values of ε are approximately equal to 1.0, which indicates that the median relationships are unbiased in predicting F and the models have central tendencies. In other words, the predictions underestimate the response just as often as they overestimate. Based on Figures 3.13, it is noted that the predictor variable V_{S30} is shown to have little or no bias

in the median relationships expressed by Equations 3.2 and 3.4, because plots of V_{S30}-ε do not show any systematic structure.

The next step involves obtaining linear regression approximations of F_p and V_{S30P} as a function of $S_{outcrop}$ (Equation 3.3). Sample F_p and V_{S30P} versus $S_{outcrop}$ plots are shown in Figure 3.15a-f for spectral periods of 0.0, 0.2, and 1.0 s. It can be seen from Figure 3.15 that F_p decreases and V_{S30P} increases with increasing $S_{outcrop}$. Based on the regressed F_p and V_{S30P}, Equations 3.2 and 3.4 are established using the entire data set for a given F.

The upper and lower bound curves shown in Figures 3.9-3.11 are drawn to bound 95% and 5%, respectively, of all the data points for a given *F*. They are drawn by multiplying Equations 3.1 and 3.3 by the average standard Z-scores (i.e., $Z_{0.95}$ or $Z_{0.05}$) listed in Table 3.2. The Z-scores are obtained from lognormal cumulative distribution of *F*-residuals for each set of data.

3.4 Discussions

Recommended Site Coefficients

For comparison, the NEHRP F_a and F_v values are also plotted in Figures 3.9, 3.10 and 3.11. It can be seen in Figure 3.9 that there is good general agreement between the computed median values and the NEHRP F_a values. However, computed median F_a values are higher than the NEHRP F_a for site class C and D when the spectral accelerations at the soft-rock outcrop for 0.2 s (S_s) are less than 0.75 g (Figures 3.10a-3.10d). This finding generally agrees with Silva et al. (2000) and Borcherdt (2002), who

also obtained F_a values greater than the NEHRP for site class D. For site class E, the computed median F_a values plot significantly lower than the NEHRP value.

Concerning F_v, it can be seen in Figure 3.11 that there is good general agreement between the computed median F_v values and the NEHRP value. For site class C, computed median F_v values are typically less than the NEHRP value. For site class D, computed median F_v values are often higher than the NEHRP value. This observation generally agrees with Silva et al. (2000), Borcherdt (2002), Stewart et al. (2003) and Choi and Stewart (2005) who also obtained F_v values greater than the NEHRP for site class D. For site class E, the computed median F_v values are more often lower than the NEHRP value.

Based on the findings discussed above and because conditions typical of Charleston are used, the relationships defined by Equations 3.2 and 3.4 are recommended for constructing design response spectra curves in the Charleston area. Differences in F_a and F_v values obtained in this study and the NEHRP may be explained by (1) differences in assumed soil/rock conditions; (2) differences in applied ground motions; and (3) the fact that the NEHRP uses a single site coefficient value for a given site class. The 95% upper bound and 5% lower bound curves shown in Figures 3.9-3.11 represent the variations that are likely for a given value of V_{S30}. The variables affecting F (in order of decreasing relative contribution) are V_{S30}, G/G_{max}-γ and D-γ, earthquake time history (return periods of 475 or 2475 years), and V_S below 30 m.

While the functional forms proposed for the site coefficient model (Equations 3.2 and 3.4) may not lend themselves well to code applications, they do provide a more accurate representation of the computed coefficients than do the NEHRP coefficients. If code developers prefer a single site coefficient value for a given seismic site class, the functional forms can be used to determine that value. For example, the largest median value within a site class could be used for design code applications.

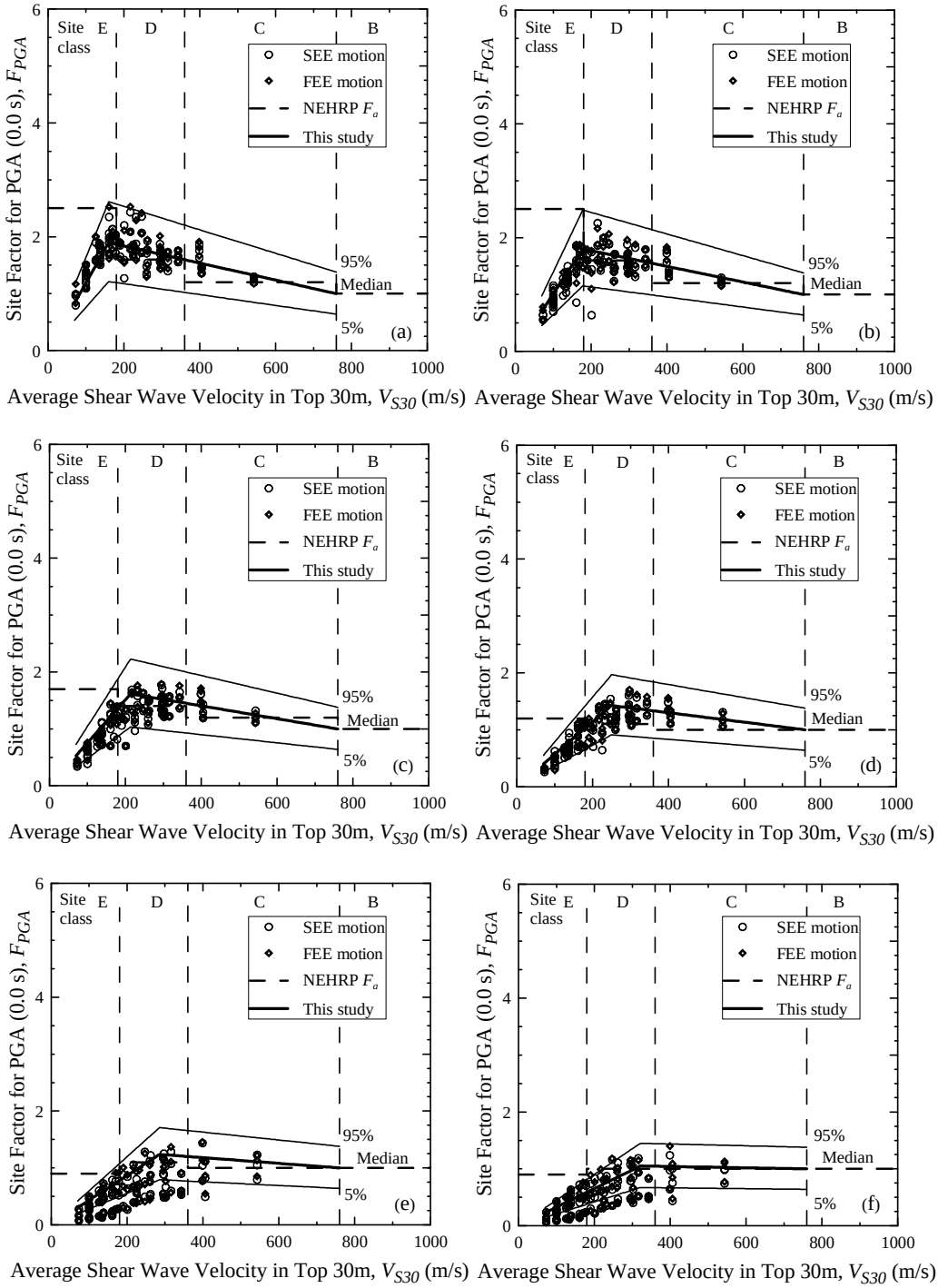

Figure 3.9 Site coefficients for 0.0 s spectral period (free-field) with *PGA* equal to (a) 0.05 g, (b) 0.1 g, (c) 0.2 g, (d) 0.3 g, (e) 0.4 g, and (f) 0.5 g.

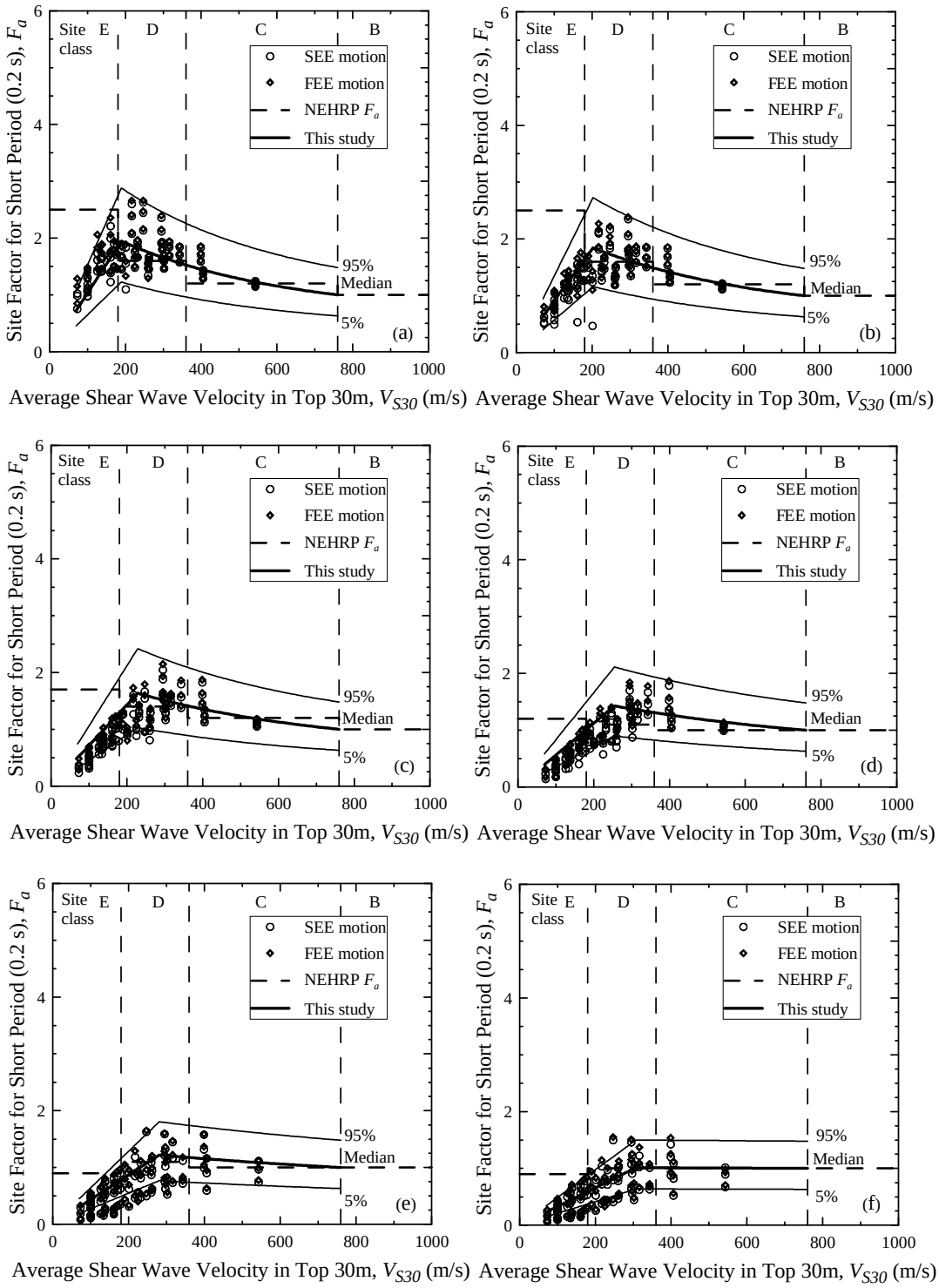

Figure 3.10 Site coefficients for 0.2 s (short) spectral period with S_s equal to (a) 0.125 g, (b) 0.25 g, (c) 0.50 g, (d) 0.75 g, (e) 1.0 g, and (f) 1.25 g.

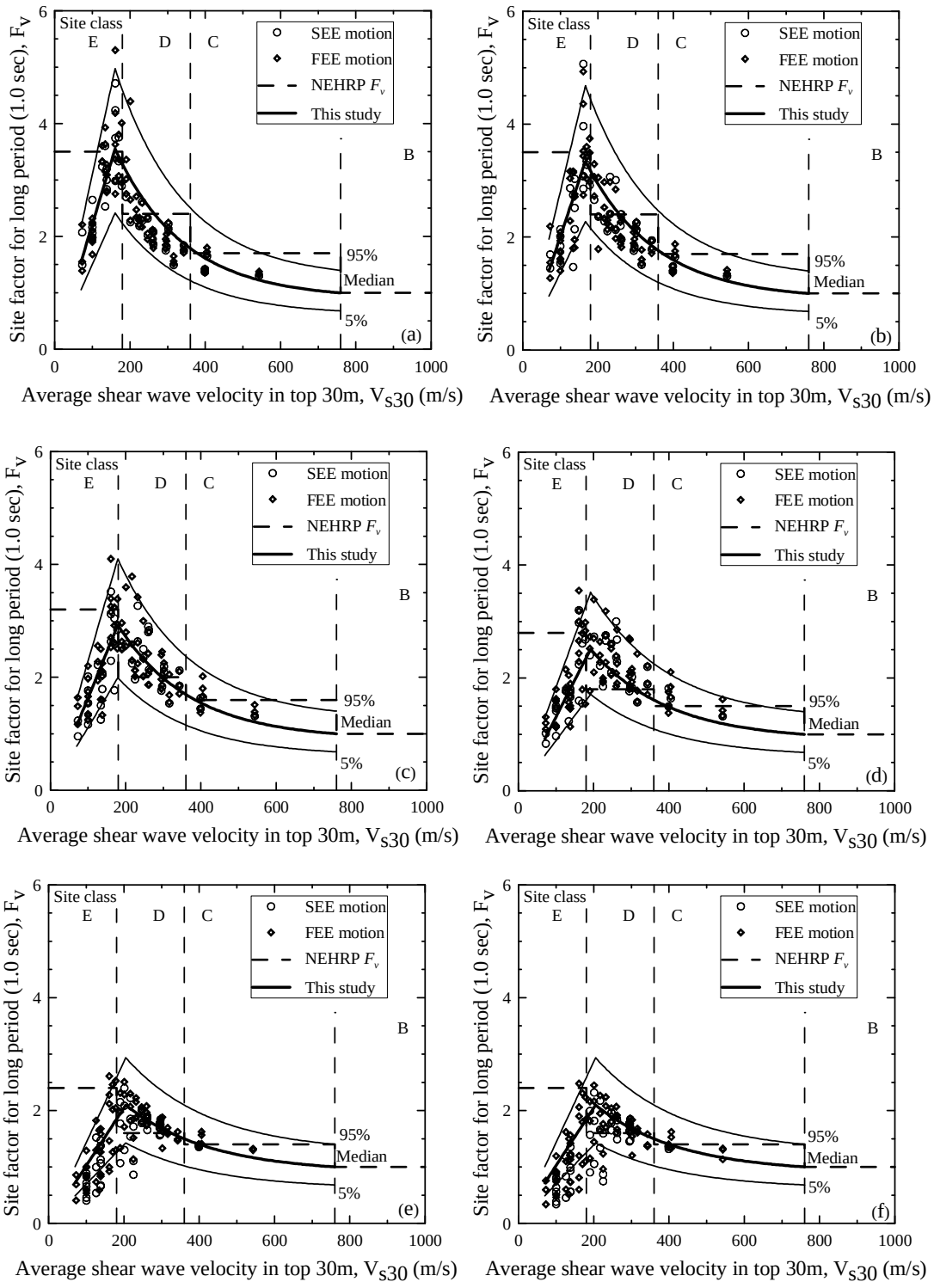

Figure 3.11 Site coefficients for 1.0 s (long) spectral period with S_1 equal to (a) 0.05 g, (b) 0.10 g, (c) 0.20 g, (d) 0.30 g, (e) 0.4 g, and (f) 0.50 g.

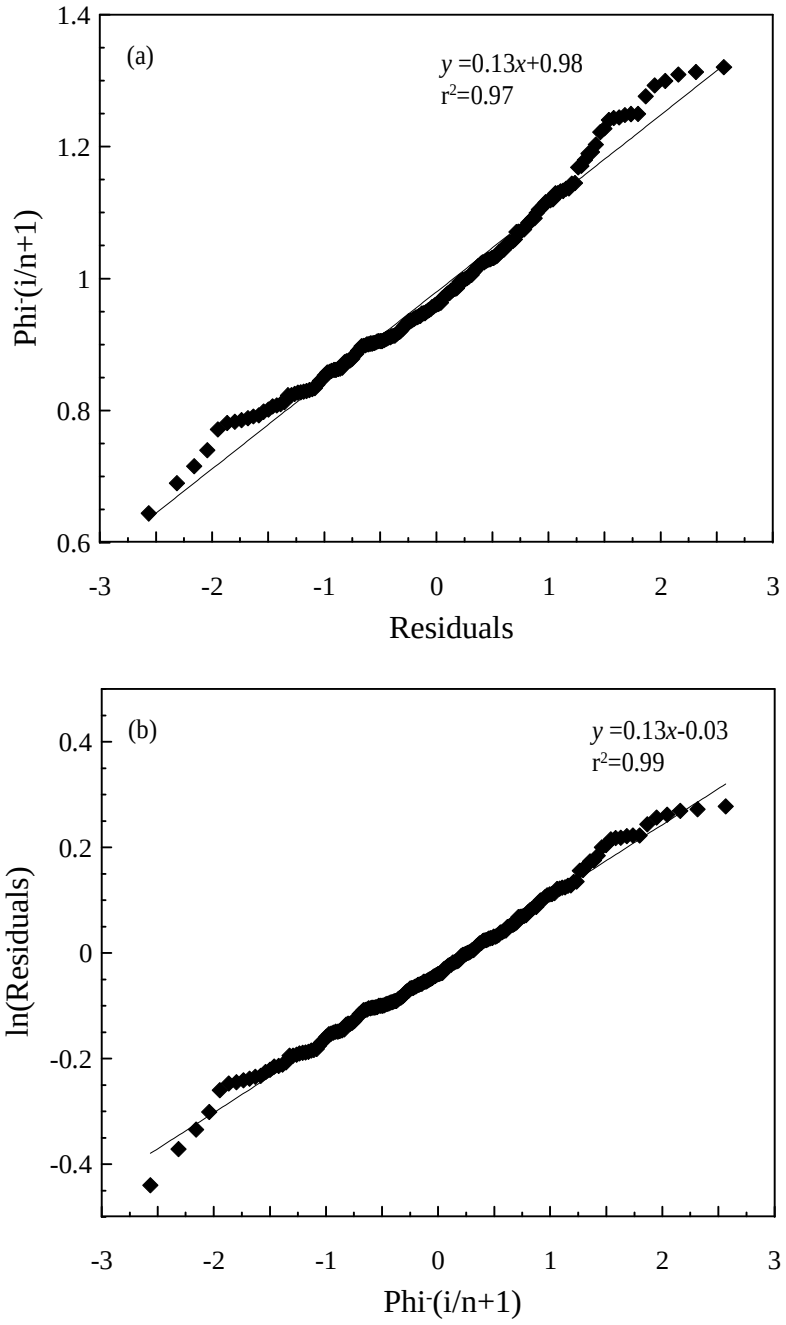

Figure 3.12 Probability plots assuming (a) normal and (b) lognormal distributions of the residuals.

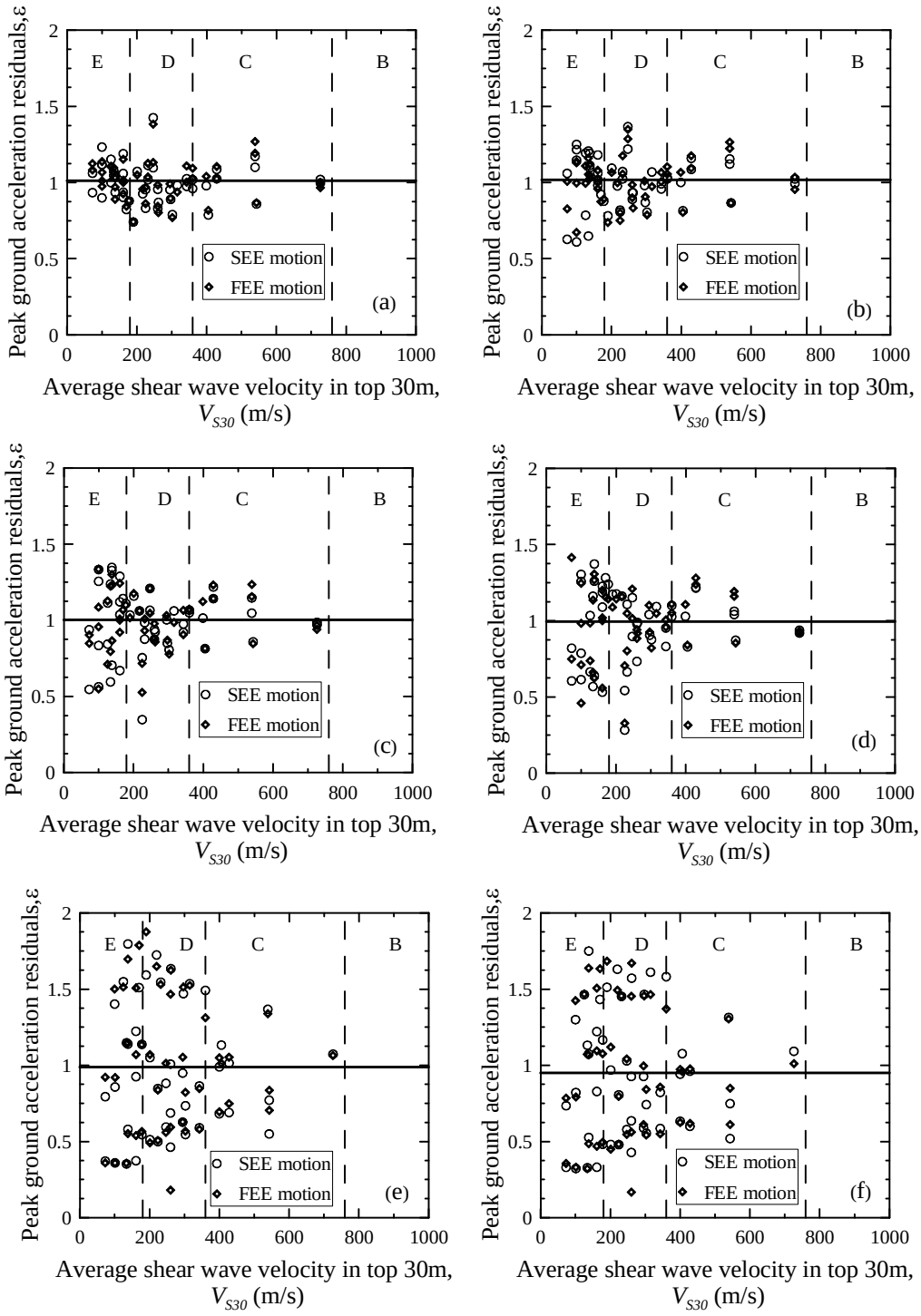

Figure 3.13 Sample residuals versus V_{S30} plot of F_{PGA} for $PGA_{outcrop}$ equal to (a) 0.05 g, (b) 0.1 g, (c) 0.2 g, (d) 0.3 g, (e) 0.4 g, and (f) 0.5 g.

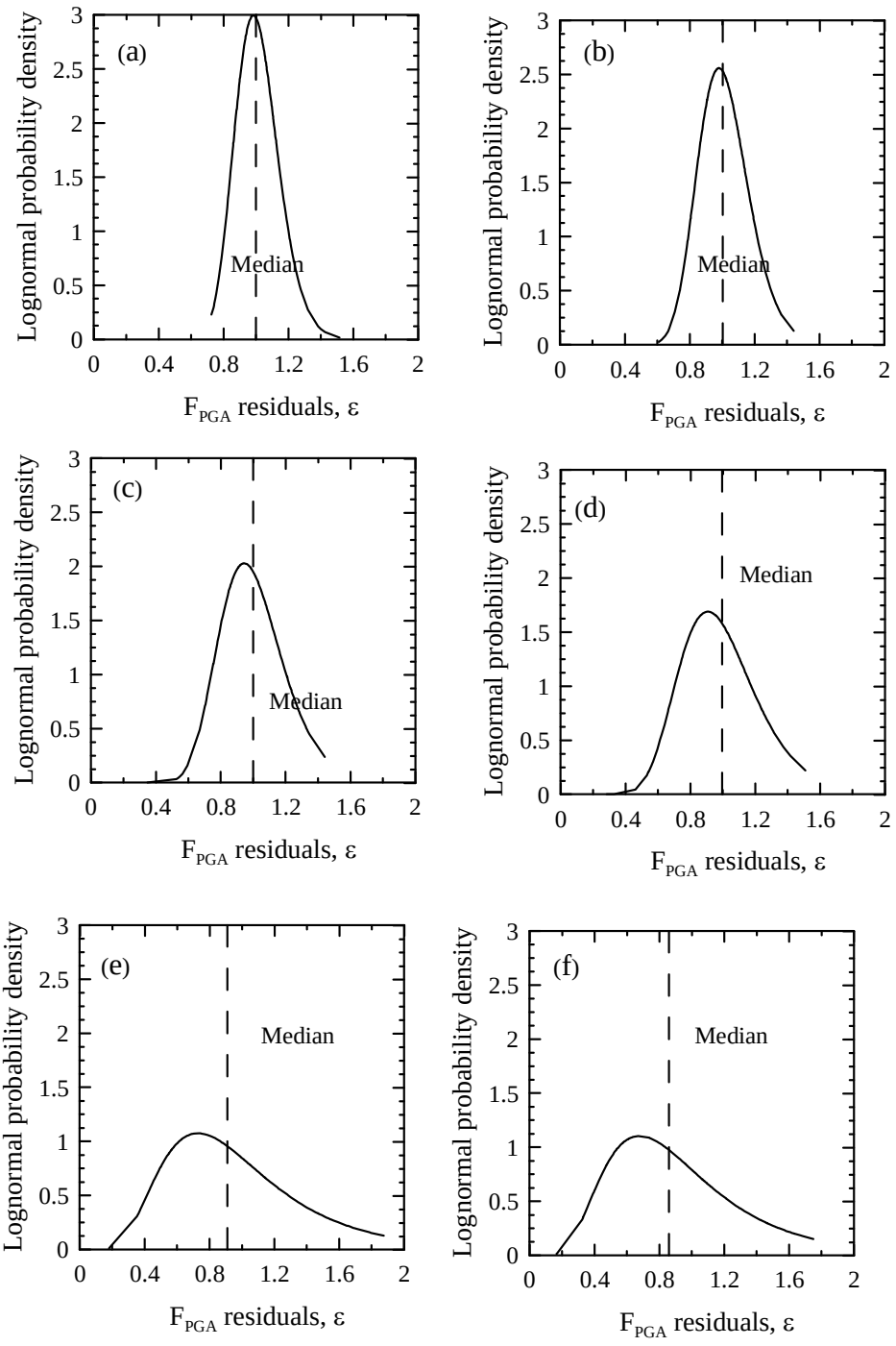

Figure 3.14 Sample lognormal probability density functions of F_{PGA} residuals for $PGA_{outcrop}$ equal to (a) 0.05 g, (b) 0.1 g, (c) 0.2 g, (d) 0.3 g, (e) 0.4 g, and (f) 0.5 g.

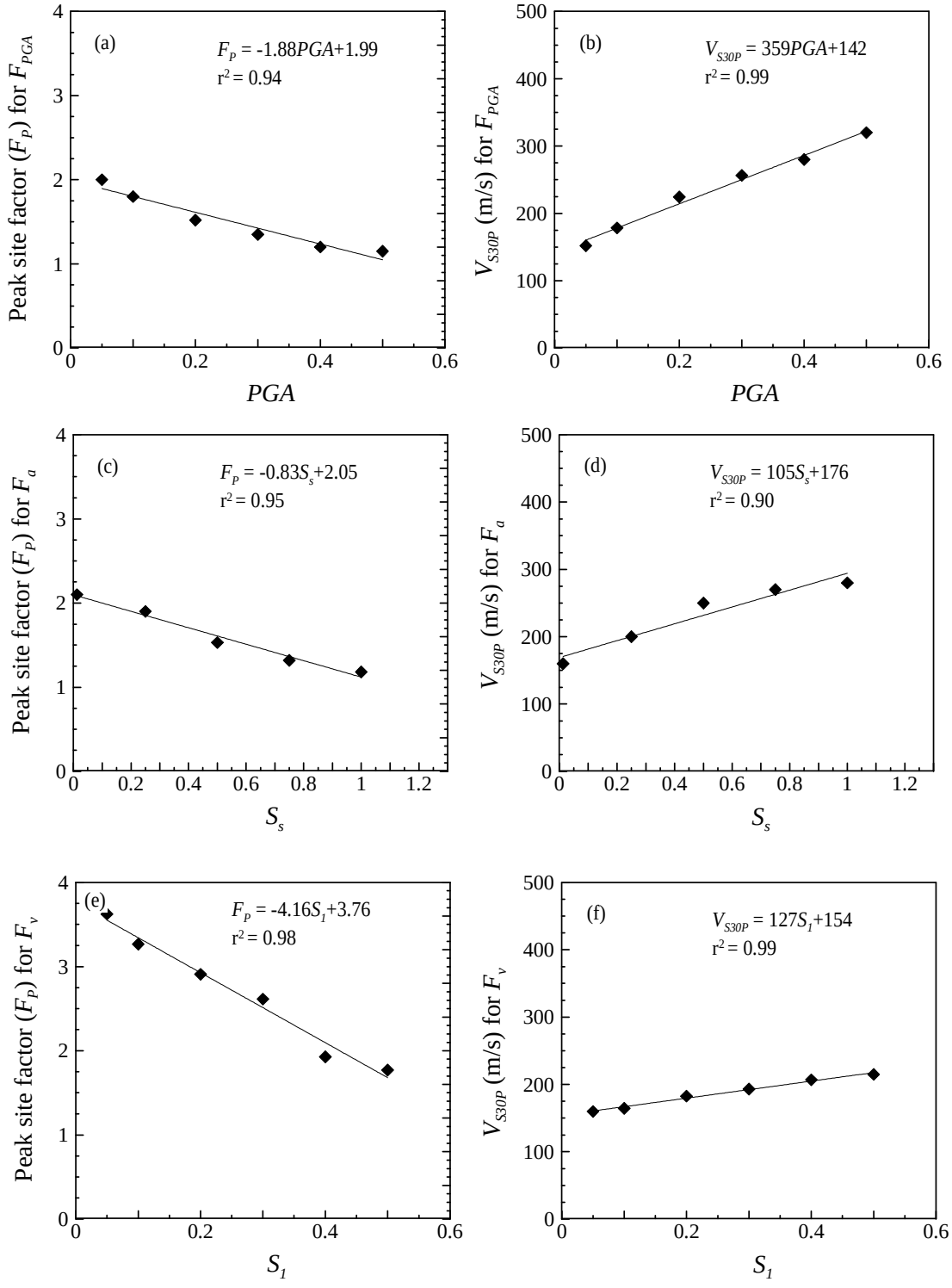

Figure 3.15 Sample F_P and V_{S30P} variation with $S_{outcrop,}$ for spectral periods of (a-b) 0.0 s, (c-d) 0.2 s, and (e-f) 1.0 s.

Application

The simplified procedure for constructing an acceleration design response spectrum (ADRS) outlined in AASHTO (2011), can be summarized in the following four steps: First, the NEHRP site class is determined. Second, $PGA_{B\text{-}C}$, S_s and S_1 are obtained from probabilistic seismic hazard maps. Third, the site class, $PGA_{B\text{-}C}$, S_s and S_1 are used to select F_{PGA}, F_a and F_v that account for the effect of local site conditions. Fourth, three points of the ADRS are obtained as follows

$$PGA = F_{PGA} * PGA_{B-C} \tag{3.7}$$

$$S_{DS} = F_a S_s \tag{3.8}$$

$$S_{D1} = F_v S_1 \tag{3.9}$$

where S_{DS} is the design short-period (0.2 s) spectral response acceleration at the ground surface; and S_{D1} is the design long-period (1.0 s) spectral response acceleration at the ground surface.

Illustrated in Figure 3.16 is the AASHTO (2011) procedure for constructing what is called the 3-point ADRS. The procedure implicitly assumes: (1) all significant peaks are expected to occur at T < 1.0 s or close to 1.0 s; (2) the plateau defined by S_{DS} provides a conservative bound for these peaks; and (3) spectral acceleration descends proportionally with 1/T, when $T > T_s$ ($T_s = S_{D1}/S_{DS}$). However, as presented below, we observed that (1) significant peaks may not always occur at shorter periods (T < 1.0 s), especially when V_{S30} < 200 m/s; and (2) the plateau cannot always be defined as S_{DS}, unless $T_s \leq 1.0$ s ($S_{D1} \leq S_{DS}$).

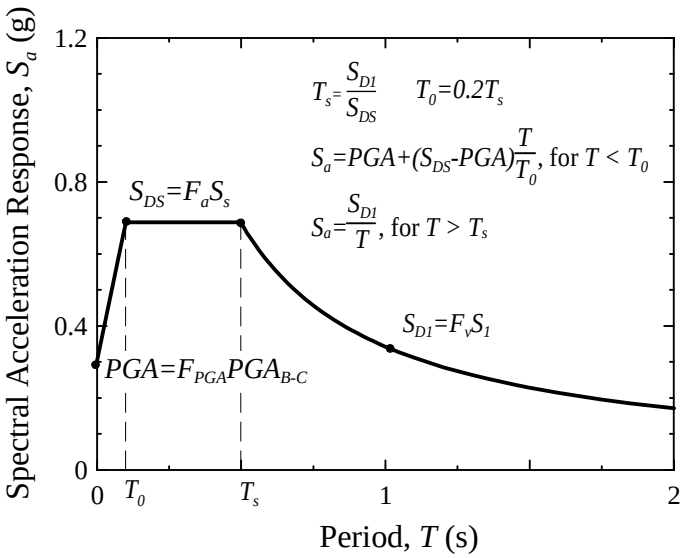

Figure 3.16 Construction of the 3-point acceleration design response spectrum based on AASHTO (2011).

Presented in Figures 3.17a-3.17d are sample response spectra for four profiles with V_s = 428, 295, 170 and 138 m/s, respectively, and PGA_{B-C} = 0.2 g. Plotted in each figure are the site-specific response spectrum and the soft-rock outcrop response spectrum. Also plotted are the 3-point ADRS curves constructed based on the AASHTO LRFD guideline, and median F_{PGA}, F_a and F_v values derived in this study. It can be seen that the AASHTO 3-point curves are unconservative when $0.2 \leq T \leq 0.5$ s for the profiles with V_s = 428 and 295 m/s; and excessively over conservative when $T < 1.0$ s for the profiles with V_s = 170 and 138 m/s. The 3-point ADRS curves based on coefficients derived in this study provide better approximations of the site-specific spectra, except for V_s = 138 m/s profile and $1.1 \leq T \leq 1.8$ s.

Because the 3-point ADRS method implicitly assumes that all significant peaks occur below T = 1.0 s, the 3-point ADRS curve based on site coefficients derived in this

study underpredicts the site-specific curve for V_{S30} = 138 m/s profile, when $1.1 \leq T \leq 1.8$ s (Figure 3.17d). Additional comparisons indicate that the 3-point ADRS method may be unconservative when $T > 1.0$ s and $V_{S30} < 200$ m/s and $PGA_{B\text{-}C} > 0.1$ g. This finding agrees with Power et al. (1998) who showed that the 3-point method can be unconservative in the Central and Eastern United States for spectral periods between 1.0 and 3.0 s. Therefore, a multi-point ADRS method is also shown in Figure 3.17d based on SCDOT (2008).

The multi-point ADRS for the V_{S30} = 138 m/s shown in Figure 3.17d is constructed by determining $S_{outcrop}$ for several spectral periods (i.e., 0.0, 0.08, 0.15, 0.2, 0.3, 0.5, 1.0, 2.0 and 3.0 s) and applying the most appropriate median F value (i.e., F_{PGA}, F_a, F_a, F_a, F_a, $F_{0.6}$, F_v, $F_{1.6}$, *and* $F_{3.0}$, respectively*).* Connecting the resulting points with straight line segments provides a reasonable fit to the site-specific spectrum, as shown in Figure 3.17d.

In practice, when $V_{S30} < 200$ m/s, it is recommended that both 3-point and multi-point ADRS curves be constructed. The values of $S_{outcrop}$ can be obtained from the uniform hazard spectrum using the USGS ground motion calculation program for 475 or 2475 year return periods (http://earthquake.usgs.gov/hazards/designmaps/javacalc.php; accessed August 20, 2011). If any point of the multi-point ADRS exceeds the 3-point ADRS, the multi-point ADRS (or a modified 3-point ADRS) should be used.

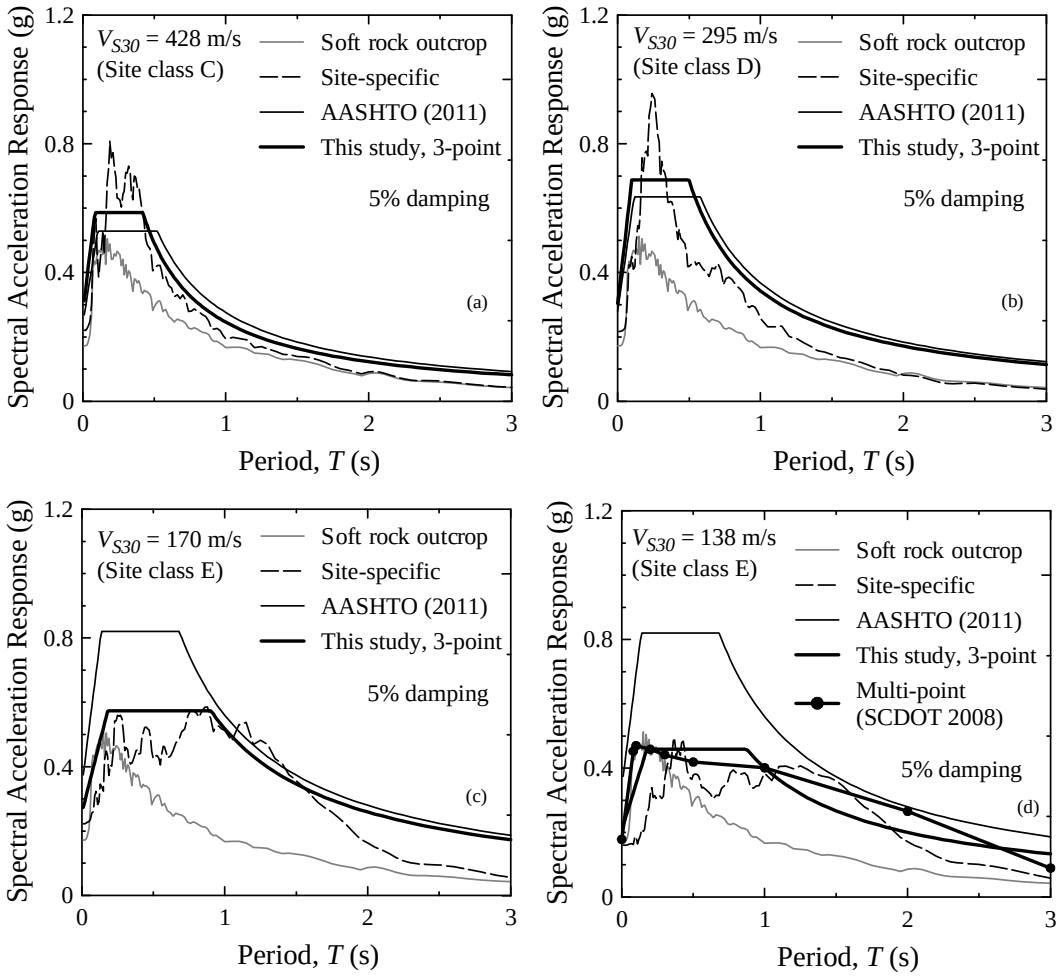

Figure 3.17 Sample acceleration response spectra for profiles with V_{S30} equal to (a) 428 m/s, (b) 295 m/s, (c) 170 m/s, and (d) 138 m/s.

Comparison of Results based on Two Rock Models

Computed surface spectral accelerations at T = 0.0, 0.2, 0.6, 1.0, 1.6, 3.0 s based on the geologic realistic and hard rock models are compared in Figure 3.18. The comparison is made such that each data point plotted in Figure 3.18 has the same V_S profile above 137 m for both models. The spectral accelerations based on the hard rock model are, on average, slightly greater than the spectral accelerations based on the geologic realistic

model for $T < 0.2$ s. For $T \geq 0.2$ s, the spectral accelerations based on the hard rock model are, on average, less than accelerations based on the geologic realistic model. The average difference in computed accelerations is most significant for $T = 3.0$ s.

Thus, the overall effect of the deeper soil stacks in the hard rock model, not captured by Scenario_PC and the assumed material properties, is to filter the low frequency amplitudes and slightly amplify the high frequency amplitudes. This observation is in good agreement with a ground response study of Columbia, South Carolina by Lester and Chapman (2005). Given that the average spectral surface accelerations for the soft and hard rock models are generally within 20% and also given that the material property information below 137 m is severely limited, the results presented in Figure 3.18 justify the use of the geologic realistic model for this study.

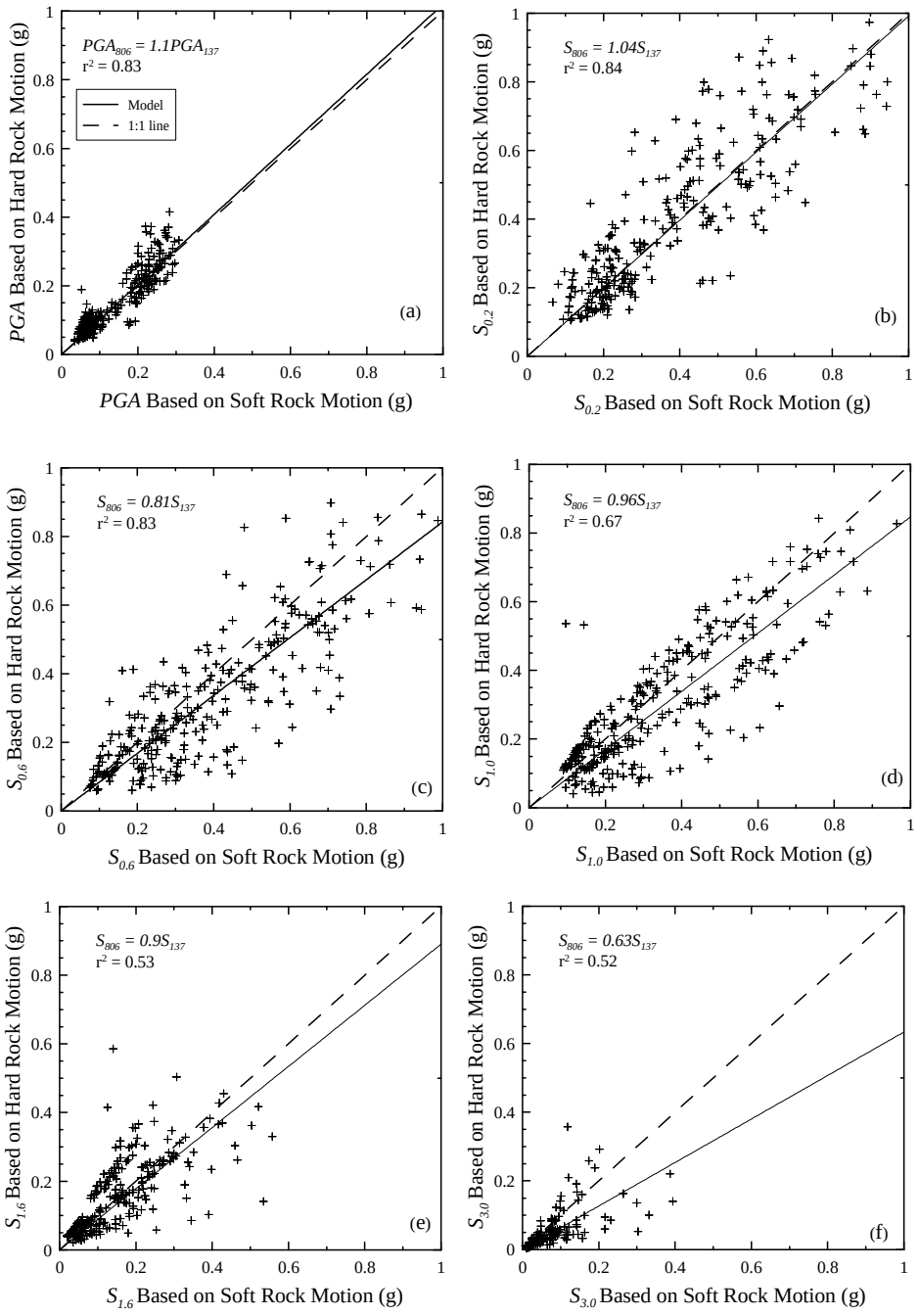

Figure 3.18 Comparison of surface accelerations obtained using hard-rock motions with V_s=3,500 m/s half-space located at 806 m and soft-rock motions with V_s=700 m/s half-space located at 137 m for (a) 0.0 s, (b) 0.2 s, (c), 0.6 s, (d) 1.0 s, (e) 1.6 s, and (f) 3.0 s spectral periods.

Limitations

There are some limitations concerning the results of this Chapter that should be noted. Although the V_s profiles shown in Figure 3.2 represent a realistic range, they are generated assuming a constant multiple of the standard deviation and ignoring any correlations between layers. The full correlation assumption is not as realistic as data driven correlated models (Toro 1995). However, accurate correlated model results require (a) information about the correlation between layers, (b) accurate upper and lower bound values, and (c) a large number of generated profiles. Even if reasonable assumptions on (a) and (b) are made, computational time is great to take care of (c), especially with the non-linear code. Graizer (2011) concluded that the Toro-type V_s generation may lead to unreasonable results, if random generations are not handled with the up-most care. Further study is needed to implement realistic random V_s generation models in the region.

Similar to the NEHRP F_a and F_v values, the site coefficients calculated in this study are amplitude dependent and return period independent. The intrinsic discrepancy between the probabilistic nature of rock accelerations and the deterministic nature of the NEHRP F_a and F_v values is not dealt in this Chapter. However, Hashash et al. (2008) and Park et al. (2012) have shown that this discrepancy may be of important significance in future studies and recommendations.

The effect of depth to V_s = 700 m/s material is not considered in this Chapter. Studies have shown that the depth to soft rock (or depth to hard rock) can produce significant variability in ground response results that is dependent on spectral period (Silva et al. 2000, Hashash et al. 2008). This effect is quantified in Chapter 4 and 5.

Finally, the results of this Chapter are most appropriate for the Charleston area, where the area is relatively flat to support the application of 1-D ground response analysis. The assumptions made do not take into account the actual topography of the bed rock and earthquake directivity effects. The results may be appropriate for other areas, but additional ground response analysis is needed to verify this conclusion.

3.5 Conclusions

Seismic site coefficients at average spectral periods of 0.0, 0.2, 0.6, 1.0, 1.6 and 3.0 s were calculated for conditions typical of Charleston based on over 12,000 ground response simulations. The site coefficients were grouped by spectral acceleration and plotted versus V_{S30}. From the plotted V_{S30}-site coefficient data pairs, median, 95% upper bound and 5% lower bound relationships were developed. Each relationship exhibited a peak value somewhere between V_{S30} of 80 and 320 m/s, depending on spectral acceleration and period. The relationships were expressed by a linear model for $V_{S30} < V_{S30P}$ and a linear or exponential model for $V_{S30} \geq V_{S30P}$. The amount of uncertainty that can be expected with estimating site coefficients using V_{S30} was represented by 95% upper bound and 5% lower bound relationships.

The computed relationships for periods of 0.0, 0.2 and 1.0 s were compared with the NEHRP F_a and F_v values. It was shown that the computed median F_{PGA} values compare well with the NEHRP F_a values. The computed median F_a values plot slightly above the NEHRP F_a values for V_{S30} > 180 m/s. The computed median F_v values plot above the NEHRP F_v values by as much as about 1.5 times for 180 ≤ V_{S30} ≤ 300 m/s. For V_{S30} < 180 m/s, the NEHRP F_a and F_v are shown to be conservative. The NEHRP F_v is also shown to be adequate for V_{S30} ≥ 360 m/s.

The computed F_{PGA}, F_a and F_v median relationships were recommended for Charleston because they are based on regional conditions and are continuous with V_{S30}. Because the relationships are continuous with V_{S30}, the NEHRP site classes (A, B, C, D and E) may not be needed.

The 3-point procedure for constructing ADRS curves was shown to be generally adequate when V_{S30} > 200 m/s. However, when V_{S30} ≤ 200 m/s, significant peaks may occur at T > 1.0 s. For this reason, it was suggested that the multi-point ADRS curve be plotted with the 3-point curve, to check if long-period accelerations are under predicted. Models to calculate site coefficients at long periods (T = 1.6 and 3.0 s) were provided to check predicted surface accelerations at long periods. The objective of the multi-point ADRS is not to replace the building code philosophy, but to present an option for the designer to make sure that longer period accelerations are not under-predicted by the 3-point ADRS design curve.

CHAPTER FOUR

SEISMIC SITE COEFFICIENT MODEL FOR DESIGN BASED ON CONDITIONS IN THE SOUTH CAROLINA COASTAL PLAIN[2]

4.1 Geology and Seismology

Presented in Figure 4.1 is the geologic map of South Carolina published by the South Carolina Department of Natural Resources (SCDNR 2005). Highlighted on the map are the Fall Line, the Brevard Fault, and the sites selected for ground response analysis. The Piedmont physiographic province lies to the west of the Fall Line and extends to the Brevard Fault. Outcrops of residual soil and highly weathered crystalline rock are common in the Piedmont. The Coastal Plain physiographic province lies to the east of the Fall Line, where relatively undeformed sediments of mainly Quaternary, Tertiary and Cretaceous ages lie on top of Mesozoic/Paleozoic folded, faulted and recrystallized basement rocks (Wheeler and Cramer 2000; Odum et al. 2003). Common depositional processes in the Coastal Plain are through marine and fluvial actions during periods of retreating ocean shoreline caused by crustal uplift and sea level fluctuations. The basement rock includes granite, schist, and gneiss (Weems and Lewis 2002).

[2] A similar version of this chapter is to be submitted for possible publication in the *Bulletin of Seismological Society of America*. Aboye, S.A., Andrus, R.D., Ravichandran, N., Bhuiyan, A.H., Martin, J.R. II, and Harman, N., "New Seismic Site Coefficient Model Based on Conditions in the South Carolina Coastal Plain.''

Based on geology and available V_S profile information, the SCCP is divided into the following four general areas: (1) Charleston-Savannah, (2) Myrtle Beach, (3) Columbia-Florence-Lake Marion, and (4) Aiken. These four general areas are similar to areas assumed by Silva et al. (2003). The Charleston-Savannah area is located within the lower part of the SCCP as displayed in Figure 4.1. Quaternary geology of the lower SCCP consists of beach/barrier ridges representing former stands of sea level, as well as fluvial and backbarrier deposits. Barrier deposits typically consist of sandy material. Backbarrier deposits typically consist of clayey material. Underlying Cretaceous and Tertiary sediments consist of marine deposits of marl, cemented sand and limestone, which were typically incised to varying degrees by stream activity prior to the deposition of Quaternary sediments.

The Myrtle Beach area also lies in the lower part of the SCCP. Near-surface sediments in the Myrtle Beach area, however, are often older and stiffer than near-surface sediments in the Charleston-Savannah area at the same depths. Theses sediments are late Cenozoic marine and fluvial deposits consisting of fine gravel, poorly sorted, stratified and coarse sand, and interbedded silts and clays (DuBar 1987, Owens 1989). Along the Little Pee Dee River valley, Holocene floodplain and Pleistocene fluvial deposits are found. Underlying Cretaceous and Tertiary strata consisting of marl, cemented sands, calcitic sandstone, and sandy limestone gently dip both to the south and to the north forming what is called the Cape Fear Arch (DuBar 1987, Owens 1989; Mosses 2002). The Cape Fear arch is a main structural feature in the SCCP, which has a northwest-

southeast trending axis between the mouth of the Cape Fear River and the North Carolina–South Carolina state line (Weems and Lewis 2002).

The Columbia-Florence-Lake Marion area is located in the middle and upper parts of the SCCP. One of Columbia's most prominent geologic features is the Fall Line. Extending east of Columbia and the Fall Line, near-surface weathered crystalline rock gently dips to the southeast beneath the overlying Pleistocene, Pliocene and upper Cretaceous sediments. These sediments were deposited in a non-marine fluvial environment and consist of sand to silty sand with interbeds of floodplain clay and channel fill sand (Maybin and Nystrom 1995; Odum et al. 2003).

The Aiken area is located in the upper part of the SCCP. Prowell (1996) indicated that Paleocene, Eocene and Miocene Tertiary sediments form the majority of surface exposures in the area. These sediments typically reflect marine and fluvial paleo-environments dominated by delta sedimentation. Paleocene deposits consist of clayey and silty quartz sand, kaolinitic clay and silt. Eocene deposits consist of silty micaceous sand, silt, silty sand and clay. Miocene deposits are dominated by sand resulting from uplift and erosion of the Piedmont province. Also present along the Savannah River valley is a mass of compact and lithified alluvial deposits derived from erosion of the local landmass. These deposits consist of fine to very coarse quartz sand in a sparse clay matrix (Prowell 1996).

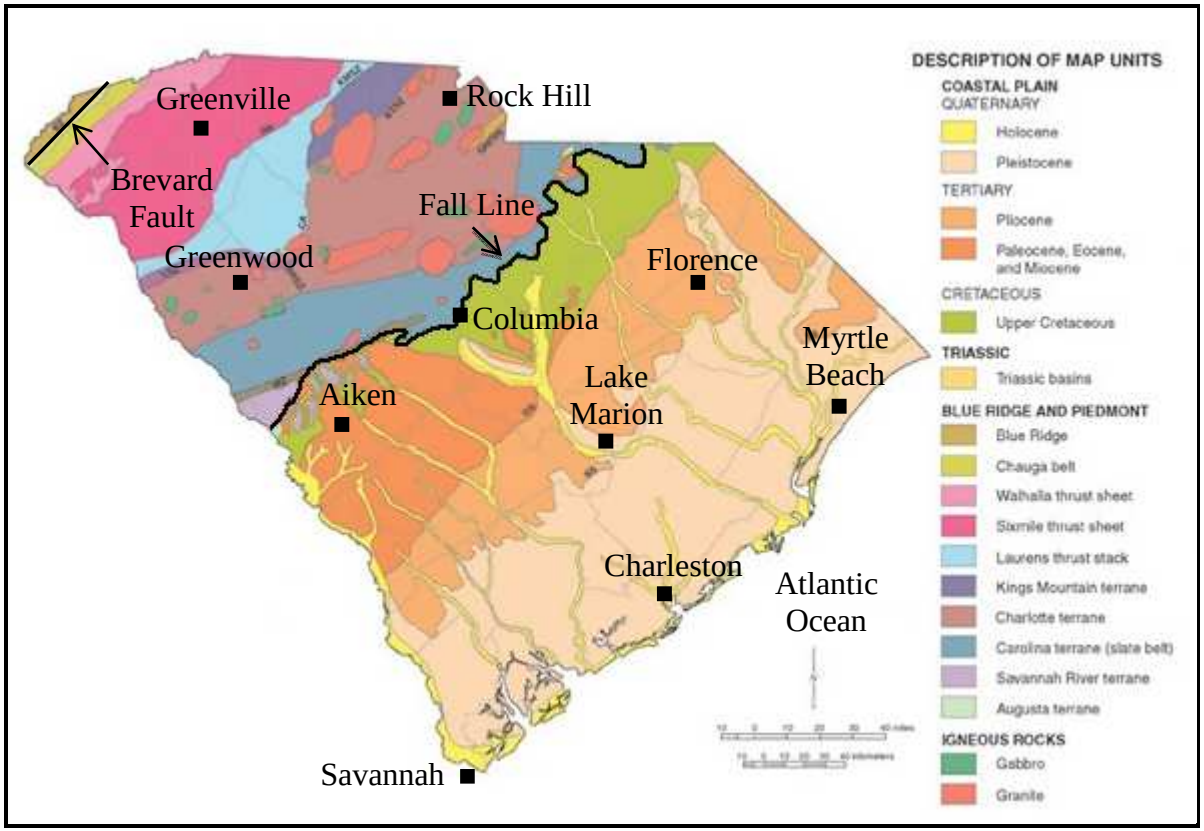

Figure 4.1 Geologic map of South Carolina (SCDNR 2005) showing the Fall Line and sites considered in ground response analysis.

Presented in Figure 4.2 is an isopach map of the Coastal Plain sediment thickness by Chapman and Talwani (2002). As illustrated in Figure 4.2, the thicknesses of sediments is 600-1,200 m in the Charleston-Savannah area; 300-600 m in the Myrtle Beach area; and 0-700 m in the Columbia-Florence-Lake Marion area; and 0-700 m in the Aiken area. These sediment thicknesses roughly correspond to the depths to weathered basement rock.

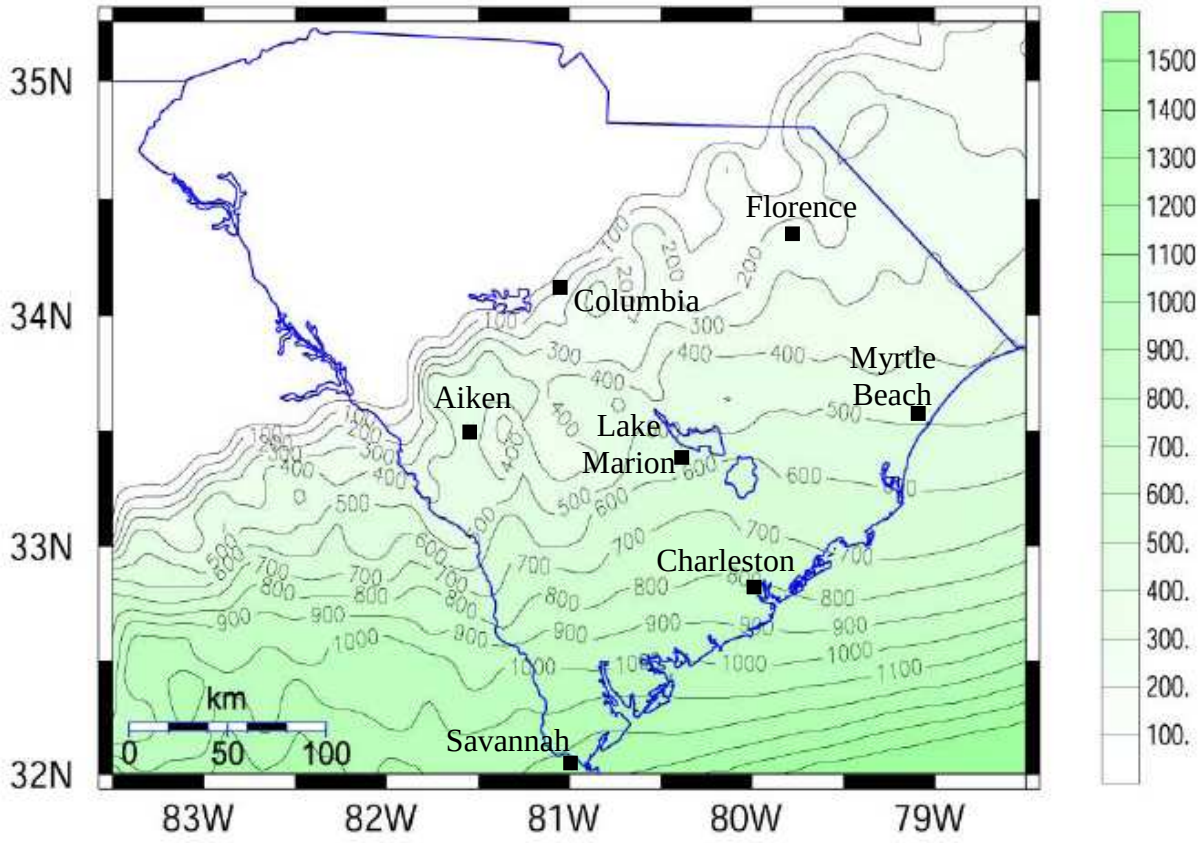

Figure 4.2 Isopach map of the Coastal Plain sediment thickness, in meters (Chapman and Talwani 2002).

Seismicity of the SCCP is dominated by the Charleston Seismic Hazard Zone located about 30 km northwest of downtown Charleston. Several major (liquefaction-inducing) earthquakes have occurred during the past 6000 years in the SCCP (Talwani and Schaeffer 2001). Among these earthquakes is the August 31, 1886 Charleston earthquake with an estimated moment magnitude (M_w) of 6.9 ± 0.3 (Bollinger 1986, Bakun and Hopper 2004, Talwani and Gassman 2008, Heidari and Andrus 2010, Cramer and Boyd 2011) to 7.3 ± 0.3 (Martin and Clough 1994, Johnston 1996). Damage in 1886 included severe lateral and vertical displacement of more than 80 km length of railroad track as well as numerous sand blows, ground fissuring, and building failures (Dutton 1889). The maximum damage intensity of the 1886 Charleston earthquake is estimated to be X on the Modified Mercalli Intensity Scale. The epicenter is roughly located at the Middleton Place. It is estimated that earthquakes of the size of the 1886 event occur, on average, every 500 years in the SCCP (Talwani and Schaffer 2001).

4.2 Dynamic Soil/Rock Model

Four reference V_s profiles and 108 other V_s profiles are used in this chapter to represent the variations in small-strain soil/rock stiffnesses in the SCCP. Presented in Figures 4.3a-d are the V_S profiles assumed for the Charleston-Savannah, Myrtle Beach, Columbia-Florence-Lake Marion and Aiken areas, respectively. The dynamic soil\rock model (including the V_S profiles) described in Chapter 3 is used for Charleston-Savannah.

For Myrtle Beach, the reference V_s profile shown in Figure 4.3b is based on averages of profiles presented in Silva et al. (2003) and Odum et al. (2003). Values of V_s in the reference profile shown in Figure 4.3b vary from 200 to 300 m/s in the top 10 m; and from 300 and 650 m/s between the depths of 10 and 150 m. A soft-rock half space with V_s of 700 m/s is assumed below the depth of 150 m.

For Columbia-Florence-Lake Marion, the reference V_s profile shown in Figure 4.3c is derived from information presented in Silva et al. (2003), Odum et al. (2003), Chapman and Lester (2005) and Andrus et al. (2006). Values of V_s in this reference profile vary between 200 and 400 m/s in the top 30 m; and from 400 to 700 m/s between the depths of 30 m and 137 m. Additional profiles shown in appendix H (Figures H1-H7) are considered to account for the likely possibility of shallower soft rock (i.e., V_s = 700 m/s) in the middle and upper parts of the SCCP. The profiles shown in Figures H1-H7 are generated by varying the depth to the V_s = 700 m/s half space shown in Figure 4.3c (i.e., depth to half space = 0.5, 1.5, 5, 10, 20, 30, 50, 100 and 137 m) and using the ground motions generated for the Columbia area.

For Aiken, the reference V_s profile shown in Figure 4.3d is the average profile presented in Silva et al. (2003) based on measurements made at the Savannah River Site. Values of V_s in this reference profile vary between 350 and 400 m/s above the depth of 50 m; and increase from 400 to 600 m/s between the depths of 50 and 145 m. The top of the soft-rock half space with V_s of 700 m/s is assumed at the depth of 145 m for Aiken.

The other V_s profiles shown in Figures 4.3a-d are derived from the reference profiles assuming estimates of standard deviation (σ) based on the study by Andrus et al. (2006). Respective histograms of V_{S30} for the V_s profiles shown in Figures 4.3a-d are presented in Figures 4.4a-d. The lognormal mean V_{S30} values for the profiles in Figures 4.3a-d are 208, 220, 270, and 260 m/s, respectively.

Predictive relationships of G/G_{max}-γ and D-γ derived by Zhang et al. (2005) for Quaternary and Tertiary and older sediments are used to describe the nonlinear behavior of each layer in the profiles. The Zhang et al. (2005) G/G_{max}-γ relationships are defined as function of mean effective stress (σ'_m) and plasticity index (PI). The D-γ relationships are defined as function of G/G_{max}, σ_m' and PI. For the σ_m' calculation, the coefficients of at-rest earth pressure is assumed to be 0.5 and 1.0 for Quaternary and Tertiary sediments, respectively. Also, for the σ_m' calculation, it is assumed that the groundwater table depth is 1.5 m. Presented in Figure 4.5 are sample mean G/G_{max}-γ and D-γ relationships assumed for the Quaternary and Tertiary layers. The uncertainty associated with the relationships is considered by ± 1σ G/G_{max}-γ and D-γ relationships (Zhang et al. 2008).

For the soft-rock half spaces in Figures 4.3a-d, purely linear relationships of G/G_{max}-γ and D-γ are assumed. This is done by entering G/G_{max} = 1 and D = 0.5% for all γ values. A damping ratio of 0.5% was assumed for soft rock in the ground motion modeling study by Chapman (2006).

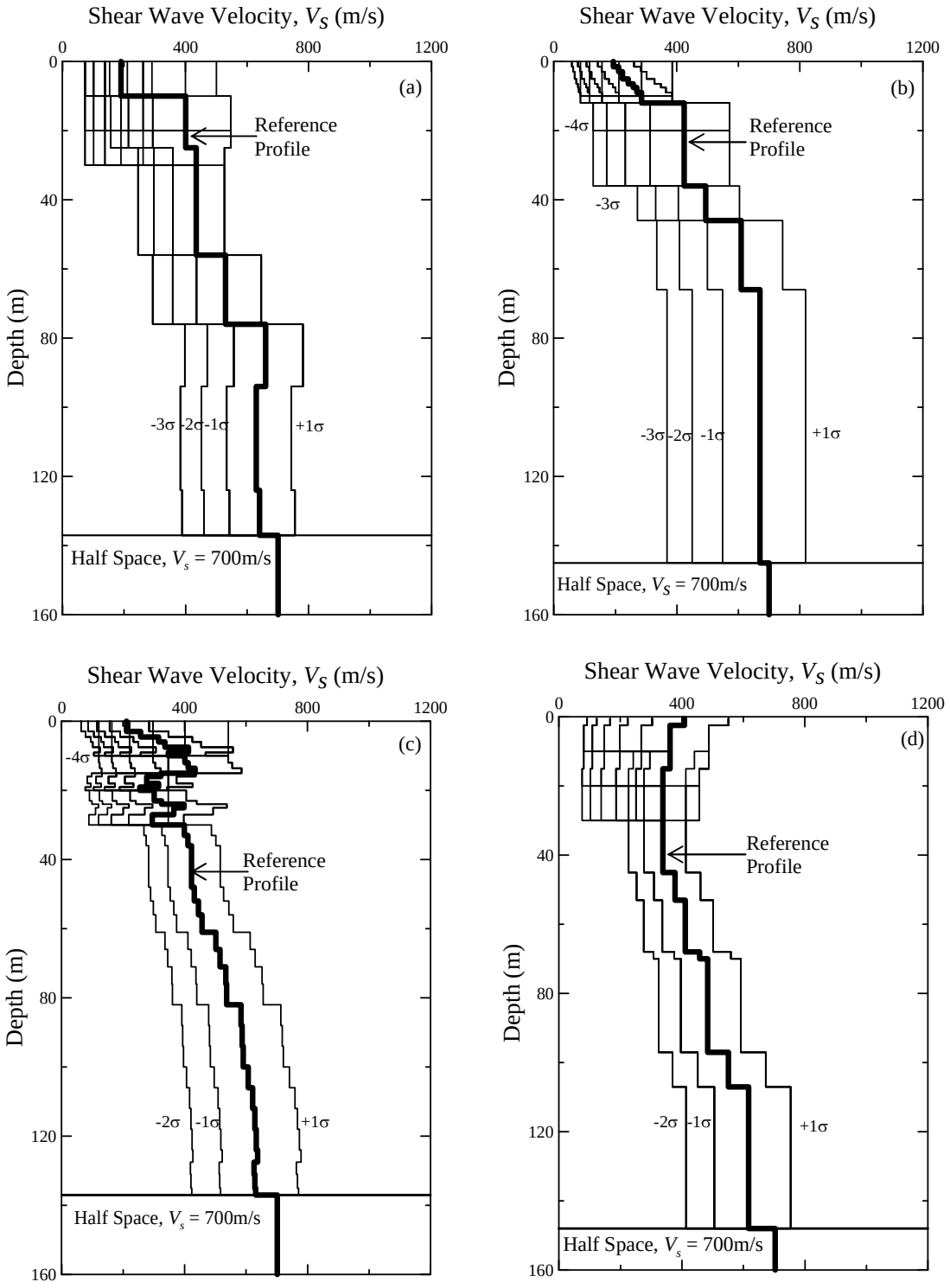

Figure 4.3 Shear wave velocity profiles considered for (a) Charleston-Savannah, (b) Myrtle Beach, (c) Columbia-Florence-Lake Marion, and (d) Aiken.

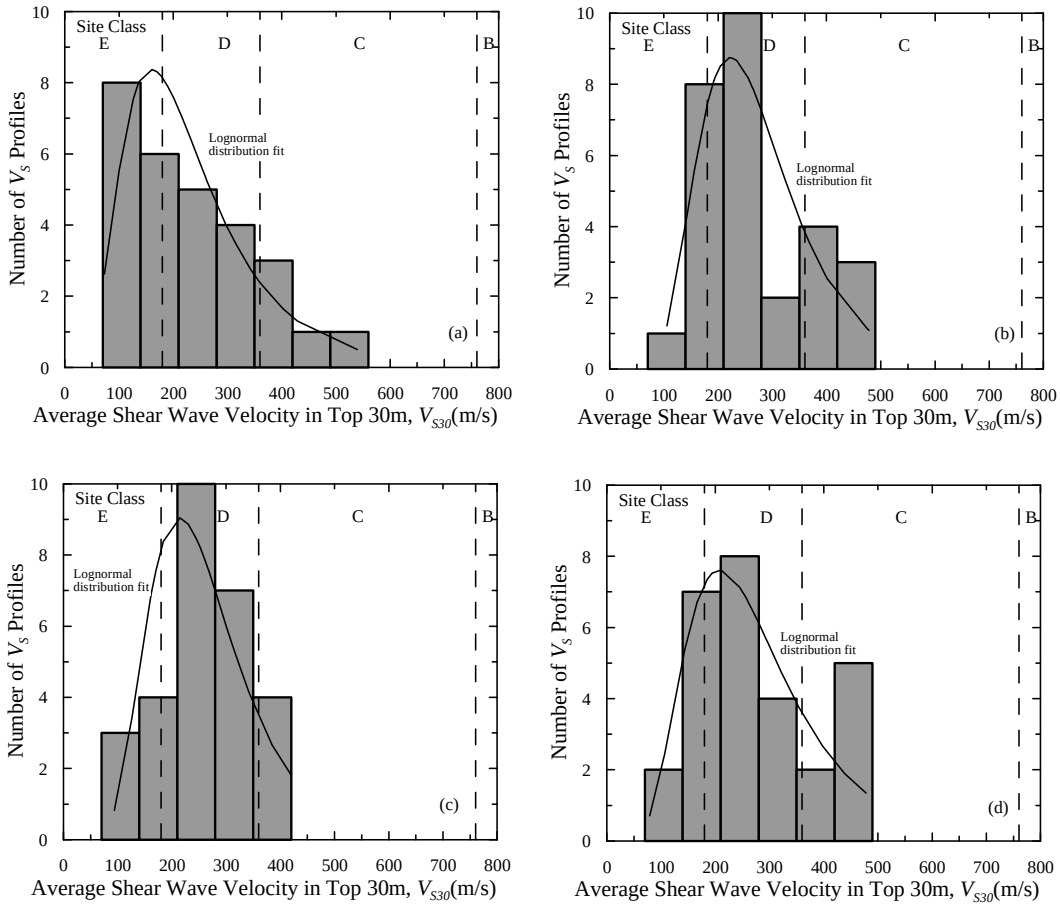

Figure 4.4 Histograms of V_{S30} for profiles assumed for (a) Charleston-Savannah, (b) Myrtle Beach, (c) Columbia-Florence-Lake Marion, and (d) Aiken.

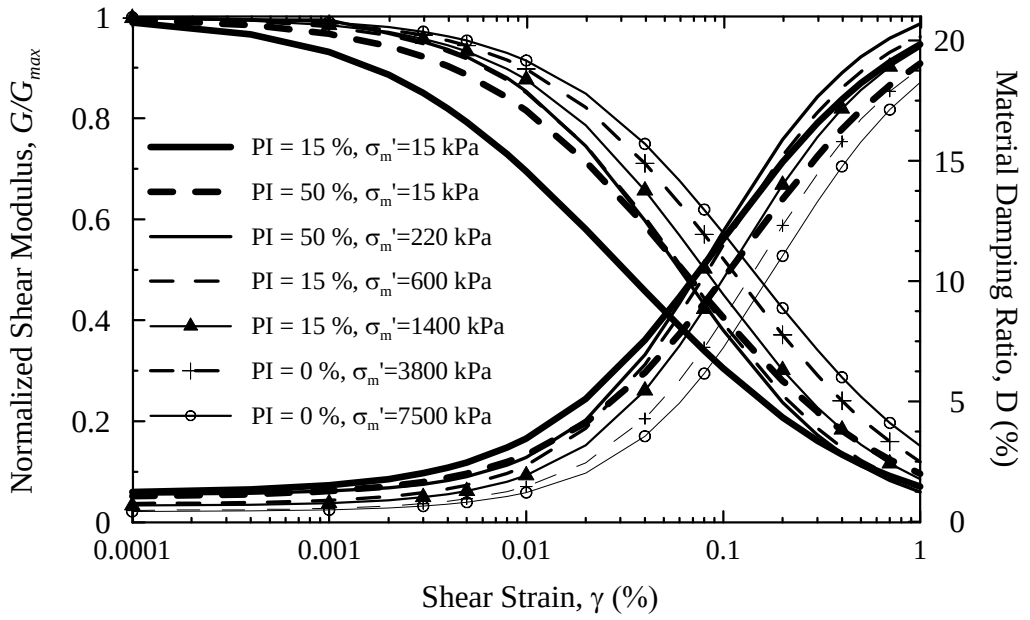

Figure 4.5 Sample mean G/G_{max}-γ and D-γ relationships used in ground response analyses.

4.3 Input Ground Motions

The deaggregated seismic hazard parameters at six oscillator frequencies (i.e., 0 Hz or free-field, 1, 2, 3.33, 5 and 10 Hz) are computed using the USGS deaggregation website (http://eqint.cr.usgs.gov/deaggint/2002/) for the centers of 12, 4, 4, 5, 4, 4 and 15, Quadrangles (1:24,000 scale) in the Charleston, Savannah, Myrtle Beach, Columbia, Florence, Lake Marion and Aiken, respectively. The return periods considered are 475 and 2,475 years (or 10% and 2% probabilities of exceedance in 50 years, respectively). The former return period is sometimes referred to as the Functional Evaluation Earthquake (FEE); and the latter return period is sometimes referred to as the Safety Evaluation Earthquake (SEE).

For all six spectral frequencies and both return periods, the modal moment M_w of 7.3 and the modal site-to-source distance for a given site are found to be practically the same, because the seismic hazard in the SCCP is dominated by the 1886 Charleston earthquake source zone (Chapman 2006). Thus, the generation of input motions matching the entire target uniform hazard spectrum is justified, and one earthquake time history representing the predominant scenario is adequate for the six spectral frequencies.

The rock model selected in Scenario_PC for the SCCP is the geologic realistic condition, which consists of an outcropping soft-rock (V_s = 700 m/s) layer over a weathered hard rock. The thickness of the soft-rock layer at any one location for the geologic realistic model is equal to the thickness of Tertiary and Cretaceous sediments (e.g., 600-1,200 m in the Charleston-Savannah area). The main advantages of selecting the geologic realistic condition are the input V_s profiles need only to extend to the top of V_s = 700 m/s material, and the computed site coefficients can be directly applied to the USGS soft-rock accelerations to estimate local accelerations.

Ninety-four synthetic input motions are used in the ground response analyses in this study. Presented in Figure 4.6 are sample FEE and SEE input motions generated for the center of the Charleston, Myrtle Beach, Columbia, and Aiken quadrangles. Values of $PGA_{outcrop}$ for the sample motions in Figure 4.6 range from 0.05 to 0.14 g for the FEE condition, and from 0.19 to 0.51 g for the SEE condition.

Presented in Figure 4.7 are Fourier amplitude plots of the motions in Figure 4.6a and 4.6b. The general frequency (or period) content of these motions can be represented in terms of the mean predominant period (T_m) defined by (Rathje et al. 1999, Stewart et al. 2001):

$$T_m = \frac{\sum_{i=1}^{n}\left(C_i^2 / f_i\right)}{\sum_{i=1}^{n} C_i^2} \tag{4.1}$$

where, f_i is the i^{th} discrete Fourier frequency between 0.25 and 20 Hz, C_i is the corresponding Fourier amplitude, and n is the number of frequency points between 0.25 and 20 Hz. The computed values of T_m are 0.24-0.43 s for the 47 FEE motions considered; and 0.23-0.37 s for the 47 SEE motions.

Because T_m characterizes the frequency content of the input time histories, it is dependent upon the site-to-source distance (R) and the depth to the top of hard rock (H_{HR}). Plotted in Figure 4.8 are values of T_m versus H_{HR} and R for the 94 soft-rock motions generated by Scenario_PC and used in this study. Values of T_m are computed from the motions using Equation 4.1; values of R are obtained from the USGS deaggregated seismic hazard output; and values of H_{HR} are provided by Scenario_PC, which are based on the isopach map by Chapman and Talwani (2002). It can be seen from Figure 4.8 that T_m increases with increasing R and H_{HR}, due to attenuation of high frequency amplitudes with increasing distance from the source.

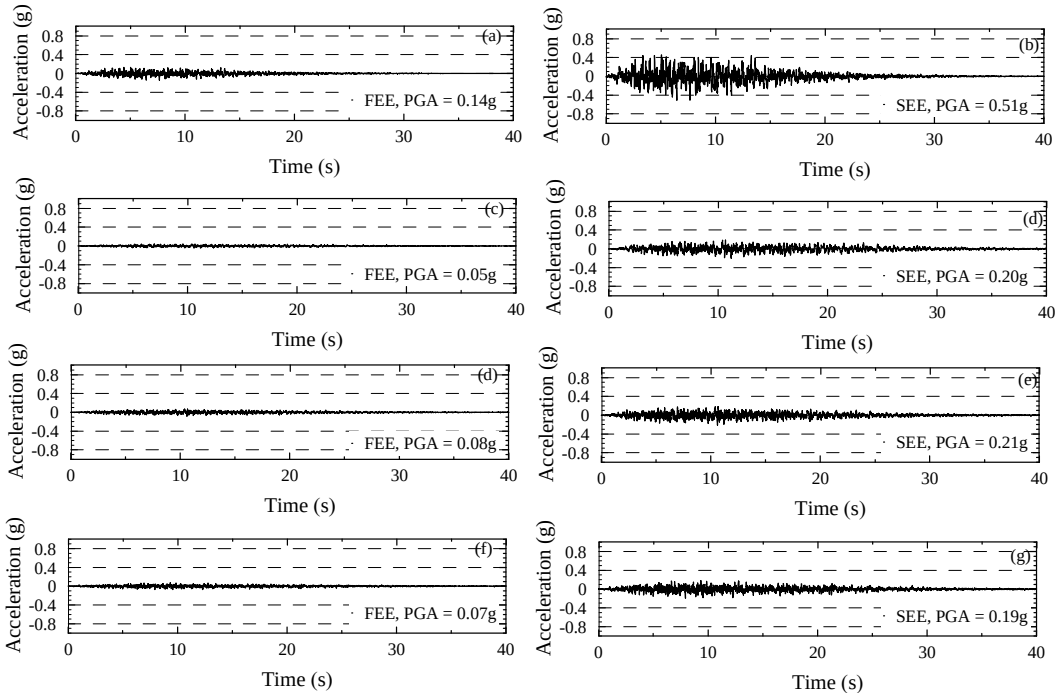

Figure 4.6 Sample synthetic soft-rock outcrop motions generated by Scenario_PC for 10% and 2% probability of exceedance in 50 years for (a-b) Charleston, (c-d) Myrtle Beach, (e-f) Columbia, and (g-h) Aiken.

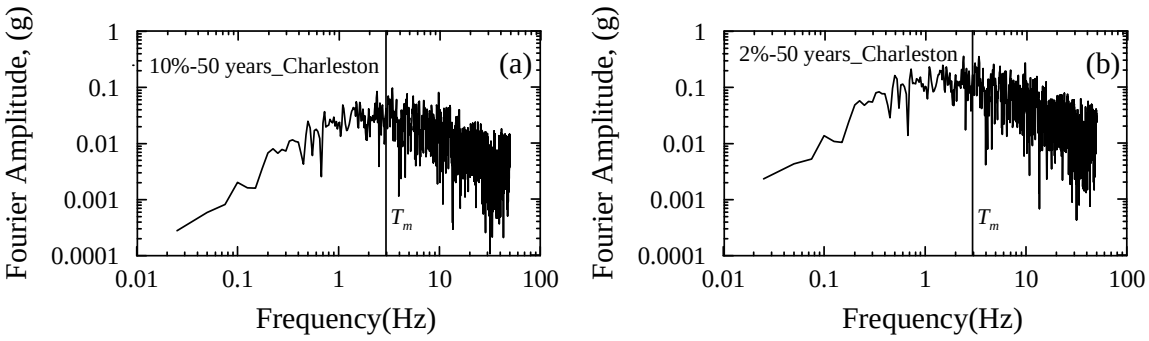

Figure 4.7 Fourier amplitude plots for (a) FEE and (b) SEE motions generated for the Charleston quadrangle.

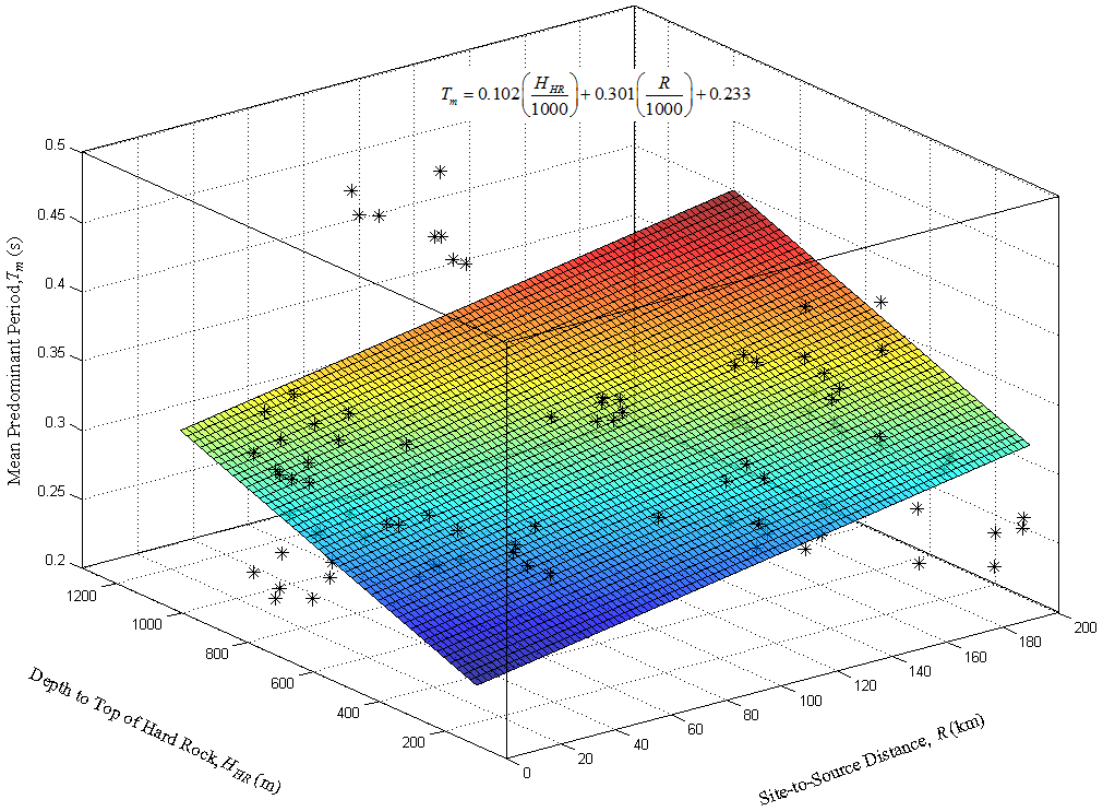

Figure 4.8 Plot of T_m versus depth to top of hard rock and site-to-source distance.

The best fit plane surface shown in Figure 4.8 is defined by:

$$T_m = 0.102\left(\frac{H_{HR}}{1000}\right) + 0.301\left(\frac{R}{1000}\right) + 0.233 \qquad (4.2)$$

From Equation 4.2, it can be seen that attenuation of higher frequency (or lower period) energy is assumed in Scenario_PC to be, on average, three times faster per distance traveled in the hard rock than in the soft rock.

Presented in Figure 4.9 are residual plots of T_m versus the predicting variables, H_{HR} and R. The residual, ε, is defined here as T_m of the plotted data obtained from the time histories generated by Scenario_PC minus T_m obtained from Equation 4.2. The mean values of ε are computed to be zero, suggesting a central tendency of the predicting equation. Equation 4.2 gives an unbiased prediction of T_m for the time histories from Scenario_PC considered, because the ε data do not exhibit a systematic pattern with H_{HR} and R. Therefore Equation 4.2 can be used for predicting T_m in the SCCP.

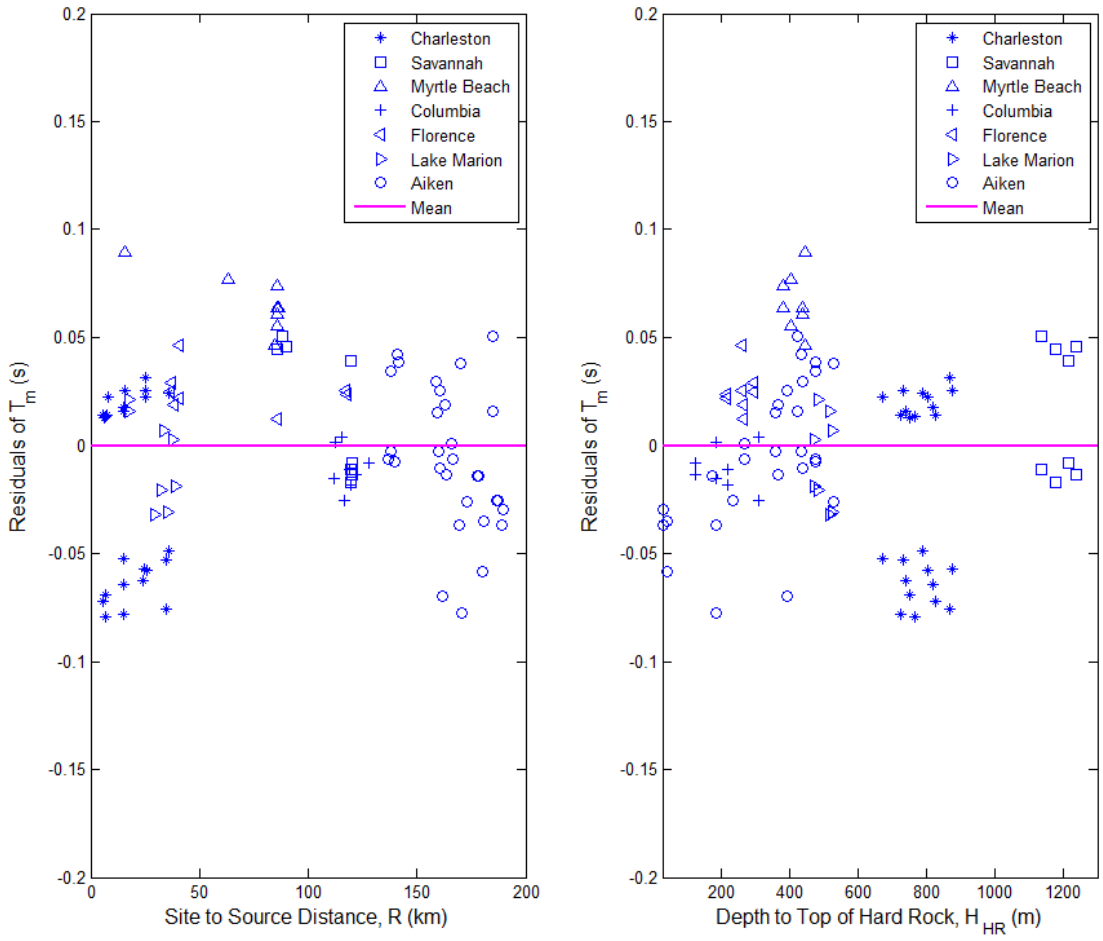

Figure 4.9 Residual plots of T_m versus H_{HR} and R.

Presented in Figures 4.10a and 4.10b are plots of $PGA_{outcrop}$ of the input motions with respect to H_{HR} and R. The anomaly in $PGA_{outcrop}$ values plotted in Figure 4.10a between H_{HR} 500 and 900 m is due to the close proximity of the Charleston Seismic Hazard Zone. This can be seen in Figure 4.10b where $PGA_{outcrop}$ values are plotted versus site-to-source distance.

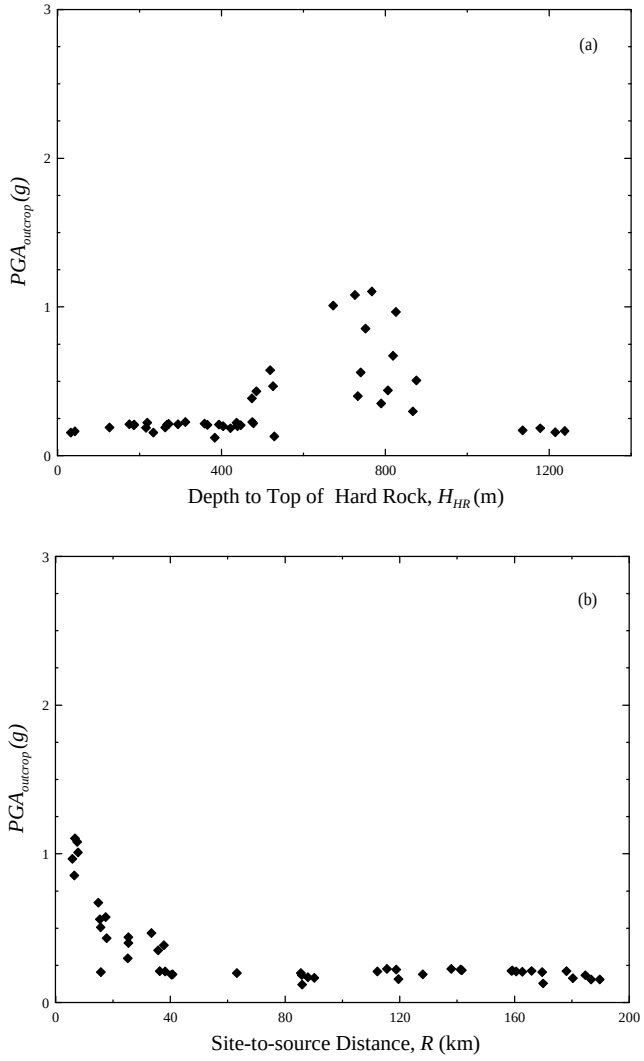

Figure 4.10 $PGA_{outcrop}$ of input motions used versus (a) H_{HR}, and (b) R.

4.4 Results

4.4.1 Generalized Model

Following the approach established in Chapter 3 for the Charleston area, average values of F are computed for six spectral period ranges (T): ≤ 0.01, 0.01-0.4, 0.41-0.8, 0.81-1.2, 1.21-2.0 and 2.01-4.0 s, respectively based on the geologic realistic, soft-rock condition. These ranges are herein referred to by their middle range periods. The respective site coefficients are denoted as $F_{PGA,}$ $F_{0.2}$ (or F_a), $F_{0.6}$, F_1 (or F_v), $F_{1.6}$ and $F_{3.0}$. Computed values of F for the SCCP sites are presented in Figures 4.11-4.13, and Appendices A-G. Each data point of F in Figures 4.11-4.13 and Appendices A-G are determined by averaging mean values from 12, 4, 4, 4, 4, 4 and 15 simulations involving different time-histories for the Charleston, Savannah, Myrtle Beach, Columbia, Florence, Lake Marion and Aiken, respectively. The data plotted in Figures 4.11-4.13 and Appendices A-G are sampled from over 36,000 SHAKE and 12,000 D-MOD simulations.

Averaging values of F over a spectral period range (e.g., 0.01-0.4 s) is consistent with the development of the NEHRP F_a and F_v recommended values. It should be noted, however, that the NEHRP F_a and F_v were determined assuming the spectral period ranges of 0.1-0.5 s and 0.4-2.0 s, respectively (Borchedt 1994). Narrower period ranges allow for better predictions of spectral accelerations, because the periods at which spectral peaks occur can vary greatly from site to site and can exceed 1.0 s.

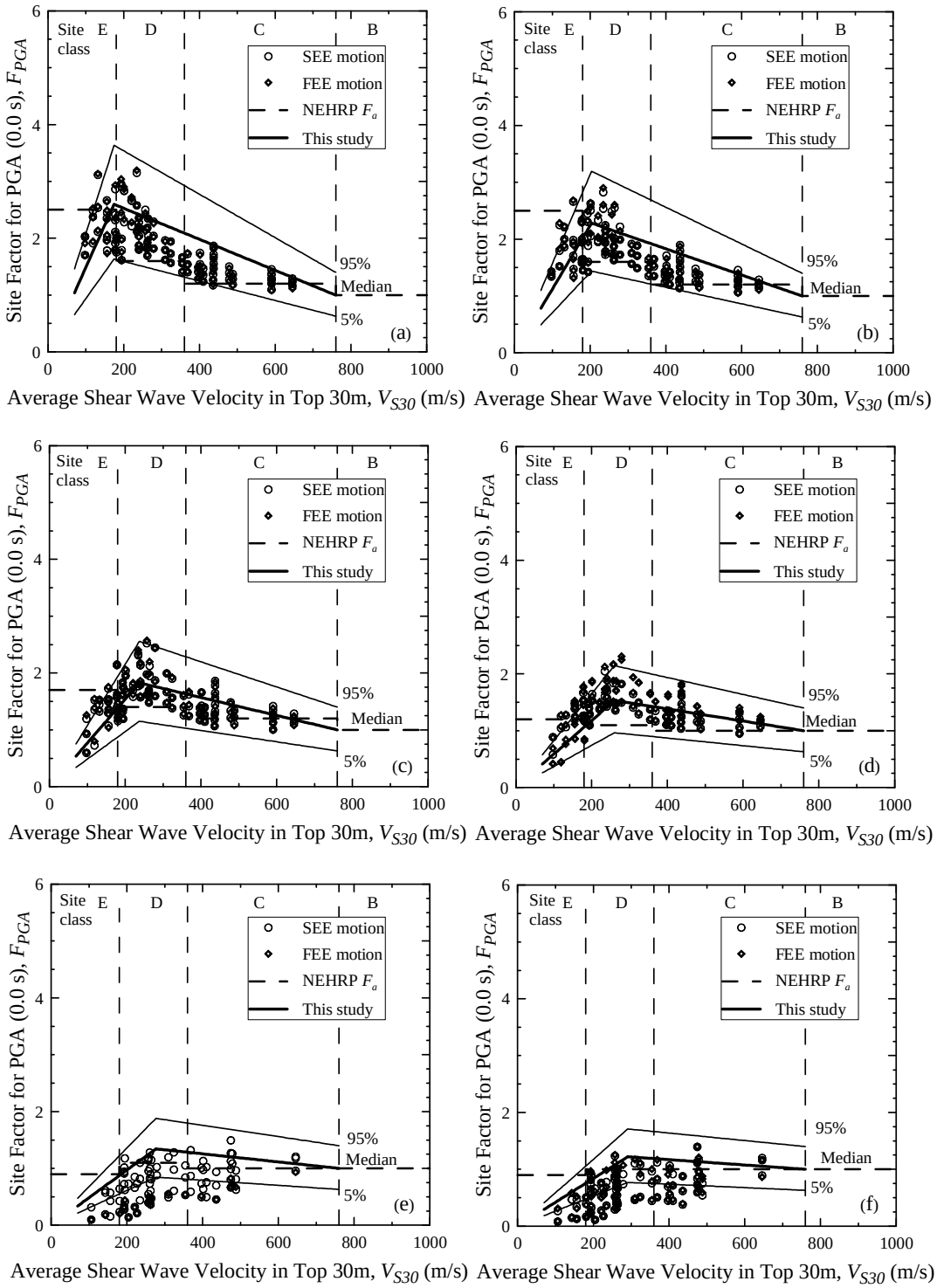

Figure 4.11 Site coefficients for 0.0 s spectral period (free-field) with *PGA* equal to (a) 0.05 g, (b) 0.1 g, (c) 0.2 g, (d) 0.3 g, (e) 0.4 g, and (f) 0.5 g, based on V_s profiles shown in Figure 4.3b for Myrtle Beach.

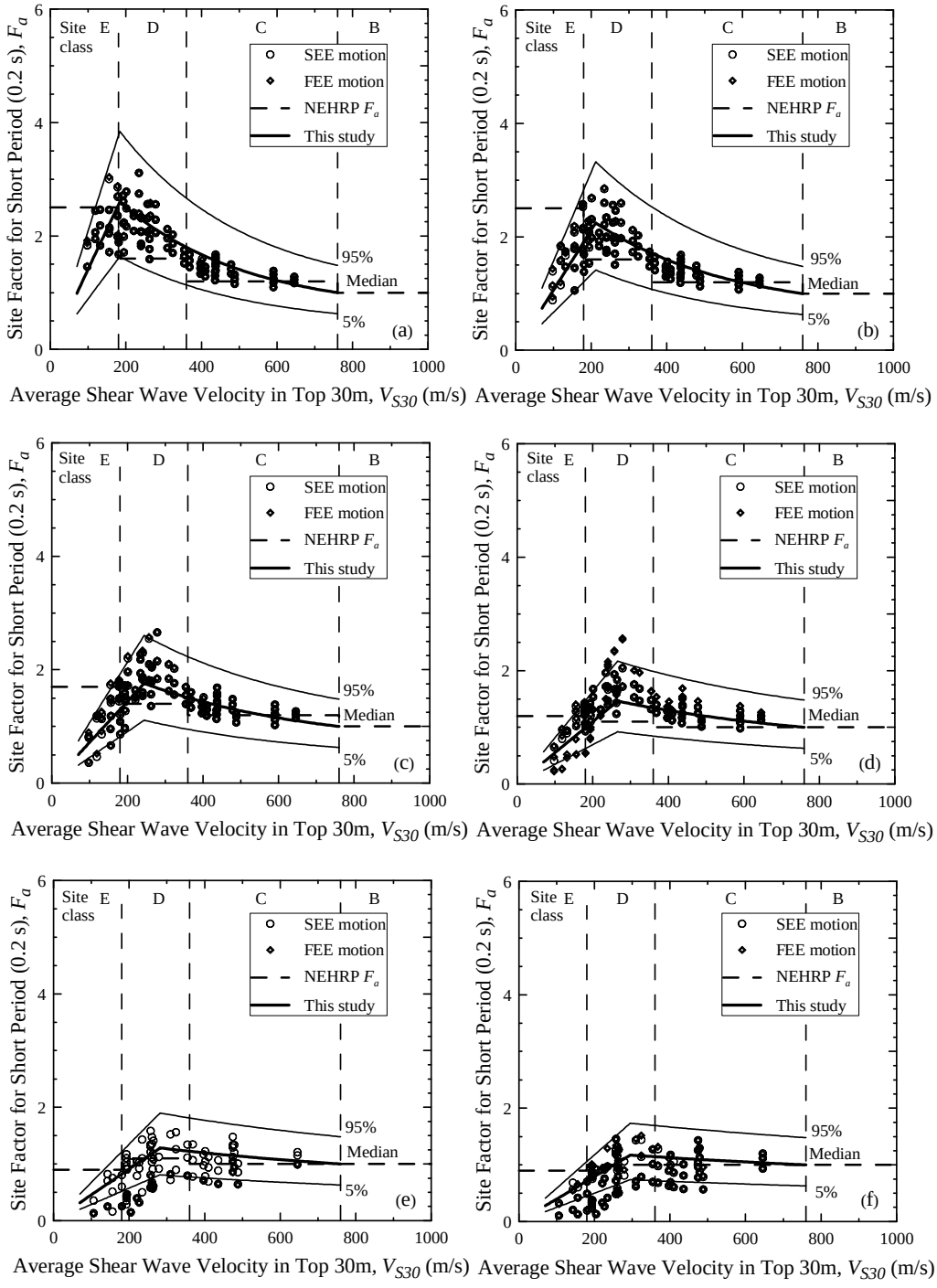

Figure 4.12 Site coefficients for 0.2 s (short) spectral period with S_s equal to (a) 0.125 g, (b) 0.25 g, (c) 0.50 g, (d) 0.75 g, (e) 1.0 g, and (f) 1.25 g, based on V_s profiles shown in Figure 4.3b for Myrtle Beach.

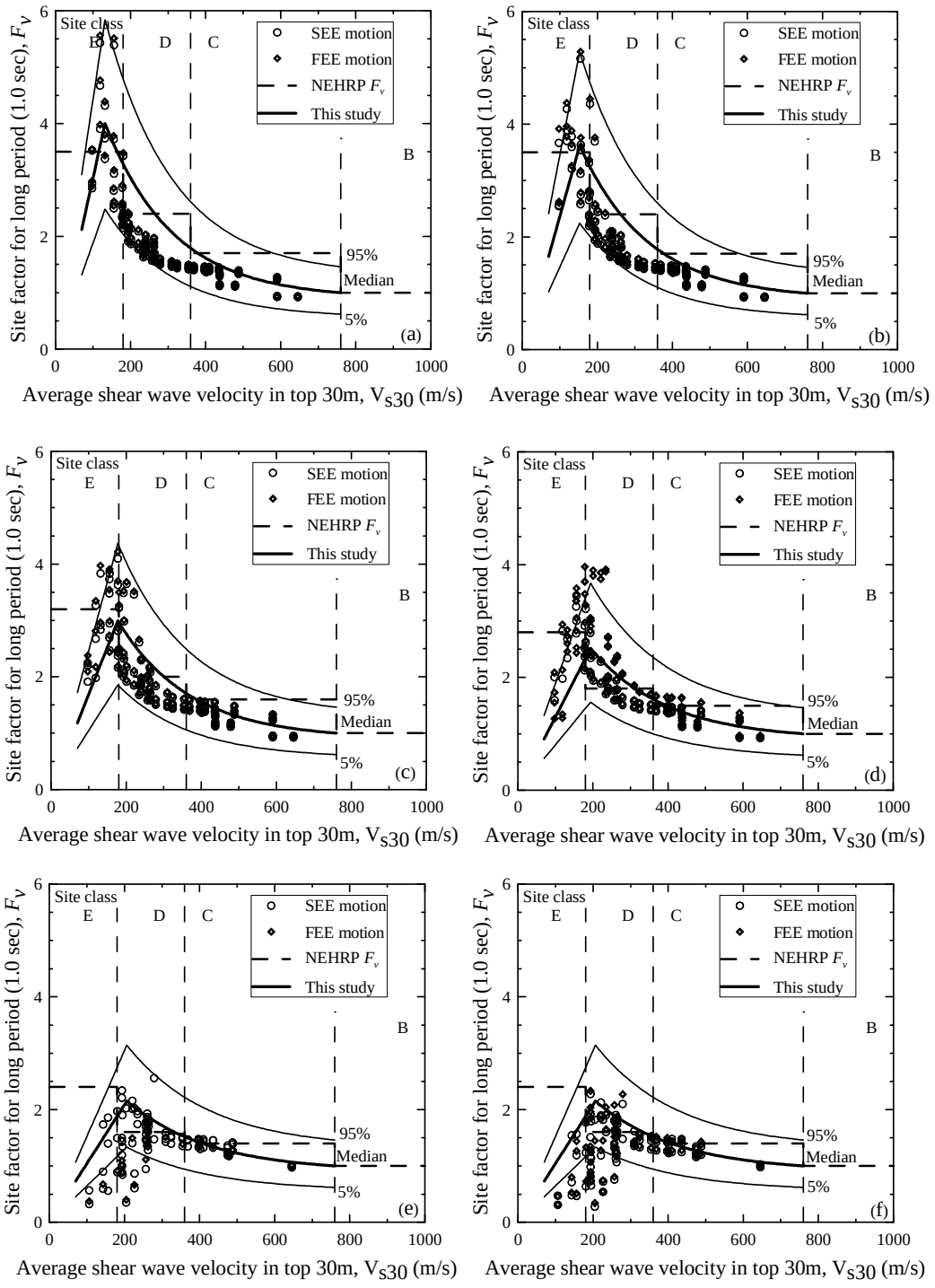

Figure 4.13 Site coefficients for 1.0 s (long) spectral period with S_1 equal to (a) 0.05 g, (b) 0.10 g, (c) 0.20 g, (d) 0.30 g, (e) 0.4 g, and (f) 0.50 g, based on V_s profiles shown in Figure 4.3b for Myrtle Beach.

As observed in the data plotted in Figures 4.11-4.13 (and all other plots in Appendices A-G), the plotted V_{S30}-F data pairs exhibit three general features--(1) an increasing trend in F as V_{S30} increases from a very low value; (2) a zone of peak F values between V_{S30} 150 to 300 m/s, depending on $S_{outcrop}$; and (3) a decreasing trend in F as V_{S30} increases beyond the zone of peak F values. Similar general features can be observed in data reported by other investigators (Silva et al. 2000; Chapman et al. 2006; Fairbanks et al. 2008) and are supported by vibration theory. These three general features are assumed in developing mathematical models of F.

4.4.1.1 Estimating the Peak Site Coefficient

Extending the site coefficient model developed in Chapter 3, the peak site coefficient within a given plot (F_P) and the corresponding average shear wave velocity in the top 30 m (V_{S30P}) can be estimated by

$$F_p = \left[x_1 \exp\left(\frac{x_2 S_{outcrop}}{g} \right) \left(\frac{T_m}{T_{100}} \right)^{x_3} + 1 \right] K_{H1} \tag{4.3a}$$

$$V_{S30P} = \left[x_4 \left(\frac{S_{outcrop}}{g} \right)^{x_5} \left(\frac{T_m}{s} \right)^{x_6} \right] K_{H2} \tag{4.3b}$$

where x_1, x_2, x_3, x_4, x_5 *and* x_6 are regression coefficients given in Table 4.1; $S_{outcrop}$ is in units of g; g is the acceleration of gravity; T_{100} is a proxy variable for the site fundamental period; s is one second to normalize T_m; and K_{H1} and K_{H2} are dimensionless adjustment coefficients to account for the influence of shallow soft rock.

The proxy variable T_{100} is defined as:

$$T_{100} = 4*100 \Big/ V_{S100} \tag{4.4}$$

where V_{S100} is the averaged shear wave velocity in the top 100 m, which is calculated similar to V_{S30}. Range and reference profile values of V_{S100} for the profiles shown in Figures 4.3a-4.3d are listed in Table 4.2. Also listed in Table 4.2 are range and reference profile values of T_{100} and T_m for the seven areas in the SCCP.

Table 4.1 Regression coefficients for estimating seismic site coefficients in the SCCP.

$S_{outcrop}$	x_1	x_2	x_3	x_4 (m/s)	x_5	x_6	a	$Z_{0.05}$	$Z_{0.95}$
PGA	7.510	-4.394	1.614	258	0.222	-0.276	-*	0.63	1.40
S_s	7.305	-1.980	1.546	245	0.206	-0.141	0.65	0.63	1.48
$S_{0.6}$	10.691	-3.382	1.487	142	0.181	-0.721	0.85	0.63	1.50
S_1	4.929	-2.734	0.437	105	0.214	-0.876	0.90	0.62	1.46
$S_{1.6}$	3.477	-2.555	0.185	128	0.228	-0.647	0.99	0.68	1.40
$S_{3.0}$	0.720	-5.638	-0.860	211	0.208	-0.036	0.99	0.65	1.30

*For *PGA*, use equation 4.6*a*.

Table 4.2 Typical values of V_{S100}, T_{100}, and T_m.

Site	V_{S100} (m/s)		T_{100} (s)		T_m (s)		Average T_m / Reference T_{100}
	Range	Reference Profile	Range	Reference Profile	Range	Average	
Charleston	158-629	377	0.64-2.53	1.06	0.24-0.35	0.29	0.27
Savannah	158-629	377	0.64-2.53	1.06	0.37-0.43	0.40	0.38
Myrtle Beach	219-680	474	0.59-1.83	0.84	0.35-0.38	0.37	0.44
Columbia	201-685	421	0.58-1.96	0.95	0.27-0.31	0.29	0.30
Florence	204-685	421	0.58-1.96	0.95	0.29-0.31	0.30	0.32
Lake Marion	204-685	421	0.58-1.96	0.95	0.26-0.31	0.28	0.29
Aiken	184-643	396	0.62-2.17	1.01	0.24-0.38	0.31	0.31

Presented in Figures 4.14a-f are F_p values plotted versus $S_{outcrop}$ and T_m/T_{100} for spectral periods of 0.0, 0.2, 0.6, 1.0, 1.6, and 3.0 s, respectively. As expected, F_p decreases with increasing $S_{outcrop}$ at all spectral periods. This is due to increased damping and nonlinear effects at higher $S_{outcrop}$. Maximum amplification is expected when the resonance frequency of a soil column matches with the frequency content of the motion. In Figures 4.14a-f, it can be seen that F_p tends to increase with increasing T_m/T_{100} for short periods ($T < 0.6$ s). For long periods ($T > 0.6$ s), however, F_P tends to decrease with increasing T_m/T_{100}. Presented in Figures 4.15a-f are respective values of V_{S30P} plotted versus $S_{outcrop}$ and T_m/T_{100} for spectral periods of 0.0, 0.2, 0.6, 1.0, 1.6, and 3.0 s, respectively. At smaller $S_{outcrop}$, maximum amplification occurs in soft soils; and at higher $S_{outcrop}$ maximum amplification occurs in stiff soils.

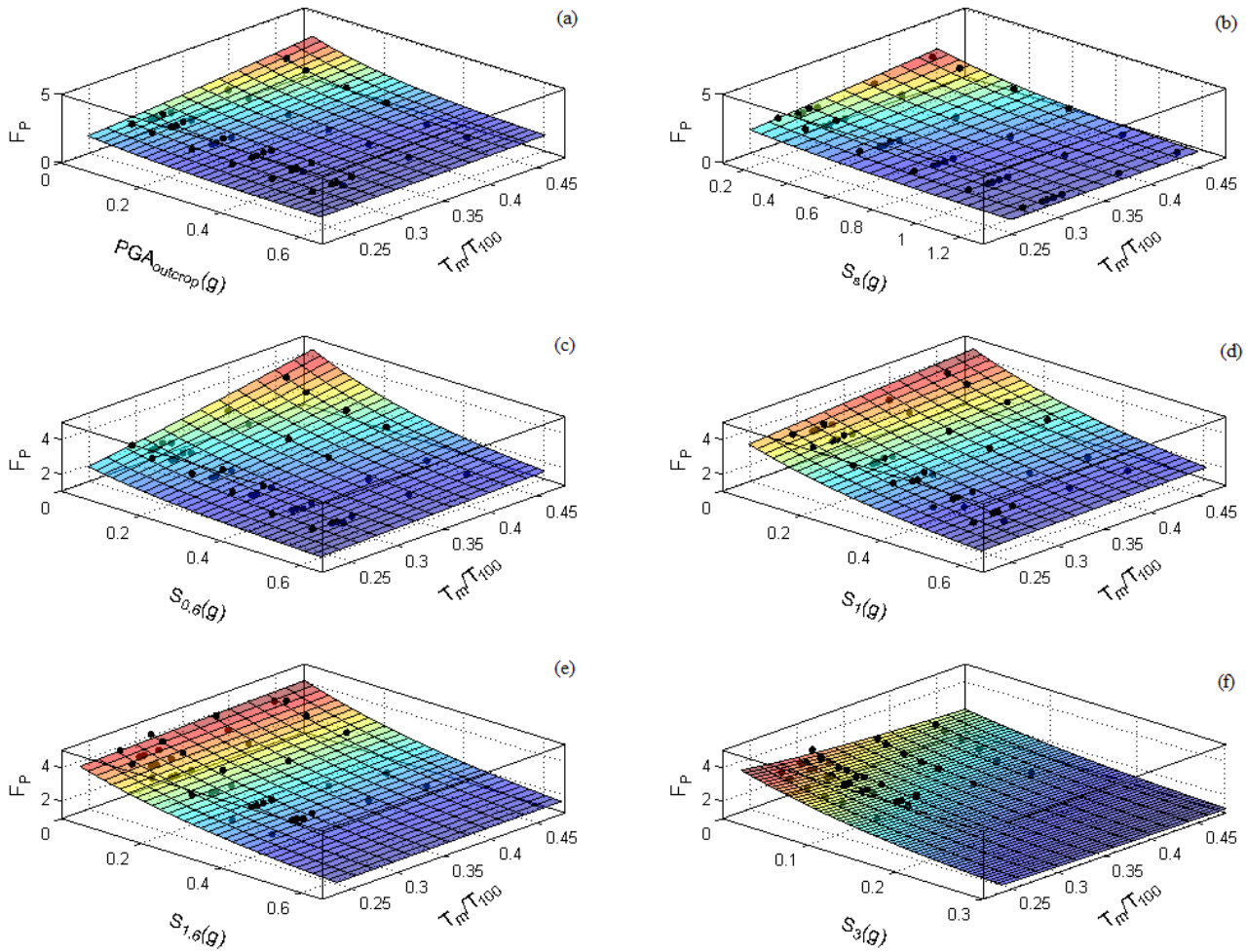

Figure 4.14 Effect of T_m/T_{100} and $S_{outcrop}$ on F_P for (a) 0.0 s, (b) 0.2 s, (c) 0.6 s, (d) 1.0 s, (e) 1.6 s, and (f) 3.0 s spectral periods.

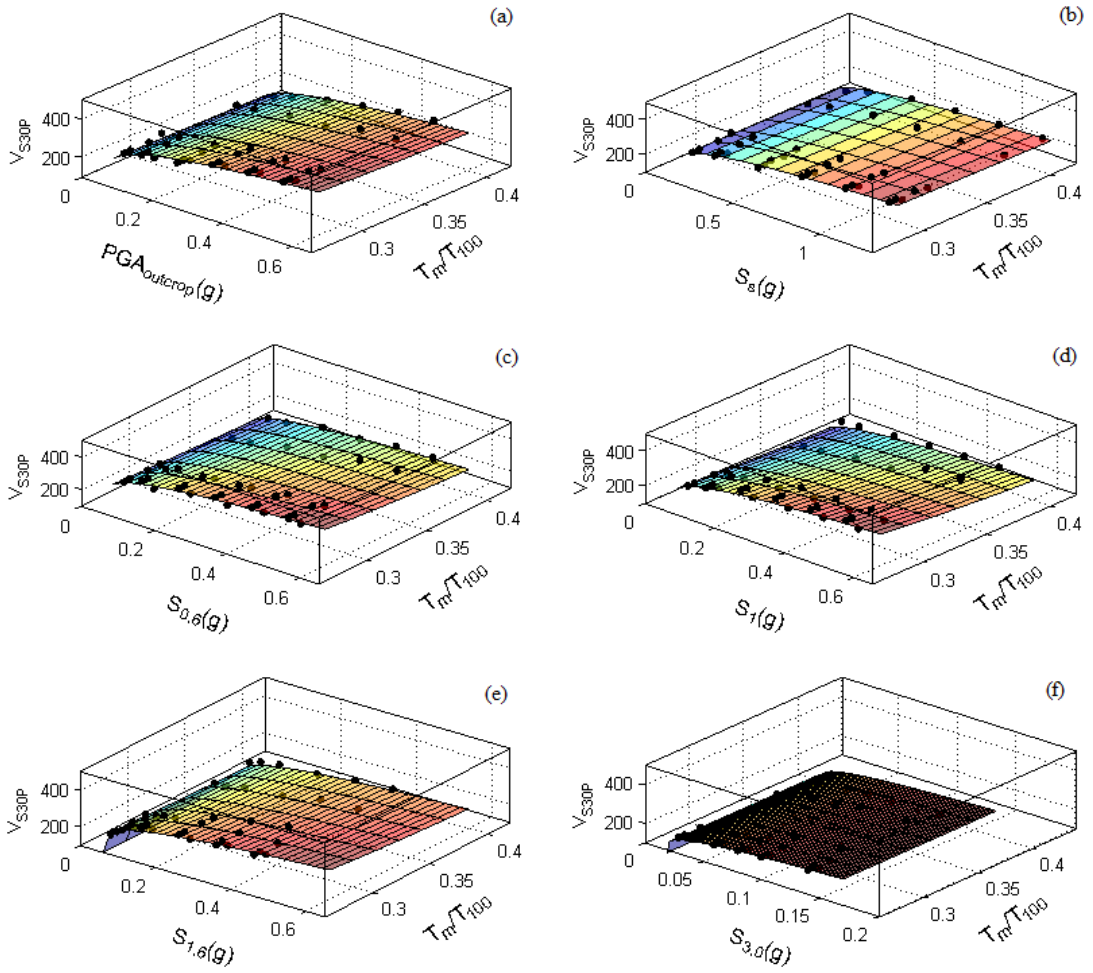

Figure 4.15 Effect of T_m/T_{100} and $S_{outcrop}$ on V_{S30P} for (a) 0.0 s, (b) 0.2 s, (c) 0.6 s, (d) 1.0 s, (e) 1.6 s, and (f) 3.0 s spectral periods.

Plotted in Figure 4.16a-4.16b, and tabulated in Table 4.3, are computed values of K_{H1} and K_{H2}, respectively, based on the results of response analysis preformed using the motions from five quadrangles near Columbia and the V_S profiles presented in Appendix H1-H6 with depths to the soft rock ($H_{B\text{-}C}$) of 0.5, 1.5, 5, 10, 20, 30, 50, and 100 m. Summary of inputs and outputs of these ground response analyses are presented in Appendix H.

It can be seen in Figure 4.16a that F_{PGA} and F_a can be much higher at sites where $H_{B\text{-}C} < 100$ m than at sites where $H_{B\text{-}C} \geq 100$ m. On the other hand, $F_{0.6}$, F_1, $F_{1.6}$, and F_3 are lower at sites where $H_{B\text{-}C} < 100$ m than at sites where $H_{B\text{-}C} \geq 100$ m. In Figure 4.16b it can be seen that soft soils exhibit greater amplification with increasing $H_{B\text{-}C}$. Similarly, stiff soils exhibit greater amplification with decreasing $H_{B\text{-}C}$.

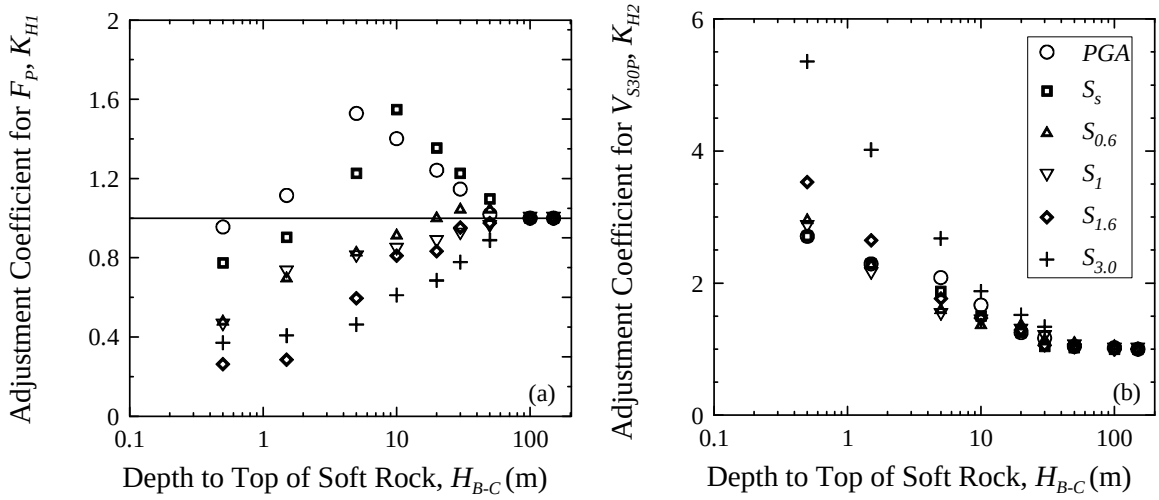

Figure 4.16 Depth to top of soft-rock adjustment coefficients, K_{H1} and K_{H2}.

Table 4.3 Recommended depth to top of soft rock adjustment coefficients.

$S_{outcrop}$	Adjustment coefficient	Depth to soft rock, $H_{B\text{-}C}$ (m)							
		0.5	1.5	5	10	20	30	50	≥ 100
PGA	K_{H1}	0.96	1.11	1.53	1.40	1.24	1.15	1.02	1.00
	K_{H2}	2.71	2.29	2.08	1.67	1.25	1.17	1.04	1.00
Ss	K_{H1}	0.77	0.90	1.23	1.55	1.35	1.23	1.10	1.00
	K_{H2}	2.71	2.29	1.88	1.50	1.25	1.04	1.02	1.00
$S_{0.6}$	K_{H1}	0.48	0.70	0.83	0.91	1.00	1.04	1.04	1.00
	K_{H2}	2.95	2.27	1.59	1.36	1.36	1.14	1.09	1.00
S_1	K_{H1}	0.46	0.73	0.80	0.84	0.88	0.92	0.96	1.00
	K_{H2}	2.86	2.14	1.52	1.43	1.29	1.19	1.05	1.00
$S_{1.6}$	K_{H1}	0.26	0.29	0.60	0.81	0.83	0.95	0.98	1.00
	K_{H2}	3.53	2.65	1.76	1.47	1.29	1.06	1.03	1.00
S_3	K_{H1}	0.37	0.41	0.46	0.61	0.69	0.78	0.89	1.00
	K_{H2}	5.36	4.02	2.68	1.88	1.52	1.34	1.07	1.00

Presented in Figures 4.17a-c are example plots of computed F_{PGA}, F_a and F_v values for $H_{B\text{-}C}$ = 10 m. Greater F_{PGA} and F_a are predicted when $H_{B\text{-}C}$ = 10 m compared to $H_{B\text{-}C}$ = 137 m for Site Class D and C. However, lesser values of F_v are predicted when $H_{B\text{-}C}$ = 10 m compared to $H_{B\text{-}C}$ = 137 m. This observation agrees with the study by Hashash et al. (2008) who also found greater F_a and lesser F_v values in shallow Site Class D profiles compared to deep Site Class D profiles in the Mississippi Embayment.

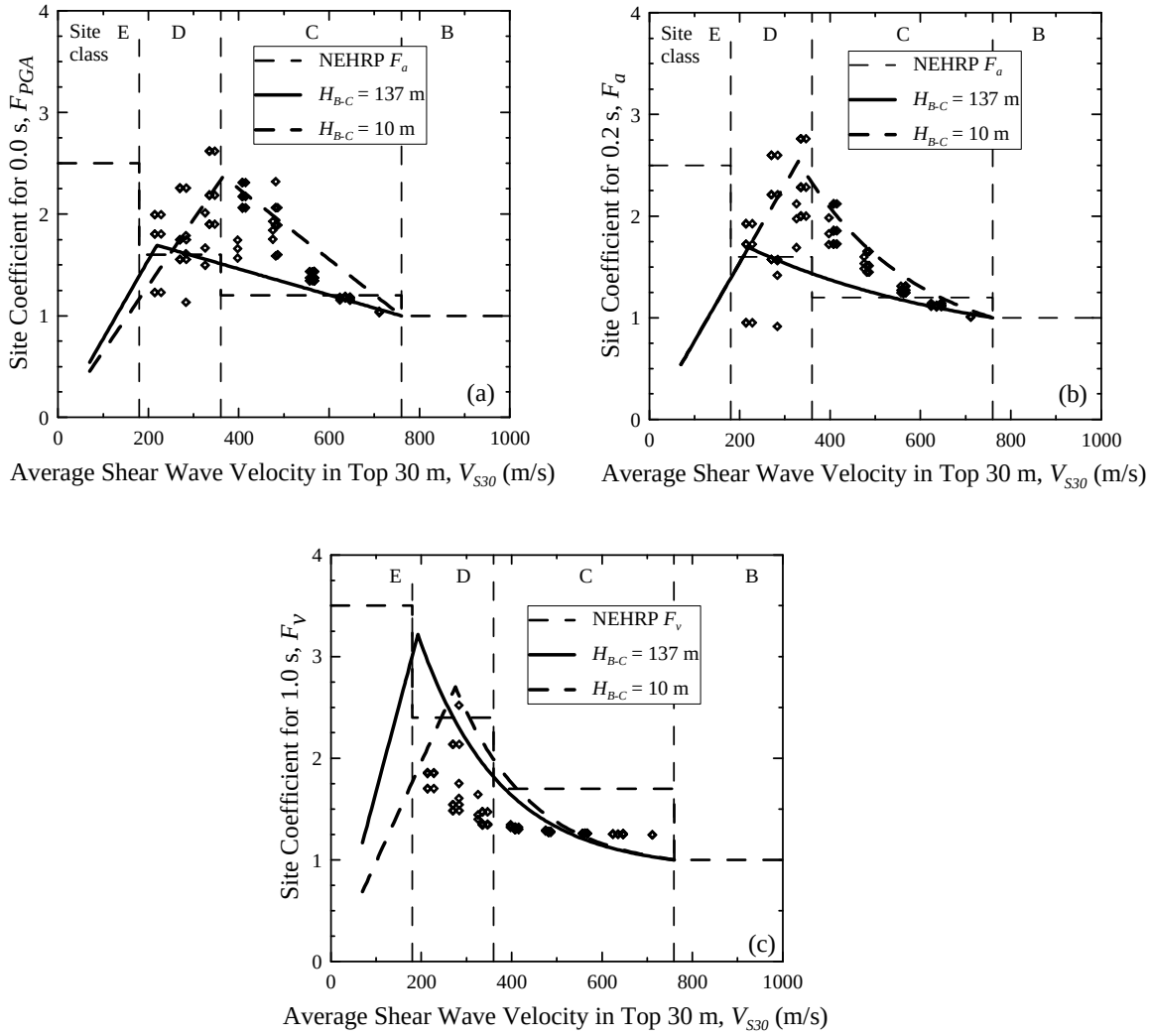

Figure 4.17 Sample median F-V_{S30} relationship for H_{B-C} = 137 and 10 m for (a) PGA = 0.1 g, (b) S_s = 0.25 g, and (c) S_1 = 0.1 g with computed values for H_{B-C} = 10 m.

4.4.1.2 Relationship between F and V_{S30}

With the estimates of F_P and V_{S30P}, the median V_{S30}-F relationships of the eighteen plots shown in Figures 4.11-4.13 (as well as Appendix A-H) can be expressed as follows (Aboye et al. 2014):

$$F = \left(\frac{F_P}{V_{S30P}}\right) V_{S30} \qquad \text{for } V_{S30} < V_{S30P} \text{ and all spectral periods } T \tag{4.5}$$

$$F = \frac{\left(F_p - 1\right)\left(760 - V_{S30}\right)}{760 - V_{S30P}} + 1 \qquad \text{for } V_{S30} \geq V_{S30P} \text{ and } T < 0.2\ s \tag{4.6a}$$

$$F = a + b\, e^{cV_{S30}} \qquad \text{for } V_{S30} \geq V_{S30P} \text{ and } T \geq 0.2\ s \tag{4.6b}$$

where a is a regression coefficient given in Table 4.1; and b and c are coefficients calculated from:

$$b = \frac{1-a}{e^{760c}} \tag{4.7}$$

$$c = \frac{\ln\left(\frac{1-a}{F_p - a}\right)}{760 - V_{S30P}} \tag{4.8}$$

Equation 4.5 is a linear relationship, and assumes F = 0 when V_{S30} = 0 m/s. Equations 4.6a and 4.6b are linear and exponential relationships, respectively; and satisfy the assumed reference soft-rock outcrop condition of F = 1.0 when V_{S30} = 760 m/s. Both Equations 4.5 and 4.6 provide the same value of F at $V_{S30} = V_{S30P}$.

Following the approach of Aboye et al. (2014), the development of Equations 4.5 and 4.6 involves a three-step procedure. First, median curves are derived by studying the residuals of the individual data subsets grouped by geologic area and spectral period. The residual, ε, is defined here as F of the computed data divided by F of the median relationship. Based on the probability plotting method, ε is shown to follow a lognormal distribution. The second step involves obtaining least-squared regression approximations of F_p and V_{S30P} as a function of $S_{outcrop}$ and T_m/T_{100}. Finally, based on F_p, V_{S30P}, K_{H1} and $K_{H2,}$ Equations 4.5 and 4.6 are established. The predictor variables V_{S30}, $S_{outcrop}$, T_m/T_{100} and $H_{B\text{-}C}$ are shown to have little or no bias in the median relationships expressed by Equations 4.5 and 4.6, because plots of variables-ε do not show any systematic structure.

The upper and lower curves shown in Figures 4.11-4.13 are drawn to bound 95% and 5%, respectively, of all the data points for a given F. They are drawn by multiplying Equations 4.5 and 4.6 by the average standard Z-scores (i.e., $Z_{0.95}$ or $Z_{0.05}$) listed in Table 4.1. The Z-scores are obtained from lognormal cumulative distribution of F-residuals for each set of data.

The new seismic site coefficient model defined by Equations 4.3, 4.5 and 4.6 is recommended for the SCCP because it provides better matches to the computed values than do the NEHRP coefficients for all values of V_{S30}. A flowchart of the procedure for obtaining the recommended site coefficients from soft-rock spectral accelerations is presented in Figure 4.18. The procedure begins with (1) determining four key site variables (i.e., V_{S30}; V_{S100} or T_{100}; H_{HR}; and $H_{B\text{-}C}$) from in situ test results and available

geologic information; and (2) obtaining three key ground motion variables (i.e., $S_{outcrop}$ = *PGA*, $S_{0.2}$, $S_{0.6}$, S_1, $S_{1.6}$, S_3; R; and T_m) from hazard maps or computer programs like Scenario_PC. With these inputs, the values of F_P and V_{S30P} are calculated from Equations 4.3a and 4.3b, respectively; and the site coefficients corresponding to each value of $S_{outcrop}$ are calculated using Equation 4.5 or 4.6.

4.4.2 Recommended Site Coefficients

Presented in Appendices A-G are computed site coefficients for the Charleston, Savannah, Myrtle Beach, Columbia, Florence, Lake Marion, and Aiken areas, respectively. In decreasing order, the computed site coefficients were generally found to be greater in Myrtle Beach, Savannah, Charleston, Florence, Columbia, Lake Marion and Aiken areas. More closely matching values of T_m and T_{100} (i.e., T_m = 0.37 and T_{100} = 0.84 for the Myrtle Beach reference profile may explain the higher site coefficients obtained for Myrtle Beach and Savannah. In this section, a selected discussion is given based on computed site coefficients for Myrtle Beach area.

Plotted in Figures 4.11, 4.12, and 4.13 are F_{PGA}, F_a, and F_v values computed for Myrtle Beach, respectively. Also plotted for comparison are the NEHRP F_a and F_v values. Maximum computed median F_{PGA} values range from 1.2 to 2.6, as shown in Figure 4.11. The computed median F_{PGA} values are generally greater than the NEHRP F_a values for all values of $S_{outcrop}$. The difference is most significant for Site Class D, and can be greater by as much as 75%. As shown in Figure 4.12, maximum computed median F_a values range from 1.25 to 2.6. The computed median F_a values are greater than the

NEHRP F_a values by as much as 1.8 times. For the Site Class E, the NEHRP F_a is found to be conservative compared to the computed median F_{PGA} and F_a values from this study. This finding generally agrees with Silva et al. (2000), Rodriguez-Marek et al. (2001), Borcherdt (2002), Stewart et al. (2003), Seyhan and Stewart (2011) and the NGA-GMPEs (http://peer.berkeley.edu/ngaeast/) whose computed F_a values are greater for Site Class D and smaller for Site Class E compared to the NEHRP (Tables 2.1-2.3).

Presented in Figure 4.13 are F_v values computed for Myrtle Beach. It can be seen in Figure 4.13 that the computed median F_v values range from 2.0 to 3.7. The computed maximum median F_v values plot relatively below the NEHRP F_v values for Site Class E and C. For Site Class D, the computed median F_v values are sometimes greater than the NEHRP values. Figure 4.13 shows that long-period amplification is critical when V_{S30} is between 180-300 m/s. This observation generally agrees with Silva et al. (2000), Borcherdt (2002), Stewart et al. (2003) and Choi and Stewart (2005) who also obtained F_v values greater than the NEHRP for Site Class D (see Tables 2.4-2.6).

It is worth noting that the recommended site coefficients are based on motions generated by Scenario_PC assuming the modal M_w of 7.3 and scaling to different values of $PGA_{outcrop}$. Additional analysis was performed with soft-rock motions generated by assuming M_w of 5, 6, 7 and 8 and scaling the motions to different values of $PGA_{outcrop}$. Although the motions exhibit varying frequency contents and durations depending on M_w, there is little to no difference between the computed site coefficients. The influence of frequency content on F is adequately captured by the T_m terms in Equations 4.3a and

4.3b; and the influence of ground motion duration on F is comparatively small compared to the influence of $PGA_{outcrop}$. Thus, the site coefficients described by Equations 4.3a, 4.3b, 4.5 and 4.6 can be applied to soft-rock spectra accelerations for all earthquake magnitudes.

Additional analysis was also performed to investigate the influence of H_{HR} versus $H_{B\text{-}C}$. It is found that much, if not all, of the variations in computed site coefficients at a given location due to the depth to top of rock can be explain by $H_{B\text{-}C}$. Thus, the adjustment coefficients K_{H1} and K_{H2} are sufficient to capture the influence of shallow depths (< 100 m) to bedrock.

4.5 Summary

In this Chapter, the model for predicting site coefficients developed in Chapter 3 was extended to a generalized seismic site coefficient model for the SCCP. Soil/rock and seismic conditions typical of sites in the SCCP (i.e., Charleston, Savannah, Myrtle Beach, Columbia, Florence, Lake Marion, and Aiken) were considered. Input ground motions were scaled to obtain good coverage over the spectral acceleration range as provided in codes and guidelines. It was shown that scaling of input motions is justified because the SCCP is dominated by a single seismic source zone. The generalized model was based on over 48,000 total stress, one-dimensional equivalent linear and nonlinear ground response analyses, and derived at spectral periods of 0.0, 0.2, 0.6, 1.0, 1.6 and 3.0 s. The respective site coefficients were referred to as F_{PGA}, F_a, $F_{0.6}$, $F_{1.0}$, $F_{1.6}$, and $F_{3.0}$, and were calculated as averages over period ranges of $\leq$ 0.1, 0.1-0.4, 0.4-0.8, 0.8-1.2, 1.2-2.0, 2.0-4.0 s.

The most important variables identified in developing the seismic site coefficient model are: V_{S30}, spectral acceleration (amplitude), mean predominant period of the input motion (T_m), approximate fundamental frequency of soil/rock column in the top 100 m (T_{100}), and depth to soft rock ($H_{B\text{-}C}$). A relationship to compute T_m based on depth to hard rock (H_{HR}) and site-to-source distance (R) was suggested for the SCCP. In decreasing order, the computed site coefficients were found to be greater in Myrtle Beach, Savannah, Charleston, Florence, Columbia, Lake Marion and Aiken. More closely matching values of T_m and T_{100} (i.e., T_m = 0.37 and T_{100} = 0.84 for the Myrtle Beach reference profile) may explain the higher site coefficients for Myrtle Beach.

The computed site coefficients for each of the seven areas in the SCCP were grouped by spectral acceleration and plotted versus V_{S30}. The site coefficient model was expressed by a linear model for $V_{S30} < V_{S30P}$ and a linear or exponential model for $V_{S30} \geq V_{S30P}$. Each set of data exhibited a peak value somewhere between V_{S30} of 73 and 320 m/s, depending on soft rock-outcrop acceleration ($S_{outcrop}$) and period. Site coefficients decrease with increasing $S_{outcrop}$ and the rate of decrease is higher when $V_{S30} < 200$ m/s. As $S_{outcrop}$ increases, the induced shear strains increase, causing higher hysteretic damping in the soil. The increased hysteretic damping dissipates the wave energy. Because softer sediments develop larger strains than stiffer sediments, this effect is more pronounced when $V_{S30} < 200$ m/s. It is also noted that F_{PGA} and F_a attenuate more rapidly with increasing $S_{outcrop}$ than F_v. The variability in computed site coefficients for sites with similar V_{S30} was characterized by 5% lower bound and 95% upper bound curves.

The computed relationships for periods of 0.0, 0.2 and 1.0 s for Myrtle Beach were compared with the NEHRP F_a and F_v values. It was shown that the computed median F_{PGA} values are greater than the NEHRP F_a values by as much as 70%. The computed median F_a values also plotted above the NEHRP F_a values for $V_{S30} > 180$ m/s. The computed median F_v values plotted above the NEHRP F_v values by as much as about 1.4 times for $180 \leq V_{S30} \leq 350$ m/s. The computed median F_v values agreed with the NEHRP F_v values for $V_{S30} \geq 360$ m/s. For $V_{S30} < 180$ m/s, the NEHRP F_a and F_v were shown to be greater than the computed median values.

The effect of $H_{B\text{-}C}$ was considered by using hypothetical $H_{B\text{-}C}$ values of 0.5, 1.5, 5, 10, 20, 30, 50, 100 and 137 m in the V_s profile in Columbia. Higher amplifications were found at lower values of $H_{B\text{-}C}$ when $T \leq 0.6$ s. When $T > 0.6$ s, higher amplifications were found at higher values of $H_{B\text{-}C.}$ The procedure for applying the seismic site coefficient model is summarized in the flow chart presented in Figure 4.18.

The computed F_{PGA}, F_a and F_v median relationships were recommended for the SCCP because they are: (1) based on regional conditions; (2) continuous with V_{S30}, (3) dependent on depth to rock, and (4) dependent on the frequency content of the design motion. This chapter addressed some of the limitations of Chapter 3 and Aboye et al. (2014).

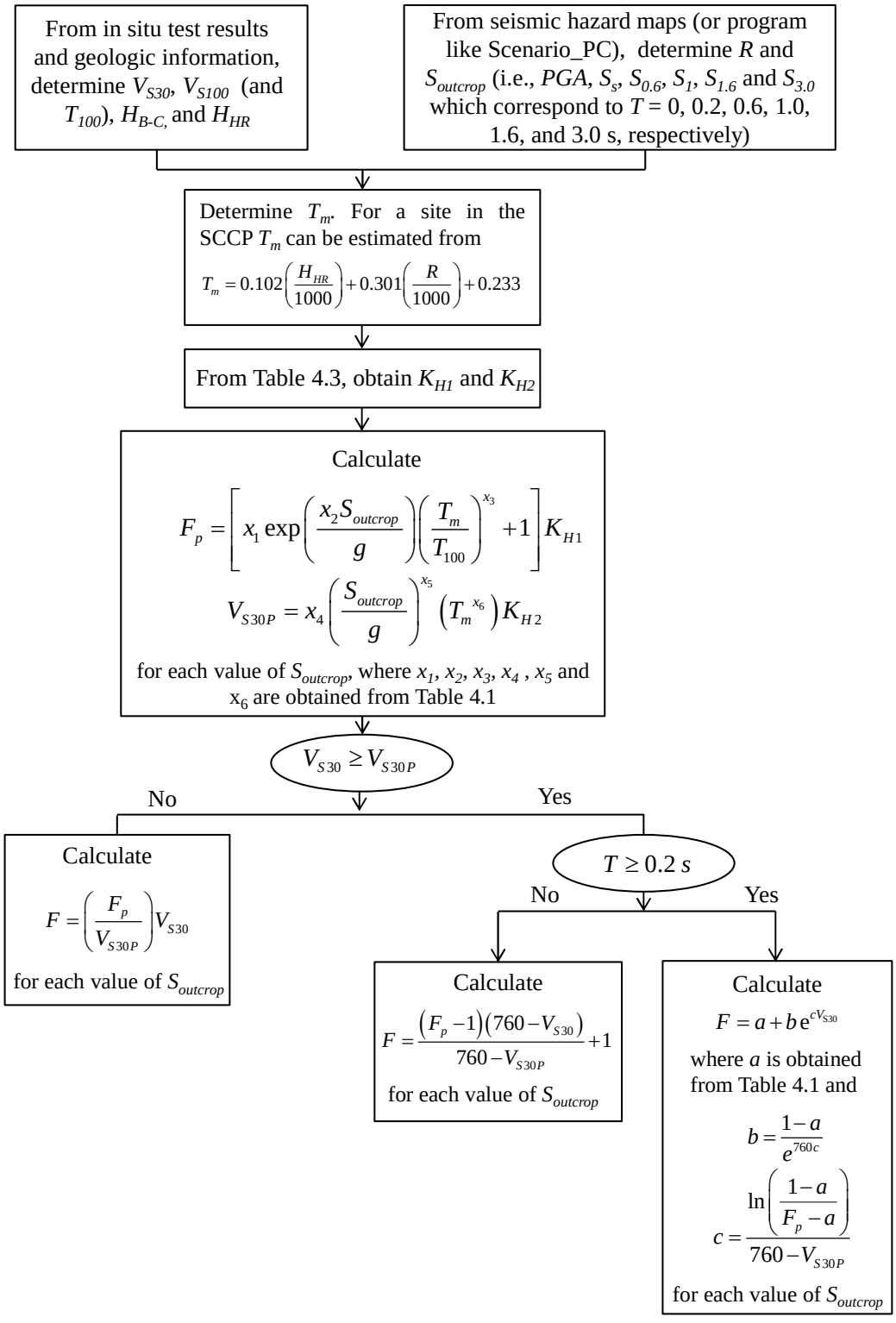

Figure 4.18 Flow chart of obtaining site coefficients for conditions in the SCCP.

CHAPTER FIVE

SEISMIC SITE COEFFICIENT MODEL FOR THE SOUTH CAROLINA PIEDMONT

5.1 Geology and Seismology

The South Carolina Piedmont (SCP) is an area of rolling hills that lies between the Fall line and the Brevard fault, as shown on the geologic map presented in Figure 5.1. The South Carolina Coastal Plain lies to the east of the Fall line. The Brevard fault is a major topographic and structural feature in South Carolina. To the west of the Brevard fault are the Blue Ridge Mountains, which is a southern continuation of the Appalachian Mountains.

The SCP is characterized by erosional remains of an ancient mountain chain with elevations ranging from 100 to 500 m. It is characterized by gently rolling topography, deeply weathered bedrock, and relatively few rock outcrops. Based on rock type and geologic structures, the SCP can be divided into several physiographic units (belts) including the Brevard fault unit and the inner Piedmont unit (Krinitzsky and Dunbar 1990).

As discussed by Krinitzsky and Dunbar (1990), the Brevard fault unit is characterized by cataclystic rocks produced by crushing and fracturing from fault movements. Other rock types existing in the Brevard fault unit are phyllites, schists

(chlorite, graphite, and mica), gneiss, amphibolite quartizites and carbonates. The age of these rocks is Paleozoic or older. The inner Piedmont contains rocks of the highest metamorphic grade found in the SCP. These include volcanic and sedimentary rocks metamorphosed to the Almandine-Amphibolite facies (amphibolite, granitic gneiss, paragneiss, metasandstone, and schist).

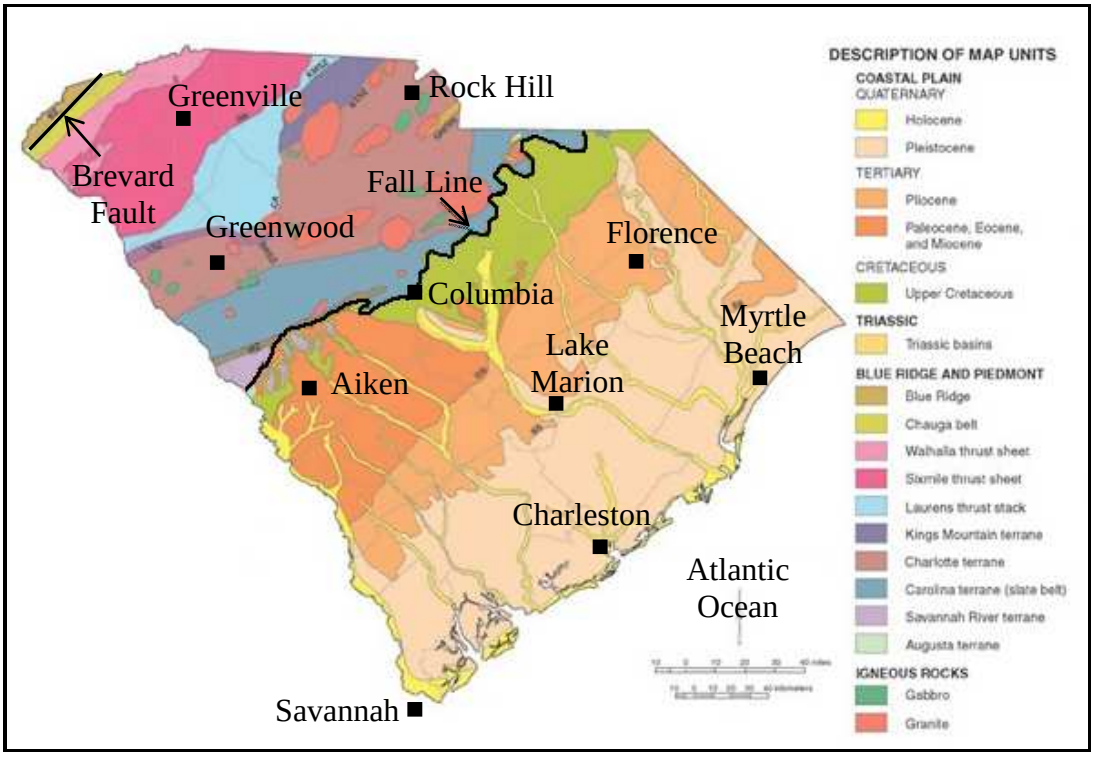

Figure 5.1 Geologic map of South Carolina (SCDNR 2005) showing the Fall Line and the Brevard Fault that bound the South Carolina Piedmont, as well the sites considered in ground response analysis.

The typical vertical stratigraphic sequence in the SCP includes 2 to 20 m of residual soils at the surface underlain by saprolites and weathered soils (SCDOT 2008). Typically, residual soils consist of clayey soils near the surface, underlain by sandy silts

and silty sands. Saprolites are physically and chemically weathered rocks that can be soft/loose to very hard and dense, and typically retain the structure of the parent rock.

Regarding the seismicity of the SCP, there are four major fault zones identified as potentially active seismic sources. These fault zones are the Brevard, the Towaliga-Middleton-Lowndesville-Kings Mountain, the Goat Rock-Modoc, and the Augusta Shear Zones (Hatcher et al. 1977). Most of these faults zones are thrust faults with strike-slip components, which were mainly formed and active during the Palezoic Era, prior the opening of the Atlantic Ocean (Krinitzsky and Dunbar 1992). Due to the absence of any active faults and a high compressional stress regime, the seismicity in the SCP is due to the interaction of an ambient stress field on pre-existing zones of weakness. The predominant zones of weakness are networks of joints, thus limiting the size of the largest earthquake in the area (Talwani 1986).

Based on Bollinger (1975), the largest recorded earthquake within the SCP occurred in Union County on January 1, 1913, which has a Modified Mercalli Intensity Index (MMI) of VII to VIII. Its magnitude has been estimated to be between 5.0 and 5.5. Geologically the estimated epicenter lies on the Kings Mountain shear zone. Other small intensity earthquakes are also known to have occurred in the SCP. These include the 1971 Oconee county earthquake (MMI = VI), and the 1971 Lake Jocasse earthquake (MMI = VI).

5.2 Seismic Hazard Assessment

The seismic hazards at the centers of sixteen quadrangles making up the four selected areas in the SCP (i.e., Columbia, Greenville, Greenwood, and Rock Hill) are assessed based on the 2008 USGS deaggregation hazard mapping (http://eqint.cr.usgs.gov/deaggint/2008/index.php, accessed December 15, 2012). The seismic hazard in these areas, except Greenville and the western half of Greenwood, is dominated by modal earthquake moment magnitudes (M_w) of about 7.3 for both the SEE and FEE conditions. The seismic hazard for the Greenville area and the western half of the Greenwood area is dominated by earthquakes with M_w = 4.8 and 7.3 for the SEE and FEE conditions, respectively. This indicates that, unlike the SCCP, the seismic hazard in the SCP is influenced by multiple sources, in addition to the Charleston-Summerville seismic source zone.

Presented in Figures 5.2 is a sample deaggregated seismic hazard output from the Rock Hill area. It can be observed that the seismic hazard includes nearer small earthquakes (M_w = 4.5 to 6.0), and farther large earthquakes (M_w = 7.0 to 7.5). Thus, the justification of single dominant seismic source, as assumed for the SCCP in Chapters 3 and 4, does not apply in the western half part of the SCP. To account for multiple seismic source zones, input motions are generated matching the seismic hazard at target frequency values, as will be discussed in Section 5.4.

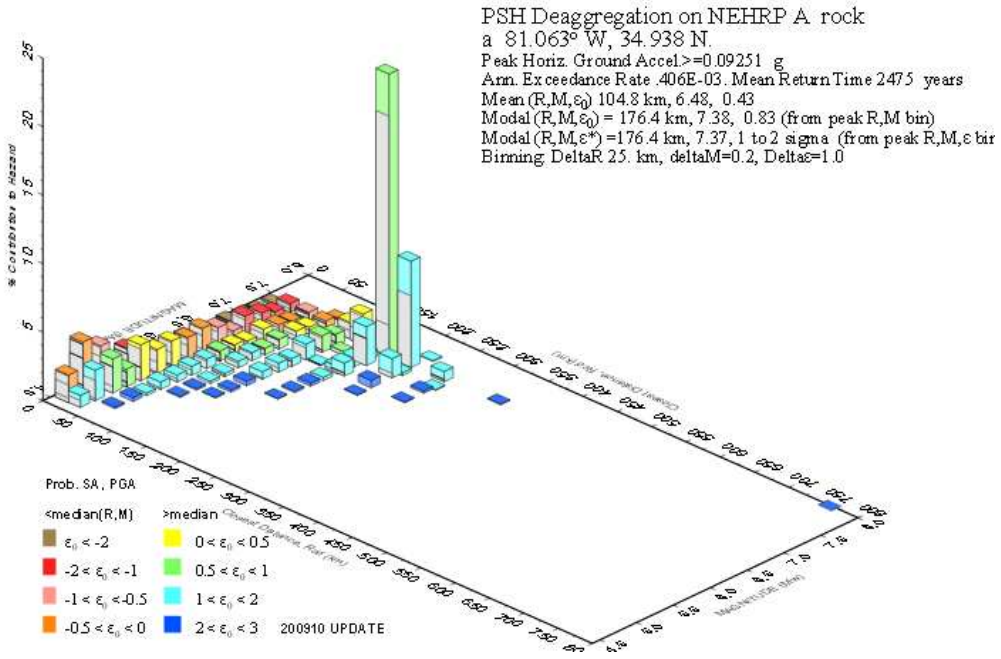

Figure 5.2 Deaggregated seismic hazard on NEHRP Site Class A rock for the Rock Hill West quadrangle (http://eqint.cr.usgs.gov/deaggint/2008/index.php, accessed December 15, 2012).

5.3 Dynamic Soil/Rock Model

Presented in Figure 5.3 are representative V_s profiles assumed in the ground response analyses for the SCP. The reference V_s profile shown in Figure 5.3a is derived by combining V_s profiles measured by/for different consultants (e.g., WPC, S&ME and URS) with the USGS V_s model used by Silva et al. (2003). Mean V_s values range from 273 to 300 m/s in the top 10 m. Between the depths of 10 and 20 m, V_s values vary from 300 to 760 m/s. Between the depths of 20 and 30 m, V_s values vary from 760 to 2,500 m/s. A V_s value of 2,500 m/s is the assumed representative value for the weathered hard rock in SCP.

In addition to the reference V_s profile, fifty-one other V_s profiles are shown in Figure 5.3. These other profiles are derived by applying ±1, -2 and -3 standard deviations of ln(V_s) to the reference profile above the weathered rock half space. Average values of σ of ln(V_s) assumed are 0.32 for the Quaternary material and 0.3 for the saprolites and residual soils. Depths to the weathered hard rock of 50, 30, 20 and 10 m are also assumed, as indicated in Figures 5.3a, 5.3b, 5.3c and 5.3d, respectively.

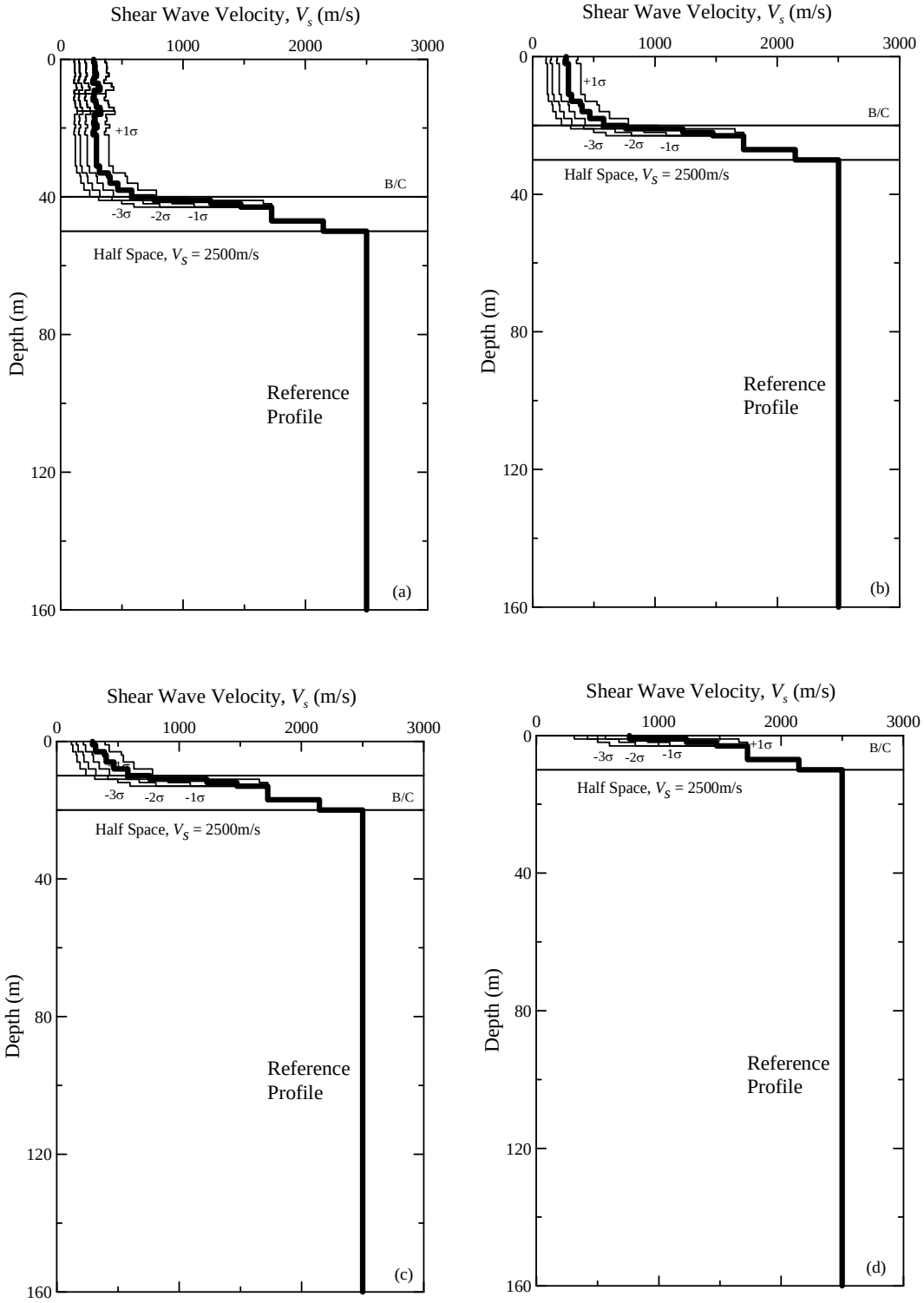

Figure 5.3 Representative profiles of V_s for the SCP with the top of V_s = 2,500 m/s material at depths of (a) 50 m, (b) 30 m, (c) 20 m and (d) 10 m.

Presented in Figure 5.4 and 5.5 are two soil/rock models assumed for determining the variation of normalized shear modulus (G/G_{max}) and material damping ratio (D) with shearing strain amplitude. The soil/rock model in Figure 5.4 contains a 10-m thick residual soil on top of a saprolite layer. Under the saprolite layer is the weathered-rock half space with V_s = 2,500 m/s. The soil/rock model in Figure 5.5 is identical to Figure 5.4 below the depth of 10 m. Above the depth of 10 m in Figure 5.5, properties typical of the Quaternary flood plain material are assumed. The ground water depth is assumed to be 5 m in both models.

Similar to Chapters 3 and 4, the Zhang et al. (2005, 2008) relationships are used to represent the variations in G/G_{max} and D with shearing strain amplitude (γ) in terms of geologic age, mean effective confining pressure, and soil plasticity index. Displayed in Figure 5.6 are sample G/G_{max}-γ and D-γ relationships for the Quaternary, and the residual soil and saprolite layers shown in Figures 5.4 and 5.5. Also used in ground response analysis are the $\pm 1\sigma$ G/G_{max}-γ and D-γ relationships according to Zhang et al. (2008). For the half space with V_{S30} = 2,500 m/s, purely linear relationships of G/G_{max}-γ and D-γ are assumed. This is done by entering G/G_{max} = 1 and D = 0.1% for all γ values. A value of D = 0.1% is taken to be representative for the weathered-rock half space in the SCP (SCDOT 2008), therefore, it is different from the soft-rock damping value assumed in Chapter 3 and 4.

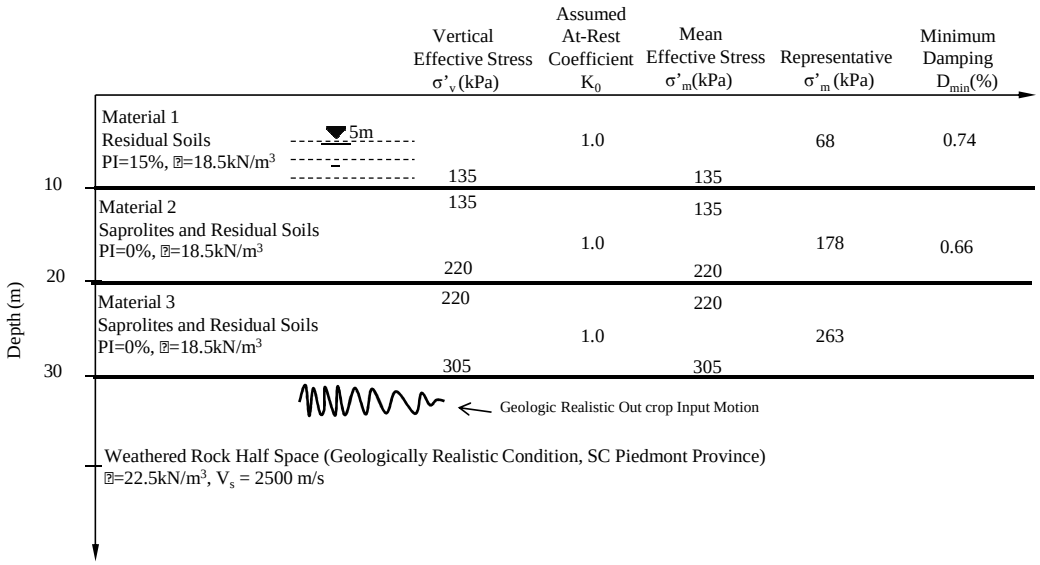

Figure 5.4 Soil/rock model for the Piedmont assuming residual soils over saprolites.

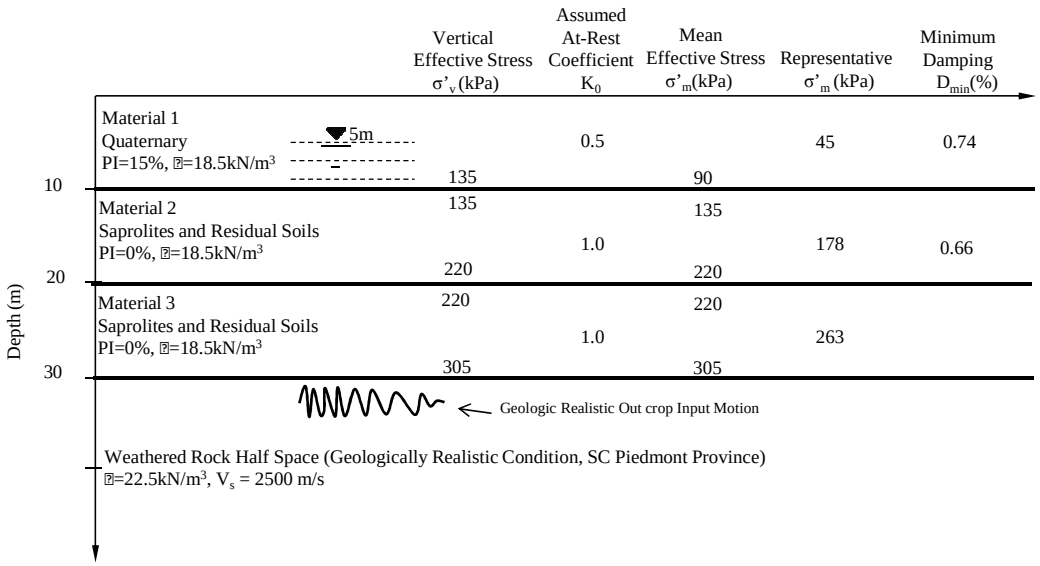

Figure 5.5 Soil/rock model for the Piedmont assuming Quaternary soils over saprolites.

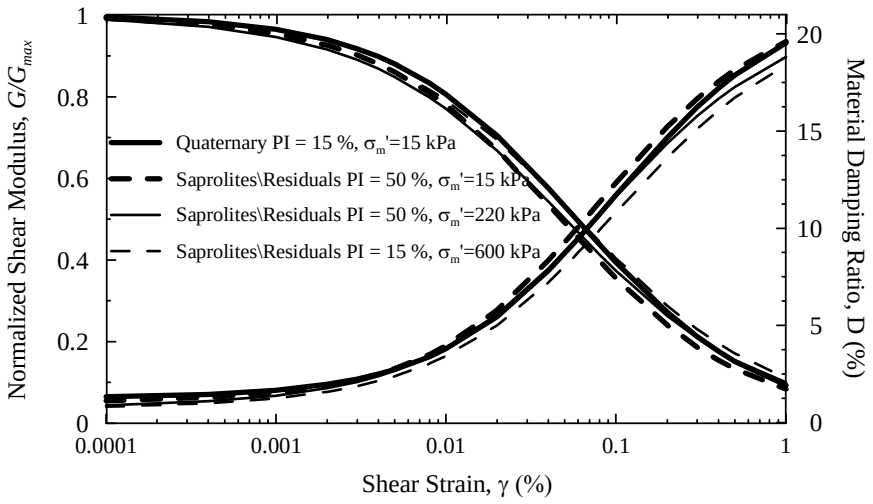

Figure 5.6 Sample mean G/G_{max}-γ and D-γ relationships used in ground response analyses based on Zhang et al. (2005).

5.4 Input Ground Motions

Synthetic ground motions for the SCP are generated using program Scenario_PC, similar to the motions used for the SCCP in Chapters 3 and 4. However, different assumptions are made for the SCP. First, the ‘‘geologic realistic’’ condition defined in Scenario_PC for the SCP consists of a 250 m thick layer of weathered rock (V_s = 2,500 m/s) over a half-space of unweathered hard rock (V_s = 3,500 m/s). Second, ground motions are generated (a) by matching the seismic hazard with the uniform hazard spectrum (UHS) points, and (b) by matching the seismic hazard at target spectral frequency (or periods) points. The latter matching is needed to account for contribution of the seismic hazard from multiple sources. The target spectral periods used are the 0.0, 0.2 and 1 s.

Presented in Figures 5.7-5.10 are sample ground motions for the Rock Hill West, Kirksey, and Columbia North quadrangles for 2 % and 10 % probability of exceedance in 50 years. The motions in Figure 5.7 were generated to match with the UHS points. The motions in Figures 5.8-5.10 were generated to match with the seismic hazard at 0.0, 0.2 and 1 s spectral periods.

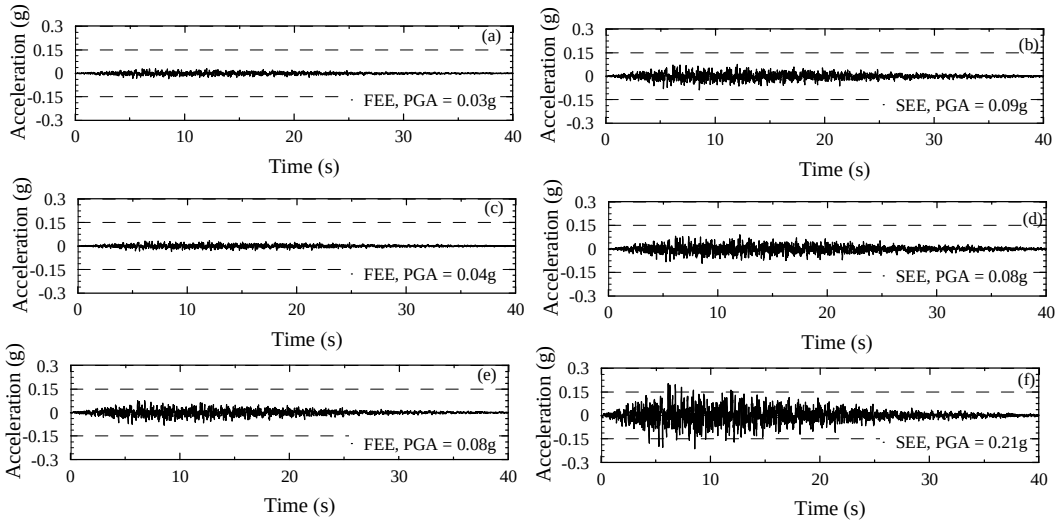

Figure 5.7 Sample synthetic weathered-rock outcrop motions matching the UHS for 10% and 2% probability of exceedance in 50 years for (a-b) Rock Hill West, (c-d) Kirksey, and (e-f) Columbia North quadrangles.

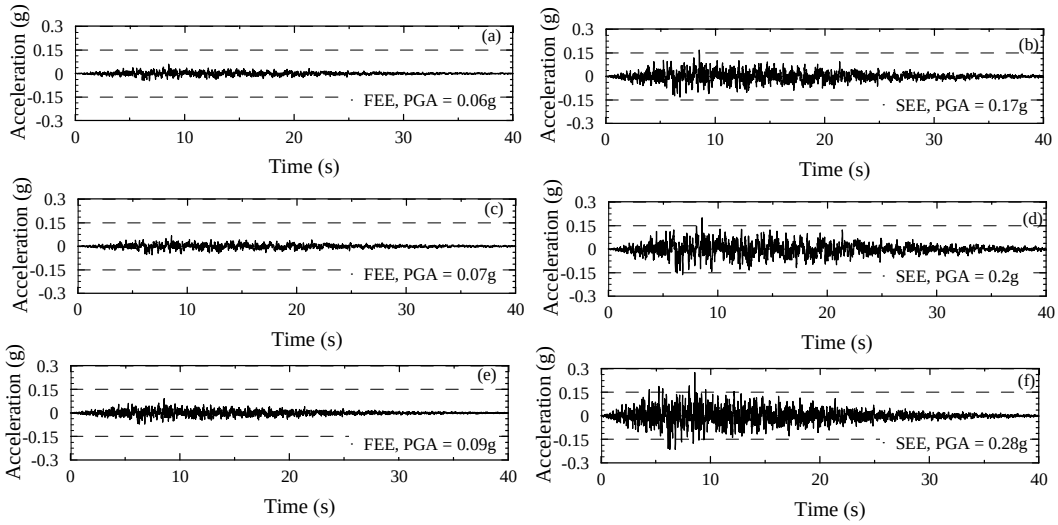

Figure 5.8 Sample synthetic weathered-rock outcrop motions matching the seismic hazard at the PGA or 0.0 s for 10% and 2% probability of exceedance in 50 years for (a-b) Rock Hill West, (c-d) Kirksey, and (e-f) Columbia North quadrangles.

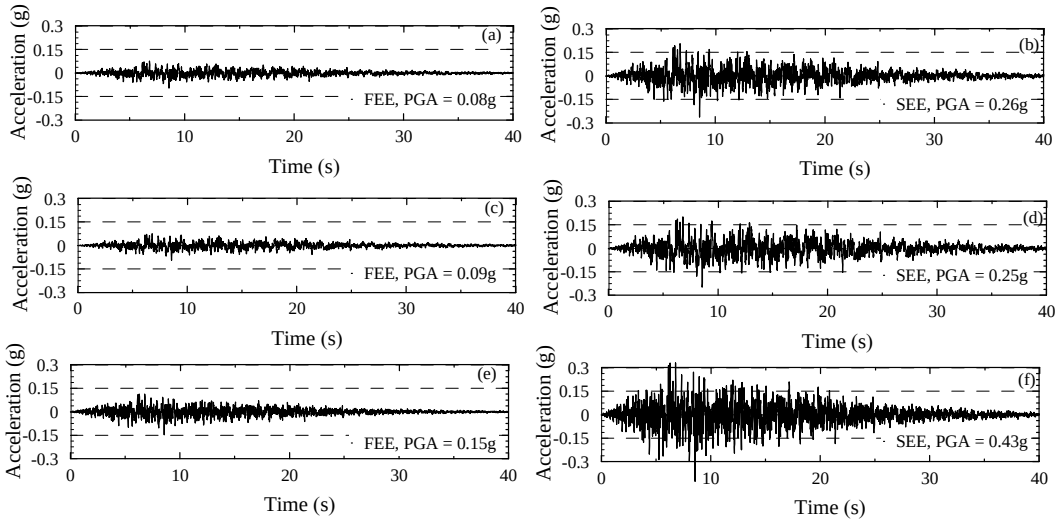

Figure 5.9 Sample synthetic weathered-rock outcrop motions matching the seismic hazard at 0.2 s for 10% and 2% probability of exceedance in 50 years for (a-b) Rock Hill West, (c-d) Kirksey, and (e-f) Columbia North quadrangles.

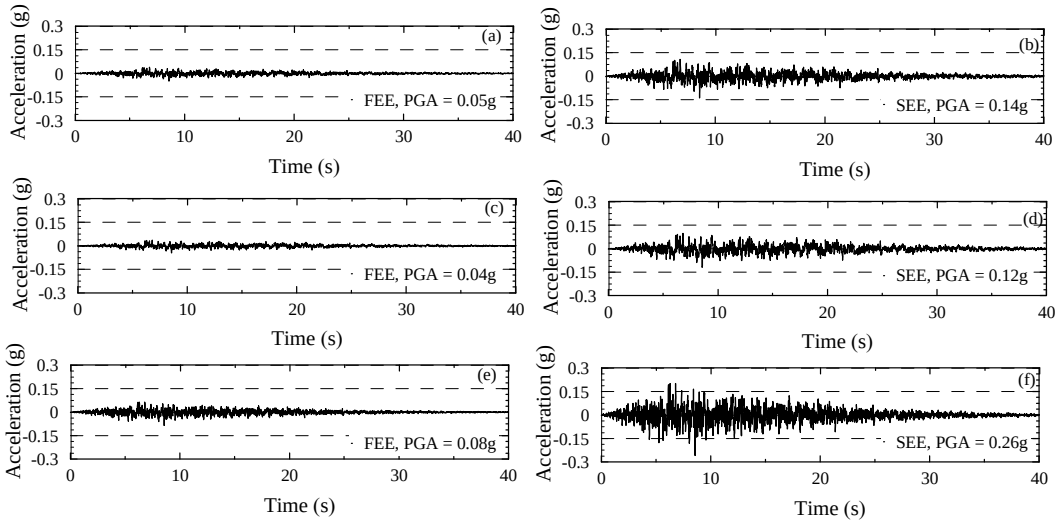

Figure 5.10 Sample synthetic weathered-rock outcrop motions matching the seismic hazard at 1.0 s for 10% and 2% probability of exceedance in 50 years for (a-b) Rock Hill West, (c-d) Kirksey, and (e-f) Columbia North quadrangles.

Compared to the UHS matched motions in Figures 5.7, the peak ground accelerations (*PGA*) of the motions in Figures 5.8 and 5.9 are greater by as much as 3.2. This is because the motions in Figures 5.8 and 5.9 are stronger, on average, at periods closer to the matching spectral periods (0.0 and 0.2 s, respectively). The difference is small for the Columbia area, and for the 1.0 s spectral period matched motions (Figure 5.10). Therefore, to obtain a conservative estimate in the Piedmont, time-histories are needed to be generated at periods of structural significance.

In this study, Figures 5.8, 5.9, and 5.10 are used to compute site coefficients for the SCP, which is decided after the sensitivity analyses presented in Figure 5.11. The analyses are intended to illustrate the effect of different assumptions that can be made in generating time histories for the Greenwood area. The reference V_s profile shown in

Figure 5.3b (i.e., profile with depth to top of V_s = 2,500 m/s material at 30 m), and motions in Figures 5.7-5.10(c-d) are used.

It can be seen in Figure 5.11(a) that the peak spectral acceleration predicted by the SEE and FEE motions occur at about the same spectral periods. As displayed in Figure 5.11(b), the *PGA* matched motion predicts higher accelerations at periods (T) < 0.15 s, and lower accelerations at periods > 0.15 s for the SEE condition. Computed spectral acceleration using the *PGA* matched FEE motion is higher than UHS matched FEE motion by as much as 1.9 times at T = 0.2 s, as shown in Figure 5.11(c). This is because the *PGA* matched motion is rich in amplitudes closer to T = 0.0 s. Compared to the UHS matched motions, the T = 0.2 s matched motions predict significantly greater spectral acceleration as shown in Figures 5.11(d) and 5.11(e). The difference can be as much as 2.6 and 2.1 times at T = 0.2 s and 0.0 s, respectively. As shown in Figure 5.11(f) the predicted spectral acceleration is greater by as much as 1.5 times for the T = 1.0 s matched motions compared to the UHS matched motions. These findings indicate that little (or no) difference between the period contents of the SEE and FEE motions

Presented in Figures 5.12 is the plot of T_m of the input motions used with respect to *R*. The anomaly of T_m at *R* value of about 15 km is for Greenville and part of Greenwood areas for the SEE condition. For the SEE condition, low T_m values were expected for Greenville and part of Greenwood areas, because these areas are dominated by modal M_w of about 4.8. However, this is not the case in Figure 5.12, which indicates that the seismology of the western half part of the SCP is a more complex than the SCCP.

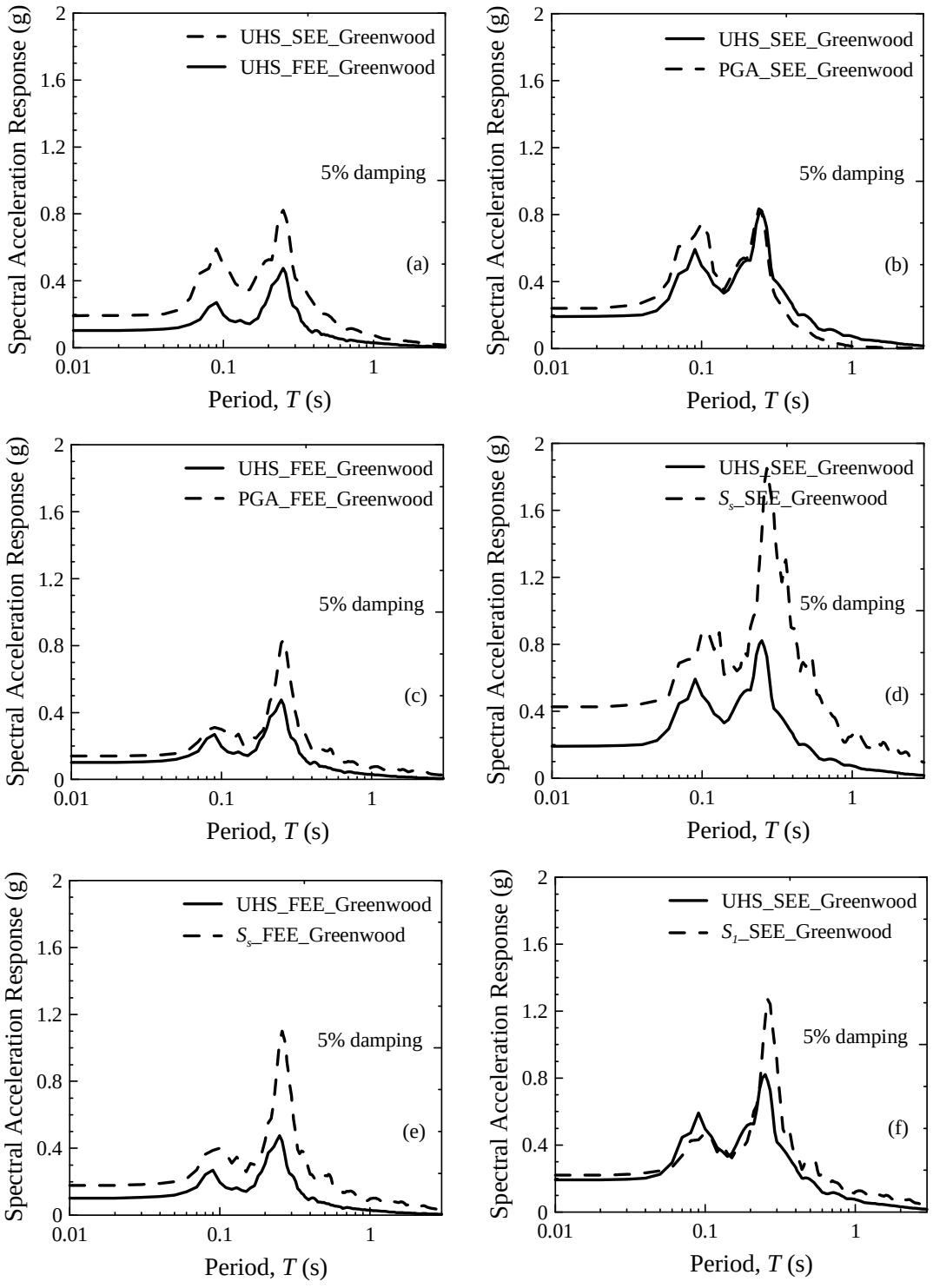

Figure 5.11 Sample sensitivity of spectral acceleration to assumption in input motion generation for the Greenwood area.

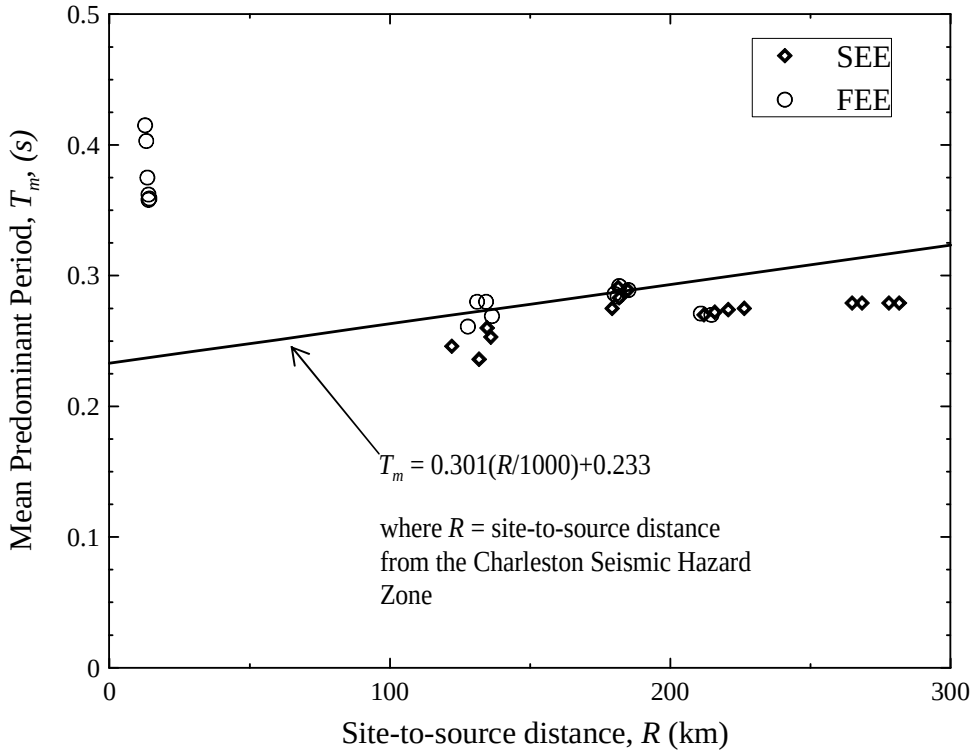

Figure 5.12 T_m of the input motions used versus R.

5.5 Ground Response Analysis

In this chapter, the computer program SHAKE2000 and DMOD2000 were used to perform one-dimensional, total stress ground response analysis. SHAKE2000 was used for all the four locations when $PGA_{outcrop}$ of the soft-rock outcrop motion is ≤ 0.3 g; and D-MOD2000 was used for selected profiles when $PGA_{outcrop}$ is > 0.3 g. For D_MOD2000, the frequency calibration pairs (i.e., viscous damping and an odd integer related to the modes at which target damping is matched) was ξ = 0.5, n = 5.

5.6 Results

Presented in Figures 5.13-5.18 are the site coefficients (i.e., F_{PGA}, F_a, $F_{0.6}$, F_v, $F_{1.6}$ and $F_{3.0}$, respectively) derived from ground response analyses plotted versus V_{S30} assuming the V_s profiles in Figure 5.3b with the weathered hard rock at 30 m. Also presented in Figures 5.12-5.18 are median, 95% bound, and 5% bound curves for the plotted data. Similar to the SCCP, the plotted V_{S30}-F data pairs in Figures 5.13-5.18 exhibit three general features--(1) an increasing trend in F as V_{S30} increases from a very low value; (2) a zone of peak F values, depending on $S_{outcrop}$; and (3) a decreasing trend in F as V_{S30} increases beyond the zone of peak F values.

The derivation of the seismic site coefficient model for the SCP is slightly different from what was proposed for the SCCP in Chapter 4. The difference is due to the assumed reference rock site. The site coefficients derived in this chapter are meant to adjust weathered-hard rock accelerations. The SCCP coefficients were meant to adjust soft-rock accelerations. Modifying the site coefficient model developed for the SCCP, the peak site coefficient within a given plot (F_p) and the corresponding average shear wave velocity in the top 30 m (V_{S30P}) can be estimated by:

$$F_p = \left[x_7 \exp\left(\frac{x_8 S_{outcrop}}{g} \right) \left(\frac{T_m}{T_{100}} \right)^{x_9} + 1 \right] K_{H3} \tag{5.1a}$$

$$V_{S30P} = \left[x_{10} \left(\frac{S_{outcrop}}{g} \right)^{x_{11}} \left(\frac{T_m}{s} \right)^{x_{12}} \right] K_{H4} \tag{5.1b}$$

where x_7, x_8, x_9, x_{10}, x_{11} *and* x_{12} are regression coefficients given in Table 5.1; $S_{outcrop}$ is in units of *g*; *g* is the acceleration of gravity; T_{100} is a proxy variable for the site fundamental period; *s* is one second to normalize T_m; and K_{H3} and K_{H4} are dimensionless adjustment coefficients to account for the influence of depth to the weathered hard rock. Presented in Table 5.2 are range and reference profile values of T_{100} and T_m for the four selected areas in the SCP. Presented in Table 5.3 is the depth to weathered hard rock adjustment coefficients.

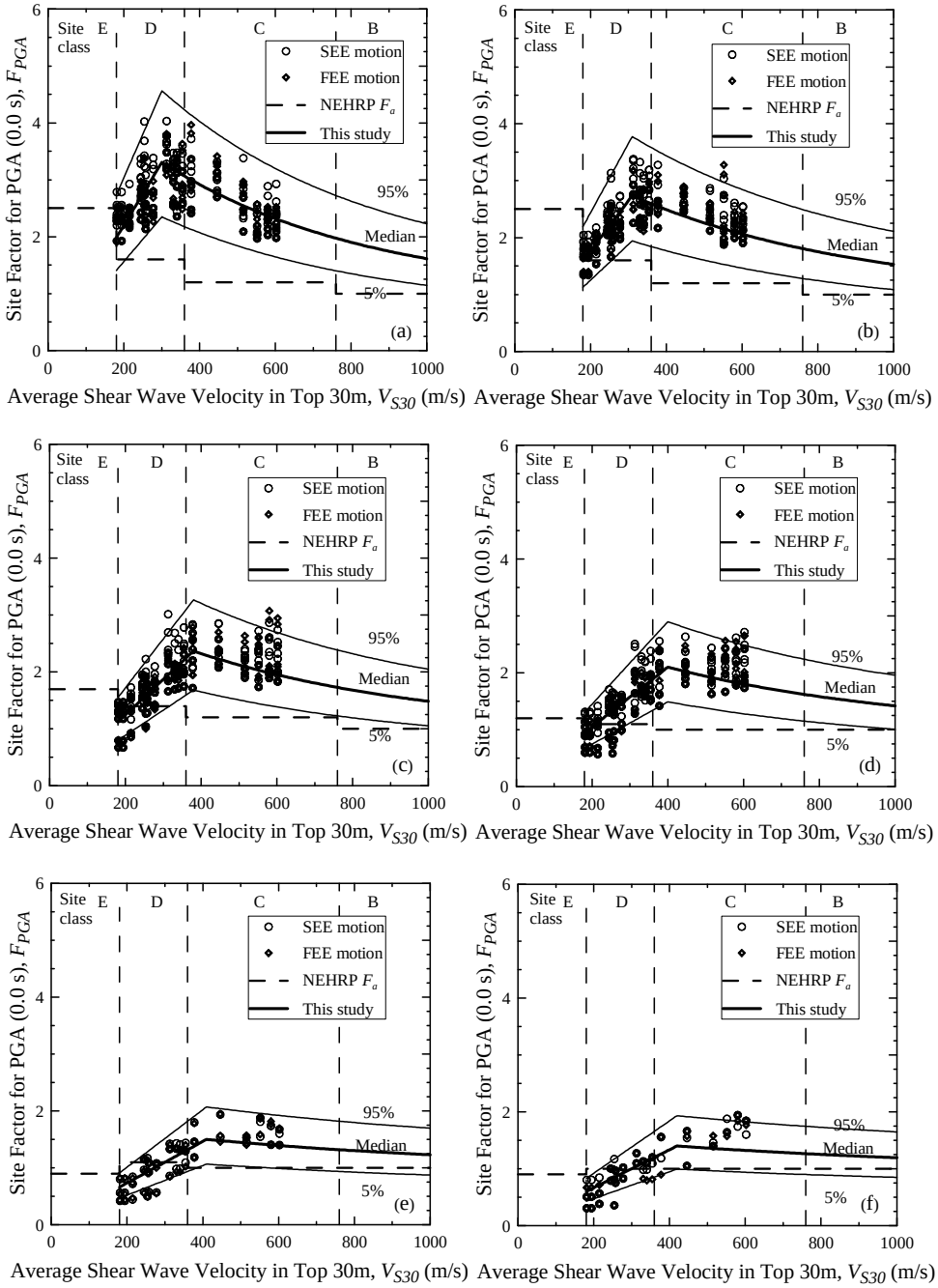

Figure 5.13 Site coefficient for 0.0 s spectral period (free-field) with *PGA* equal to (a) 0.05 g, (b) 0.1 g, (c) 0.2 g, (d) 0.3 g, (e) 0.4 g, and (f) 0.5 g for the SCP with top of V_s = 2,500 m/s at depth of 30 m depth.

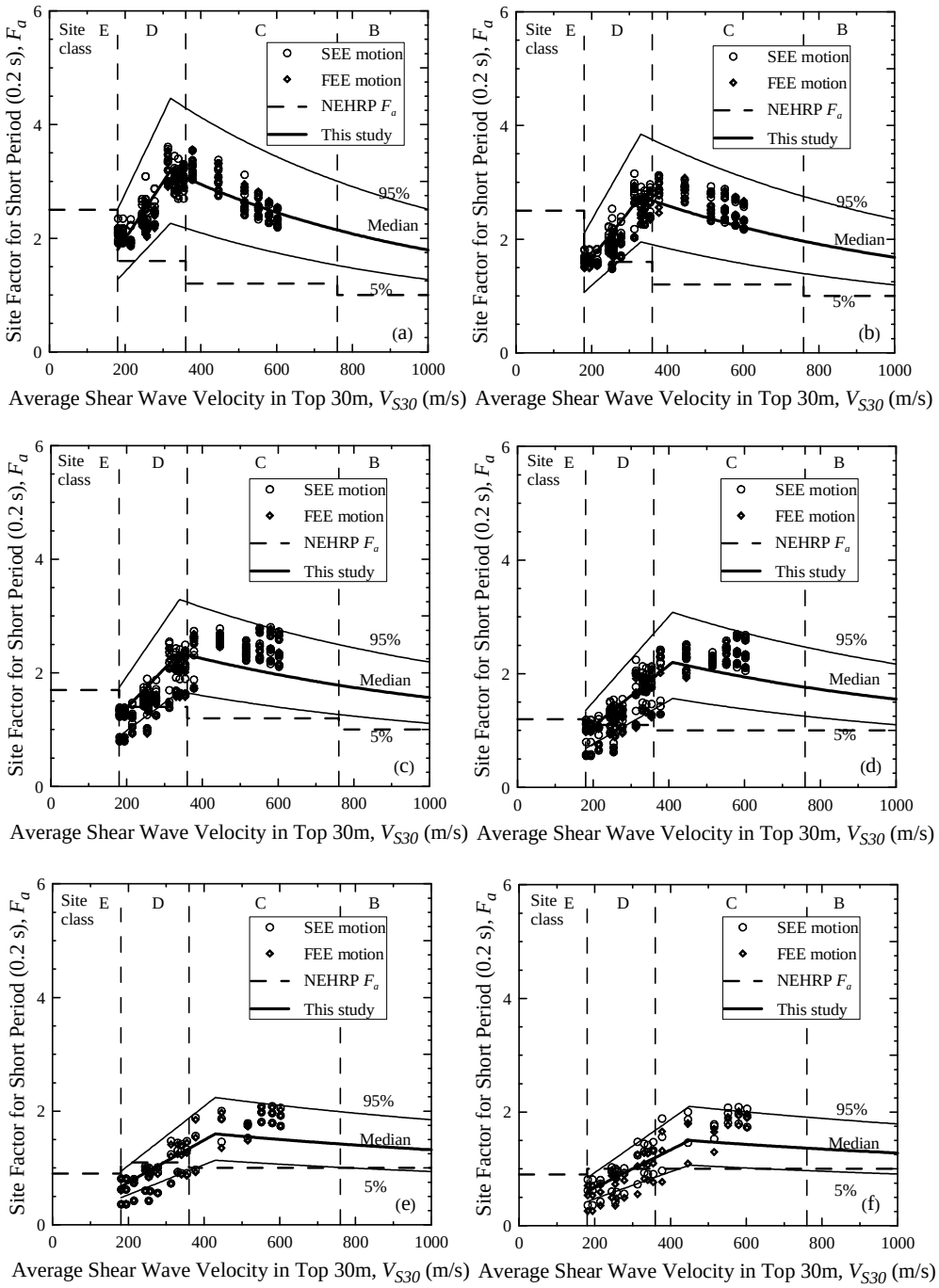

Figure 5.14 Site coefficient for 0.2 s (short) spectral period with S_s equal to (a) 0.125 g, (b) 0.25 g, (c) 0.50 g, (d) 0.75 g, (e) 1.0 g, and (f) 1.25 g for the SCP with top of V_s = 2,500 m/s at depth of 30 m depth.

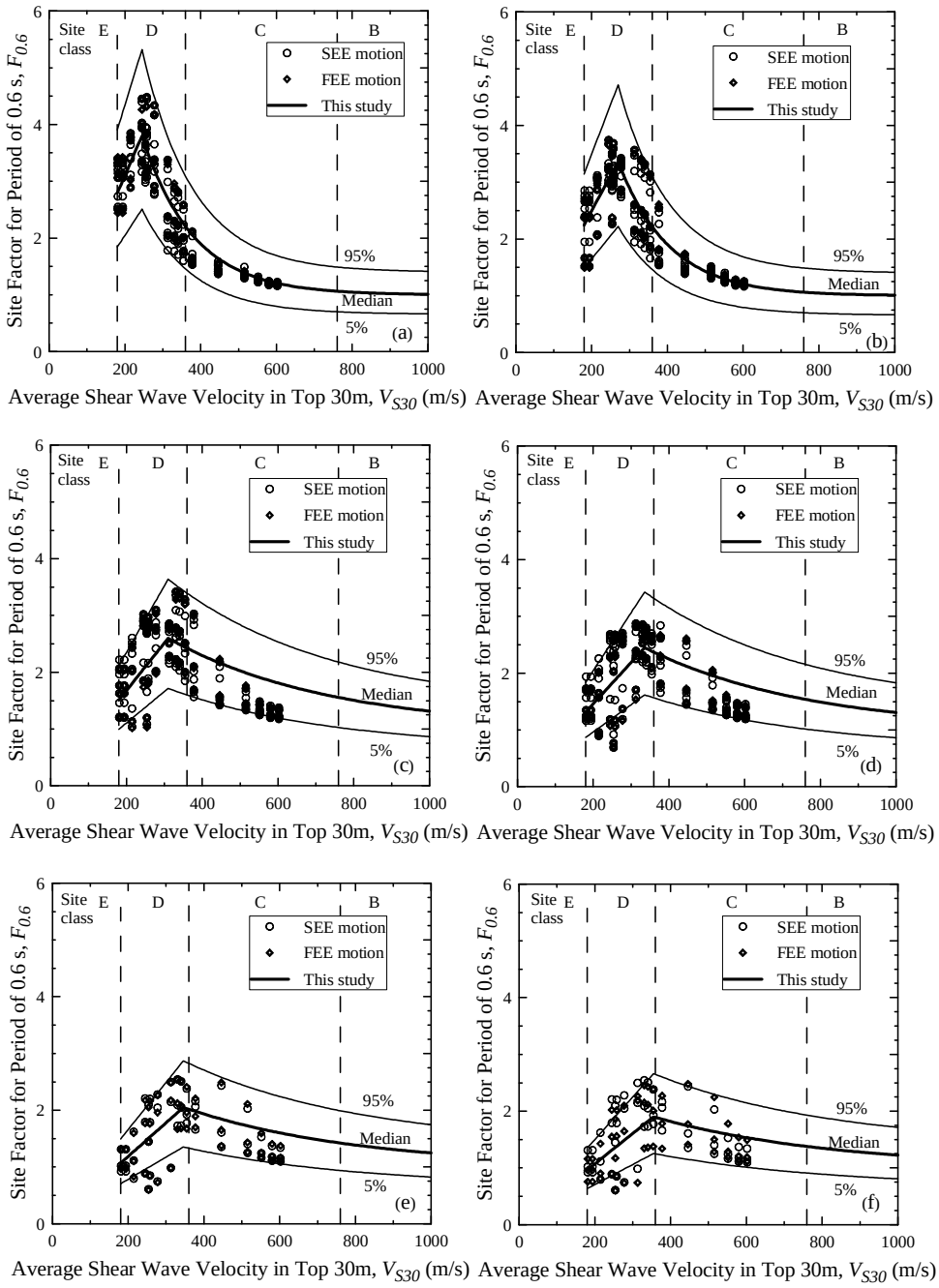

Figure 5.15 Site coefficient for 0.6 s spectral period with $S_{0.6}$ equal to (a) 0.05 g, (b) 0.10g, (c) 0.20 g, (d) 0.30 g, (e) 0.40 g, and (f) 0.50 g for the SCP with top of V_s = 2,500 m/s at depth of 30 m depth.

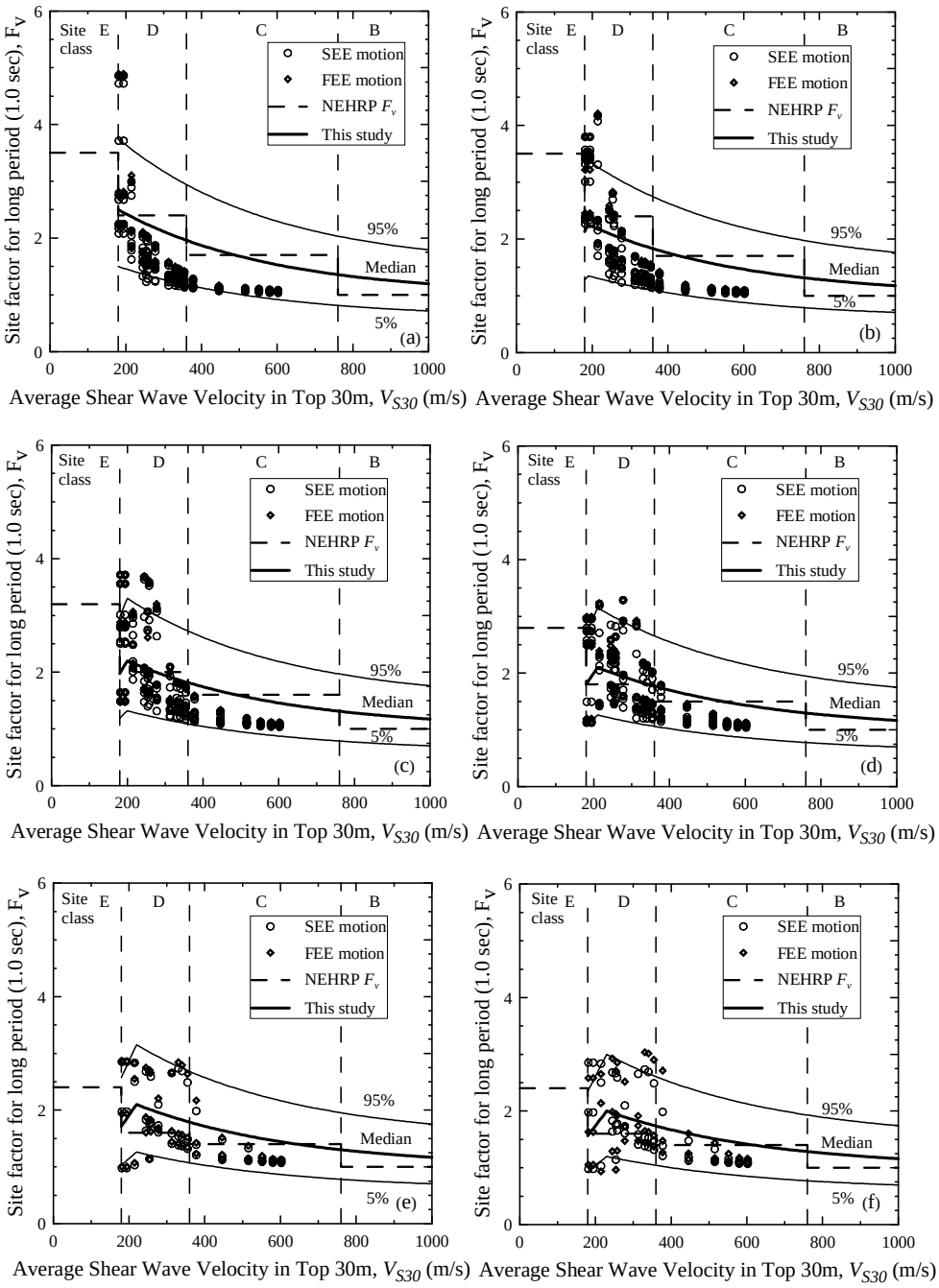

Figure 5.16 Site coefficient for 1.0 s (long) spectral period with S_1 equal to (a) 0.05 g, (b) 0.10 g, (c) 0.20 g, (d) 0.30 g, (e) 0.40 g, and (f) 0.50 g for the SCP with top of V_s = 2,500 m/s at depth of 30 m depth.

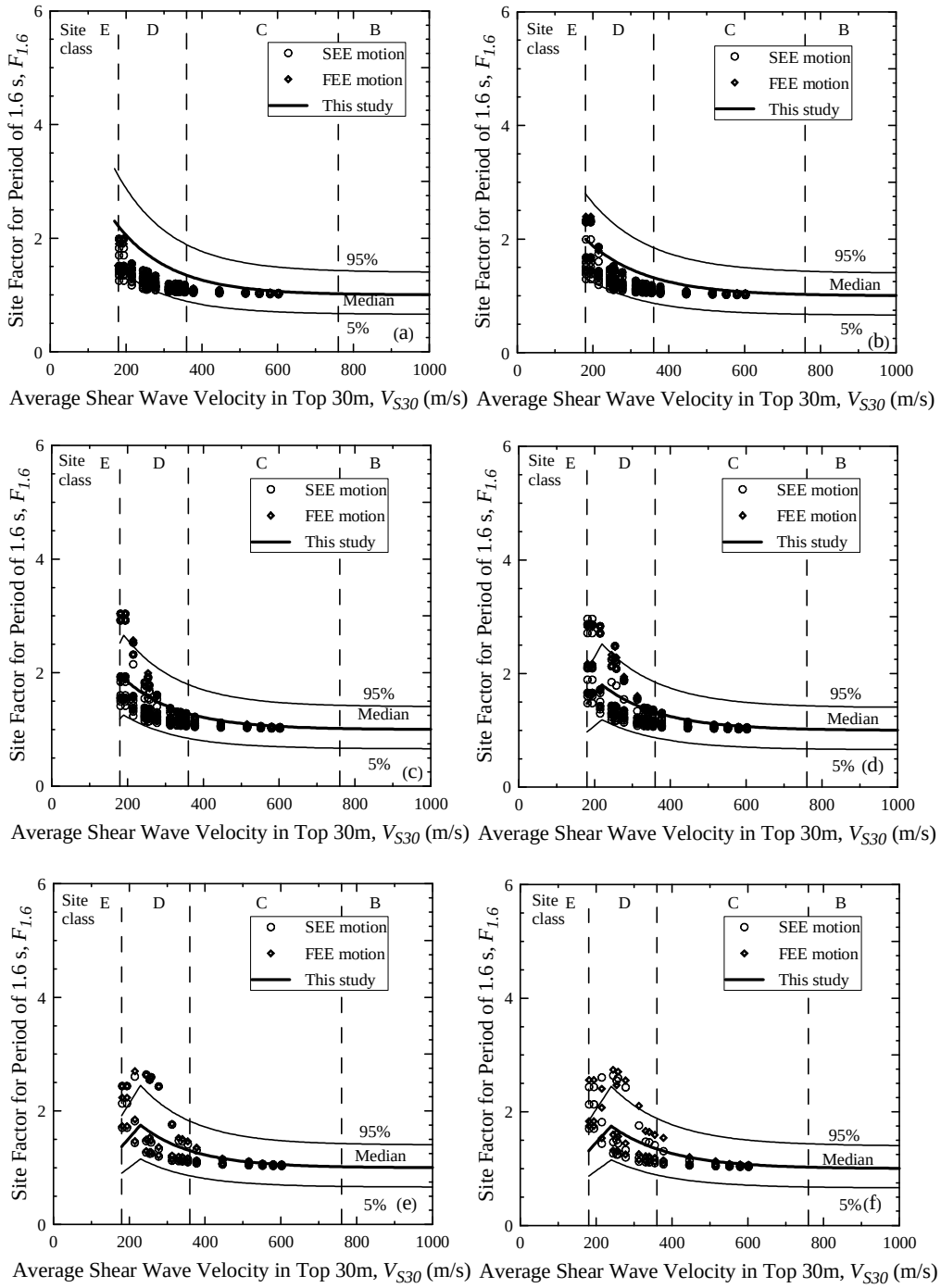

Figure 5.17 Site coefficient for 1.6 s spectral period with $S_{1.6}$ equal to (a) 0.02 g, (b) 0.05 g, (c) 0.1 g, (d) 0.15 g, (e) 0.20 g, and (f) 0.4g for the SCP with top of V_s = 2,500 m/s at depth of 30 m depth.

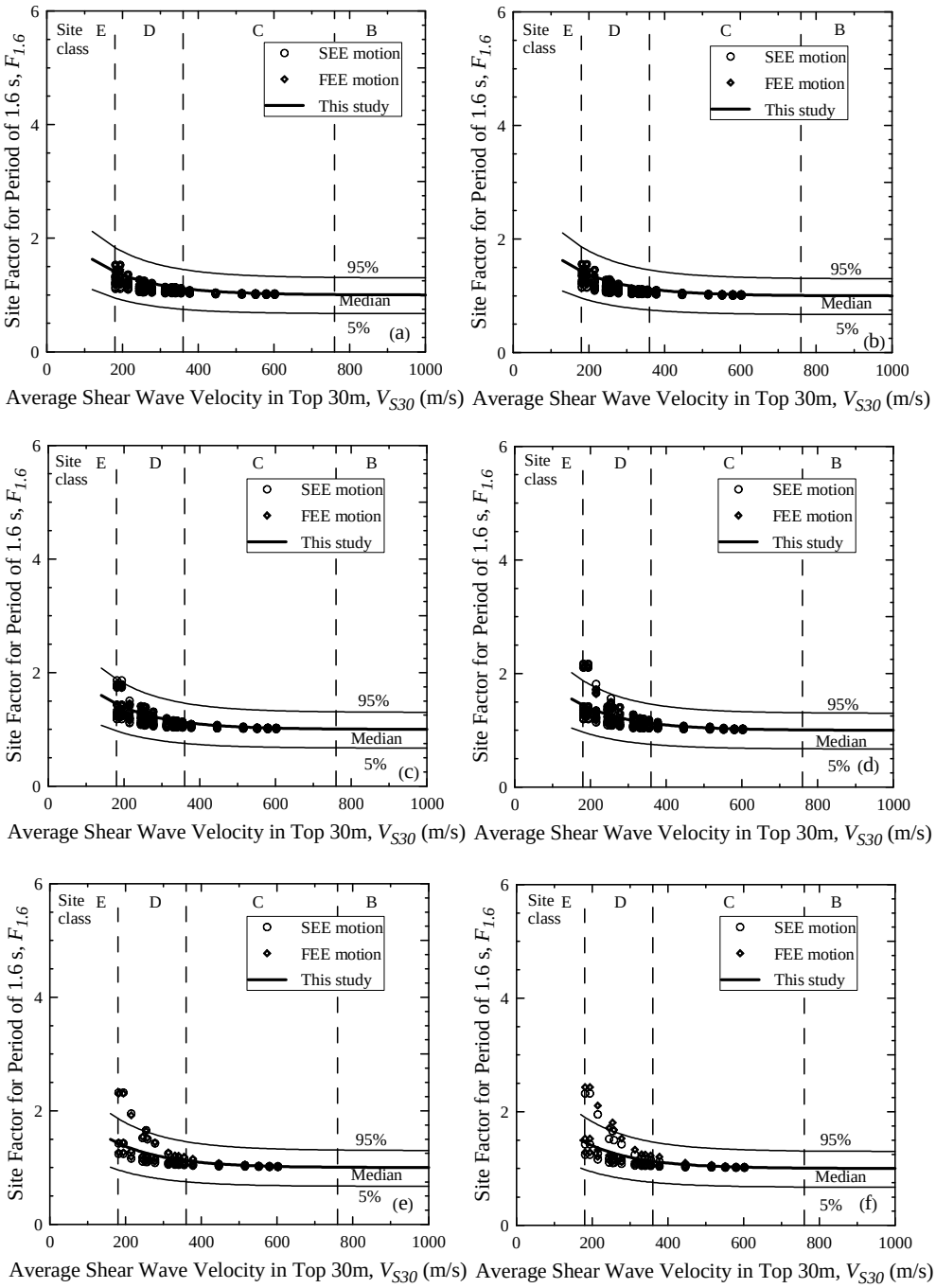

Figure 5.18 Site coefficient for 3.0 s spectral period with $S_{3.0}$ equal to (a) 0.01 g, (b) 0.02 g, (c) 0.04 g, (d) 0.06 g, (e) 0.08 g and (f) 0.12 g for the SCP with top of V_s = 2,500 m/s at depth of 30 m depth.

Table 5.1 Regression coefficients for estimating seismic site coefficients in the SCP.

$S_{outcrop}$	x_7	x_8	x_9	x_{10} (m/s)	x_{11}	x_{12}	a	$Z_{0.05}$	$Z_{0.95}$
PGA	2.861	-4.064	-0.562	606	0.157	0.187	-	0.71	1.38
S_s	2.659	-1.381	-0.657	538	0.162	0.182	0.88	0.71	1.41
$S_{0.6}$	3.245	-2.981	-0.445	538	0.162	0.228	0.98	0.66	1.40
S_1	1.496	-0.912	-0.759	374	0.090	0.333	0.98	0.60	1.50
$S_{1.6}$	1.159	-1.420	-0.003	405	0.153	0.333	0.99	0.66	1.40
$S_{3.0}$	0.712	-5.638	-0.860	212	0.208	-0.036	0.99	0.67	1.30

*For *PGA*, use equation without *a*.

Table 5.2 Typical values of V_{S100}, T_{100}, and T_m for the SCP.

Site	V_{S100} (m/s)		T_{100} (s)		T_m (s)		$\frac{\text{Average } T_m}{\text{Reference } T_{100}}$
	Range	Reference Profile	Range	Reference Profile	Range	Average	
Columbia	1025-1833	1553	0.21-0.39	0.26	0.25-0.28	0.27	1.04
Rock Hill					0.27-0.29	0.28	1.07
Greenwood					0.27-0.42	0.35	1.35
Greenville					0.28-0.38	0.33	1.27

Table 5.3 Depth to weathered-hard rock adjustment coefficients.

$S_{outcrop}$	Adjustment coefficient	Depth to soft rock, H_{HR} (m)						
		5	10	20	30	40	50	100
PGA	K_{H3}	0.33	0.35	1.00	1.00	0.94	0.88	0.58
	K_{H4}	7.83	7.33	1.67	1.00	0.97	0.93	0.77
Ss	K_{H3}	0.33	0.34	1.13	1.00	0.92	0.84	0.45
	K_{H4}	7.03	6.25	1.41	1.00	0.97	0.94	0.78
$S_{0.6}$	K_{H3}	0.27	0.29	0.58	1.00	1.03	1.05	1.18
	K_{H4}	9.69	9.39	2.86	1.00	0.97	0.94	0.79
S_1	K_{H3}	0.35	0.33	0.43	1.00	1.17	1.33	2.17
	K_{H4}	12.63	12.11	3.79	1.00	0.95	0.89	0.63
$S_{1.6}$	K_{H3}	0.59	0.59	0.76	1.00	1.01	1.03	1.10
	K_{H4}	12.00	11.00	3.60	1.00	0.95	0.90	0.65
S_3	K_{H3}	0.76	0.76	0.91	1.00	1.02	1.03	1.11
	K_{H4}	13.16	11.58	3.79	1.00	0.89	0.79	0.26

Presented in Figure 5.19 is a sample residual plot of F_P versus the predicting variables in Equation 5.1a, $S_{outcrop}$ and T_m/T_{100}, for short-period spectral acceleration and depth to weathered-hard rock equals 30 m. The residual, ε, is defined here as F_P of the plotted data minus F_P obtained from Equation 5.1a. The mean values of ε are computed to be about zero, suggesting the central tendency of the predicting Equation 5.1a. Equation 5.1a gives an unbiased prediction of F_P, because the ε data do not exhibit a systematic pattern with $S_{outcrop}$ and T_m/T_{100}.

Plotted in Figure 5.20 is a sample residual plot of V_{S30P} versus the predicting variables, $S_{outcrop}$ and T_m for short-period spectral acceleration and depth to weathered-hard rock equals 30 m. The residual, ε, is defined here as V_{S30P} of the plotted data minus

V_{S30P} obtained from Equation 5.1b. Similar to Figure 5.19, the mean values of ε plotted in Figure 5.20 are scattered about zero, and the ε data do not exhibit a systematic pattern with $S_{outcrop}$ and T_m.

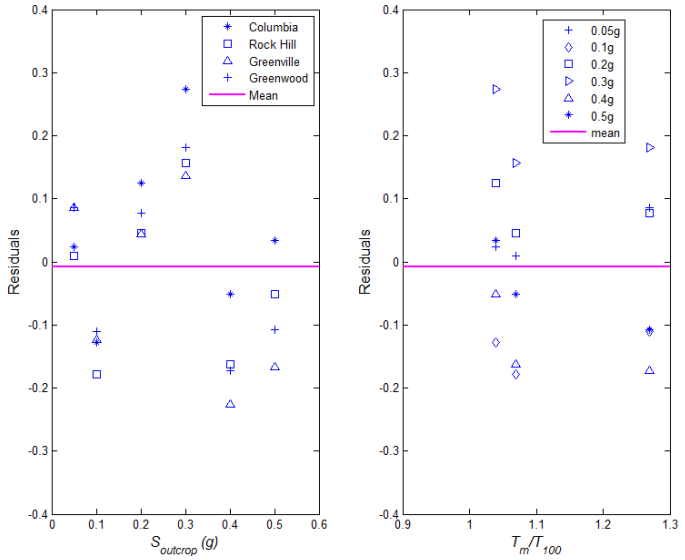

Figure 5.19 Residual plots of F_P versus $S_{outcrop}$ and T_m/T_{100}.

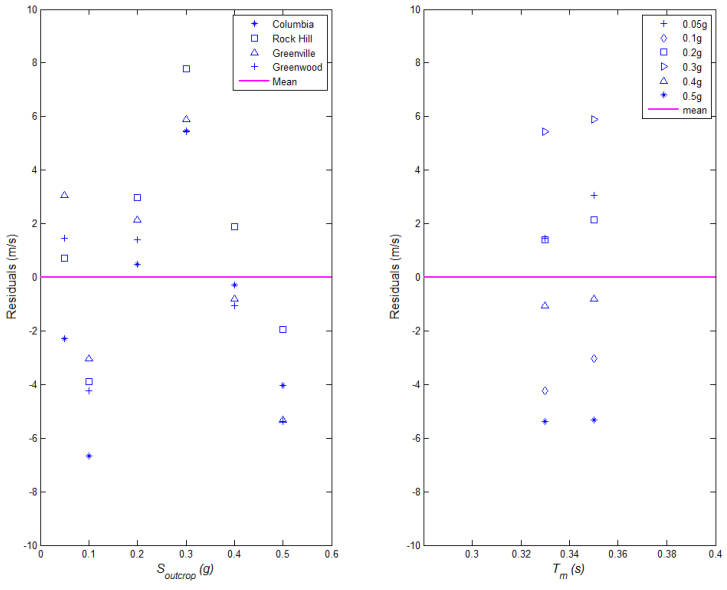

Figure 5.20 Residual plots of V_{S30P} versus $S_{outcrop}$ and T_m.

Plotted in Figure 5.21 are computed values of F_{PGA} for $PGA_{outcrop}$ = 0.05 g, and H_{HR} = 50, 30, 20, and 10 m. It can be seen from Figure 5.21 that V_{S30P} increases with decreasing H_{HR}, and maximum amplification occurs when H_{HR} is somewhere between 50 and 30 m. This is confirmed by computed T_m/T_{100} values using reference profiles with H_{HR} = 50, 30, 20, and 10 m. The T_m/T_{100} values are 0.49, 1.18, 1.21 and 1.44, when H_{HR} = 50, 30, 20, and 10 m, respectively. This confirms that matching between T_m and T_{100} occurs when H_{HR} is between 50 and 30 m.

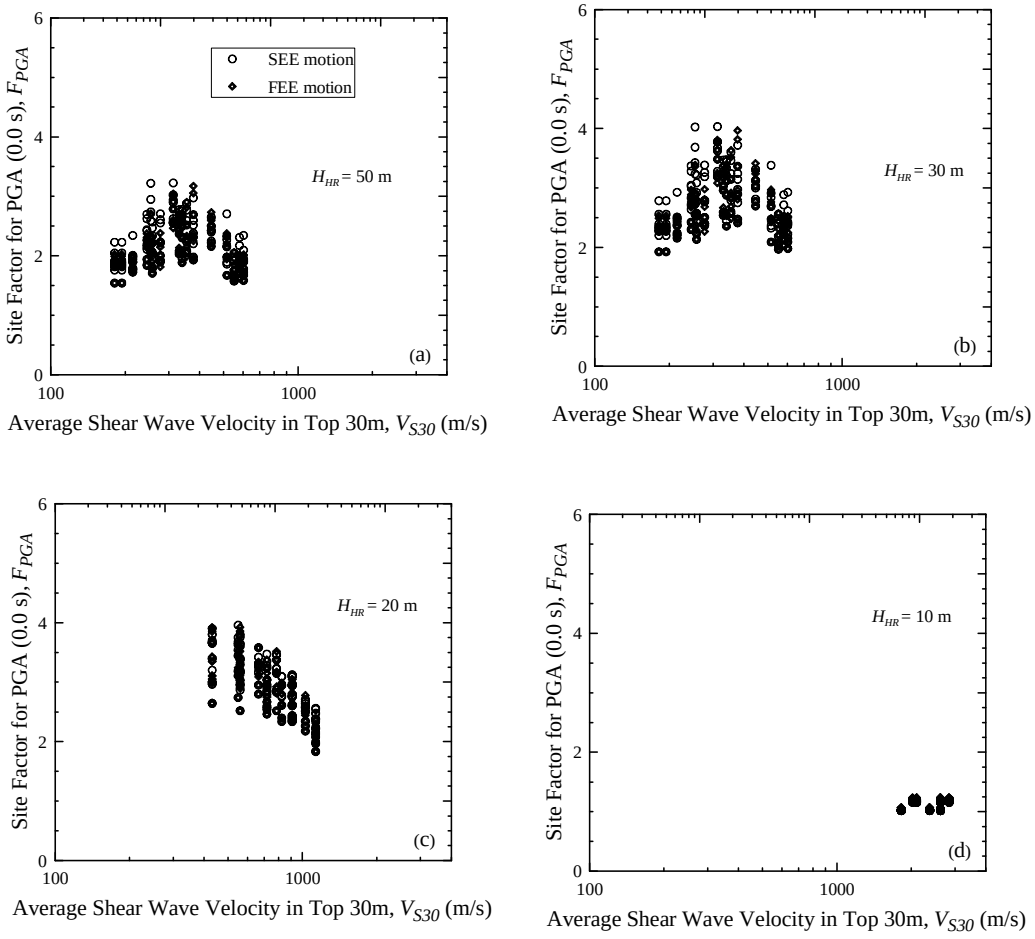

Figure 5.21 Computed F_{PGA} for $PGA_{outcrop}$ = 0.05 g and depth to weathered hard-rock (H_{HR}) of (a) 50 m, (b) 30 m, and (c) 10 m.

With the estimates of F_P and V_{S30P} from Equation 5.1a and 5.1b, the median V_{S30}-F relationships of the plots shown in Figures 5.13-5.18 can be expressed as follows:

$$F = \left(\frac{F_P}{V_{S30P}} \right) V_{S30} \qquad \text{for } V_{S30} < V_{S30P} \text{ and all spectral periods } T \tag{5.2}$$

$$F = \frac{\left(F_p - 1\right)\left(2500 - V_{S30}\right)}{2500 - V_{S30P}} + 1 \qquad \text{for } V_{S30} \geq V_{S30P} \text{ and } T < 0.2\ s \tag{5.3a}$$

$$F = a + b\, \mathrm{e}^{cV_{S30}} \qquad \text{for } V_{S30} \geq V_{S30P} \text{ and } T \geq 0.2\ s \tag{5.3b}$$

where a is a regression coefficient given in Table 5.1; and b and c are coefficients calculated from:

$$b = \frac{1 - a}{e^{2500c}} \tag{5.4}$$

$$c = \frac{\ln\left(\frac{1 - a}{F_p - a} \right)}{2500 - V_{S30P}} \tag{5.5}$$

Equation 5.2 is a linear relationship, and assumes F = 0 when V_{S30} = 0 m/s. Equations 5.3a and 5.3b are linear and exponential relationships, respectively; and satisfy the assumed reference soft-rock outcrop condition of F = 1.0 when V_{S30} = 2,500 m/s. Both Equations 5.2 and 5.3 provide the same value of F at V_{S30P}.

5.7 Recommended Site Coefficients

Maximum computed median F_{PGA} values range from 1.5 to 3.3, as shown in Figure 5.13. The computed median F_{PGA} values are significantly greater than the NEHRP F_a values for all values of $S_{outcrop}$. The difference is significant for Site Class C and D, and can be as much as 2.2 times. As shown in Figure 5.14, the maximum computed median F_a values range from 1.5 to 3.25. The computed median F_a values are greater than the NEHRP F_a values by as much as 2.0 times. Thus, the use of the NEHRP F_a values to adjust short-period accelerations ($PGA_{outcrop}$ and S_s) in the SCP is very unconservative. For the Site Class E, the NEHRP F_a values generally agree with the computed values.

Concerning F_v, the maximum computed median value can be between 1.8 and 2.6, as shown in Figure 5.15. Maximum computed F_v occurs at D-sites with V_{S30} between 180 and 250 m/s. Compared to the NEHRP F_v, the computed values are slightly higher when $S_1 > 0.2$ g.

5.8 Summary

A seismic ground response study based on conditions in the South Carolina Piedmont (SCP) was presented in this Chapter. Soil/rock and seismic conditions typical of four locations within the SCP (i.e., Columbia, Rock Hill, Greenville, and Greenwood) were considered. Because the seismic hazard in the SCP is dominated by multiple seismic sources, time-histories generated by matching target frequencies provided better results compared to time-histories generated by matching the uniform hazard spectra points.

Over 10,000 total stress, one-dimensional equivalent linear and nonlinear ground response analyses were used to derive a model for estimating seismic site coefficients in the SCP. Proxy variables used were: V_{S30}, spectral acceleration (amplitude), mean predominant period of the input motion (T_m), approximate fundamental frequency of soil/rock column in the top 100 m (T_{100}), and depth to weathered-hard rock (H_{HR}). The model was expressed by a linear relationship for $V_{S30} < V_{S30P}$ and a linear or exponential relationship for $V_{S30} \geq V_{S30P}$. Adjustment coefficients for H_{HR} were also proposed. It was found that maximum amplification occurs when H_{HR} is somewhere between 30 and 50 m. The procedure for applying the seismic site coefficient model is summarized in the flow chart presented in Figure 5.22.

Maximum computed median F_{PGA}, F_a and F_v were found to be 3.3, 3.25 and 2.6, respectively. The computed F_{PGA} and F_a were found to be significantly greater than the NEHRP F_a for Site Class C and D. The computed F_v values also plotted slightly above the NEHRP F_v value. Thus, the use of the NEHRP F_a and F_v in the SCP is unjustified.

The seismic site coefficient model developed in this chapter is recommended for constructing ADRS curves in the SCP. However, it should be used exclusively used for adjusting weathered hard rock outcropping spectral accelerations. The coefficients derived in this chapter should not be used to adjust soft-rock (B-C boundary) accelerations.

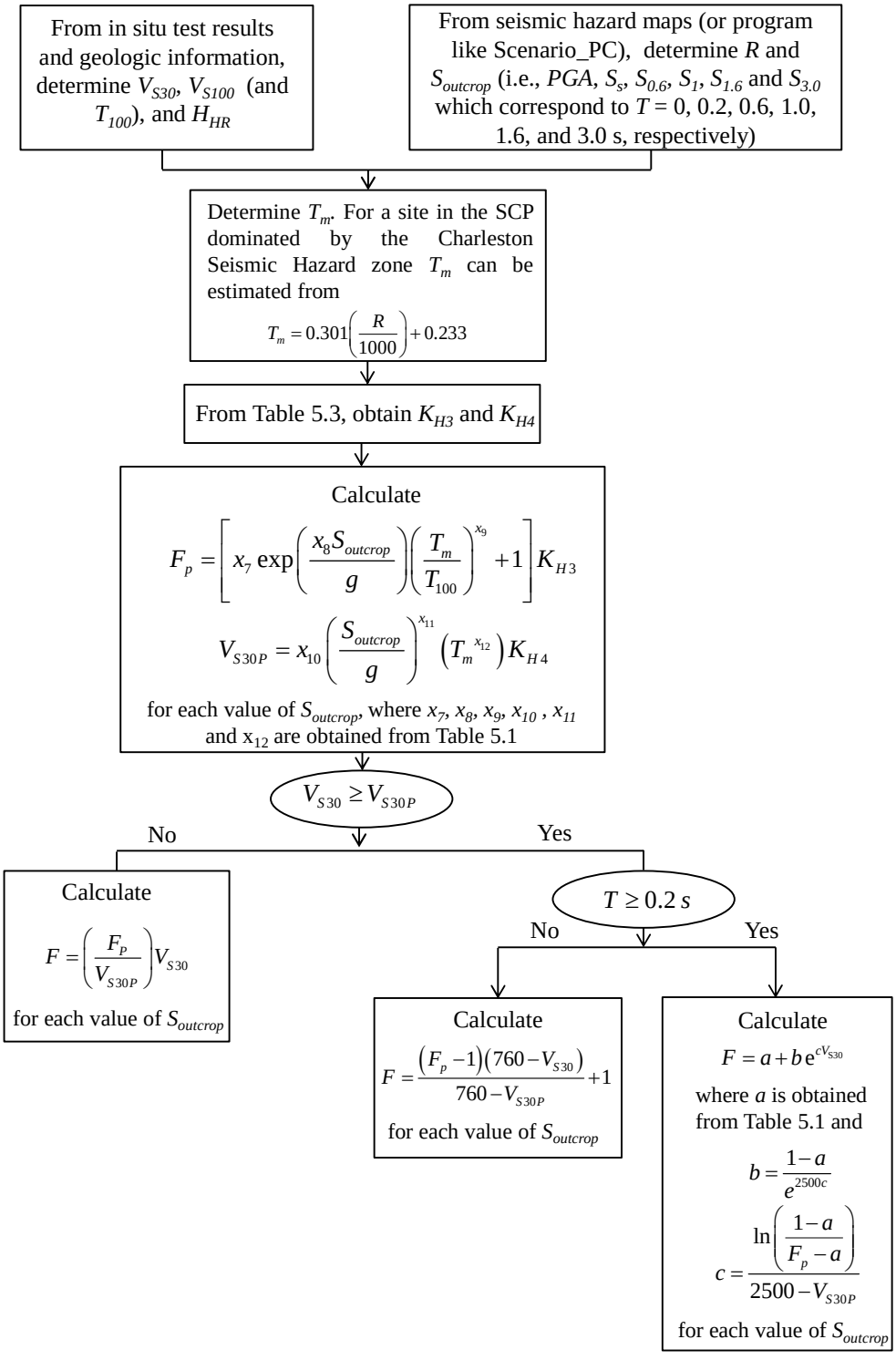

Figure 5.22 Flow chart of obtaining site coefficients and constructing ADRS curve for conditions in the SCP.

CHAPTER SIX

IMPROVED PROCEDURE FOR CONSTRUCTING ACCELERATION DESIGN RESPONSE SPECTRUM

6.1 Introduction

Summarized in this chapter are recommended procedures for constructing the horizontal acceleration design response spectrum (ADRS) to improve Chapter 12 of SCDOT (2008). The procedures are based on results presented in Chapters 4 and 5. Presented in Chapter 4 were results of ground response analysis from seven areas in the SCCP (i.e., Charleston, Savannah, Myrtle Beach, Columbia, Florence, Lake Marion, and Aiken). Presented in Chapter 5 were results of ground response analysis from four areas in the SC Piedmont (i.e., Columbia, Greenwood, Rock Hill, and Greenville). Tabulated site coefficients recommended in SCDOT (2008) are compared with maximum median site coefficients within a seismic site class derived for the SCCP and SC Piedmont. The maximum median values within site classes are presented for a conservative comparison.

6.2 Local Site Effect on PGA

In SCDOT (2008), the local site peak horizontal ground surface acceleration (i.e., free-field or spectral period T = 0 s) is determined by adjusting the mapped rock peak horizontal ground surface acceleration using the following equation:

$$PGA = F_{PGA} \times PGA_{outcrop} \tag{6.1}$$

where PGA is the peak horizontal ground acceleration at the site ground surface adjusted for local conditions; $PGA_{outcrop}$ is the mapped rock peak horizontal ground acceleration obtained from the SC Seismic Hazard maps for the appropriate design earthquake (i.e., Functional Evaluation Earthquake, FEE, or Safety Evaluation Earthquake, SEE); and F_{PGA} is the site coefficient based on the site class and mapped $PGA_{outcrop}$.

Presented in Table 6.1 are F_{PGA} values recommended in SCDOT (2008). The selection of these F_{PGA} values for design is based solely on seismic site class (i.e., A, B, C, D, E, and F) and $PGA_{outcrop}$.

Presented in Tables 6.2-6.5 are computed maximum median F_{PGA} values within a site class derived in Chapter 4 for four selected areas in the SCCP: (1) Charleston (2) Myrtle Beach, (3) Columbia, and (4) Aiken, respectively. The tabulated site coefficients for Site Classes C, D and E in the SCCP are for six different depths to the B-C boundary ($H_{B\text{-}C}$ = 5, 10, 20, 30, 50, and ≥ 100 m). It can be seen from Tables 6.2-6.5 that the F_{PGA} values derived in this study are sometimes much greater than the values recommended in SCDOT (2008).

Presented in Tables 6.6 are computed maximum median F_{PGA} values within a site class derived in Chapter 5 for SC Piedmont area. The tabulated site coefficients for Site Classes C, D and E in the Piedmont are for six different depths to material with V_S = 2,500 m/s (H_{HR} = 5, 10, 15, 20, 30, and ≥ 50 m).

It is important to note that when using Tables 6.2-6.5, $PGA_{outcrop}$ is for B-C boundary condition ($PGA_{B\text{-}C}$); and when using Table 6.6, $PGA_{outcrop}$ is for weathered hard rock condition (PGA_{HR}).

Table 6.1 F_{PGA} as a Function of Site Class and Mapped $PGA_{B\text{-}C}$ SCDOT (2008).

Site Class	Peak Horizontal Ground Acceleration[(1)], $PGA_{B\text{-}C}$ (Period = 0.0 s)				
	≤ 0.10 g	0.20 g	0.30 g	0.40 g	≥ 0.50 g
A	0.8	0.8	0.8	0.8	0.8
B	1.0	1.0	1.0	1.0	1.0
C	1.2	1.2	1.1	1.0	1.0
D	1.6	1.4	1.2	1.1	1.0
E	2.5	1.7	1.2	0.9	0.9
F[(2)]	N/A	N/A	N/A	N/A	N/A

[(1)]Use linear interpolation for intermediate values of $PGA_{B\text{-}C}$.
[(2)]Site-specific response analysis shall be performed.

Table 6.2 Maximum Median F_{PGA} as a Function of Site Class and $PGA_{B\text{-}C}$ Derived in this Study for Charleston.

Site Class	$H_{B\text{-}C}$, m	Peak Ground Acceleration[1] $PGA_{B\text{-}C}$ (Period = 0.0 s)					
		≤ 0.05 g	0.1 g	0.2 g	0.3 g	0.4 g	≥ 0.5 g
A[2]	-	-	-	-	-	-	-
B	0	1.0	1.0	1.0	1.0	1.0	1.0
C	5	3.2	2.9	2.4	2.1	1.9	1.8
	10	2.7	2.6	2.2	1.9	1.7	1.6
	20	2.2	2.1	1.8	1.7	1.5	1.4
	30	2.0	1.9	1.7	1.5	1.4	1.3
	50	1.8	1.7	1.5	1.3	1.2	1.2
	≥100	1.8	1.6	1.4	1.3	1.2	1.1
D	5	3.1	2.4	1.7	1.4	1.1	1.0
	10	2.9	2.6	1.9	1.5	1.3	1.2
	20	2.6	2.3	1.9	1.7	1.5	1.4
	30	2.4	2.2	1.8	1.6	1.4	1.3
	50	2.1	1.9	1.6	1.4	1.3	1.2
	≥100	2.1	1.9	1.6	1.4	1.2	1.2
E	5	1.5	1.2	0.8	0.7	0.6	0.5
	10	1.8	1.4	1.0	0.8	0.7	0.6
	20	2.1	1.6	1.1	0.9	0.8	0.7
	30	2.1	1.6	1.1	0.9	0.8	0.7
	50	2.1	1.6	1.1	0.9	0.8	0.7
	≥100	2.1	1.6	1.2	0.9	0.8	0.7
F[3]	N/A	N/A	N/A	N/A	N/A	N/A	N/A

[1]Use linear interpolation for intermediate values of $PGA_{B\text{-}C}$.
[2]Site-specific response analysis shall be performed.
[3]Site Class A not presented in the Charleston area. No response analysis performed.

Table 6.3 Maximum Median F_{PGA} as a Function of Site Class and $PGA_{B\text{-}C}$ Derived in this Study for Myrtle Beach.

Site Class	$H_{B\text{-}C}$, m	Peak Ground Acceleration[(1)] $PGA_{B\text{-}C}$ (Period = 0.0 s)					
		≤ 0.05 g	0.1 g	0.2 g	0.3 g	0.4 g	≥ 0.5 g
A[(2)]	-	-	-	-	-	-	-
B	0	1.0	1.0	1.0	1.0	1.0	1.0
C	5	4.0	3.5	2.8	2.3	2.1	1.9
	10	3.3	3.1	2.6	2.1	1.9	1.7
	20	2.6	2.5	2.1	1.8	1.6	1.5
	30	2.4	2.2	1.9	1.7	1.5	1.4
	50	2.1	2.0	1.7	1.5	1.3	1.2
	≥100	2.1	1.9	1.6	1.4	1.3	1.2
D	5	3.9	3.0	2.0	1.6	1.3	1.1
	10	3.6	3.2	2.3	1.8	1.5	1.3
	20	3.2	2.8	2.3	1.9	1.7	1.5
	30	3.0	2.6	2.1	1.8	1.5	1.4
	50	2.6	2.3	1.9	1.6	1.4	1.2
	≥100	2.6	2.3	1.8	1.5	1.3	1.2
E	5	2.0	1.5	1.0	0.8	0.6	0.6
	10	2.2	1.7	1.2	0.9	0.7	0.6
	20	2.7	2.0	1.4	1.1	0.9	0.7
	30	2.6	2.0	1.4	1.0	0.9	0.7
	50	2.6	2.0	1.4	1.0	0.9	0.7
	≥100	2.6	2.0	1.4	1.1	0.9	0.8
F[(3)]	N/A	N/A	N/A	N/A	N/A	N/A	N/A

[(1)]Use linear interpolation for intermediate values of $PGA_{B\text{-}C}$.

[(2)]Site-specific response analysis shall be performed.

[(3)]Site Class A not presented in the Myrtle Beach. No response analysis performed.

Table 6.4 Maximum Median F_{PGA} as a Function of Site Class and $PGA_{B\text{-}C}$ Derived in this Study for the Columbia area in SCCP.

Site Class	$H_{B\text{-}C}$, m	Peak Ground Acceleration[1] $PGA_{B\text{-}C}$ (Period = 0.0 s)					
		≤ 0.05 g	0.1 g	0.2 g	0.3 g	0.4 g	≥ 0.5 g
A[2]	-	-	-	-	-	-	-
B	0	1.0	1.0	1.0	1.0	1.0	1.0
C	5	3.0	2.7	2.3	2.0	1.8	1.7
	10	2.6	2.5	2.1	1.8	1.7	1.6
	20	2.1	2.0	1.8	1.6	1.5	1.4
	30	1.9	1.8	1.6	1.5	1.4	1.3
	50	1.7	1.6	1.4	1.3	1.2	1.1
	≥100	1.7	1.6	1.4	1.3	1.2	1.1
D	5	2.8	2.2	1.6	1.3	1.1	1.0
	10	2.7	2.5	1.8	1.4	1.2	1.1
	20	2.4	2.2	1.8	1.6	1.5	1.3
	30	2.2	2.0	1.7	1.5	1.4	1.3
	50	2.0	1.8	1.5	1.3	1.2	1.2
	≥100	2.0	1.8	1.5	1.3	1.2	1.1
E	5	1.4	1.1	0.8	0.6	0.5	0.5
	10	1.6	1.2	0.9	0.7	0.6	0.5
	20	1.9	1.5	1.1	0.8	0.7	0.6
	30	1.9	1.4	1.0	0.8	0.7	0.6
	50	1.9	1.4	1.0	0.8	0.7	0.6
	≥100	1.9	1.5	1.1	0.9	0.7	0.7
F[3]	N/A	N/A	N/A	N/A	N/A	N/A	N/A

[1]Use linear interpolation for intermediate values of $PGA_{B\text{-}C}$.
[2]Site-specific response analysis shall be performed.
[3]Site Class A not presented in the Columbia area in SCCP. No response analysis performed

Table 6.5 Maximum Median F_{PGA} as a Function of Site Class and $PGA_{B\text{-}C}$ Derived in this Study for Aiken.

Site Class	$H_{B\text{-}C}$, m	Peak Ground Acceleration[1] $PGA_{B\text{-}C}$ (Period = 0.0 s)					
		≤ 0.05 g	0.1 g	0.2 g	0.3 g	0.4 g	≥ 0.5 g
A[2]	-	-	-	-	-	-	-
B	0	1.0	1.0	1.0	1.0	1.0	1.0
C	5	2.9	2.6	2.2	2.0	1.8	1.7
	10	2.5	2.4	2.1	1.8	1.7	1.6
	20	2.0	1.9	1.7	1.6	1.5	1.4
	30	1.9	1.8	1.6	1.5	1.4	1.3
	50	1.7	1.6	1.4	1.3	1.2	1.1
	≥100	1.6	1.5	1.4	1.2	1.2	1.1
D	5	2.8	2.1	1.6	1.3	1.1	1.0
	10	2.7	2.4	1.8	1.4	1.2	1.1
	20	2.4	2.1	1.8	1.6	1.5	1.3
	30	2.2	2.0	1.7	1.5	1.4	1.3
	50	1.9	1.8	1.5	1.3	1.2	1.1
	≥100	1.9	1.7	1.5	1.3	1.2	1.1
E	5	1.4	1.1	0.8	0.6	0.5	0.5
	10	1.6	1.2	0.9	0.7	0.6	0.6
	20	1.9	1.4	1.1	0.9	0.7	0.7
	30	1.8	1.4	1.0	0.8	0.7	0.7
	50	1.8	1.4	1.0	0.8	0.7	0.7
	≥100	1.9	1.5	1.1	0.9	0.7	0.7
F[3]	N/A	N/A	N/A	N/A	N/A	N/A	N/A

[1]Use linear interpolation for intermediate values of $PGA_{B\text{-}C}$.
[2]Site-specific response analysis shall be performed.
[3]Site Class A not presented in the Aiken area. No response analysis performed

Table 6.6 Maximum Median F_{PGA} as a Function of Site Class and PGA_{HR} Derived in this Study for Columbia in SCP.

Site Class	H_{HR}, m	Peak Ground Acceleration[1] PGA_{HR} (Period = 0.0 s)					
		≤ 0.05 g	0.10 g	0.20 g	0.30 g	0.40 g	≥ 0.50 g
A	-	1.0	1.0	1.0	1.0	1.0	1.0
B	5	0.6	0.5	0.4	0.3	0.3	0.3
	10	0.7	0.6	0.4	0.3	0.3	0.2
	20	2.7	2.4	2.0	1.7	1.5	1.3
	30	2.8	2.5	2.0	1.7	1.5	1.4
	50	2.3	2.0	1.7	1.4	1.2	1.1
	100	1.6	1.4	1.2	1.0	0.9	0.9
C	5	0.9	0.9	0.9	0.9	0.9	0.9
	10	0.9	0.9	0.9	0.9	0.9	0.9
	20	3.0	2.6	2.1	1.7	1.5	1.3
	30	3.2	2.9	2.3	1.9	1.6	1.5
	50	2.6	2.3	1.8	1.5	1.3	1.2
	100	1.7	1.5	1.2	1.0	0.9	0.9
D	5	0.3	0.3	0.3	0.3	0.3	0.3
	10	0.3	0.3	0.3	0.3	0.3	0.3
	20	2.2	1.7	1.2	0.9	0.8	0.7
	30	3.3	2.9	2.2	1.7	1.4	1.2
	50	2.6	2.3	1.8	1.5	1.2	1.1
	100	1.7	1.5	1.2	1.0	0.9	0.8
E	5	-	-	-	-	-	-
	10	-	-	-	-	-	-
	20	1.1	0.9	0.6	0.5	0.4	0.3
	30	2.0	1.6	1.1	0.9	0.7	0.6
	50	1.7	1.3	1.0	0.7	0.6	0.5
	100	1.4	1.1	0.8	0.6	0.5	0.4
F[2]	N/A	N/A	N/A	N/A	N/A	N/A	N/A

[1]Use linear interpolation for intermediate values of PGA_{HR}.

[2]Site-specific response analysis shall be performed.

6.3 Local Site Effects on Short- and Long-Period Spectral Accelerations

The local site short-period (T = 0.2 s) and the long-period (T = 1.0 s) horizontal spectral response accelerations are determined by adjusted mapped rock spectral values using the following equations:

$$S_{DS} = F_a \times S_S \tag{6.2}$$

$$S_{D1} = F_v \times S_1 \tag{6.3}$$

where S_{DS} in the design short-period horizontal spectral response acceleration adjusted for local site conditions; S_{D1} is the design long-period horizontal spectral response acceleration adjusted for local site conditions; F_a is the short-period site coefficient; F_v is the long-period site coefficient; S_S is the mapped short-period horizontal spectral response acceleration, and S_1 the mapped long-period horizontal spectral response acceleration.

Presented in Tables 6.7 and 6.8 are respective F_a and F_v values recommended in SCDOT (2008). Presented in Tables 6.9-6.12 and Tables 6.14-6.17 are computed F_a and F_v values, respectively, for the SCCP. Presented in Tables 6.13 and 6.18 are respective F_a and F_v values for the SCP. It should be noted that when using Tables 6.9-6.12 and Tables 6.14-6.17, $PGA_{outcrop}$ is for B-C boundary condition ($PGA_{B\text{-}C}$); and when using Tables 6.13 and 6.18, $PGA_{outcrop}$ is for weathered hard rock condition (PGA_{HR}).

Table 6.7 F_a as a Function of Site Class and S_s Recommended in SCDOT (2008) for B-C Boundary Mapped Soft-Rock Acceleration.

Site Class	Mapped Horizontal Spectral Acceleration at Period of 0.2 s[(1)], S_S				
	≤ 0.25 g	0.50 g	0.75 g	1.00 g	≥ 1.25 g
A	0.8	0.8	0.8	0.8	0.8
B	1.0	1.0	1.0	1.0	1.0
C	1.2	1.2	1.1	1.0	1.0
D	1.6	1.4	1.2	1.1	1.0
E	2.5	1.7	1.2	0.9	0.9
F[(2)]	N/A	N/A	N/A	N/A	N/A

[(1)]Use linear interpolation for intermediate values of S_S.
[(2)]Site-specific response analysis shall be performed.

Table 6.8 F_v as a Function of Site Class and S_1 Recommended in SCDOT (2008) for B-C Boundary Mapped Soft-Rock Acceleration.

Site Class	Mapped Horizontal Spectral Acceleration at Period of 1.0 s[(1)], S_1				
	≤ 0.10 g	0.20 g	0.30 g	0.40 g	≥ 0.50 g
A	0.8	0.8	0.8	0.8	0.8
B	1.0	1.0	1.0	1.0	1.0
C	1.7	1.6	1.5	1.4	1.3
D	2.4	2.0	1.8	1.6	1.5
E	3.5	3.2	2.8	2.4	2.4
F[(2)]	N/A	N/A	N/A	N/A	N/A

[(1)]Use linear interpolation for intermediate values of S_1.
[(2)]Site-specific response analysis shall be performed.

Table 6.9 Maximum Median F_a as a Function of Site Class and Mapped S_s for the B-C Condition Derived in this Study for Charleston.

Site Class	H_{B-C}, m	Mapped Spectral Acceleration at Short-Period[(1)] for the B-C Condition (Period = 0.2 sec)					
		≤ 0.15 g	0.25 g	0.50 g	0.75 g	1.00 g	1.25 g
A[(3)]	-	-	-	-	-	-	-
B	0	1.0	1.0	1.0	1.0	1.0	1.0
C	5	2.5	2.3	1.9	1.6	1.5	1.4
	10	2.5	2.6	2.4	2.1	1.9	1.7
	20	2.1	2.0	1.9	1.7	1.6	1.5
	30	1.8	1.8	1.6	1.5	1.4	1.3
	50	1.7	1.6	1.5	1.3	1.3	1.2
	≥100	1.6	1.5	1.4	1.2	1.2	1.1
D	5	2.6	2.1	1.5	1.2	1.0	0.9
	10	3.3	2.9	2.3	1.8	1.6	1.4
	20	2.9	2.5	2.1	1.8	1.6	1.5
	30	2.6	2.3	1.9	1.6	1.5	1.4
	50	2.3	2.1	1.7	1.5	1.3	1.2
	≥100	2.1	1.9	1.5	1.3	1.2	1.1
E	5	1.3	1.0	0.7	0.6	0.5	0.4
	10	2.1	1.6	1.2	0.9	0.8	0.7
	20	2.2	1.7	1.2	1.0	0.8	0.7
	30	2.4	1.9	1.3	1.0	0.9	0.8
	50	2.2	1.7	1.2	1.0	0.8	0.7
	≥100	2.0	1.6	1.1	0.9	0.8	0.7
F[(2)]	N/A	N/A	N/A	N/A	N/A	N/A	N/A

[(1)] Use linear interpolation for intermediate values of S_S.
[(2)]Site-specific response analysis shall be performed.
[(3)]Site Class A not presented in the Charleston area. No response analysis performed.

Table 6.10 Maximum Median F_a as a Function of Site Class and Mapped S_S for the B-C Condition Derived in this Study for Myrtle Beach.

Site Class	$H_{B\text{-}C}$, m	Mapped Spectral Acceleration at Short-Period[(1)] for the B-C Condition (Period = 0.2 sec)					
		≤ 0.15 g	≤ 0.15 g	≤ 0.15 g	≤ 0.15 g	≤ 0.15 g	≤ 0.15 g
A[(3)]	-	-	-	-	-	-	-
B	0	1.0	1.0	1.0	1.0	1.0	1.0
C	5	3.0	2.8	2.2	1.8	1.6	1.4
	10	2.9	3.0	2.7	2.3	2.0	1.8
	20	2.4	2.3	2.1	1.9	1.7	1.6
	30	2.1	2.0	1.8	1.6	1.5	1.4
	50	1.9	1.8	1.6	1.4	1.3	1.2
	≥100	1.8	1.7	1.5	1.3	1.2	1.1
D	5	3.2	2.5	1.7	1.3	1.1	0.9
	10	4.0	3.5	2.7	2.1	1.7	1.5
	20	3.5	3.0	2.4	2.0	1.7	1.5
	30	3.2	2.8	2.2	1.8	1.6	1.4
	50	2.8	2.5	1.9	1.6	1.4	1.3
	≥100	2.6	2.2	1.8	1.5	1.3	1.2
E	5	1.7	1.3	0.8	0.6	0.5	0.5
	10	2.6	2.0	1.3	1.0	0.8	0.7
	20	2.8	2.1	1.4	1.1	0.9	0.8
	30	3.0	2.3	1.5	1.2	1.0	0.8
	50	2.8	2.1	1.4	1.1	0.9	0.8
	≥100	2.6	1.9	1.3	1.0	0.8	0.7
F[(2)]	N/A	N/A	N/A	N/A	N/A	N/A	N/A

[(1)] Use linear interpolation for intermediate values of S_S.
[(2)]Site-specific response analysis shall be performed.
[(3)]Site Class A not presented in the Myrtle Beach area. No response analysis performed.

Table 6.11 Maximum Median F_a as a Function of Site Class and Mapped S_S for the B-C Condition Derived in this Study for Columbia in SCCP.

Site Class	$H_{B\text{-}C}$, m	Mapped Spectral Acceleration at Short-Period[(1)] for the B-C Condition (Period = 0.2 sec)					
		≤ 0.15 g	≤ 0.15 g	≤ 0.15 g	≤ 0.15 g	≤ 0.15 g	≤ 0.15 g
A[(3)]	-	-	-	-	-	-	-
B	0	1.0	1.0	1.0	1.0	1.0	1.0
C	5	2.4	2.2	1.8	1.6	1.4	1.4
	10	2.4	2.5	2.3	2.0	1.8	1.7
	20	2.0	2.0	1.8	1.7	1.6	1.5
	30	1.8	1.7	1.6	1.4	1.4	1.3
	50	1.6	1.6	1.4	1.3	1.2	1.2
	≥100	1.5	1.5	1.3	1.2	1.1	1.1
D	5	2.4	1.9	1.4	1.1	0.9	0.9
	10	3.1	2.7	2.2	1.7	1.5	1.3
	20	2.7	2.4	2.0	1.7	1.6	1.4
	30	2.4	2.2	1.8	1.6	1.4	1.4
	50	2.2	1.9	1.6	1.4	1.3	1.2
	≥100	2.0	1.8	1.5	1.3	1.2	1.1
E	5	1.2	0.9	0.7	0.6	0.5	0.4
	10	1.9	1.5	1.1	0.9	0.7	0.7
	20	2.0	1.6	1.1	0.9	0.8	0.7
	30	2.2	1.7	1.2	1.0	0.9	0.8
	50	2.0	1.6	1.1	0.9	0.8	0.7
	≥100	1.9	1.4	1.0	0.8	0.7	0.7
F[(2)]	N/A	N/A	N/A	N/A	N/A	N/A	N/A

[(1)] Use linear interpolation for intermediate values of S_S.
[(2)]Site-specific response analysis shall be performed.
[(3)]Site Class A not presented in the Columbia area. No response analysis performed.

Table 6.12 Maximum Median F_a as a Function of Site Class and Mapped S_S for the B-C Condition Derived in this Study for Aiken.

Site Class	$H_{B\text{-}C}$, m	Mapped Spectral Acceleration at Short-Period[(1)] for the B-C Condition (Period = 0.2 sec)					
		≤ 0.15 g	≤ 0.15 g	≤ 0.15 g	≤ 0.15 g	≤ 0.15 g	≤ 0.15 g
A[(3)]	-	-	-	-	-	-	-
B	0	1.0	1.0	1.0	1.0	1.0	1.0
C	5	2.3	2.1	1.8	1.6	1.4	1.4
	10	2.4	2.4	2.2	2.0	1.8	1.7
	20	2.0	1.9	1.8	1.7	1.6	1.5
	30	1.7	1.7	1.5	1.4	1.4	1.3
	50	1.6	1.6	1.4	1.3	1.2	1.2
	≥100	1.5	1.5	1.3	1.2	1.1	1.1
D	5	2.4	1.9	1.4	1.1	0.9	0.9
	10	3.0	2.7	2.1	1.7	1.5	1.4
	20	2.6	2.3	1.9	1.7	1.6	1.4
	30	2.4	2.1	1.8	1.6	1.4	1.4
	50	2.1	1.9	1.6	1.4	1.3	1.2
	≥100	1.9	1.7	1.4	1.3	1.2	1.1
E	5	1.2	0.9	0.7	0.5	0.5	0.4
	10	1.9	1.5	1.1	0.9	0.7	0.7
	20	2.0	1.5	1.1	0.9	0.8	0.7
	30	2.2	1.7	1.2	1.0	0.9	0.8
	50	2.0	1.5	1.1	0.9	0.8	0.7
	≥100	1.8	1.4	1.0	0.8	0.7	0.7
F[(2)]	N/A	N/A	N/A	N/A	N/A	N/A	N/A

[(1)] Use linear interpolation for intermediate values of S_S.
[(2)]Site-specific response analysis shall be performed.
[(3)]Site Class A not presented in the Aiken area. No response analysis performed.

Table 6.13 Maximum Median F_a as a Function of Site Class and Mapped S_s for the Weathered Hard Rock Condition Derived in this Study for Columbia in SCP.

Site Class	H_{HR}, m	Mapped Spectral Acceleration at Short-Period [(1)] for the Weathered Hard Rock Condition (Period = 0.2 sec)					
		≤ 0.15 g	0.25 g	0.50 g	0.75 g	1.00 g	≥ 1.25 g
A	-	1.0	1.0	1.0	1.0	1.0	1.0
B	5	0.6	0.6	0.6	0.6	0.6	0.6
	10	0.6	0.6	0.6	0.6	0.6	0.6
	20	1.9	1.9	1.8	1.6	1.5	1.4
	30	1.6	1.6	1.5	1.4	1.3	1.2
	50	1.5	1.4	1.3	1.2	1.2	1.1
	100	1.1	1.1	0.6	0.6	0.6	0.6
C	5	0.6	0.6	0.6	0.6	0.6	0.6
	10	0.6	0.6	0.6	0.6	0.6	0.6
	20	3.2	2.9	2.4	2.0	1.7	1.6
	30	2.6	2.5	2.1	1.8	1.5	1.4
	50	2.2	2.0	1.8	1.5	1.3	1.2
	100	1.2	1.1	0.6	0.6	0.6	0.6
D	5	0.6	0.6	0.6	0.6	0.6	0.6
	10	0.6	0.6	0.6	0.6	0.6	0.6
	20	2.7	2.2	1.6	1.3	1.1	0.9
	30	2.8	2.5	2.0	1.6	1.3	1.1
	50	2.4	2.1	1.8	1.4	1.2	1.0
	100	1.3	1.1	0.6	0.6	0.6	0.6
E	5	-	-	-	-	-	-
	10	-	-	-	-	-	-
	20	1.4	1.1	0.8	0.6	0.6	0.6
	30	1.7	1.4	1.0	0.8	0.7	0.6
	50	1.5	1.2	0.9	0.7	0.6	0.6
	100	1.0	0.8	0.6	0.6	0.6	0.6
F[(2)]	N/A	N/A	N/A	N/A	N/A	N/A	N/A

[(1)] Use linear interpolation for intermediate values of S_S.

[(2)]Site-specific response analysis shall be performed.

Table 6.14 Maximum Median F_v as a Function of Site Class and Mapped S_1 for the B-C Boundary Condition Derived in this Study for Charleston.

Site Class	$H_{B\text{-}C}$, m	Mapped Horizontal Spectral Acceleration at Period of 1.0 s[(1)] for the B-C Boundary Condition					
		≤ 0.05 g	0.1 g	0.2 g	0.3 g	0.4 g	≥ 0.5 g
A[(3)]	-	-	-	-	-	-	-
B	0	1.0	1.0	1.0	1.0	1.0	1.0
C	5	1.9	1.9	1.9	1.7	1.6	1.4
	10	1.8	1.9	1.8	1.7	1.6	1.5
	20	1.8	1.8	1.8	1.7	1.6	1.4
	30	1.8	1.8	1.8	1.7	1.5	1.4
	50	1.8	1.8	1.7	1.6	1.5	1.4
	≥100	1.8	1.8	1.7	1.6	1.5	1.4
D	5	2.9	2.7	2.2	1.9	1.6	1.4
	10	3.1	2.8	2.3	2.0	1.7	1.5
	20	3.3	2.9	2.5	2.1	1.8	1.6
	30	3.3	3.1	2.6	2.2	1.9	1.6
	50	3.2	3.2	2.7	2.3	2.0	1.7
	≥100	3.2	3.2	2.8	2.4	2.0	1.8
E	5	2.4	1.9	1.4	1.0	0.8	0.7
	10	2.7	2.1	1.5	1.2	0.9	0.8
	20	3.1	2.4	1.8	1.4	1.1	0.9
	30	3.4	2.8	2.0	1.5	1.2	1.0
	50	3.5	3.2	2.3	1.8	1.5	1.2
	≥100	3.7	3.4	2.6	2.0	1.6	1.4
F[(2)]	N/A	N/A	N/A	N/A	N/A	N/A	N/A

[(1)] Use linear interpolation for intermediate values of S_1.
[(2)]Site-specific response analysis shall be performed.
[(3)]Site Class A not presented in the Charleston area. No response analysis performed.

Table 6.15 Maximum Median F_v as a Function of Site Class and Mapped S_1 for the B-C Boundary Condition Derived in this Study for Myrtle Beach.

Site Class	H_{B-C}, m	Mapped Horizontal Spectral Acceleration at Period of 1.0 s[(1)] for the B-C Boundary Condition					
		≤ 0.05 g	0.1 g	0.2 g	0.3 g	0.4 g	≥ 0.5 g
A[(3)]	-	-	-	-	-	-	-
B	0	1.8	1.9	1.8	1.7	1.6	1.4
C	5	1.8	1.9	1.8	1.7	1.6	1.4
	10	1.8	1.8	1.8	1.7	1.5	1.4
	20	1.8	1.8	1.7	1.6	1.5	1.4
	30	1.8	1.8	1.7	1.6	1.5	1.4
	50	1.8	1.8	1.7	1.6	1.5	1.4
	≥100	3.2	2.9	2.4	2.0	1.7	1.5
D	5	3.3	3.0	2.5	2.1	1.8	1.6
	10	3.4	3.2	2.6	2.2	1.9	1.6
	20	3.4	3.3	2.7	2.3	2.0	1.7
	30	3.3	3.2	2.8	2.4	2.1	1.8
	50	3.3	3.3	3.0	2.5	2.1	1.9
	≥100	2.9	2.2	1.6	1.2	1.0	0.8
E	5	3.2	2.5	1.8	1.4	1.1	0.9
	10	3.5	2.9	2.1	1.6	1.3	1.1
	20	3.6	3.3	2.3	1.8	1.5	1.2
	30	3.8	3.5	2.8	2.1	1.7	1.4
	50	4.0	3.6	3.0	2.3	1.9	1.6
	≥100	1.8	1.9	1.8	1.7	1.6	1.4
F[(2)]	N/A	N/A	N/A	N/A	N/A	N/A	N/A

[(1)] Use linear interpolation for intermediate values of S_1.
[(2)]Site-specific response analysis shall be performed.
[(3)]Site Class A not presented in the Myrtle Beach area. No response analysis performed.

Table 6.16 Maximum Median F_v as a Function of Site Class and Mapped S_1 for the B-C Boundary Condition Derived in this Study for Columbia in SCCP.

Site Class	H_{B-C}, m	Mapped Horizontal Spectral Acceleration at Period of 1.0 s[(1)] for the B-C Boundary Condition					
		≤ 0.05 g	0.1 g	0.2 g	0.3 g	0.4 g	≥ 0.5 g
A[(3)]	-	-	-	-	-	-	-
B	0	1.9	2.0	2.0	1.9	1.6	1.4
C	5	1.9	2.0	2.0	1.9	1.7	1.5
	10	1.9	1.9	1.9	1.8	1.6	1.5
	20	1.9	1.9	1.8	1.7	1.6	1.5
	30	1.8	1.8	1.8	1.7	1.6	1.5
	50	1.8	1.8	1.8	1.7	1.6	1.5
	≥100	2.9	2.6	2.2	1.8	1.5	1.2
D	5	3.0	2.7	2.3	1.9	1.7	1.4
	10	3.2	2.9	2.4	2.0	1.8	1.6
	20	3.3	3.0	2.5	2.1	1.8	1.6
	30	3.4	3.1	2.6	2.2	1.9	1.7
	50	3.4	3.3	2.7	2.3	2.0	1.8
	≥100	2.1	1.6	1.2	0.9	0.7	0.6
E	5	2.3	1.8	1.3	1.0	0.8	0.7
	10	2.7	2.1	1.5	1.2	1.0	0.8
	20	3.1	2.4	1.7	1.3	1.1	0.9
	30	3.4	2.8	2.0	1.6	1.3	1.1
	50	3.6	3.1	2.2	1.7	1.4	1.2
	≥100	1.9	2.0	2.0	1.9	1.6	1.4
F[(2)]	N/A	N/A	N/A	N/A	N/A	N/A	N/A

[(1)] Use linear interpolation for intermediate values of S_1.
[(2)]Site-specific response analysis shall be performed.
[(3)]Site Class A not presented in the Columbia in SCCP area. No response analysis performed.

Table 6.17 Maximum Median F_v as a Function of Site Class and Mapped S_1 for the B-C Boundary Condition Derived in this Study for Aiken.

Site Class	H_{B-C}, m	Mapped Horizontal Spectral Acceleration at Period of 1.0 s[(1)] for the B-C Boundary Condition					
		≤ 0.05 g	0.1 g	0.2 g	0.3 g	0.4 g	≥ 0.5 g
A[(3)]	-	-	-	-	-	-	-
B	0	1.0	1.0	1.0	1.0	1.0	1.0
C	5	1.9	1.9	1.9	1.8	1.6	1.4
	10	1.9	1.9	1.9	1.8	1.6	1.5
	20	1.8	1.8	1.8	1.7	1.6	1.5
	30	1.8	1.8	1.8	1.7	1.6	1.5
	50	1.8	1.8	1.7	1.6	1.5	1.4
	≥100	1.8	1.8	1.7	1.6	1.5	1.4
D	5	2.9	2.6	2.2	1.8	1.6	1.3
	10	3.0	2.7	2.3	1.9	1.7	1.5
	20	3.1	2.8	2.4	2.0	1.7	1.5
	30	3.3	3.0	2.5	2.1	1.8	1.6
	50	3.2	3.1	2.6	2.2	1.9	1.7
	≥100	3.2	3.2	2.7	2.3	2.0	1.7
E	5	2.2	1.7	1.2	1.0	0.8	0.7
	10	2.5	1.9	1.4	1.1	0.9	0.7
	20	2.8	2.2	1.6	1.2	1.0	0.9
	30	3.2	2.5	1.8	1.4	1.2	1.0
	50	3.4	3.0	2.1	1.7	1.4	1.1
	≥100	3.6	3.2	2.4	1.8	1.5	1.2
F[(2)]	N/A	N/A	N/A	N/A	N/A	N/A	N/A

[(1)] Use linear interpolation for intermediate values of S_1.
[(2)]Site-specific response analysis shall be performed.
[(3)]Site Class A not presented in the Aiken area. No response analysis performed.

Table 6.18 Maximum Median F_v as a Function of Site Class and Mapped S_1 for the Weathered Hard Rock Condition Derived in this Study for Columbia in SCP.

Site Class	H_{HR}, m	Mapped Horizontal Spectral Acceleration at Period of 1.0 s[(1)] for the Weathered Hard Rock Condition					
		≤ 0.05 g	0.1 g	0.2 g	0.3 g	0.4 g	≥ 0.5 g
A	-	1.0	1.0	1.0	1.0	1.0	1.0
B	5	0.6	0.6	0.6	0.6	0.6	0.6
	10	0.6	0.6	0.6	0.6	0.6	0.6
	20	1.2	1.1	0.6	0.6	0.6	0.6
	30	1.6	1.6	1.5	1.4	1.3	1.2
	50	1.8	1.8	1.6	1.5	1.5	1.4
	100	2.1	2.0	1.9	1.8	1.7	1.6
C	5	1.2	1.2	1.2	1.2	1.2	1.2
	10	1.2	1.2	1.2	1.2	1.2	1.2
	20	1.2	1.2	1.2	1.2	1.2	1.2
	30	2.6	2.5	2.1	1.8	1.5	1.4
	50	3.2	3.1	2.7	2.4	2.1	1.8
	100	4.3	4.1	3.6	3.2	2.9	2.6
D	5	2.1	2.1	2.1	2.1	2.1	2.1
	10	2.1	2.1	2.1	2.1	2.1	2.1
	20	2.1	2.1	2.1	2.1	2.1	2.1
	30	2.8	2.5	2.1	2.1	2.1	2.1
	50	3.8	3.4	2.8	2.4	2.1	2.1
	100	6.1	5.5	4.5	3.9	3.3	3.0
E	5	-	-	-	-	-	-
	10	-	-	-	-	-	-
	20	2.1	2.1	2.1	2.1	2.1	2.1
	30	2.1	2.1	2.1	2.1	2.1	2.1
	50	2.5	2.1	2.1	2.1	2.1	2.1
	100	5.8	4.7	3.4	2.7	2.3	2.1
F[(2]		NA	NA	NA	NA	NA	NA

[(1)] Use linear interpolation for intermediate values of S_S.

[(2)]Site-specific response analysis shall be performed.

6.4 Three-Point Acceleration Design Response Spectrum

This section discusses the procedure for constructing an acceleration design response spectrum (ADRS) recommended in SCDOT (2008) and AASHTO (2011a). First, the site V_{S30} is determined. Second, $PGA_{outcrop}$, S_s and S_1 are obtained from probabilistic seismic hazard maps. Third, the V_{S30}, $PGA_{outcrop}$, S_s and S_1 are used to calculate site coefficients, F_{PGA}, F_a and F_v using Equations 6.4, 6.5 and 6.6 that account for the effect of local site conditions. Fourth, three points of the ADRS are obtained as follows:

$$PGA = F_{PGA} * PGA_{outcrop} \tag{6.4}$$

$$S_{DS} = F_a S_s \tag{6.5}$$

$$S_{D1} = F_v S_1 \tag{6.6}$$

where PGA, S_{DS}, and S_{D1} are the design peak ground acceleration, short-period (0.2 s) acceleration and long-period (1.0 s) spectral response acceleration, respectively, at the site. Finally the ADRS is constructed as illustrated in Figure 6.1.

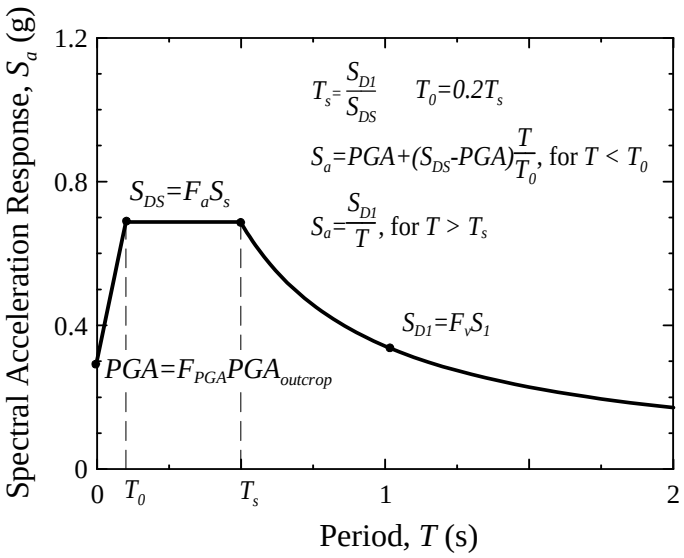

Figure 6.1 Three-point ADRS curve (SCDOT 2008).

The procedure illustrated in Figure 6.1 implicitly assumes: (1) all significant peaks are expected to occur at $T \leq 1.0$ s; (2) the plateau defined by S_{DS} provides a conservative bound for these peaks; and (3) spectral acceleration descends proportionally with $1/T$, when $T > T_s$ ($T_s = S_{D1}/S_{DS}$). However, it was shown in Chapter 3 that (1) significant peaks may not always occur at shorter periods ($T \leq 1.0$ s), especially when $V_{S30} < 200$ m/s; and (2) the plateau cannot always be defined as S_{DS}, unless $T_s \leq 1.0$ s ($S_{D1} \leq S_{DS}$).

The 3-point procedure for constructing ADRS curves was shown in Chapter 3 to be generally adequate when $V_{S30} > 200$ m/s. However, when $V_{S30} \leq 200$ m/s, significant peaks may occur at $T > 1.0$ s. For this reason, it was suggested that the multi-point ADRS curve be plotted with the 3-point curve, to check if long-period accelerations are under predicted. Models to calculate site coefficients at long periods (T = 1.6 and 3.0 s) were provided in Chapters 4 and 5.

6.5 Multi-Point Acceleration Design Response Spectrum

The objective of the multi-point ADRS is to present a check for the designer to make sure that longer period accelerations are not under-predicted by the 3-point ADRS design curve. The multi-point ADRS is drawn by first constructing the three-point ADRS curve and then overlaying on the same graph the multi-point ADRS values as illustrated in Figure 6.2.

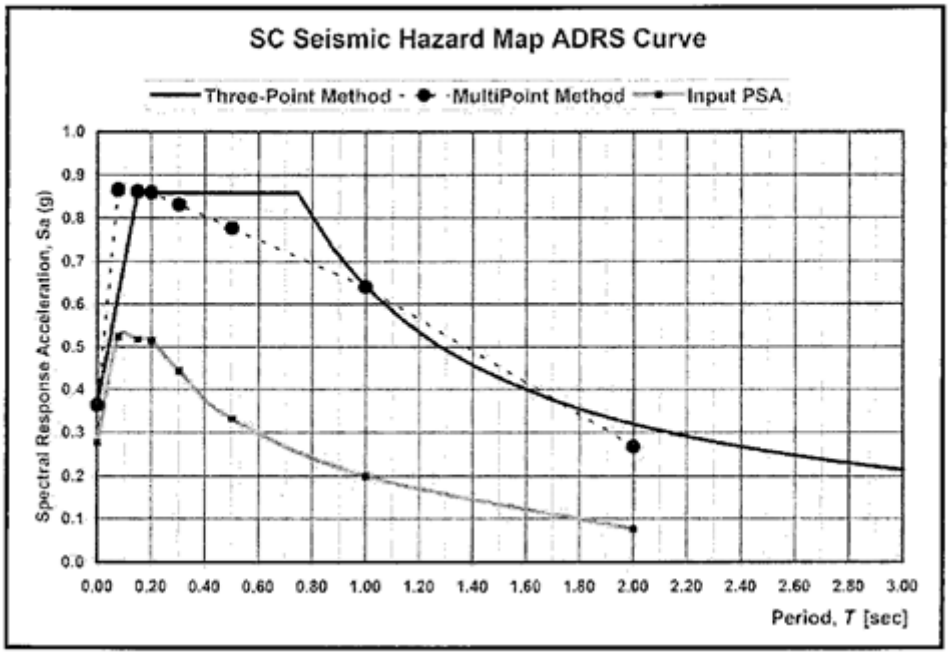

Figure 6.2 Example three-point/multi-point ADRS curves for a Site Class C location (SCDOT 2008).

After the multi-point horizontal ADRS curve has been constructed, the three-point ADRS is checked to see if it is underestimating spectral accelerations or if it is not representative of the acceleration response spectrum. In certain circumstances there may

be a shift that is not captured by the three-point ADRS; this is particularly true in the Eastern United States where the peak of the acceleration response spectrum is shifted towards the 1.0 s period. This shift appears to occur at locations where the soil column is deep and V_{S30} < 200 m/s (SCDOT 2008).

The ADRS curves shown in Figure 6.3 provide an example where discrepancies between the three-point and the multi-point methods indicate spectral accelerations significantly underestimated at the 1.0 s period and significantly dissimilar acceleration response spectrum shape. For this particularly example, the Site Class is E and the difference is important because the fundamental period of the bridge being designed was 1.0 s (SCDOT 2008).

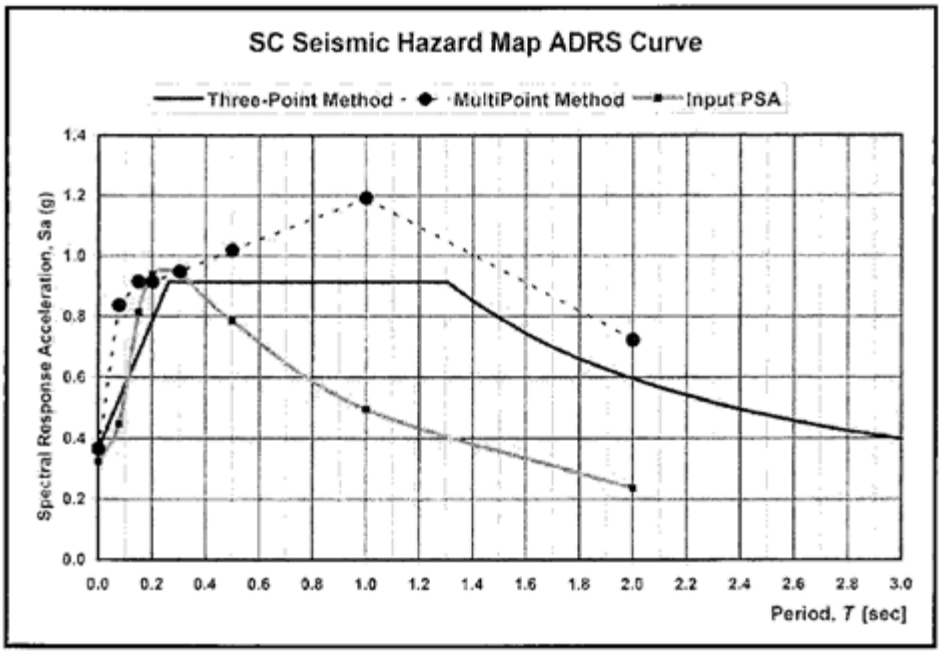

Figure 6.3 Example three-point/multi-point ADRS curves for a Site Class D location (SCDOT 2008).

It should be noted that the multi-point method currently described in SCDOT (2008) can give ambiguous results (Power and Chiou 2000), because F_a is used for all T less than or equal to 0.2 s and F_v is used for all T greater than or equal to 1.0 s to compute the response spectrum. To improve the current multi-point method, additional site coefficients $F_{0.6}$, $F_{1.6}$ and $F_{3.0}$ were developed in this study for T values of 0.6, 1.6 and 3.0 s, respectively. Recommended $F_{0.6}$, $F_{1.6}$ and $F_{3.0}$ values can be calculated from the models developed in Chapters 4 and 5.

6.6 Discussion

Presented in Figure 6.4, 6.5 and 6.6 are bar charts showing maximum median F_{PGA}, F_a, and F_v, respectively, grouped by the NEHRP site classes for Charleston, Myrtle Beach, Columbia and Aiken. Also plotted are the NEHRP F_{PGA}, F_a, and F_v values for comparison. It can be seen in Figure 6.4 that the maximum median F_{PGA} for the four selected areas are within 20%. The maximum median F_{PGA} decrease by area in the following order: Myrtle Beach, Charleston, Columbia, and Aiken. For Site Class C and D, the NEHRP F_{PGA} can be exceeded by as much as 70%.

As shown in Figure 6.5, the computed maximum median F_a values are the highest for Myrtle Beach. For Site Class D, the computed maximum median F_a in Mytrle Beach, Charleston, Columbia, and Aiken can be as much as 1.6, 1.4, 1.3, and 1.2 times the NEHRP F_a, respectively. For Site Class E, the NEHRP F_a is found to be greater than the computed values. The computed F_a values for Columbia are found to be very close to the computed F_a values for Aiken.

Presented in Figure 6.6 are bar charts comparing maximum median F_v values for the four selected SCCP sites and the NEHRP F_v. It can be seen that the computed F_v values are all close for Site Classes C and D. For Site Class D, the computed F_v in Mytrle Beach, Charleston, Columbia, and Aiken can be as much as 1.5, 1.4, 1.4, and 1.4 times the NEHRP F_v. For Site Class C, the computed F_v values are slightly greater than the NEHRP $F_{v.}$

Presented in Figures 6.7-6.9 are sample depth-dependent F_{PGA}, F_a, and F_v values grouped by amplitude and site class for Charleston. Also plotted are the corresponding depth-independent NEHRP values. The plots show the sensitivity of site amplification at shallow depths to soft rock ($H_{B\text{-}C} \leq 50$ m).

As shown in Figure 6.7, F_{PGA} and F_a generally increase with decreasing $H_{B\text{-}C}$, for Site Classes C and D. For Site Class E, however, F_{PGA} and F_a slightly decrease with decreasing $H_{B\text{-}C}$. Concerning F_v, the computed depth-dependent coefficients do not differ much for Site Class C. For Site Classes D and E, F_v decreases with decreasing $H_{B\text{-}C}$. These observations agree fairly well with a depth-dependent site response study for the Mississippi Embayment (Hashash et al. 2008). Hashash et al. (2008) obtained increasing F_a and decreasing F_v with decreasing depth for Site Class D.

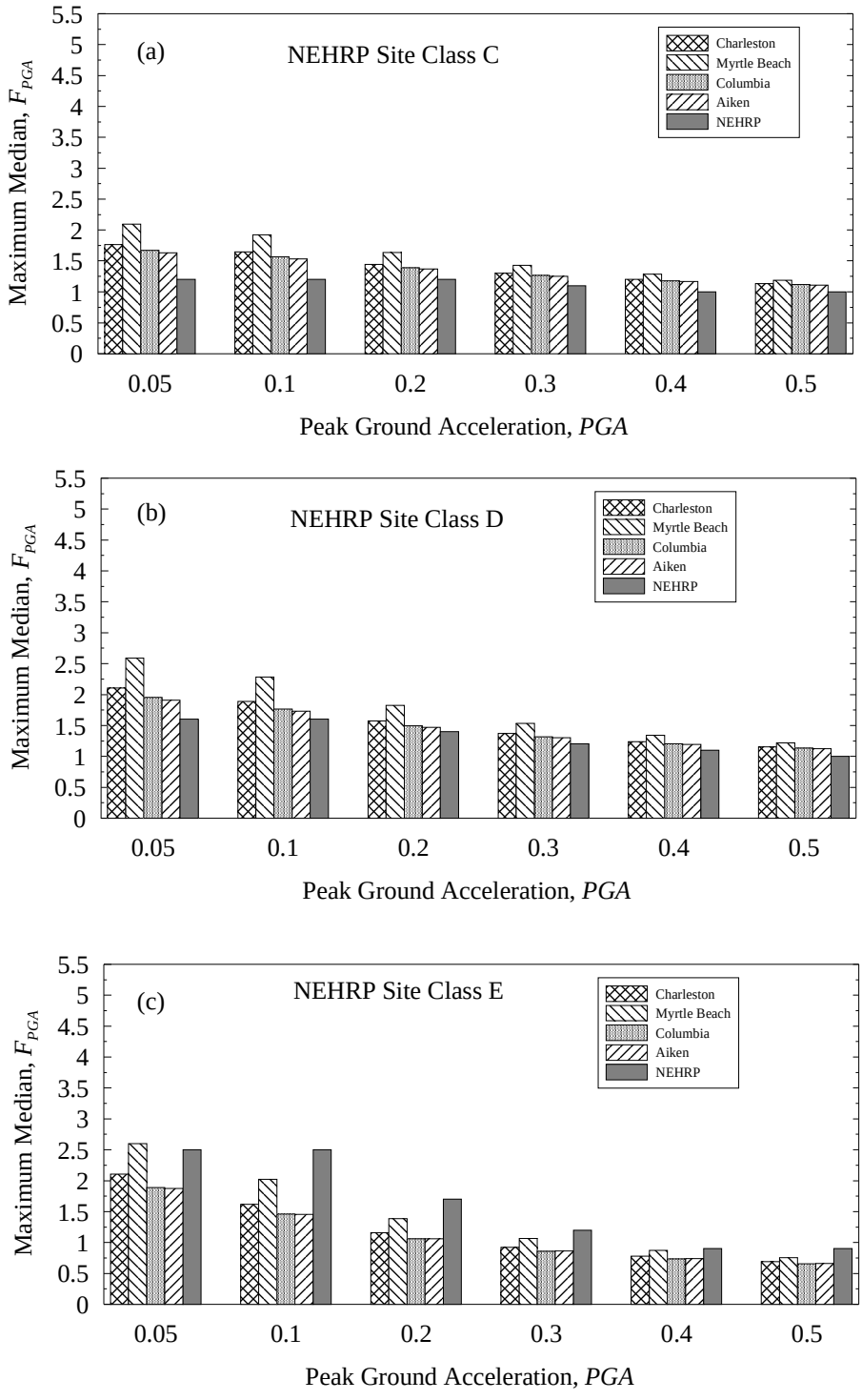

Figure 6.4 Maximum median F_{PGA} within site classes for four site response areas in the SCCP with $H_{B\text{-}C}$ > 100 m compared with the NEHRP F_{PGA}.

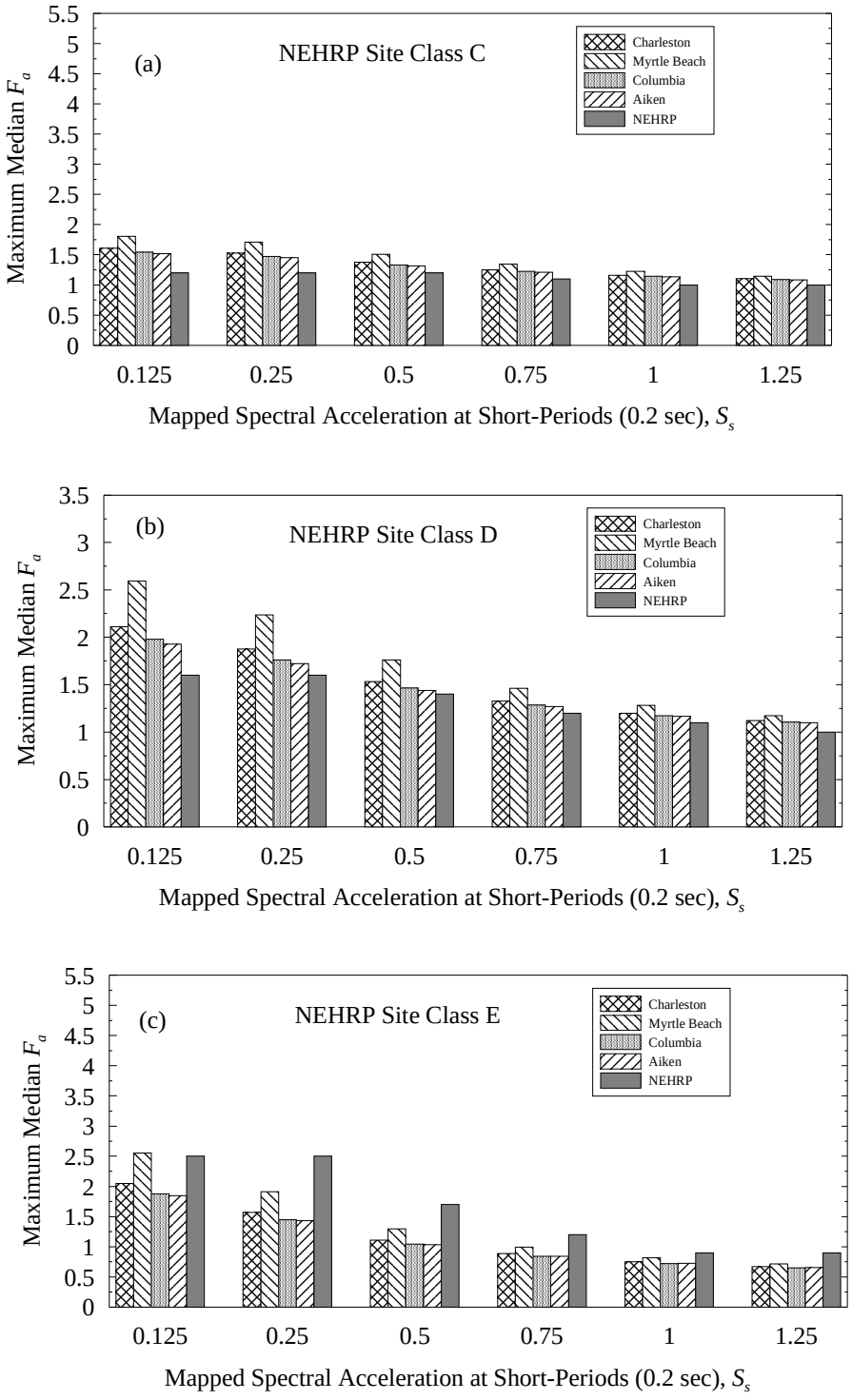

Figure 6.5 Maximum median F_a within site classes for site response areas in the SCCP compared with the NEHRP F_a.

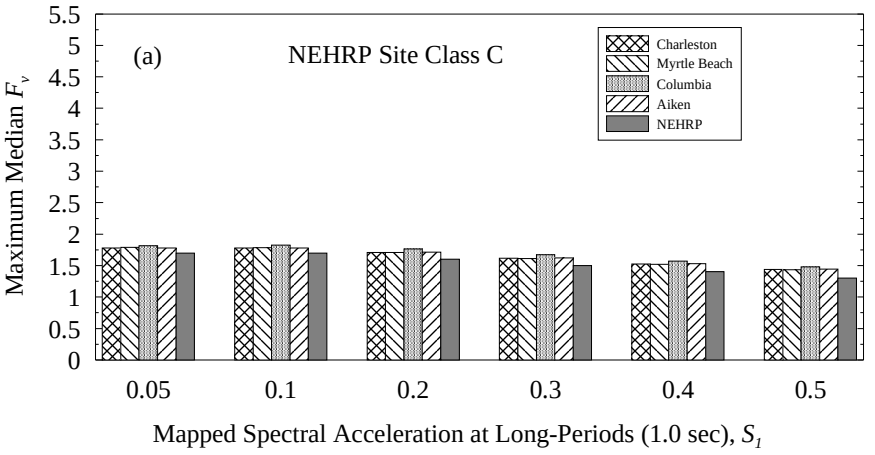

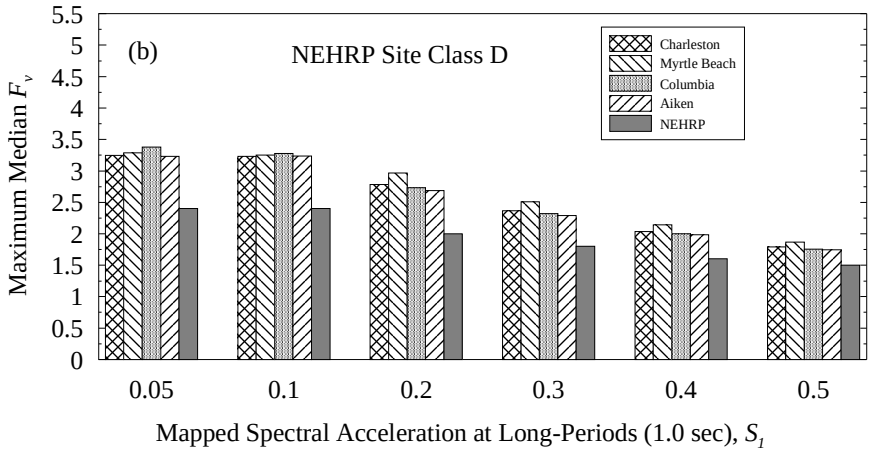

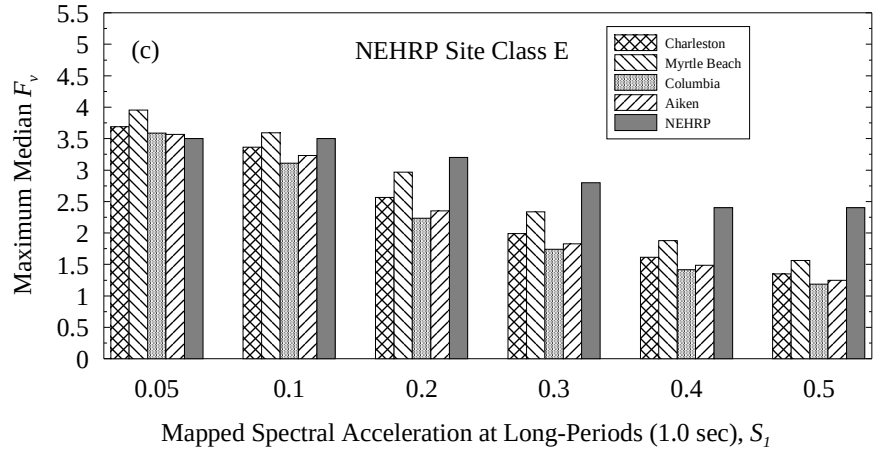

Figure 6.6 Maximum median F_v within site classes for site response areas in the SCCP compared with the NEHRP F_v.

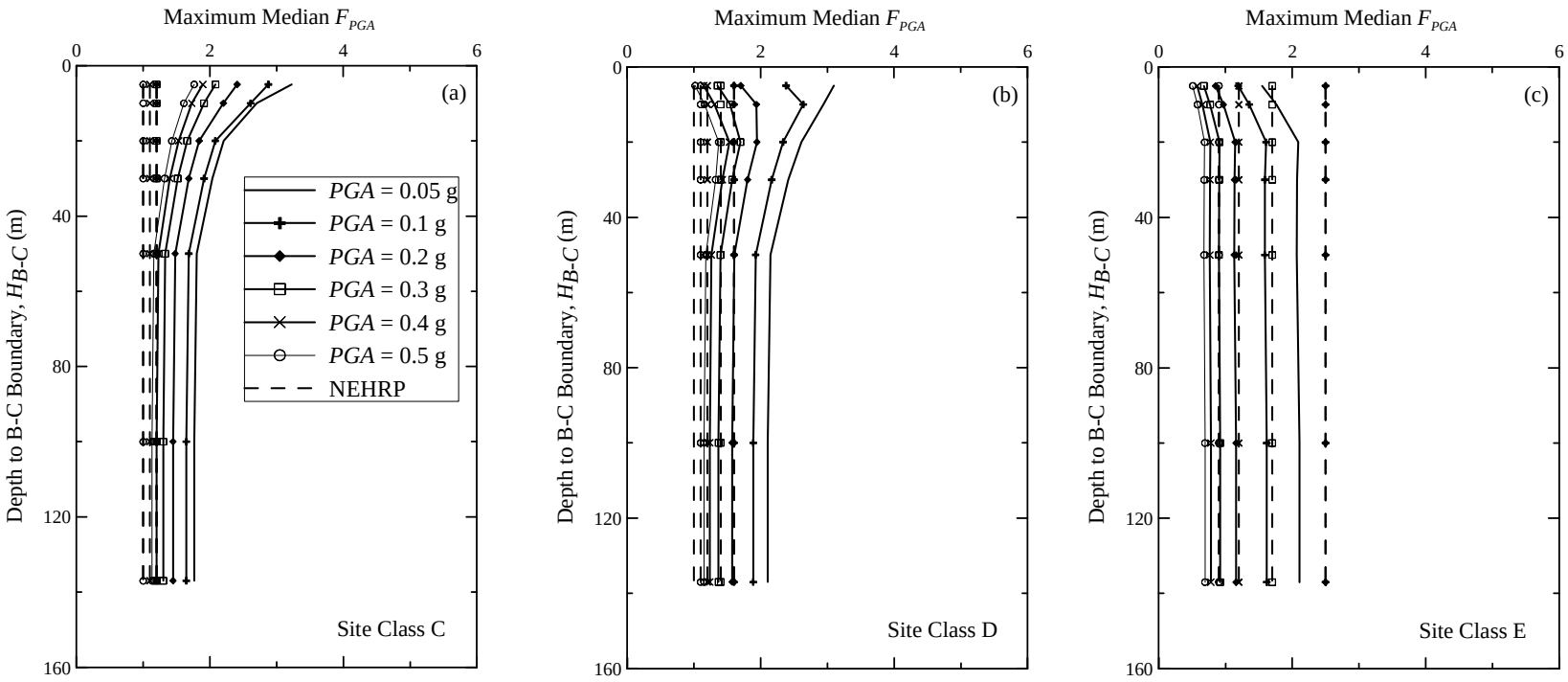

Figure 6.7 Sample depth dependent maximum median F_{PGA} for Charleston area.

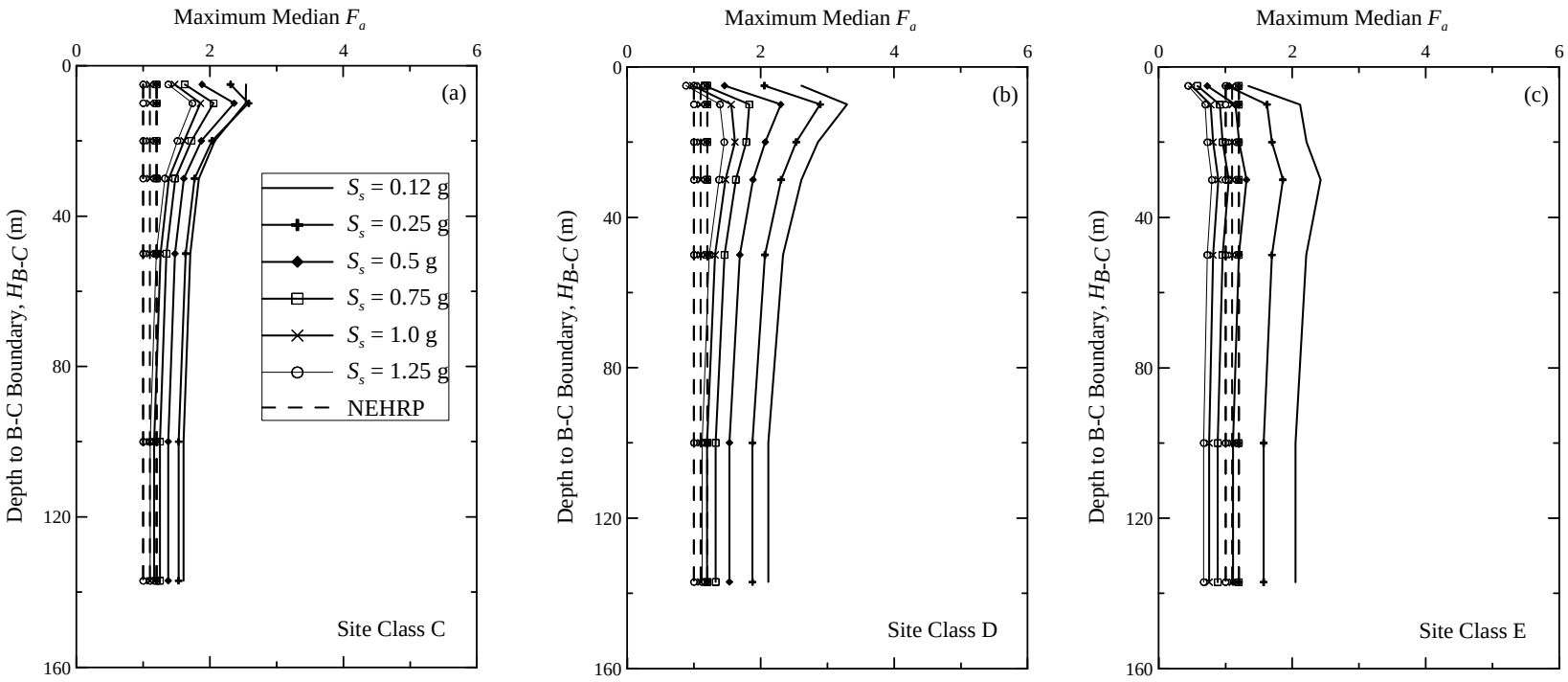

Figure 6.8 Sample depth dependent maximum median F_a for Charleston area.

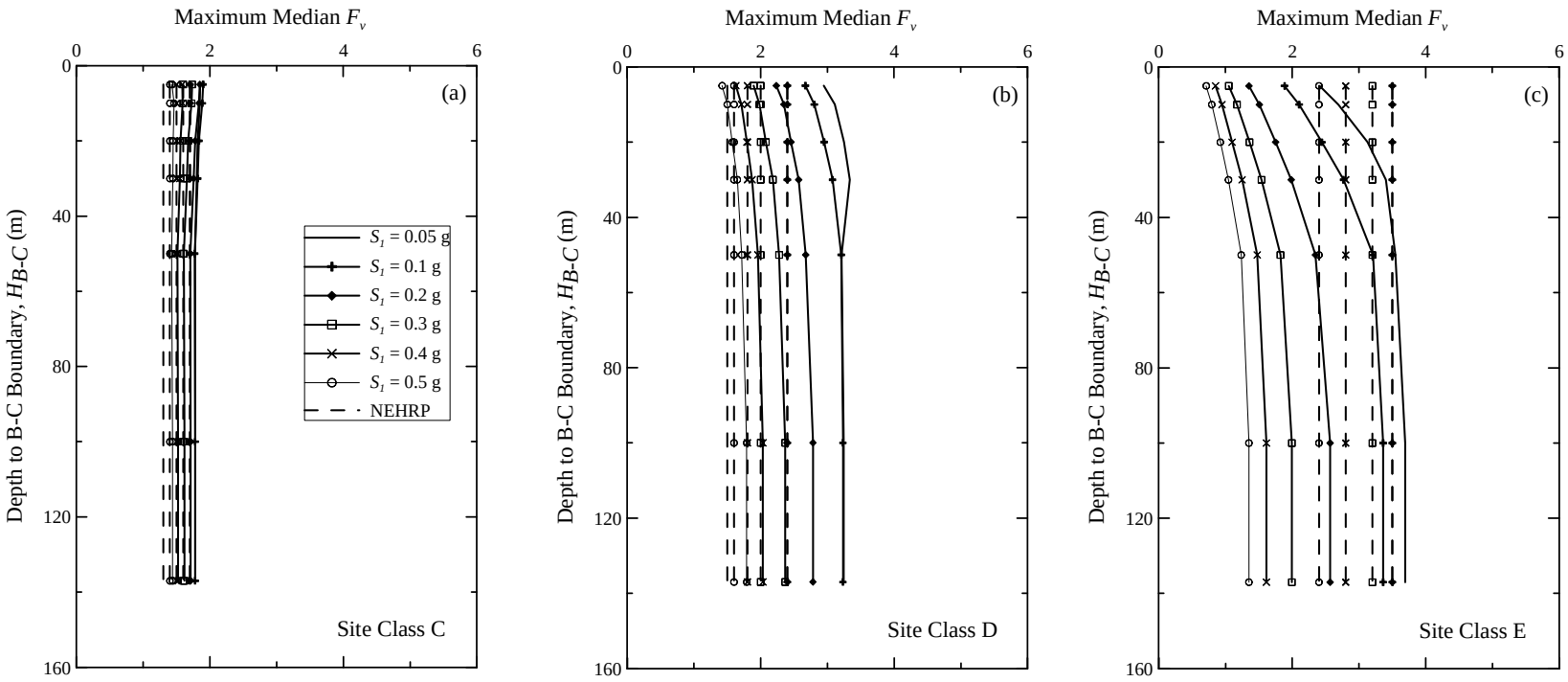

Figure 6.9 Sample depth dependent maximum median F_v for Charleston area.

6.7 Summary

In this Chapter, seismic site coefficients recommended in SCDOT (2008) are compared with site coefficients computed in this study. It was shown that the computed F_{PGA} for areas in the SCCP are within 20%. For Site Class D and C, the NEHRP F_{PGA} can be exceeded by as much as 70% in the SCCP. The computed maximum median F_a in Mytrle Beach, Charleston, Columbia, and Aiken can be as much as 1.6, 1.4, 1.3, and 1.2 times the NEHRP F_a, respectively. Similarly, the computed F_v in Mytrle Beach, Charleston, Columbia, and Aiken can be as much as 1.5, 1.4, 1.4, and 1.4 times the NEHRP $F_{v.}$

Unlike the NEHRP values, the coefficients derived in this study are depth dependent. F_{PGA} and F_a generally increase with decreasing $H_{B\text{-}C}$ for Site Classes C and D. F_v decreases with decreasing $H_{B\text{-}C}$ for Site Classes D and E. F_{PGA}, F_a and F_v slightly decrease with decreasing $H_{B\text{-}C}$ for Site Class E.

It was shown that multiple tables will be needed to accurately represent the new site coefficients and to account for all significant conditions. Thus, the use of the continuous relationships of site coefficients with V_{S30} presented in Chapters 4 and 5 is a more efficient approach to defining the recommended site coefficients for seismic design.

CHAPTER SEVEN

CONCLUSIONS AND RECOMMENDATIONS

7.1 Conclusions

New generalized models for predicting seismic site coefficients were developed in this dissertation based on over 60,000 total stress, one-dimensional equivalent linear and nonlinear ground response analyses. Soil/rock and seismic conditions typical of sites in the SCCP (i.e., Charleston, South Carolina side of Savannah, Myrtle Beach, Columbia, Florence, Lake Marion, and Aiken), and sites in the SCP (i.e., Columbia, Greenwood, Rock Hill and Greenville) were considered. Input ground motions were scaled to obtain good coverage over the spectral acceleration range, as provided in seismic design codes and guidelines.

The initial model for predicting seismic site coefficients was developed for the Charleston area in Chapter 3, and was defined at spectral periods of 0.0, 0.2, 0.6, 1.0, 1.6 and 3.0 s. The respective site coefficients were referred to as F_{PGA}, F_a, $F_{0.6}$, $F_{1.0}$, $F_{1.6}$, and $F_{3.0}$, and were calculated as averages over period ranges of $\leq$ 0.1, 0.1-0.4, 0.4-0.8, 0.8-1.2, 1.2-2.0, 2.0-4.0 s. The site coefficients were grouped by spectral acceleration, and plotted versus V_{S30}. From the plotted V_{S30}-site coefficient data pairs, median relationships were developed. Each relationship exhibited a peak value somewhere between V_{S30} of 80 and 320 m/s, depending on spectral acceleration and period. The relationships were

expressed by a linear model for $V_{S30} < V_{S30P}$ and a linear or exponential model for $V_{S30} \geq V_{S30P}$. The variability in computed site coefficients for sites with similar V_{S30} was characterized by 5% lower bound and 95% upper bound curves.

The computed relationships for periods of 0.0, 0.2 and 1.0 s were compared with the NEHRP F_a and F_v values. The computed median F_{PGA} and F_a values typically plotted above the NEHRP F_a values for $V_{S30} > 180$ m/s. The computed median F_v values also typically plotted above the NEHRP F_v values by as much as about 1.5 times for $180 \leq V_{S30} \leq 300$ m/s. For $V_{S30} < 180$ m/s, the computed F_a and F_v values plotted below the NEHRP values. Because the computed site coefficients in chapter 3 are based on local conditions, they were recommended for the Charleston area.

Also, in Chapter 3, the 3-point procedure for constructing ADRS curves was shown to be generally adequate when $V_{S30} > 200$ m/s. When $V_{S30} \leq 200$ m/s, peaks exceeding the 3-point ADRS curves can occur at $T > 1.0$ s. For this reason, it was recommended that multi-point ADRS curves also be plotted to check if long-period accelerations are under predicted. Models needed to calculate the long-period site coefficients were proposed.

In Chapter 4, the model for predicting site coefficients developed in Chapter 3 was modified to accommodate variations in the entire SCCP. It was shown that scaling of input motions is justified because the SCCP is dominated by a single seismic source zone. Site coefficients decrease with increasing $S_{outcrop}$ and the rate of decrease is higher

when V_{S30} < 200 m/s. It was noted that F_{PGA} and F_a attenuate more rapidly with increasing $S_{outcrop}$ than F_v.

The most important variables identified in developing the seismic site coefficient model in Chapter 4 are: V_{S30}, spectral acceleration (amplitude), mean predominant period (T_m), approximate fundamental period of soil/rock column in the top 100 m (T_{100}), and depth to soft rock ($H_{B\text{-}C}$). A relationship to compute T_m based on depth to weathered hard rock (H_{HR}) and site-to-source distance (R) was suggested for use in the SCCP. It was shown that attenuation of higher frequency (or lower period) energy is three times faster per distance traveled in the hard basement rock than in the soft rock. In decreasing order, the computed site coefficients were found to be greater in Myrtle Beach, Savannah, Charleston, Florence, Columbia, Lake Marion and Aiken. More closely matching values of T_m and T_{100} (e.g., T_m = 0.37 and T_{100} = 0.84 for the Myrtle Beach reference profile) may explain the higher site coefficients in Myrtle Beach.

The computed site coefficients for Myrtle Beach were compared with the NEHRP site coefficients. The computed F_a and F_v values for Myrtle Beach were found to be significantly greater than the NEHRP F_a and F_v when the depth to soft rock < 100 m, particularly for F_a. The results clearly indicated that the assumption of a single value of F_a and F_v for a wide range of V_{S30} values (a Site Class) is an overly simplified approach.

In Chapter 5, the model for predicting site coefficients was extended to the South Carolina Piedmont. Because there was limited V_s information, a single dynamic soil/rock model was assumed for the entire SCP and adjusted to account for variations in stiffness

and depth to weathered hard rock (V_S = 2,500 m/s). It is found that both the FEE and SEE conditions in the SCP were dominated by earthquakes with modal M_w = 7.3, except in the western half of the SCP where the SEE condition was dominated by earthquakes with modal M_w = 4.8. Because the seismic hazard in the SCP can be dominated by multiple sources, generation of input motions matching the uniform hazard points was shown to give unconservative results. Therefore, input motions matching target frequencies were used. The site coefficients developed in Chapter 5 for the SCP were not comparable with the NEHRP F_a and F_v values, because the input motions used in the SCP were generated for weathered hard rock (V_S = 2500 m/s) and the NEHRP coefficients should be applied to accelerations for the B-C boundary condition.

In Chapter 6, the models developed in Chapters 4 and 5 were used to calculate and tabulate maximum site coefficients of the median curve within a site class. The coefficients were then compared with coefficients recommended by the NEHRP. Multiple tables were needed for the new site coefficients to account for all significant conditions. Thus, use of the continuous models presented in Chapters 4 and 5 are more efficient in defining the recommended site coefficients.

The computed F_{PGA}, F_a and F_v median relationships were recommended for South Carolina because they are: (1) based on regional conditions; (2) continuous with V_{S30}, (3) dependent on depth to rock, and (4) dependent on the period content of the design motion.

Much of the new seismic site coefficient models can be directly applied to other areas of the world. In addition to the need for soft-rock and weathered-rock spectral accelerations, an estimate of the mean predominant period will be needed.

7.2 Recommendations

The following future studies are recommended:

1. Additional ground response analyses are needed to refine the seismic site coefficient models, particularly in the SCP. This work should further characterize the effect of the mean predominant period on the derived site coefficients.

2. Because only synthetic ground motions were used in this study, the results are limited to the assumptions made in generating the ground motions. Real (recorded) ground motions should be considered to compare with the recommended site coefficients based on synthetic motions.

3. Characterization of mean predominant periods for different regions of the United States and other parts of the world will allow for the application of the proposed site coefficient model in these areas.

4. Because this study is based on one-dimensional assumption. It will be interesting to investigate the effects of two-dimensional assumption on computed site coefficients.

5. Additional work is needed to investigate the influence of layer correlation on the seismic site coefficient models and to make refinements as needed. In the ground

response analyses conducted in this dissertation, reasonable ranges of shear wave velocity (V_S) profiles for the SCCP and the SCP were considered by assuming a reference profile and applying reasonable standard deviation values. Thus, the influence of layer correlation is one of the limitations of this study and should be investigated.

APPENDIX A

SUMMARY OF INPUTS AND OUTPUTS OF SITE RESPONSE ANALYSIS FOR THE CHARLESTON AREA

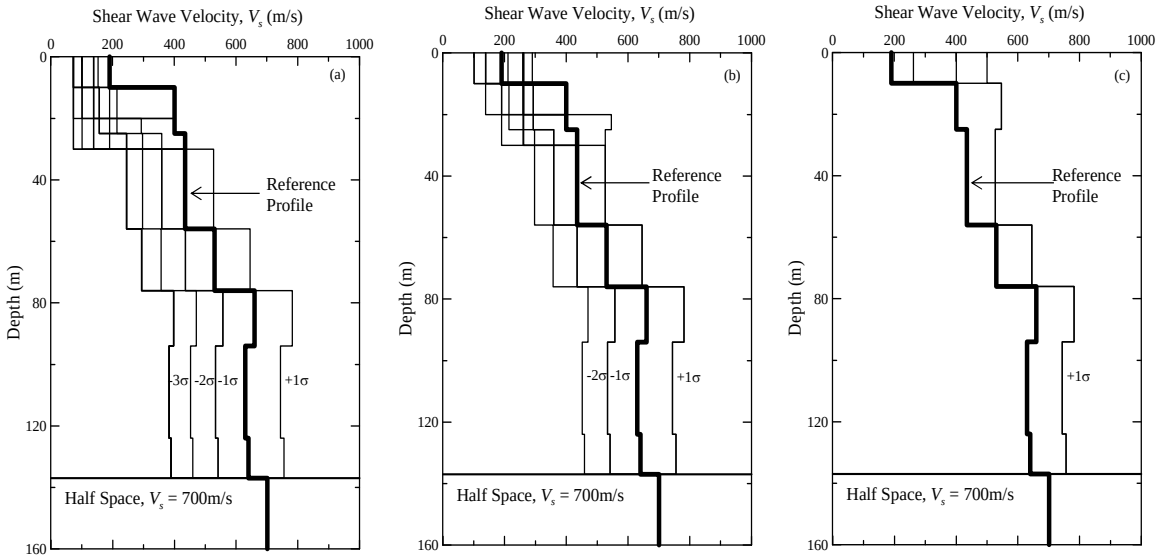

Figure A.1: Shear wave velocity profiles considered for the Charleston area without a low velocity layer at depth = 125 to 135 m, and soft rock half space at depth = 137 m. The reference profile and standard deviation values are based on Andrus et al. (2006).

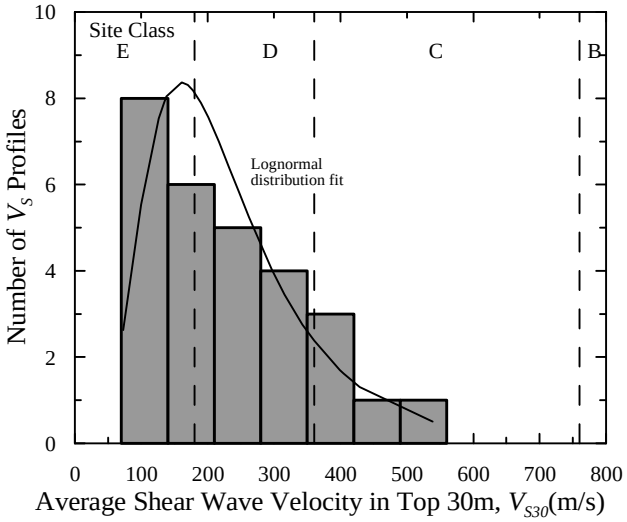

Figure A.2: V_{S30} histogram of shear wave velocity profiles in Figure A.1.

Table A.1: Table of best fit values of F_P and V_{S30P}

Figure	F_p	V_{S30P}	a
A.3a	2.0	152	-
A.3b	1.8	179	-
A.3c	1.5	224	-
A.3d	1.4	256	-
A.3e	1.0	320	-
A.3f	1.0	350	-
A.4a	2.0	160	0.63
A.4b	1.7	180	0.63
A.4c	1.5	250	0.65
A.4d	1.4	290	0.65
A.4e	1.1	310	0.67
A.4f	1.0	330	0.67
A.5a	3.0	160	0.84
A.5b	2.6	170	0.86
A.5c	2.5	214	0.85
A.5d	2.1	217	0.85
A.5e	1.5	245	0.85
A.5f	1.4	250	0.84
A.6a	3.7	160	0.98
A.6b	3.3	165	0.96
A.6c	2.9	183	0.88
A.6d	2.7	193	0.70
A.6e	1.9	207	0.80
A.6f	1.8	215	0.71
A.7a	4.1	114	1.00
A.7b	3.5	134	1.00
A.7c	3.1	149	0.99
A.7d	2.8	159	0.98
A.7e	2.0	184	0.93
A.7f	1.9	195	0.91
A.8a	1.9	100	0.99
A.8b	2.0	120	0.99
A.8c	2.3	145	0.99
A.8d	2.3	150	1.00
A.8e	1.7	155	0.97
A.8f	1.6	160	0.85

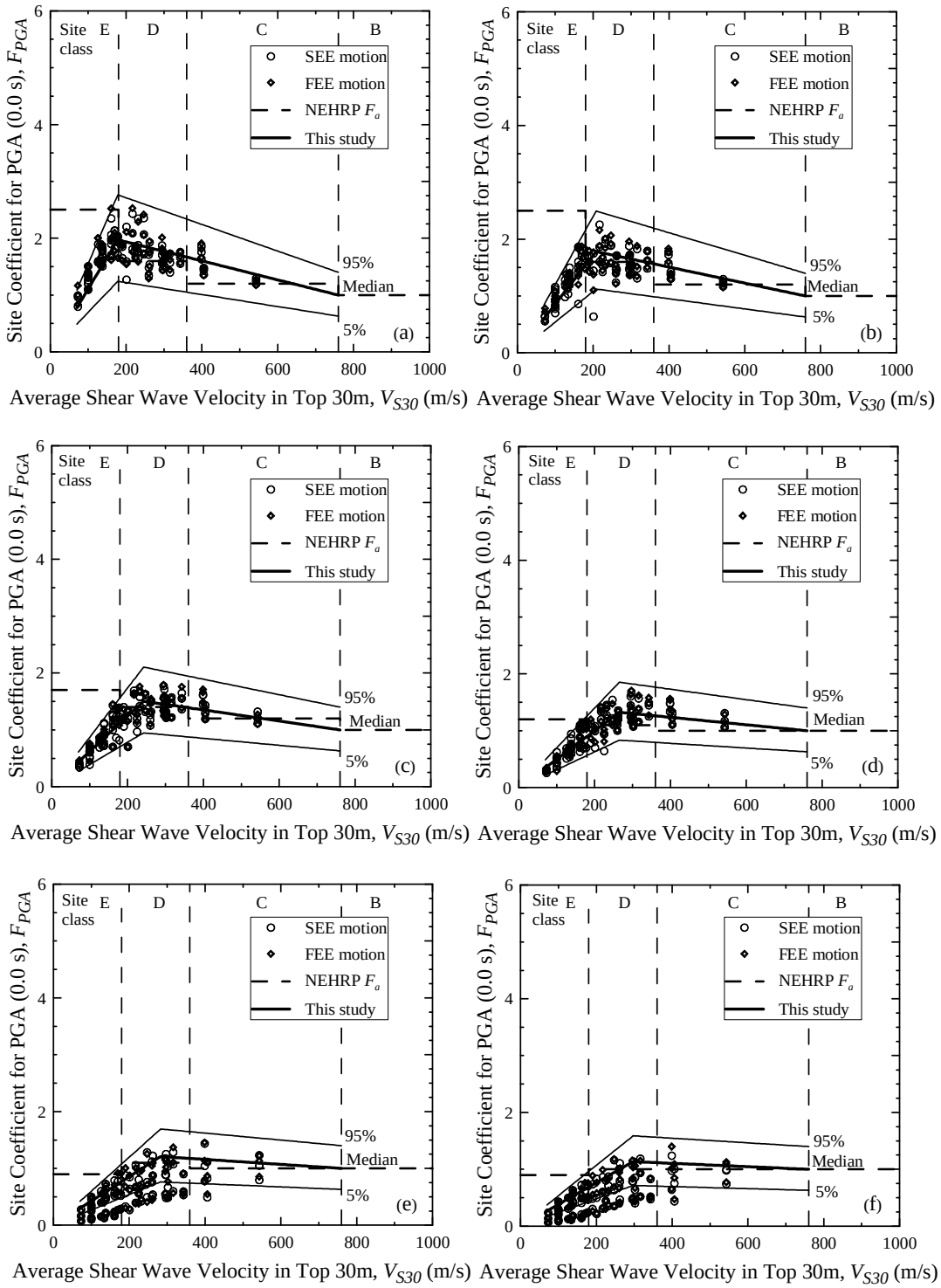

Figure A.3: Site coefficients for 0.0 s spectral period (free-field) with *PGA* equal to (a) 0.05 g, (b) 0.1 g, (c) 0.2 g, (d) 0.3 g, (e) 0.4 g, and (f) 0.5 g based on V_s profiles shown in Figure A.1 for the Charleston area.

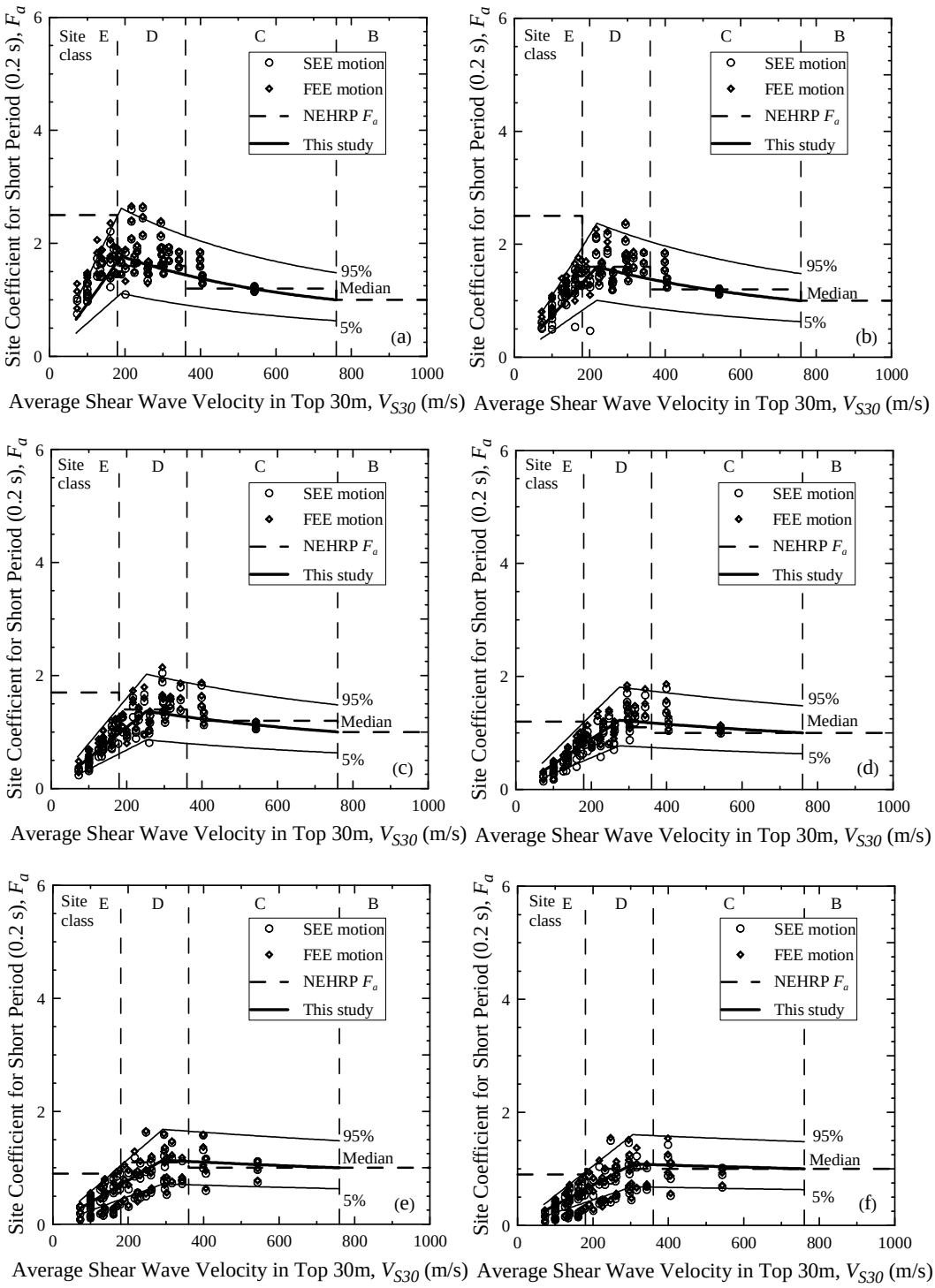

Figure A.4: Site coefficients for 0.2 s (short) spectral period with S_s equal to (a) 0.125 g, (b) 0.25 g, (c) 0.50 g, (d) 0.75 g, (e) 1.0 g, and (f) 1.25 g, based on V_s profiles shown in Figure A.1 for the Charleston area.

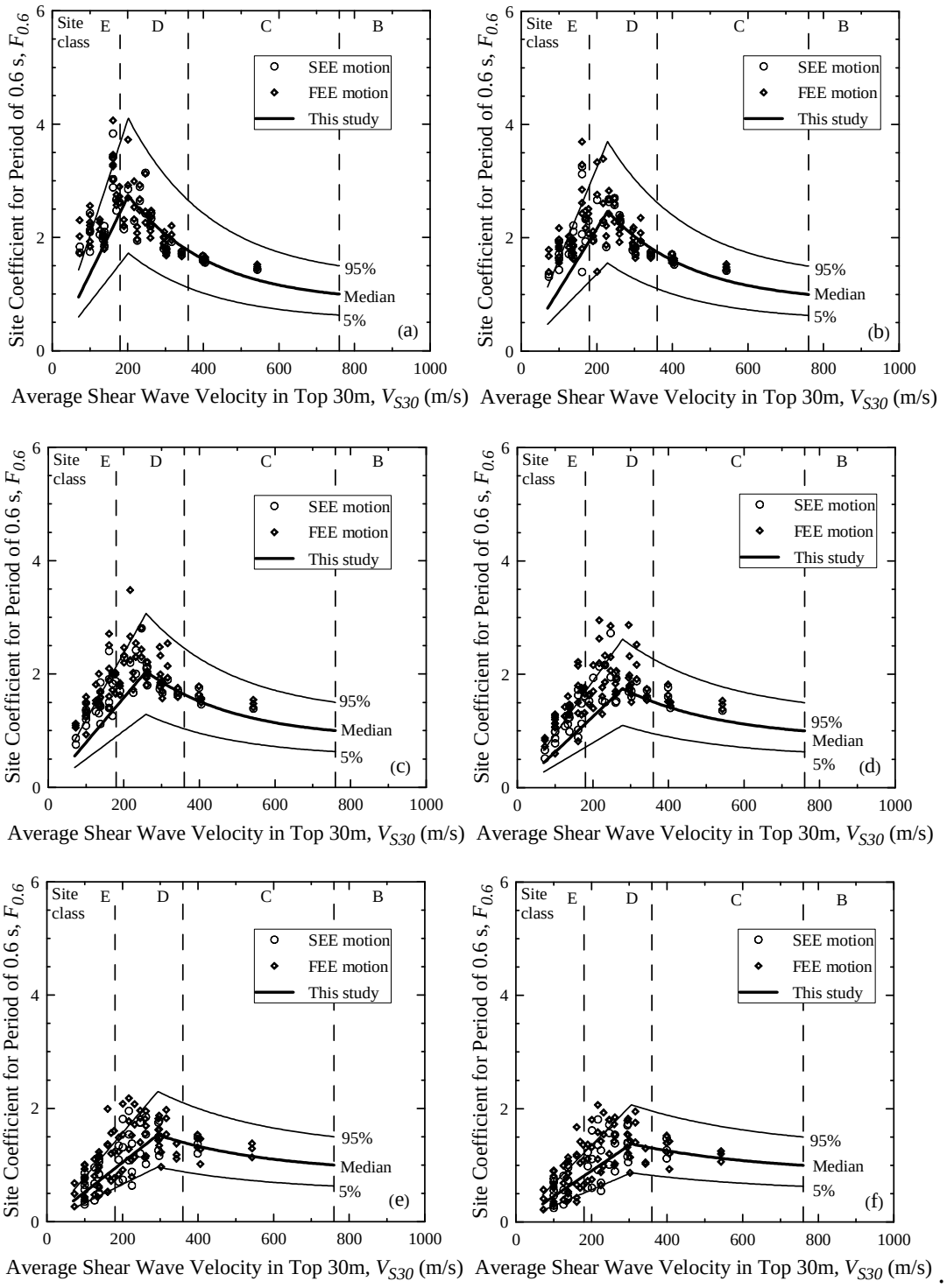

Figure A.5: Site coefficients for 0.6 s spectral period with $S_{0.6}$ equal to (a) 0.05 g, (b) 0.10g, (c) 0.20 g, (d) 0.30 g, (e) 0.40 g, and (f) 0.50 g, based on V_s profiles shown in Figure A.1 for the Charleston area.

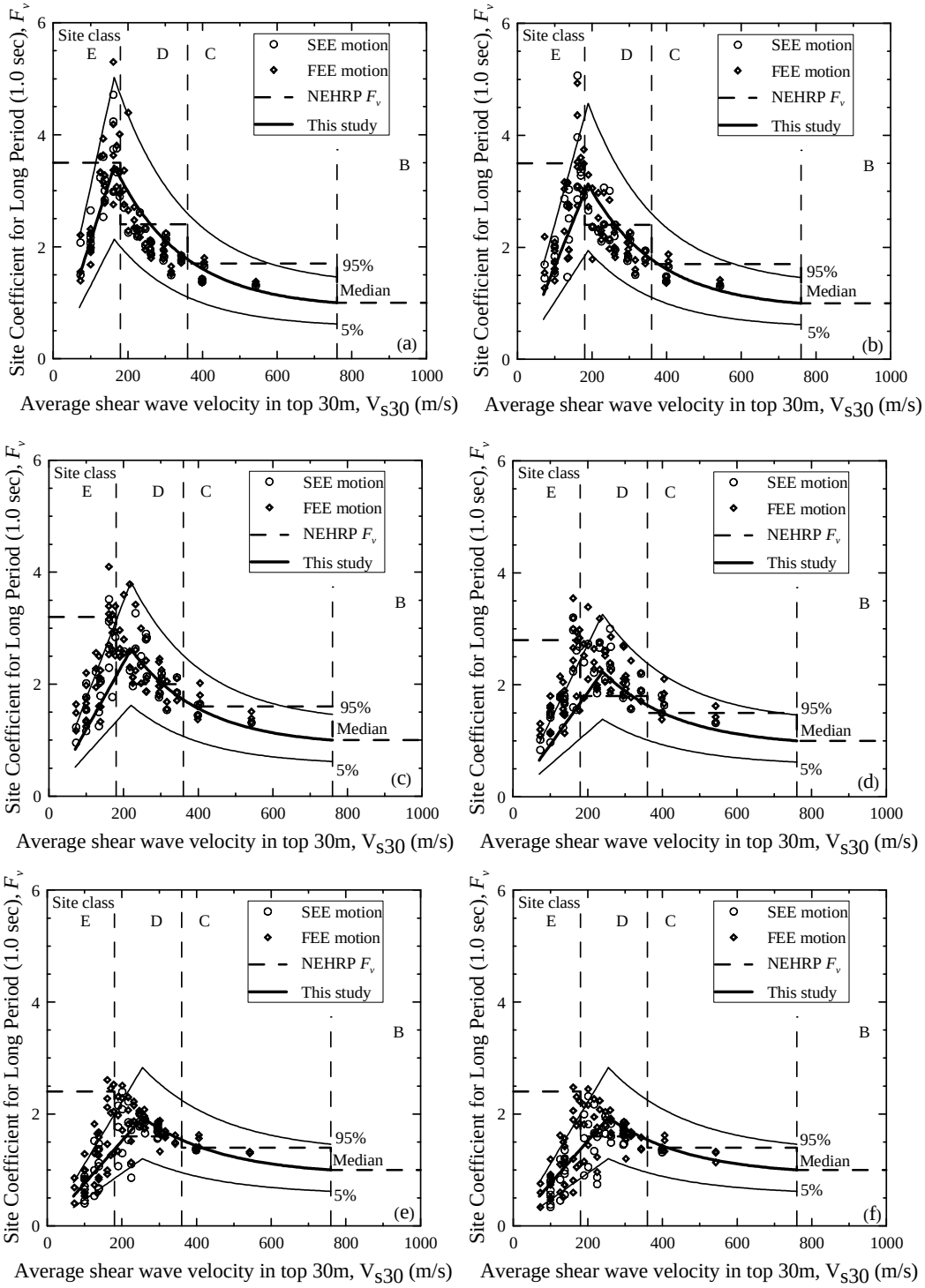

Figure A.6: Site coefficients for 1.0 s (long) spectral period with S_1 equal to (a) 0.05 g, (b) 0.10 g, (c) 0.20 g, (d) 0.30 g, (e) 0.40 g, and (f) 0.50 g, based on V_s profiles shown in Figure A.1 for the Charleston area.

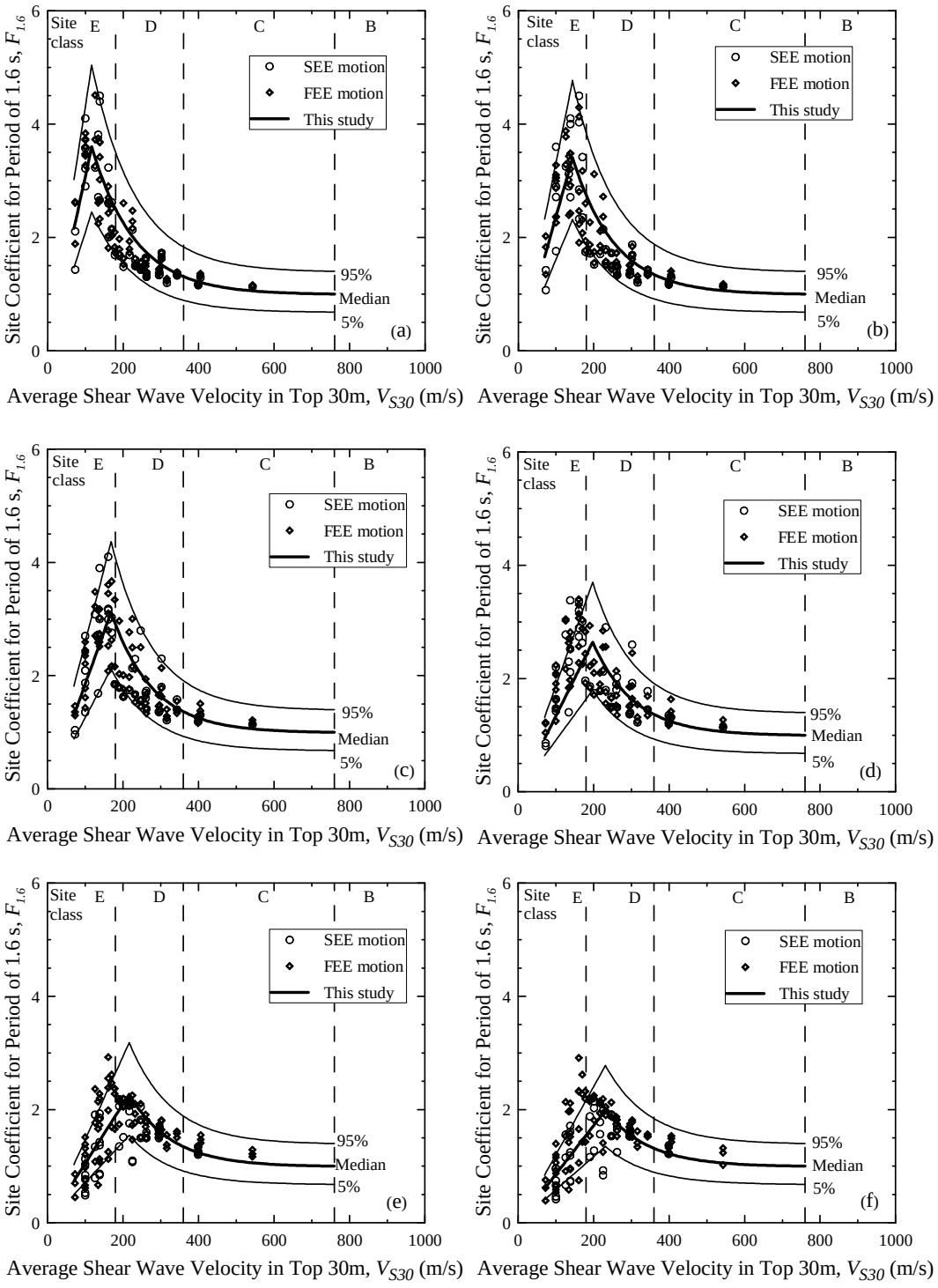

Figure A.7: Site coefficients for 1.6 s spectral period with $S_{1.6}$ equal to (a) 0.02 g, (b) 0.05 g, (c) 0.10 g, (d) 0.20 g, (e) 0.30 g, and (f) 0.40g, based on V_s profiles shown in Figure A.1 for the Charleston area.

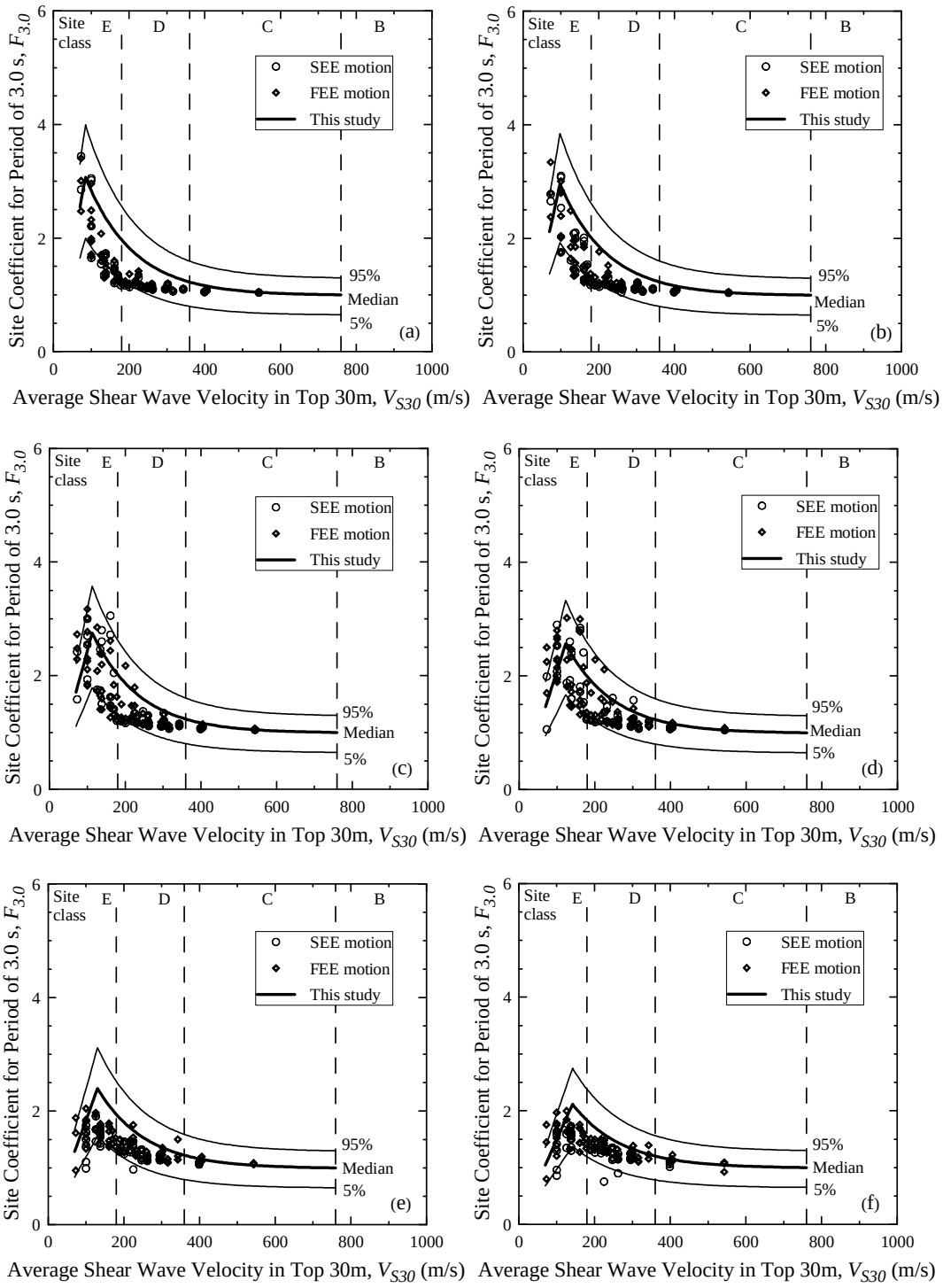

Figure A.8: Site coefficients for 3.0 s spectral period with $S_{3.0}$ equal to (a) 0.01 g, (b) 0.02 g, (c) 0.04 g, (d) 0.06 g, (e) 0.08 g and (f) 0.12 g, based on V_s profiles shown in Figure A.1 for the Charleston area.

APPENDIX B

SUMMARY OF INPUTS AND OUTPUTS OF SITE RESPONSE ANALYSIS FOR THE MYRTLE BEACH AREA

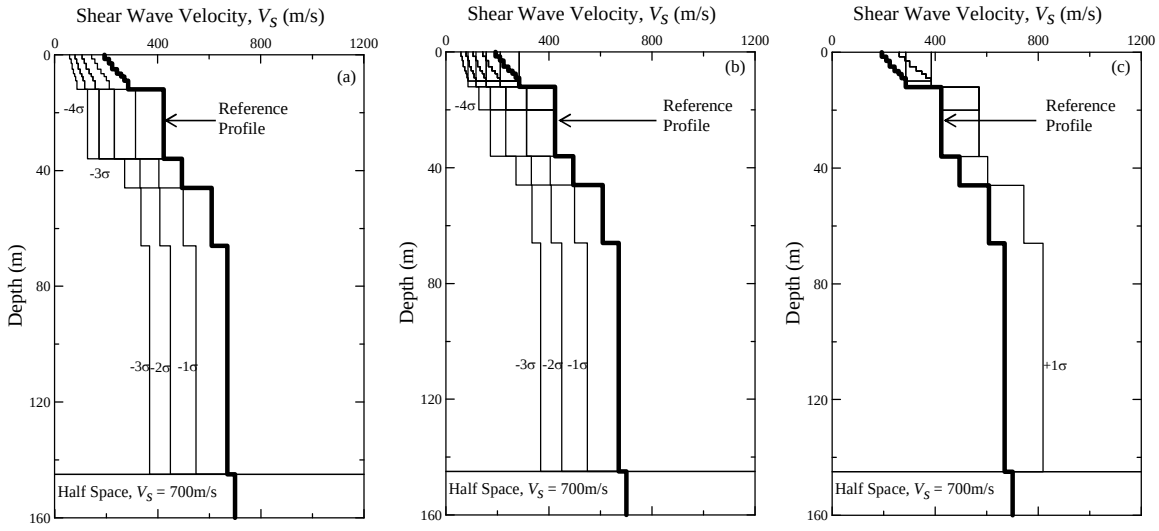

Figure B.1: Shear wave velocity profiles considered for Myrtle Beach with soft rock half space at depth = 145 m. The reference profile is from Silva et al. (2003), and the standard deviation values are based on a study by Andrus et al. (2006).

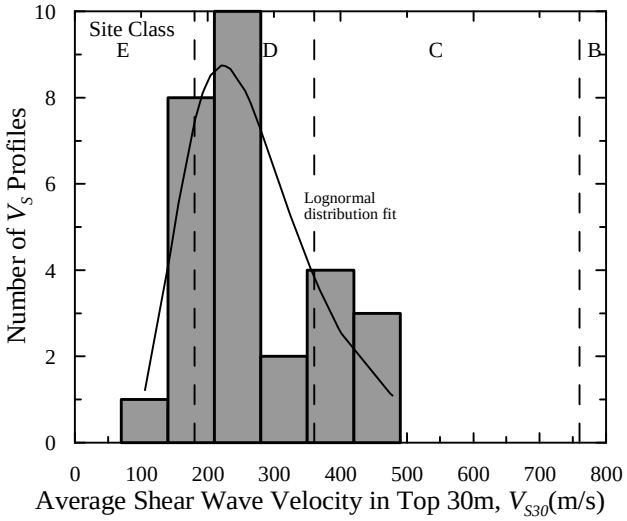

Figure B.2: V_{S30} histogram of shear wave velocity profiles in Figure B.1.

Table B.1: Table of best fit values of F_P and V_{S30P}

Figure	F_p	V_{S30P}	a
B.3a	2.8	152	-
B.3b	2.4	179	-
B.3c	2.0	224	-
B.3d	1.8	256	-
B.3e	1.0	360	-
B.3f	1.0	380	-
B.4a	2.7	160	0.80
B.4b	2.3	200	0.85
B.4c	2.0	250	0.91
B.4d	1.9	270	0.95
B.4e	1.0	300	0.99
B.4f	1.0	320	0.99
B.5a	3.7	160	0.97
B.5b	3.2	170	0.92
B.5c	2.9	214	0.95
B.5d	2.7	217	0.93
B.5e	1.4	245	0.94
B.5f	1.4	250	0.96
B.6a	3.9	140	0.99
B.6b	3.7	150	0.99
B.6c	3.4	170	0.99
B.6d	3.2	190	0.99
B.6e	1.6	210	0.65
B.6f	1.6	220	0.60
B.7a	4.0	114	1.00
B.7b	3.9	134	1.00
B.7c	3.4	149	1.00
B.7d	3.2	159	1.00
B.7e	1.6	184	0.99
B.7f	1.5	195	0.99
B.8a	1.7	73	0.99
B.8b	1.7	80	0.99
B.8c	1.7	130	0.96
B.8d	1.6	160	1.00
B.8e	1.5	180	0.97
B.8f	1.4	210	0.85

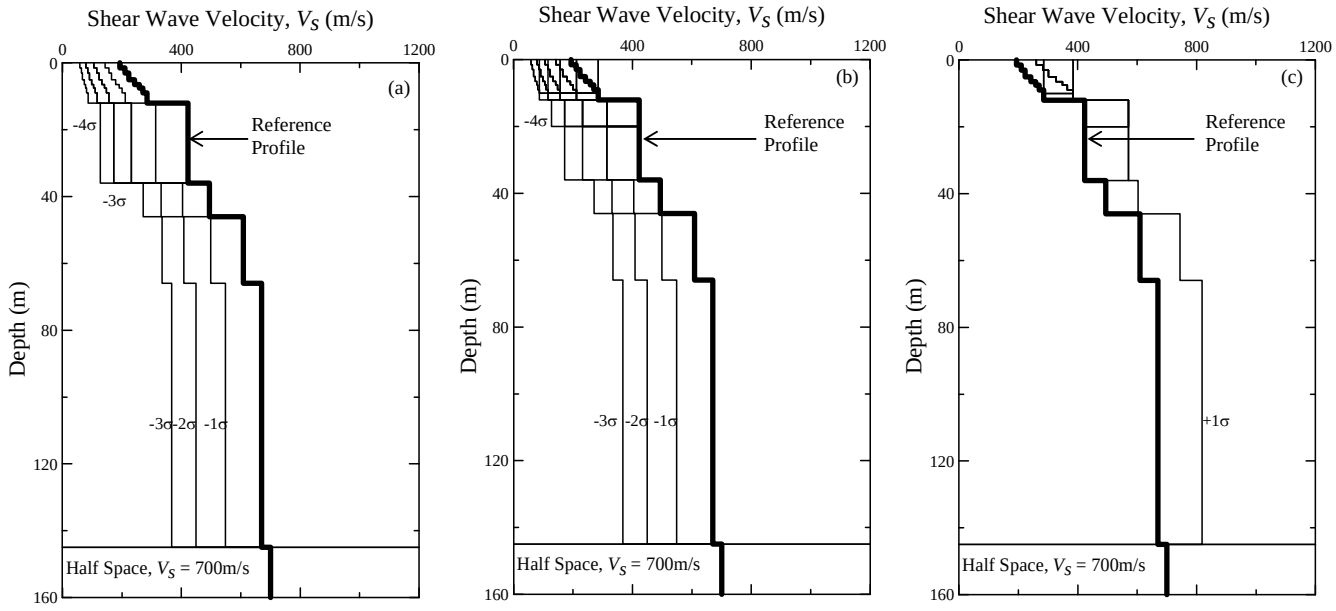

Figure B.1: Shear wave velocity profiles considered for Myrtle Beach with soft rock half space at depth = 145 m. The reference profile is from Silva et al. (2003), and the standard deviation values are based on a study by Andrus et al. (2006).

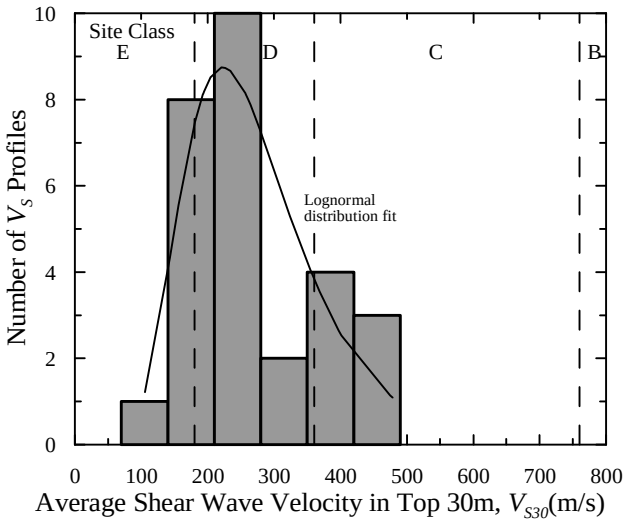

Figure B.2: V_{S30} histogram of shear wave velocity profiles in Figure B.1.

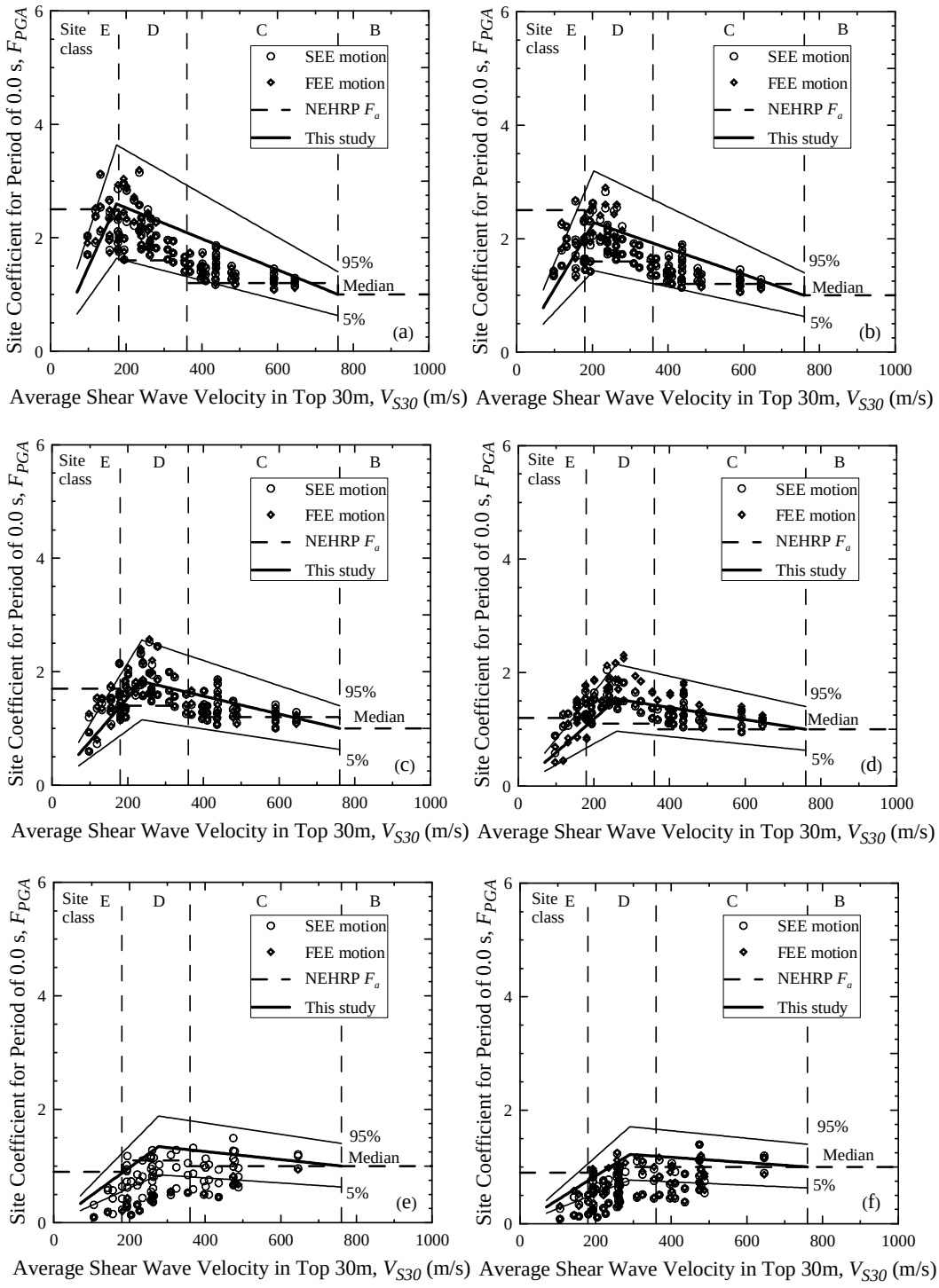

Figure B.3: Site coefficients for 0.0 s spectral period (free-field) with *PGA* equal to (a) 0.05 g, (b) 0.1 g, (c) 0.2 g, (d) 0.3 g, (e) 0.4 g, and (f) 0.5 g, based on V_s profiles shown in Figure B.1 for the Myrtle Beach area.

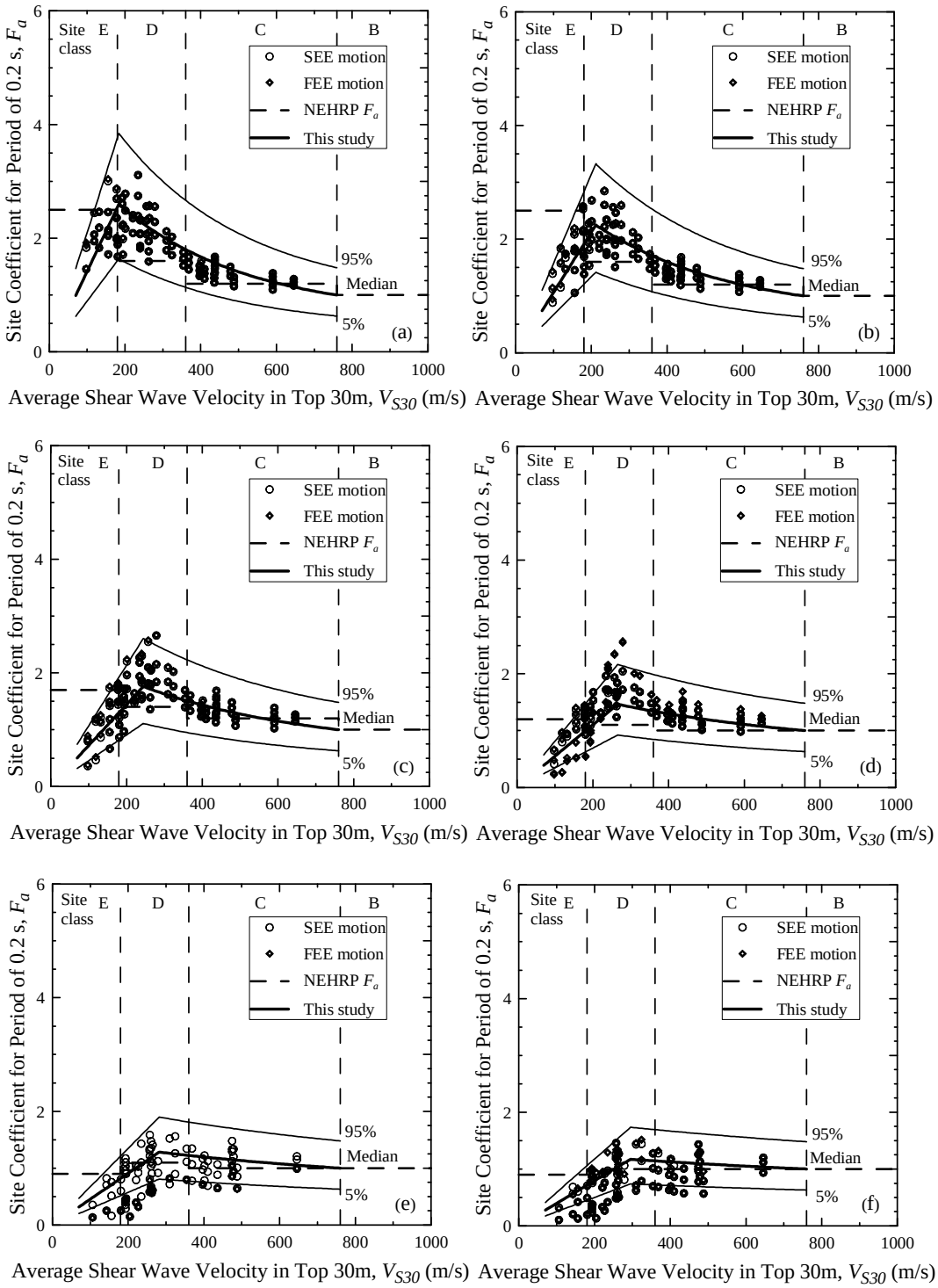

Figure B.4: Site coefficients for 0.2 s (short) spectral period with S_s equal to (a) 0.125 g, (b) 0.25 g, (c) 0.50 g, (d) 0.75 g, (e) 1.0 g, and (f) 1.25 g, based on V_s profiles shown in Figure B.1 for the Myrtle Beach area.

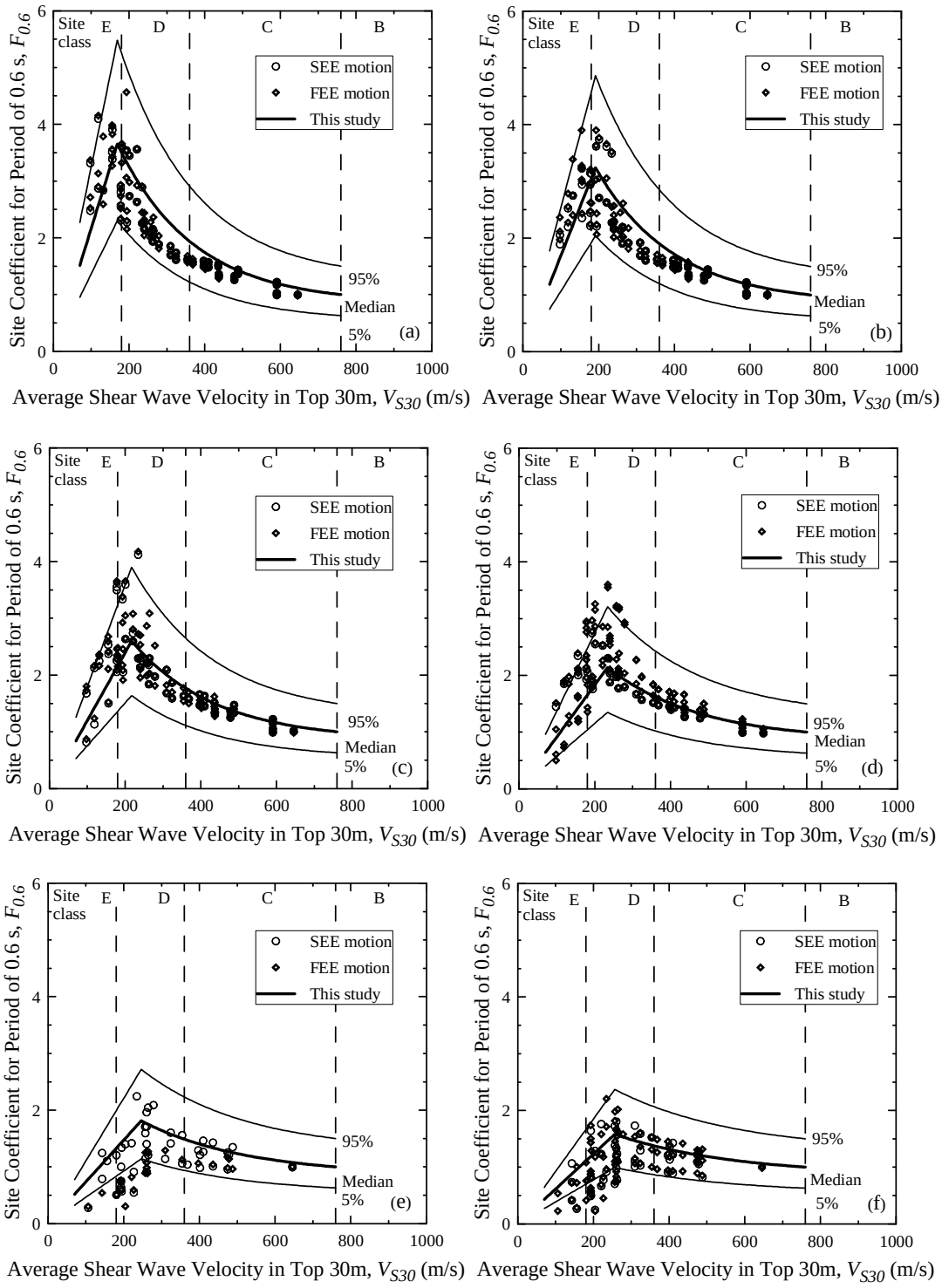

Figure B.5: Site coefficients for 0.6 s spectral period with $S_{0.6}$ equal to (a) 0.05 g, (b) 0.10g, (c) 0.20 g, (d) 0.30 g, (e) 0.40 g, and (f) 0.50 g, based on V_s profiles shown in Figure B.1 for the Myrtle Beach area.

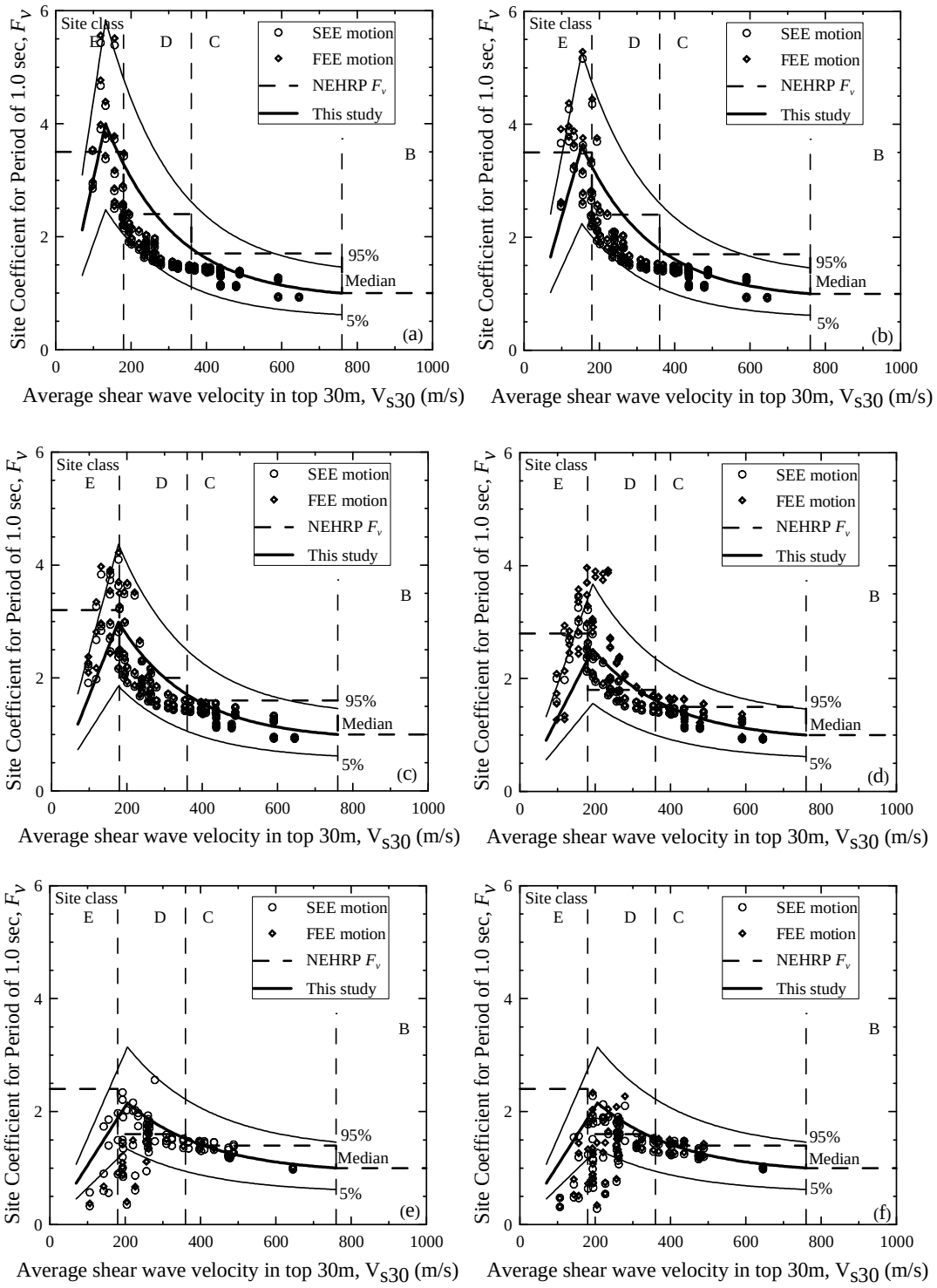

Figure B.6: Site coefficients for 1.0 s (long) spectral period with S_1 equal to (a) 0.05 g, (b) 0.10 g, (c) 0.20 g, (d) 0.30 g, (e) 0.40 g, and (f) 0.50 g, based on V_s profiles shown in Figure B.1 for the Myrtle Beach area.

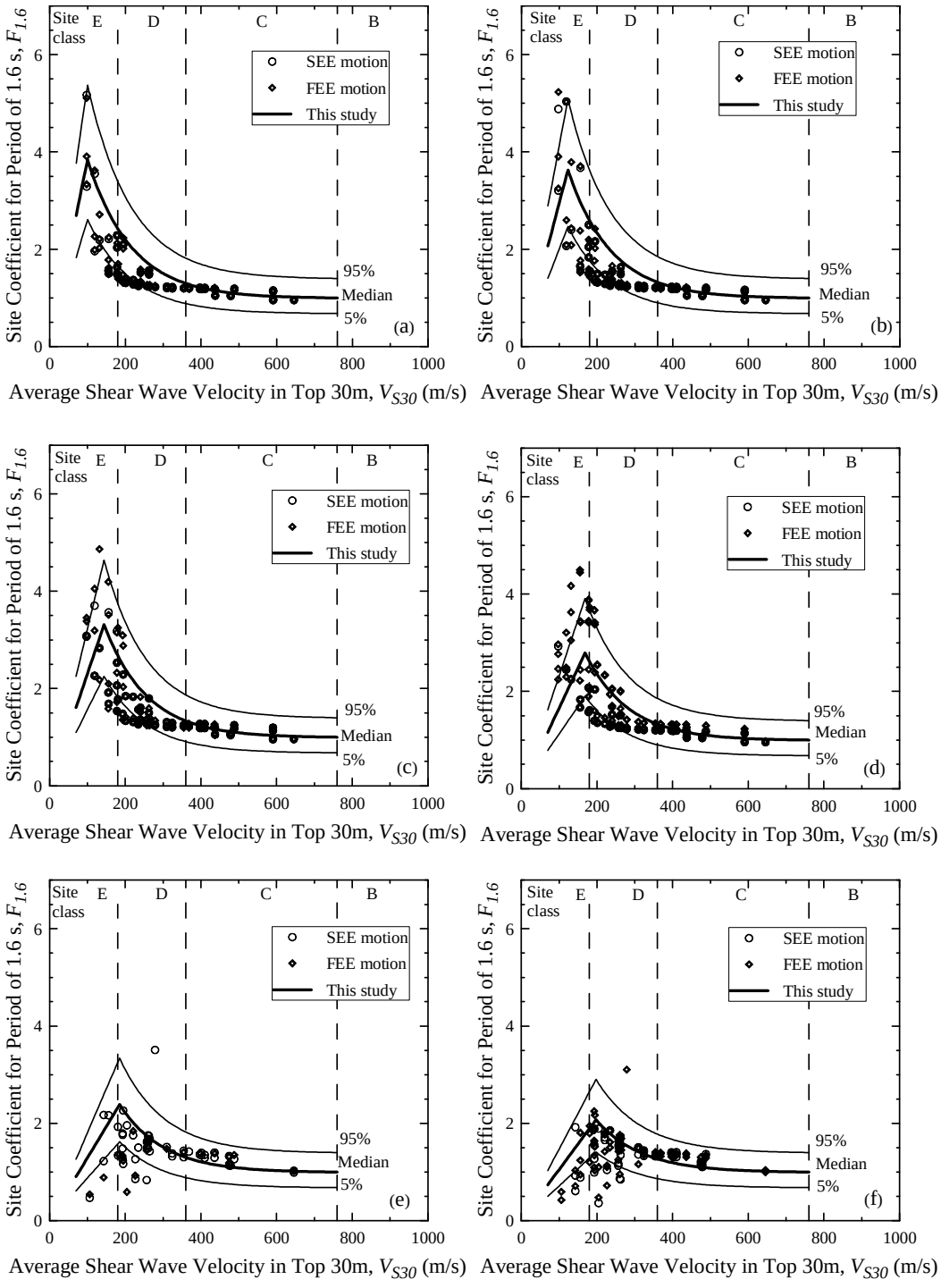

Figure B.7 Site coefficients for 1.6 s spectral period with $S_{1.6}$ equal to (a) 0.02 g, (b) 0.05 g, (c) 0.10 g, (d) 0.20 g, (e) 0.30 g, and (f) 0.40g, based on V_s profiles shown in Figure B.1 for the Myrtle Beach area.

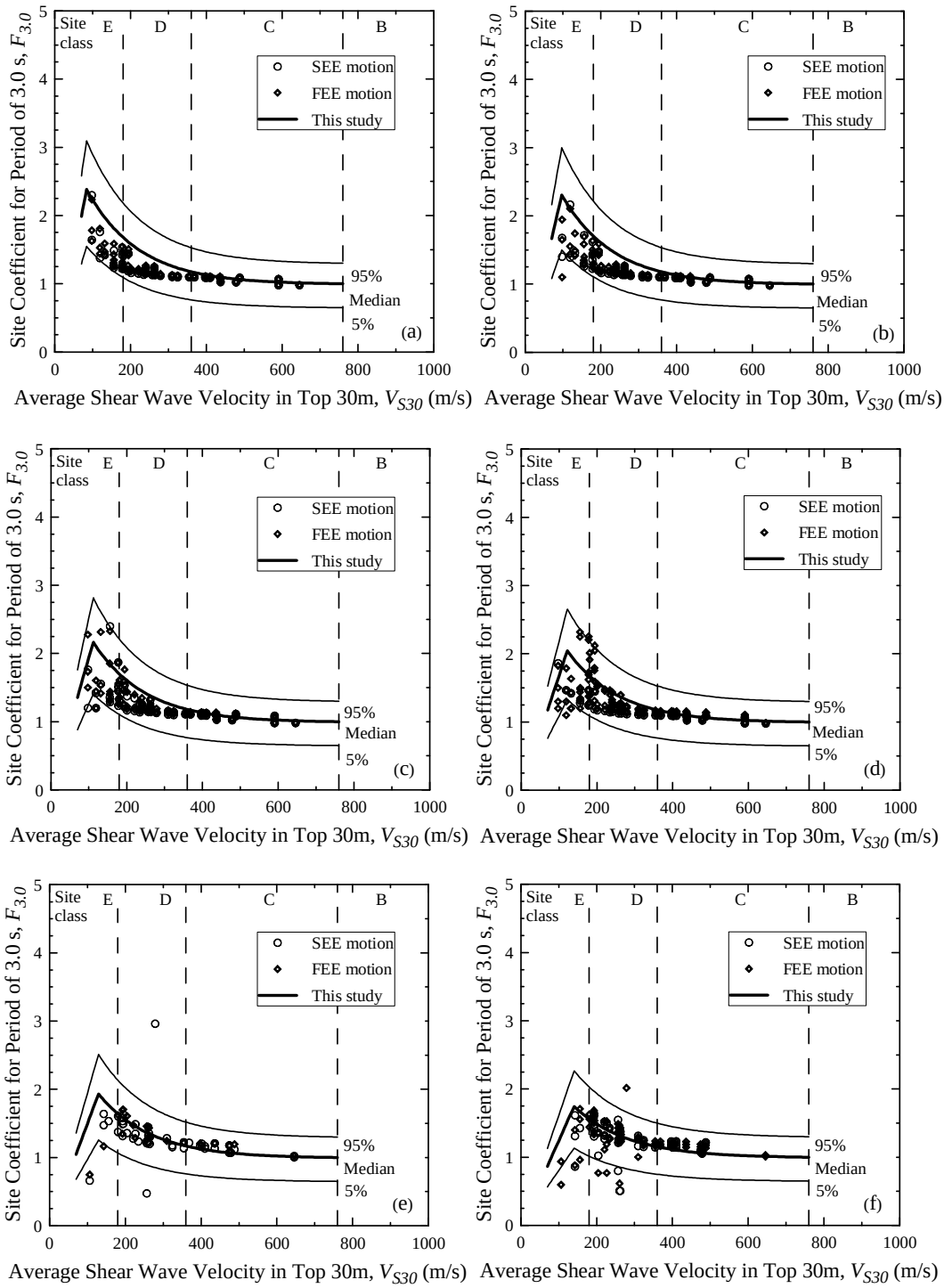

Figure B.8: Site coefficients for 3.0 s spectral period with $S_{3.0}$ equal to (a) 0.01 g, (b) 0.02 g, (c) 0.04 g, (d) 0.06 g, (e) 0.08 g and (f) 0.12 g, based on V_s profiles shown in Figure B.1 for the Myrtle Beach area.

APPENDIX C

SUMMARY OF INPUTS AND OUTPUTS OF SITE RESPONSE ANALYSIS FOR THE COLUMBIA AREA

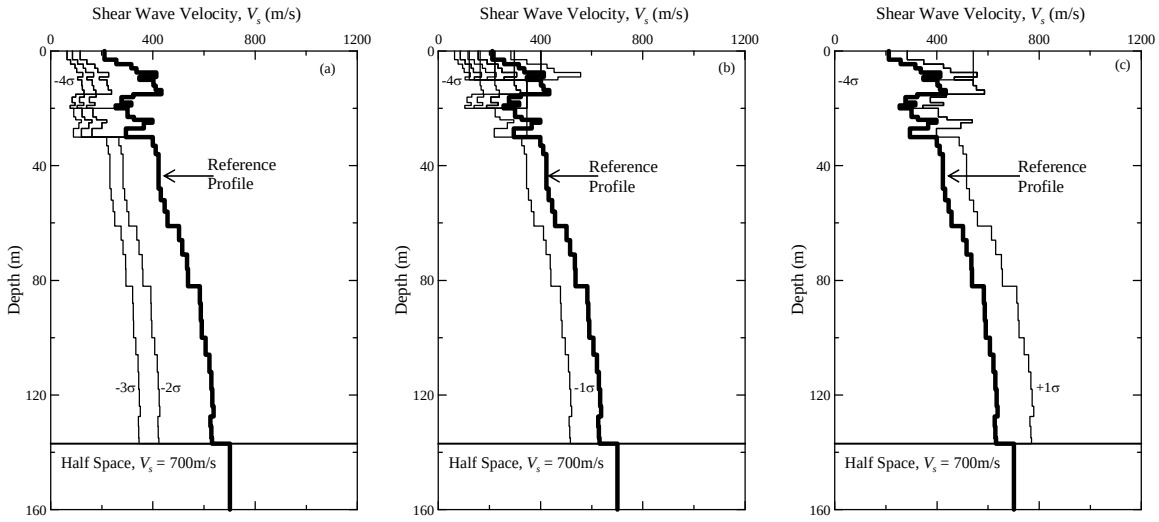

Figure C.1: Shear wave velocity profiles considered for Columbia-Florence-Lake Marion area with soft rock half space at depth = 137 m. The reference profile is compiled from Odum et al. (2003), Silva et al. (2003), Chapman et al. (2006) and Andrus et al. (2006), and the standard deviation values are based on Andrus et al. (2006).

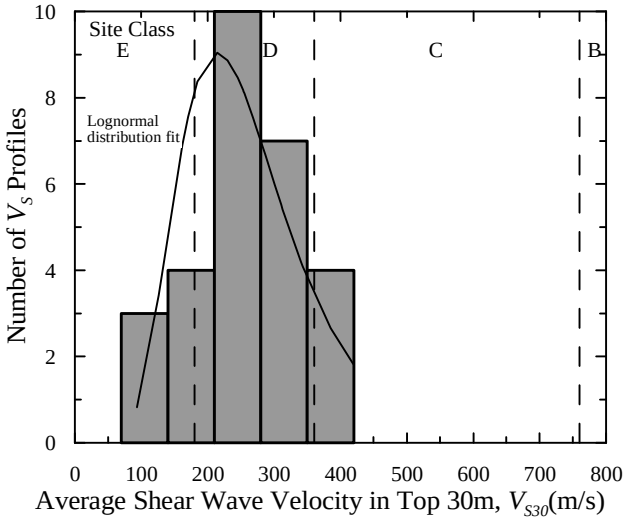

Figure C.2: V_{S30} histogram of shear wave velocity profiles in Figure C.1.

Table C.1: Table of best fit values of F_P and V_{S30P}

Figure	F_p	V_{S30P}	a
C.3a	2.0	198	-
C.3b	1.6	240	-
C.3c	1.1	270	-
C.3d	1.1	350	-
C.3e	1.0	300	-
C.3f	1.0	310	-
C.4a	2.2	140	0.99
C.4b	1.5	220	0.99
C.4c	1.1	300	0.70
C.4d	1.0	360	0.70
C.4e	1.0	250	0.70
C.4f	1.0	280	0.70
C.5a	2.4	220	0.72
C.5b	2.0	230	0.46
C.5c	1.8	240	0.99
C.5d	1.4	260	0.99
C.5e	1.4	260	0.99
C.5f	1.3	290	0.99
C.6C	2.8	173	0.83
C.6b	2.6	198	0.83
C.6c	2.3	251	0.83
C.6d	2.0	278	0.83
C.6e	2.0	280	0.83
C.6f	1.9	300	0.83
C.7a	3.0	125	0.98
C.7b	2.6	150	0.94
C.7c	2.3	170	0.59
C.7d	2.2	200	0.31
C.7e	2.4	220	0.73
C.7f	2.4	250	0.75
C.8a	2.3	90	0.99
C.8b	2.2	110	0.99
C.8c	2.0	130	0.96
C.8d	2.4	150	1.00
C.8e	2.4	190	0.75
C.8f	2.4	220	0.80

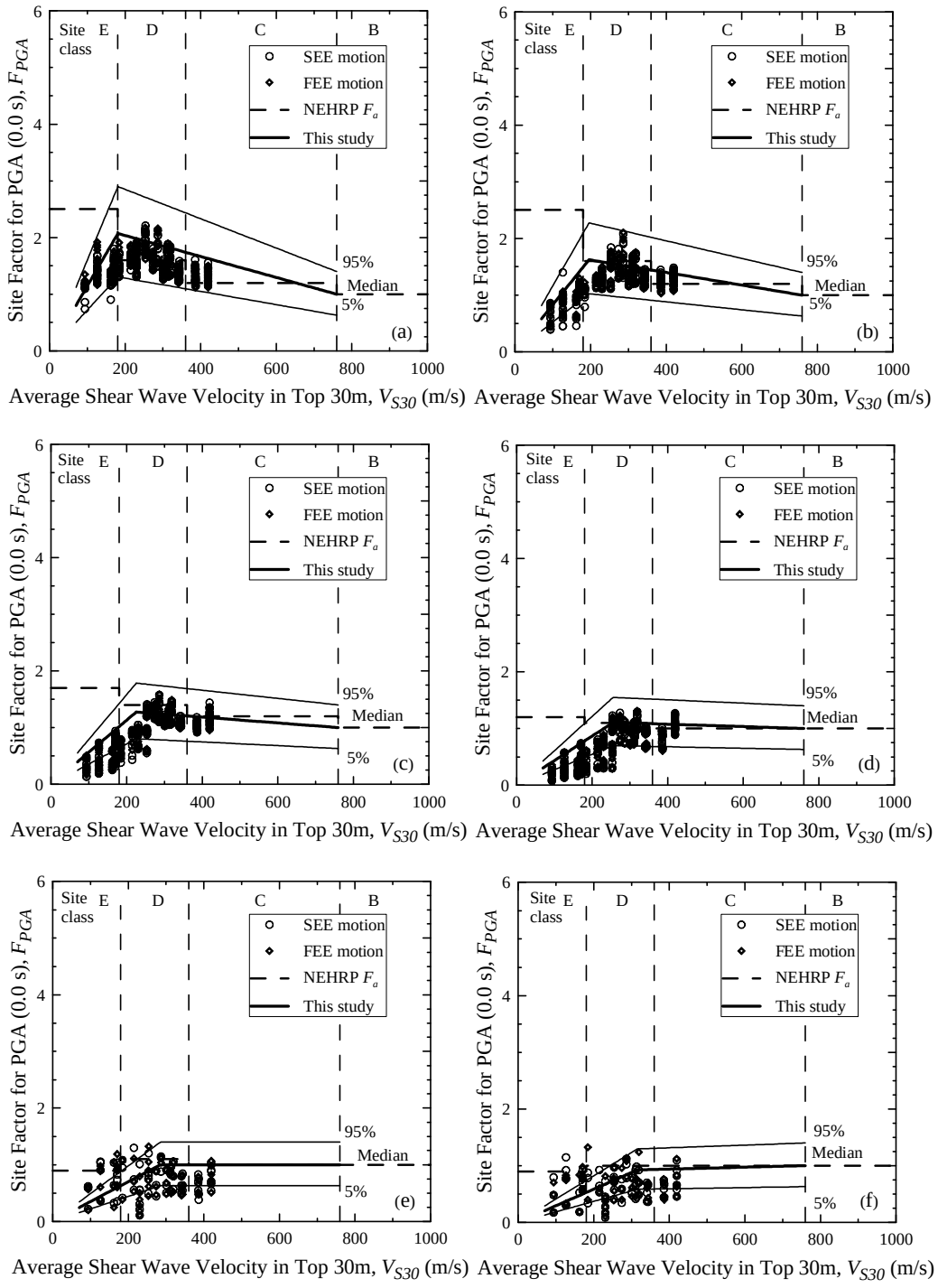

Figure C.3: Site coefficients for 0.0 s spectral period (free-field) with *PGA* equal to (a) 0.05 g, (b) 0.1 g, (c) 0.2 g, (d) 0.3 g, (e) 0.4 g, and (f) 0.5 g, based on V_s profiles shown in Figure C.1 for the Columbia area.

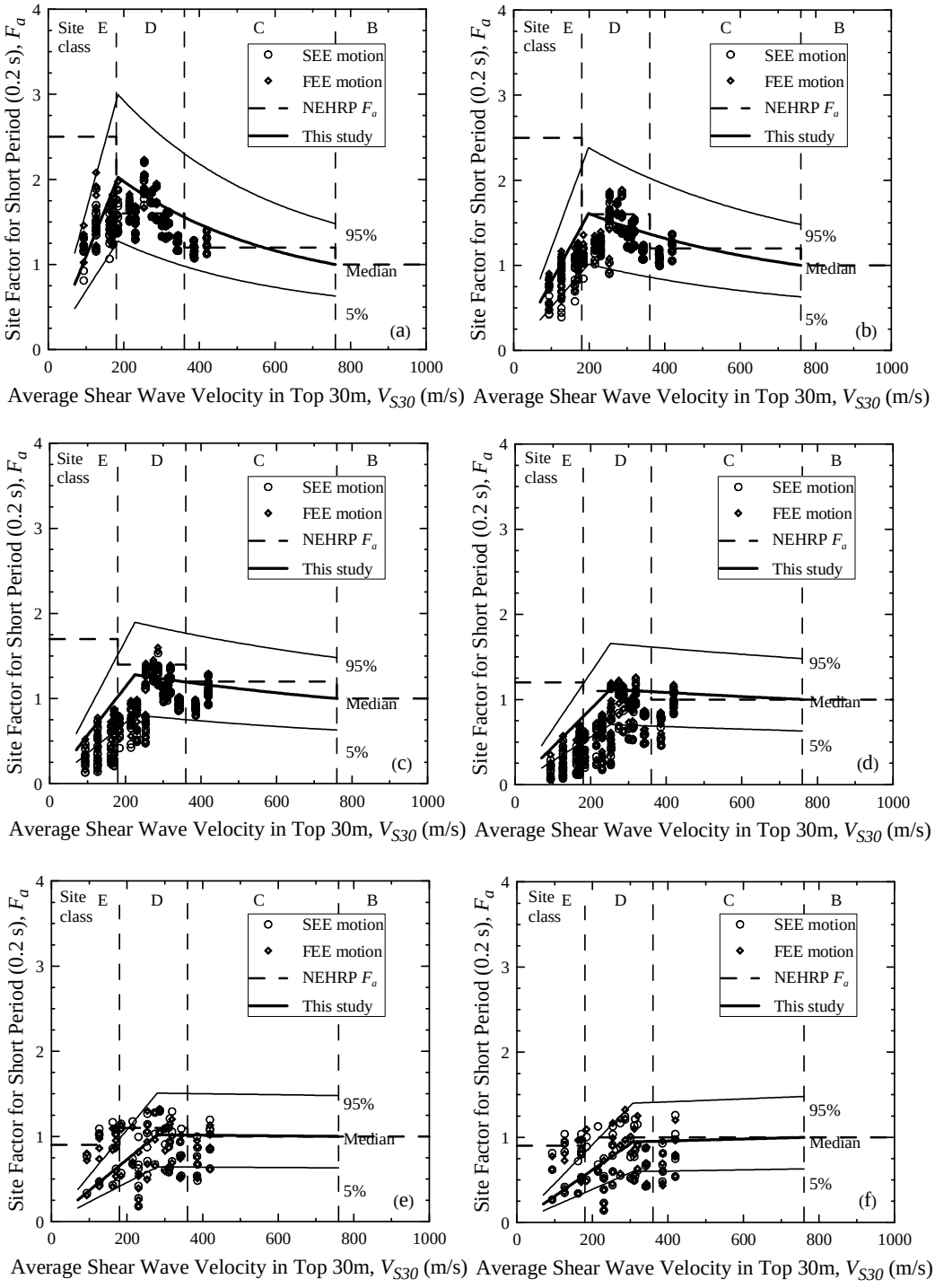

Figure C.4: Site coefficients for 0.2 s (short) spectral period with S_s equal to (a) 0.125 g, (b) 0.25 g, (c) 0.50 g, (d) 0.75 g, (e) 1.0 g, and (f) 1.25 g, based on V_s profiles shown in Figure C.1 for the Columbia area.

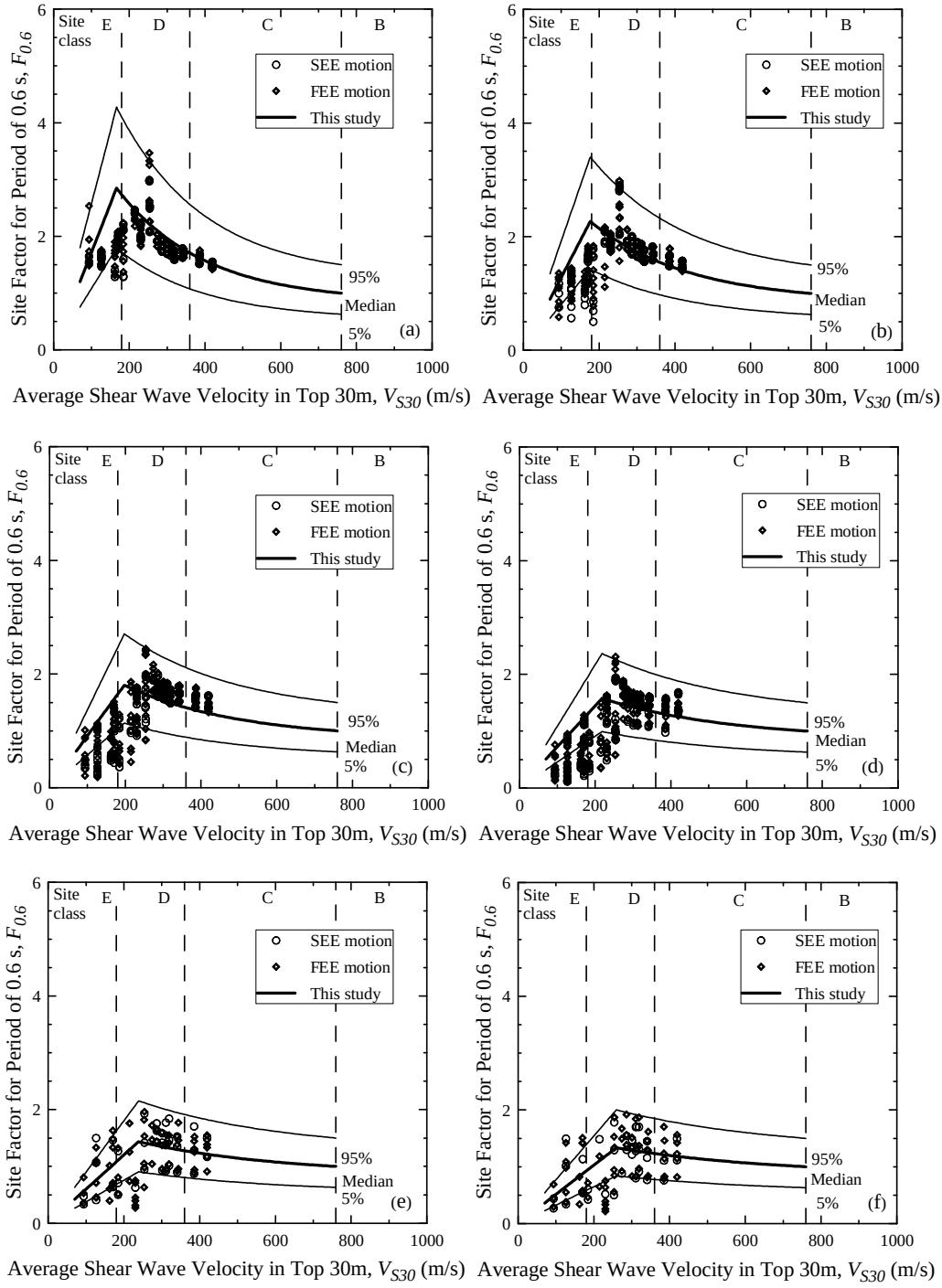

Figure C.5: Site coefficients for 0.6 s spectral period with $S_{0.6}$ equal to (a) 0.05 g, (b) 0.10g, (c) 0.20 g, (d) 0.30 g, (e) 0.40 g, and (f) 0.50 g, based on V_s profiles shown in Figure C.1 for the Columbia area.

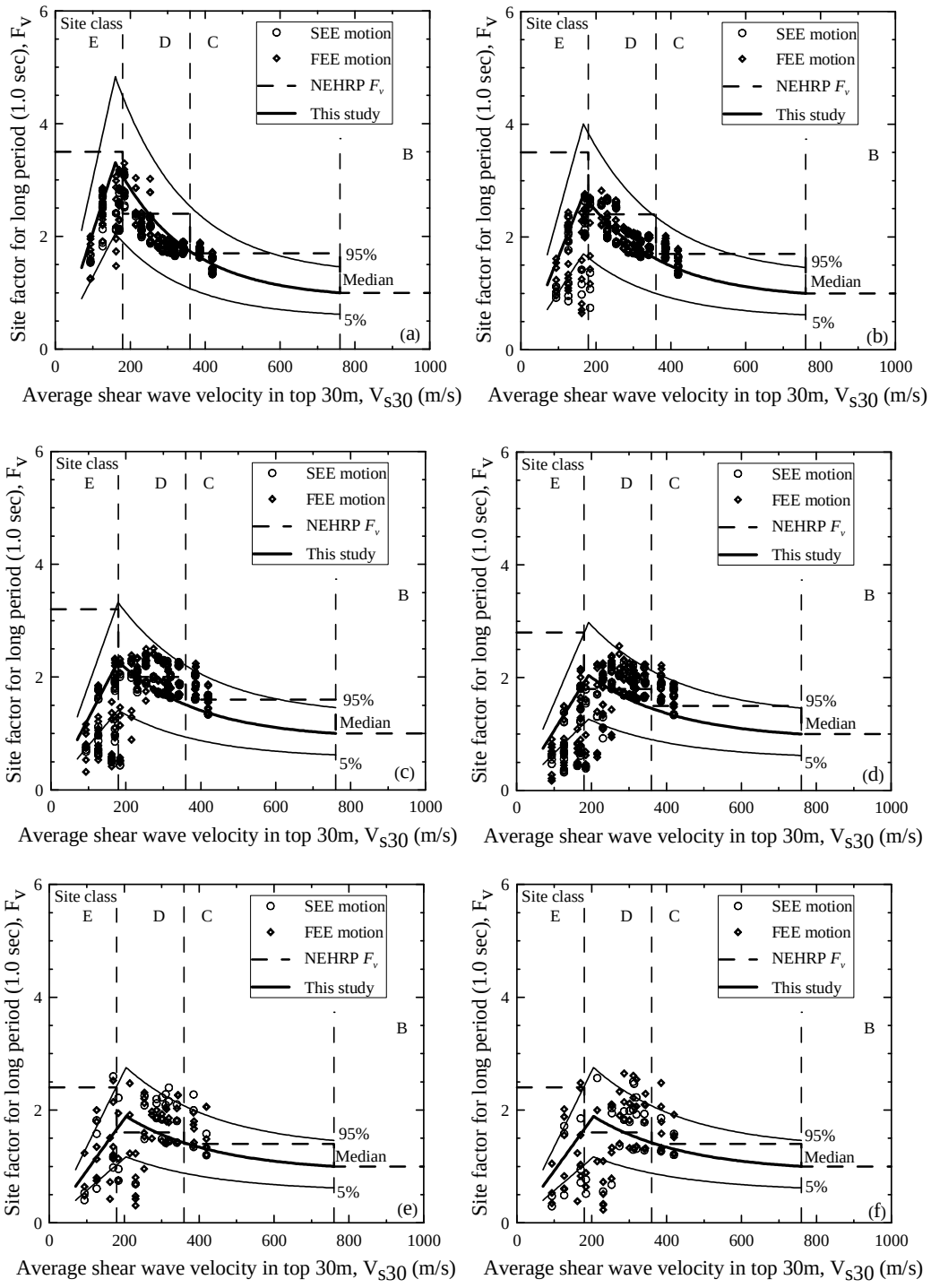

Figure C.6: Site coefficients for 1.0 s (long) spectral period with S_1 equal to (a) 0.05 g, (b) 0.10 g, (c) 0.20 g, (d) 0.30 g, (e) 0.40 g, and (f) 0.50 g, based on V_s profiles shown in Figure C.1 for the Columbia area.

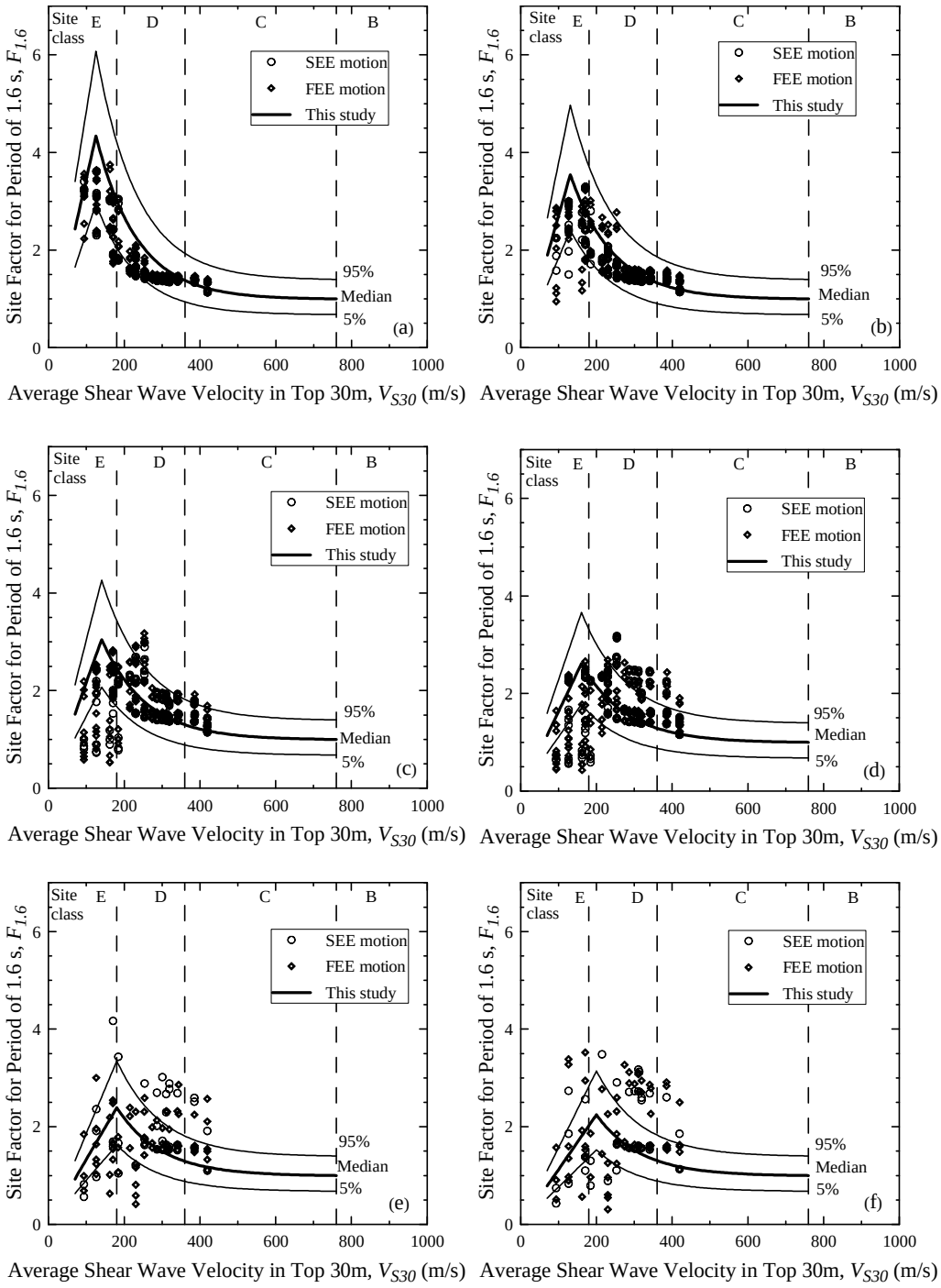

Figure C.7: Site coefficients for 1.6 s spectral period with $S_{1.6}$ equal to (a) 0.02 g, (b) 0.05 g, (c) 0.10 g, (d) 0.20 g, (e) 0.30 g, and (f) 0.40 g, based on V_s profiles shown in Figure C.1 for the Columbia area.

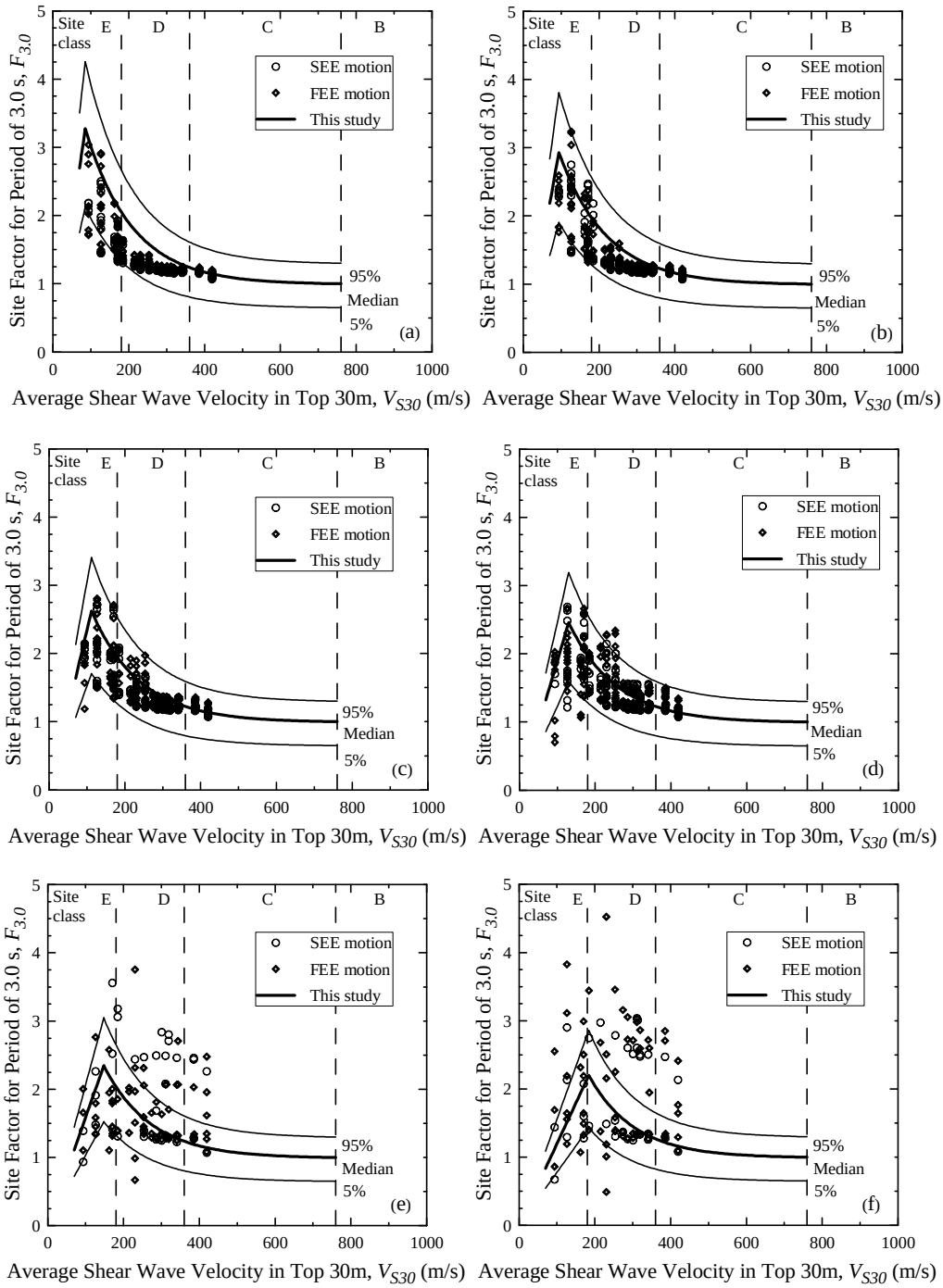

Figure C.8: Site coefficients for 3.0 s spectral period with $S_{3.0}$ equal to (a) 0.01 g, (b) 0.02 g, (c) 0.04 g, (d) 0.06 g, (e) 0.08 g and (f) 0.12 g, based on V_s profiles shown in Figure C.1 for the Columbia area.

APPENDIX D

SUMMARY OF INPUTS AND OUTPUTS OF SITE RESPONSE ANALYSIS FOR THE AIKEN AREA

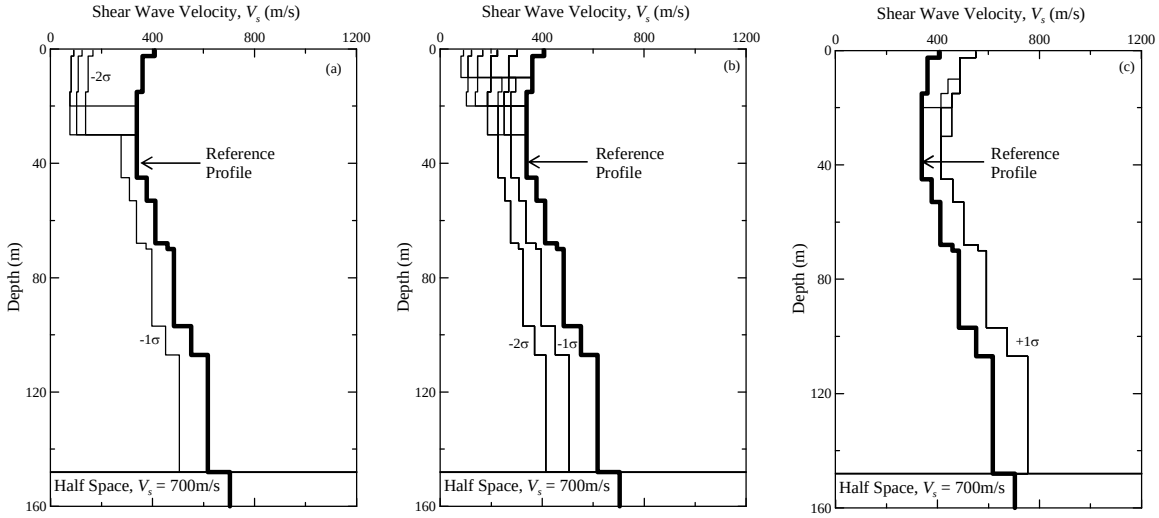

Figure D.1: Shear wave velocity profiles considered for the Aiken area with soft rock half space at depth = 148 m. The reference profile is from Silva et al. (2003), and the standard deviation values are based on a study by Andrus et al. (2006).

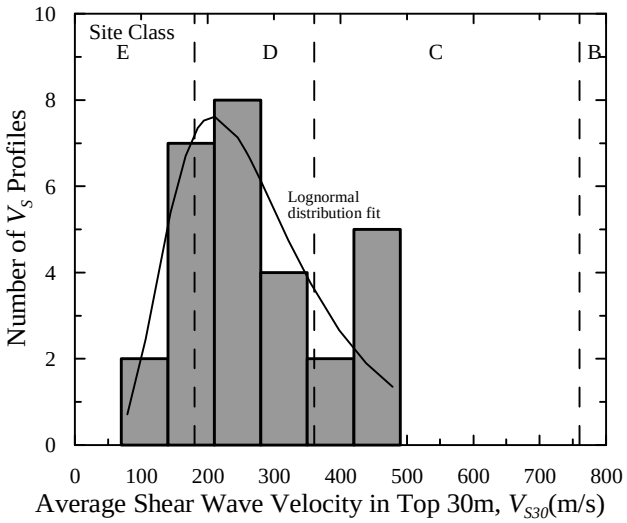

Figure D.2: V_{S30} histogram of shear wave velocity profiles in Figure D.1.

Table D.1: Table of best fit values of F_P and V_{S30P}

Figure	V_{S30P}	F_p	a
D.3a	160	2.3	-
D.3b	185	1.8	-
D.3c	230	1.7	-
D.3d	260	1.3	-
D.3e	450	1.0	-
D.3f	460	1.0	-
D.4a	180	2.1	0.98
D.4b	220	1.8	0.98
D.4c	250	1.4	0.99
D.4d	270	1.2	0.99
D.4e	410	1.0	0.99
D.4f	440	1.0	0.99
D.5a	180	2.6	0.72
D.5b	190	2.3	0.46
D.5c	214	2.2	0.90
D.5d	260	1.8	0.70
D.5e	320	1.1	0.99
D.5f	320	1.0	0.99
D.6a	180	3.2	0.85
D.6b	190	3.0	0.85
D.6c	200	2.8	0.85
D.6d	220	2.5	0.85
D.6e	290	1.1	0.85
D.6f	300	1.1	0.85
D.7a	114	3.5	0.85
D.7b	134	3.3	0.85
D.7c	149	3.0	0.83
D.7d	200	2.9	0.85
D.7e	270	1.4	0.85
D.7f	280	1.4	0.85
D.8a	73	2.4	0.90
D.8b	90	2.3	0.90
D.8c	180	2.2	0.90
D.8d	200	2.1	0.90
D.8e	210	1.7	0.90
D.8f	280	1.6	0.90

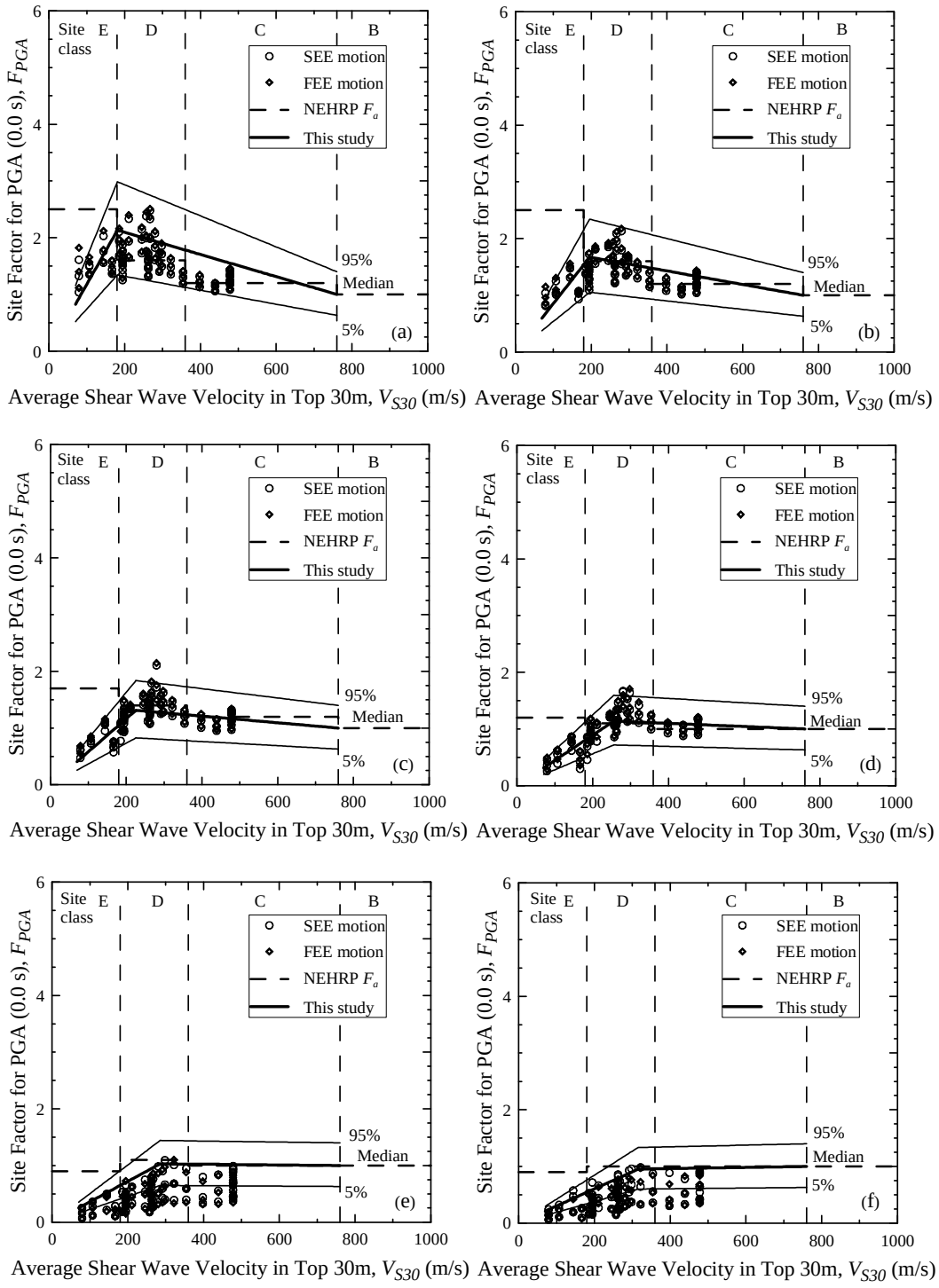

Figure D.3: Site coefficients for 0.0 s spectral period (free-field) with *PGA* equal to (a) 0.05 g, (b) 0.1 g, (c) 0.2 g, (d) 0.3 g, (e) 0.4 g, and (f) 0.5 g, based on V_s profiles shown in Figure D.1 for the Aiken area.

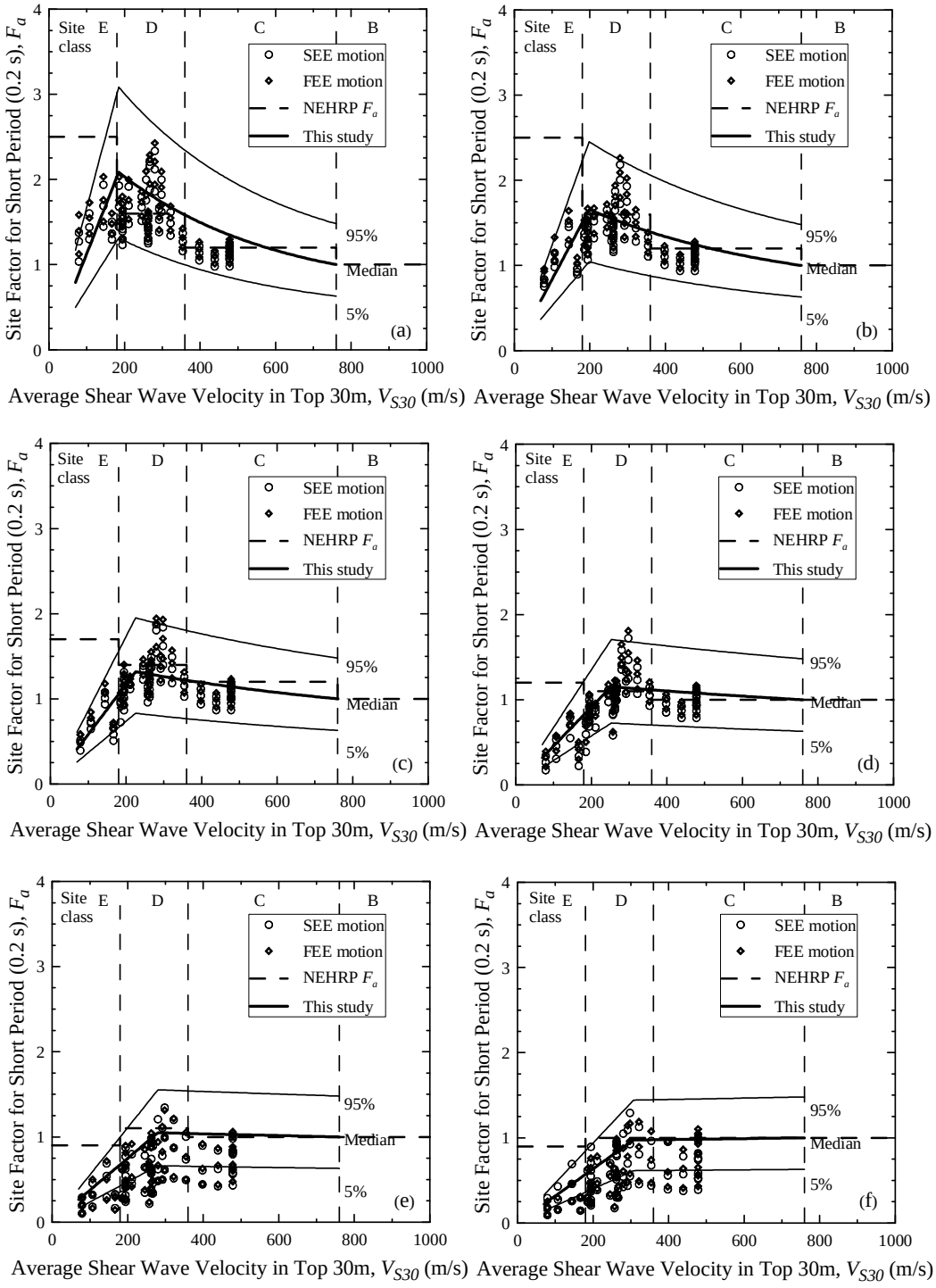

Figure D.4: Site coefficients for 0.2 s (short) spectral period with S_s equal to (a) 0.125 g, (b) 0.25 g, (c) 0.50 g, (d) 0.75 g, (e) 1.0 g, and (f) 1.25 g, based on V_s profiles shown in Figure D.1 for the Aiken area.

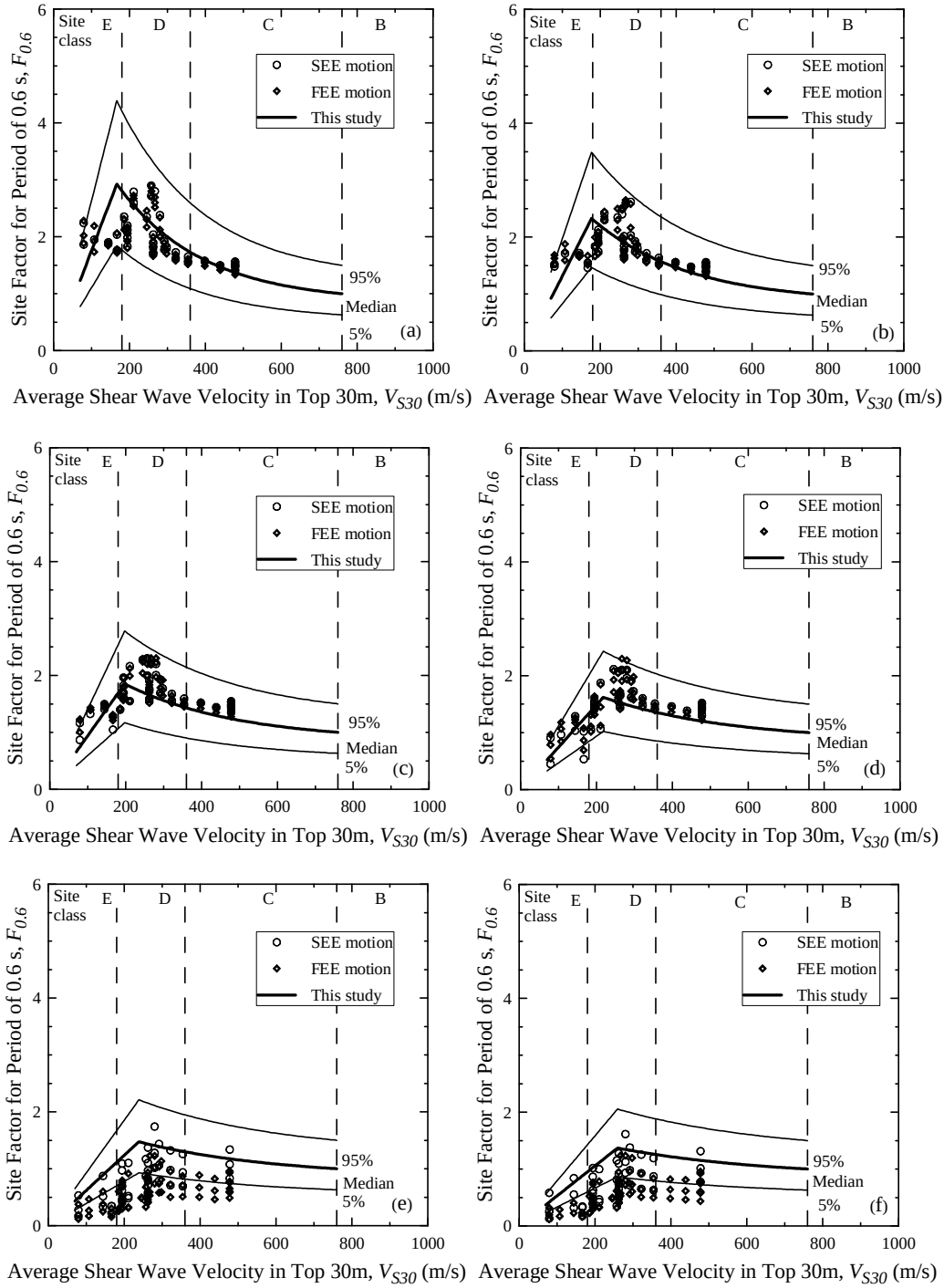

Figure D.5: Site coefficients for 0.6 s spectral period with $S_{0.6}$ equal to (a) 0.05 g, (b) 0.10g, (c) 0.20 g, (d) 0.30 g, (e) 0.40 g, and (f) 0.50 g, based on V_s profiles shown in Figure D.1 for the Aiken area.

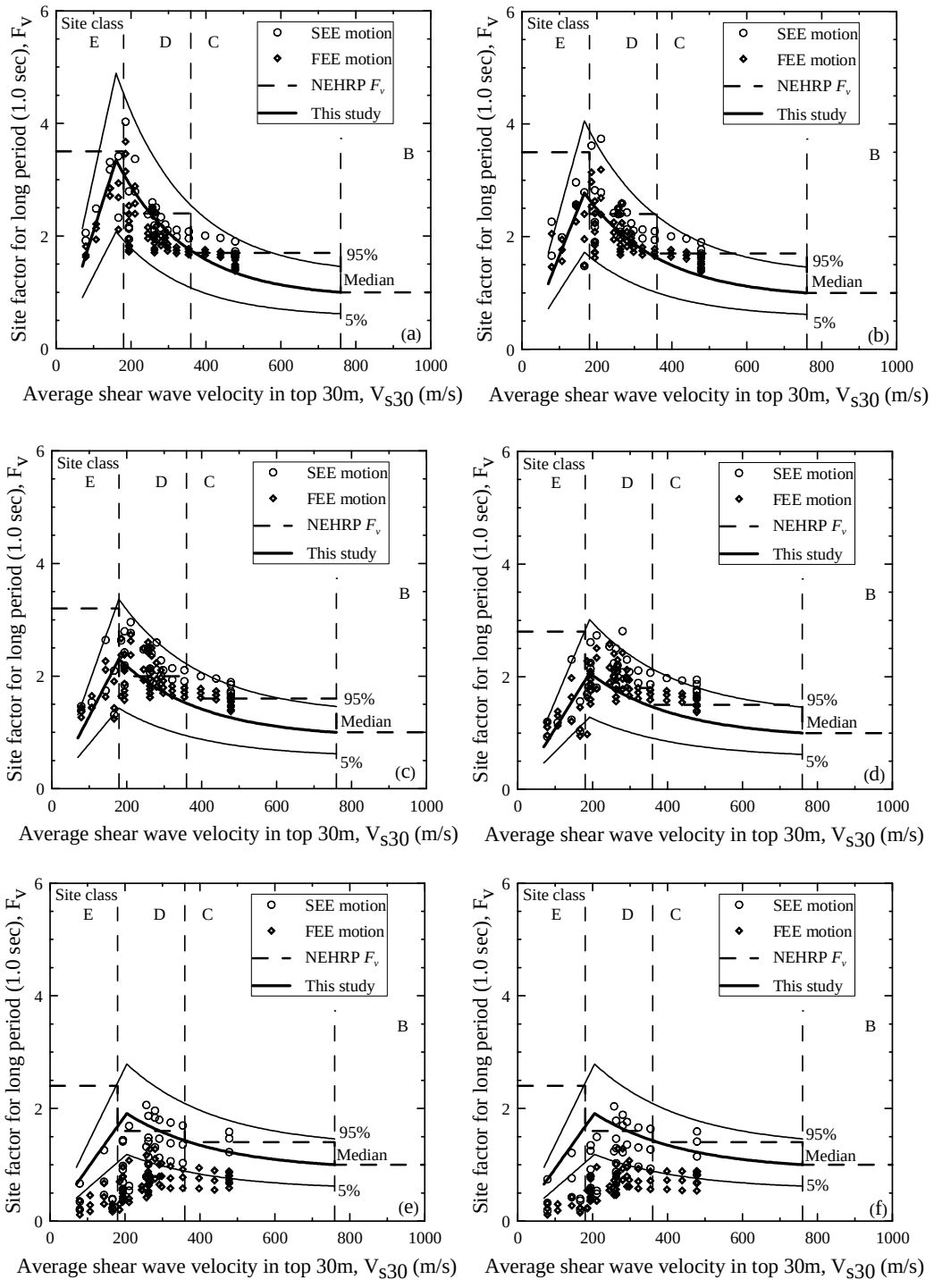

Figure D.6: Site coefficients for 1.0 s (long) spectral period with S_1 equal to (a) 0.05 g, (b) 0.10 g, (c) 0.20 g, (d) 0.30 g, (e) 0.40 g, and (f) 0.50 g, based on V_s profiles shown in Figure D.1 for the Aiken area.

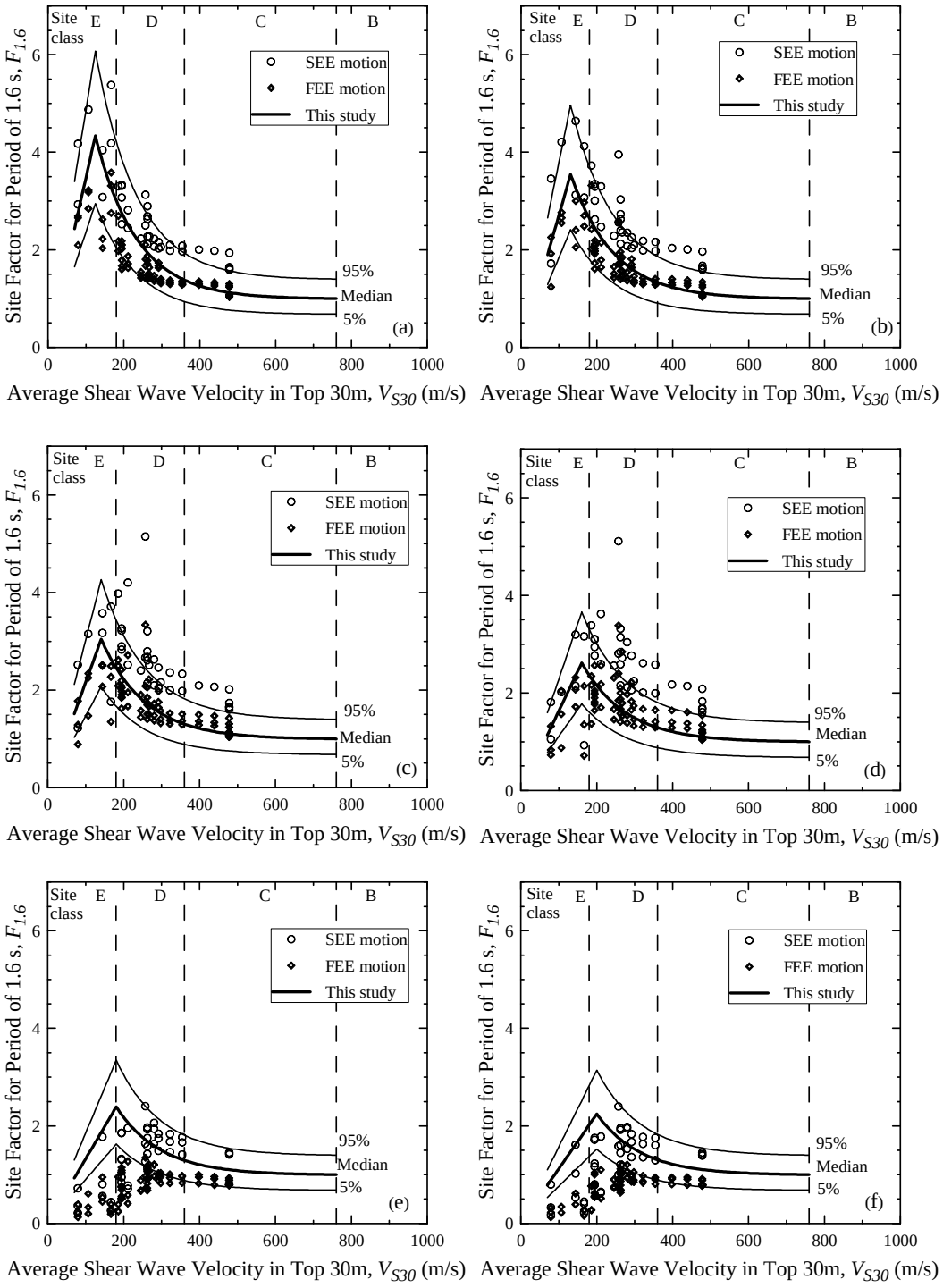

Figure D.7: Site coefficient for 1.6 s spectral period with $S_{1.6}$ equal to (a) 0.02 g, (b) 0.05 g, (c) 0.10 g, (d) 0.20 g, (e) 0.30 g, and (f) 0.40 g, based on V_s profiles shown in Figure D.1 for the Aiken area.

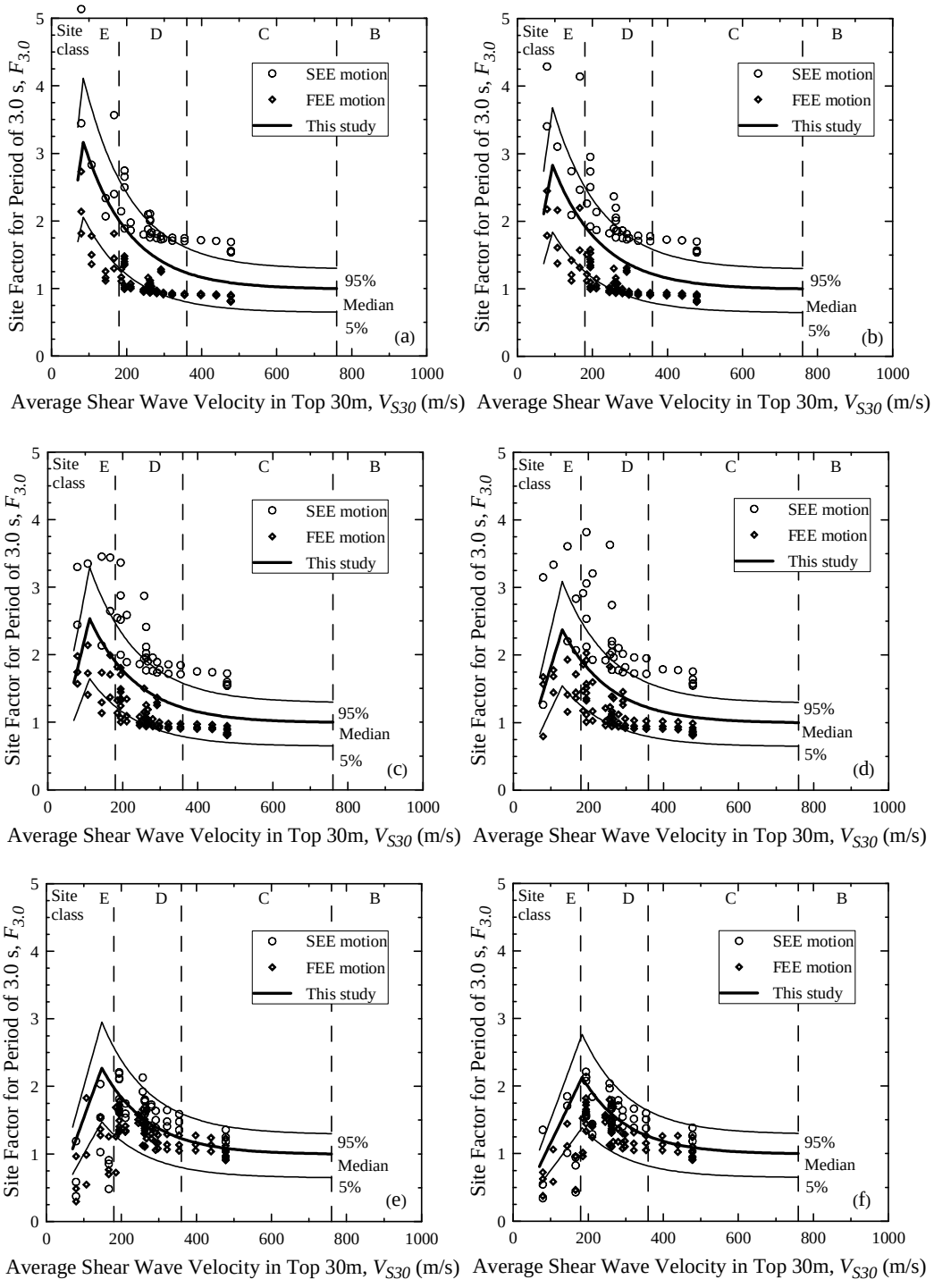

Figure D.8: Site coefficient for 3.0 s spectral period with $S_{3.0}$ equal to (a) 0.01 g, (b) 0.02 g, (c) 0.04 g, (d) 0.06 g, (e) 0.08 g and (f) 0.12 g, based on V_s profiles shown in Figure D.1 for the Aiken area.

APPENDIX E

SUMMARY OUTPUTS OF SITE RESPONSE ANALYSIS FOR THE SAVANNAH AREA

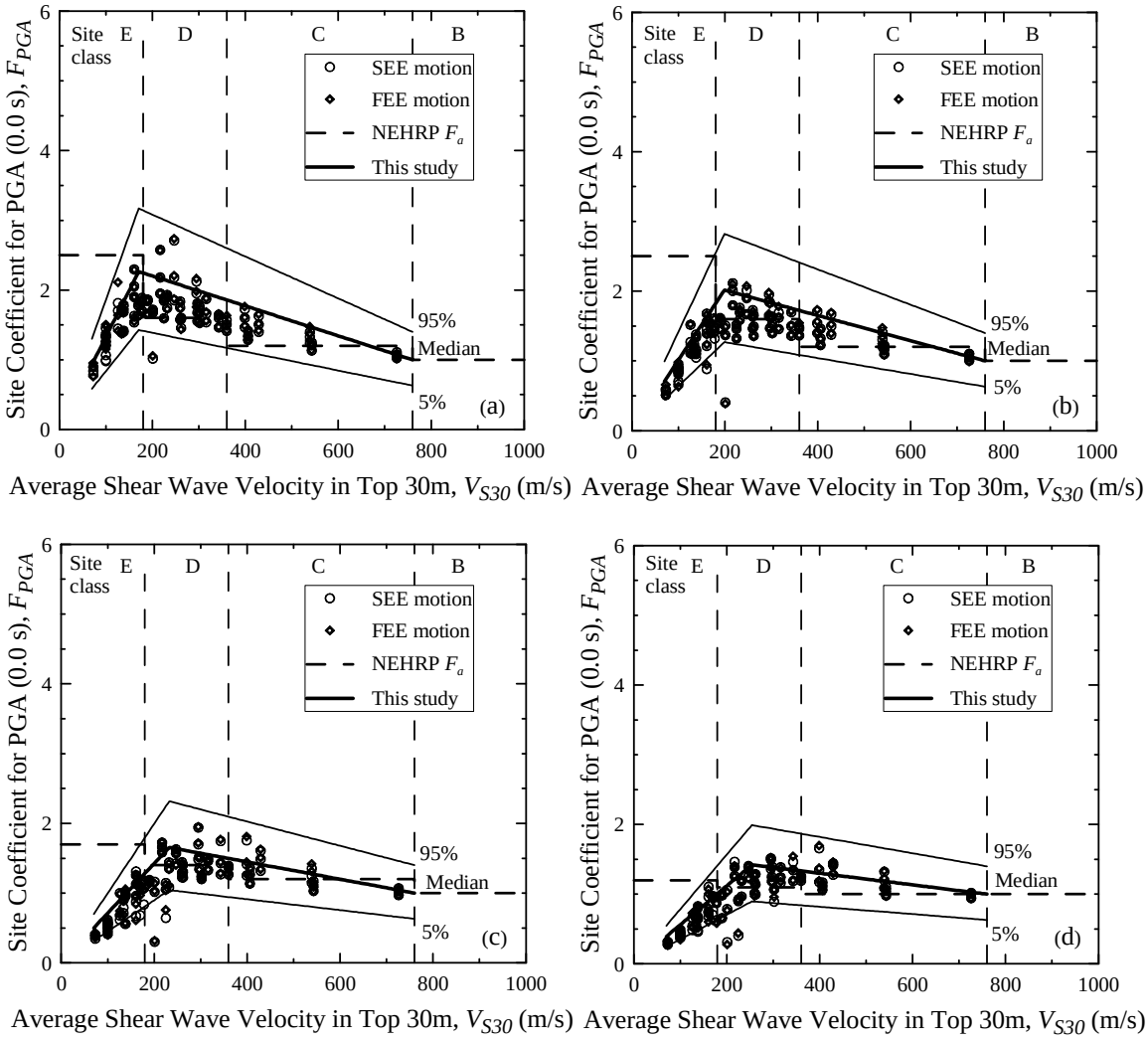

Figure E.1: Site coefficients for 0.0 s spectral period (free-field) with *PGA* equal to (a) 0.05 g, (b) 0.1 g, (c) 0.2 g, (d) 0.3 g, and (e) 0.4 g for Savannah.

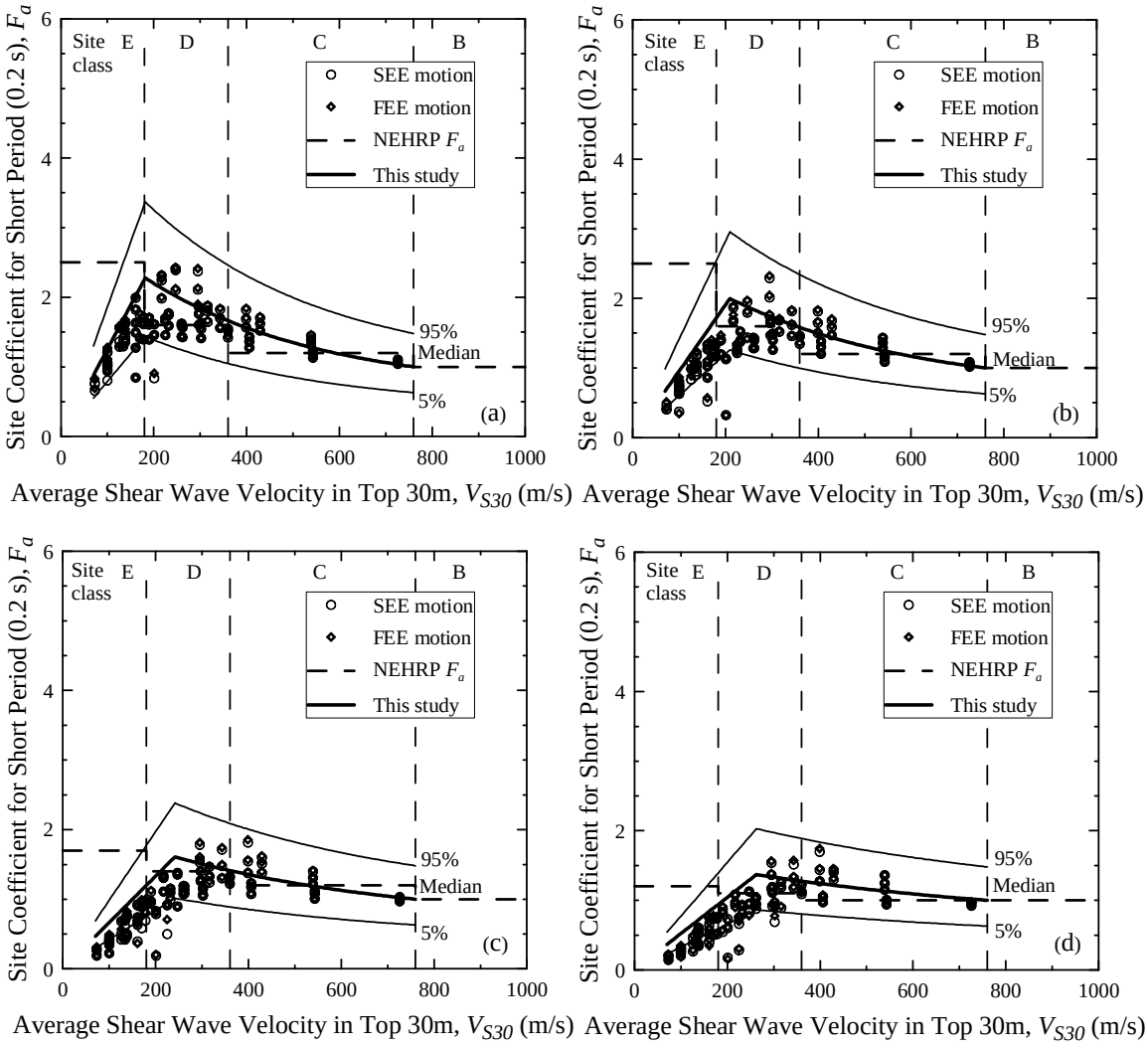

Figure E.2: Site coefficients for 0.2 s (short) spectral period with S_s equal to (a) 0.125 g, (b) 0.25 g, (c) 0.50 g, and (d) 0.75 g, for Savannah.

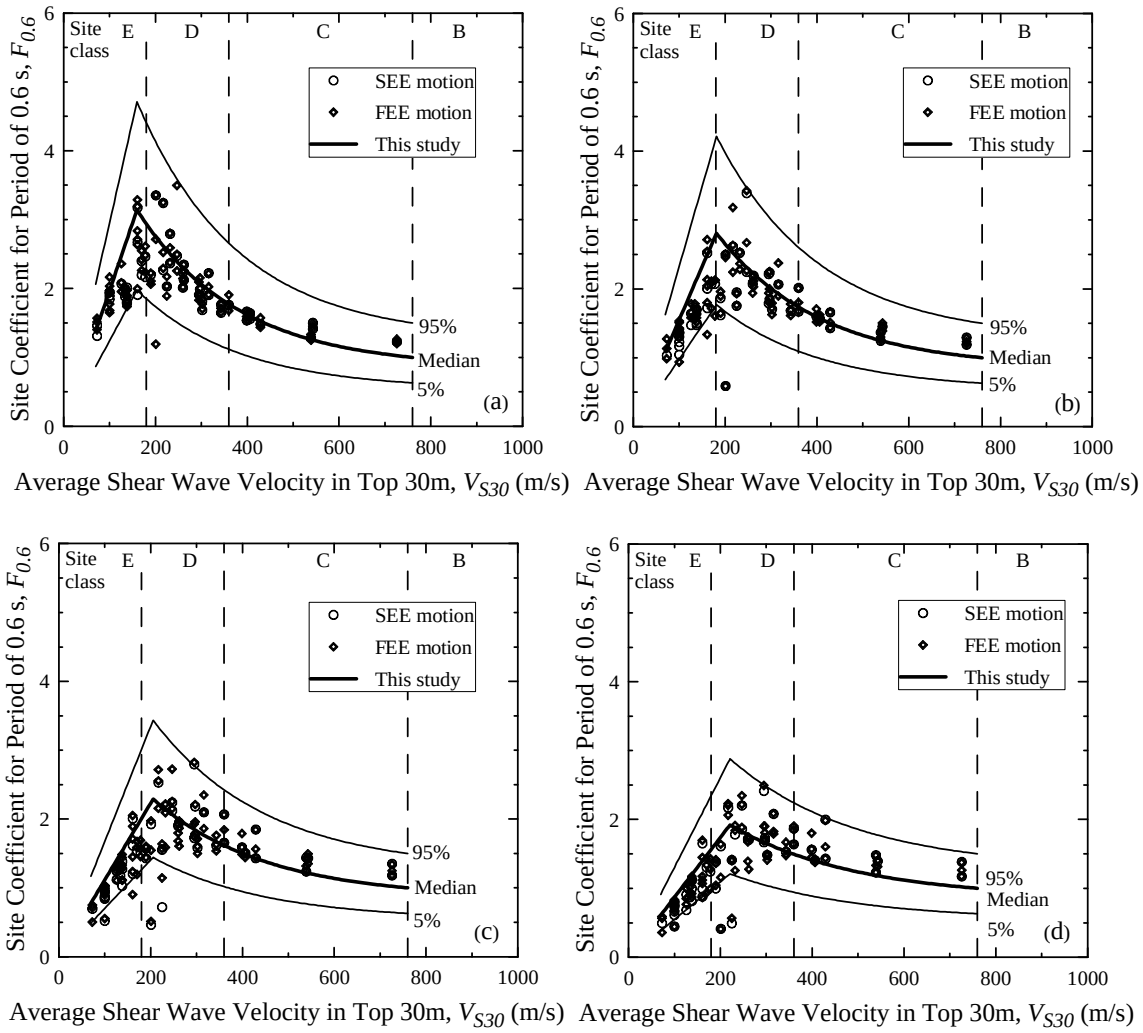

Figure E.3: Site coefficients for 0.6 s spectral period with $S_{0.6}$ equal to (a) 0.05 g, (b) 0.10g, (c) 0.20 g, and (d) 0.30 g for Savannah.

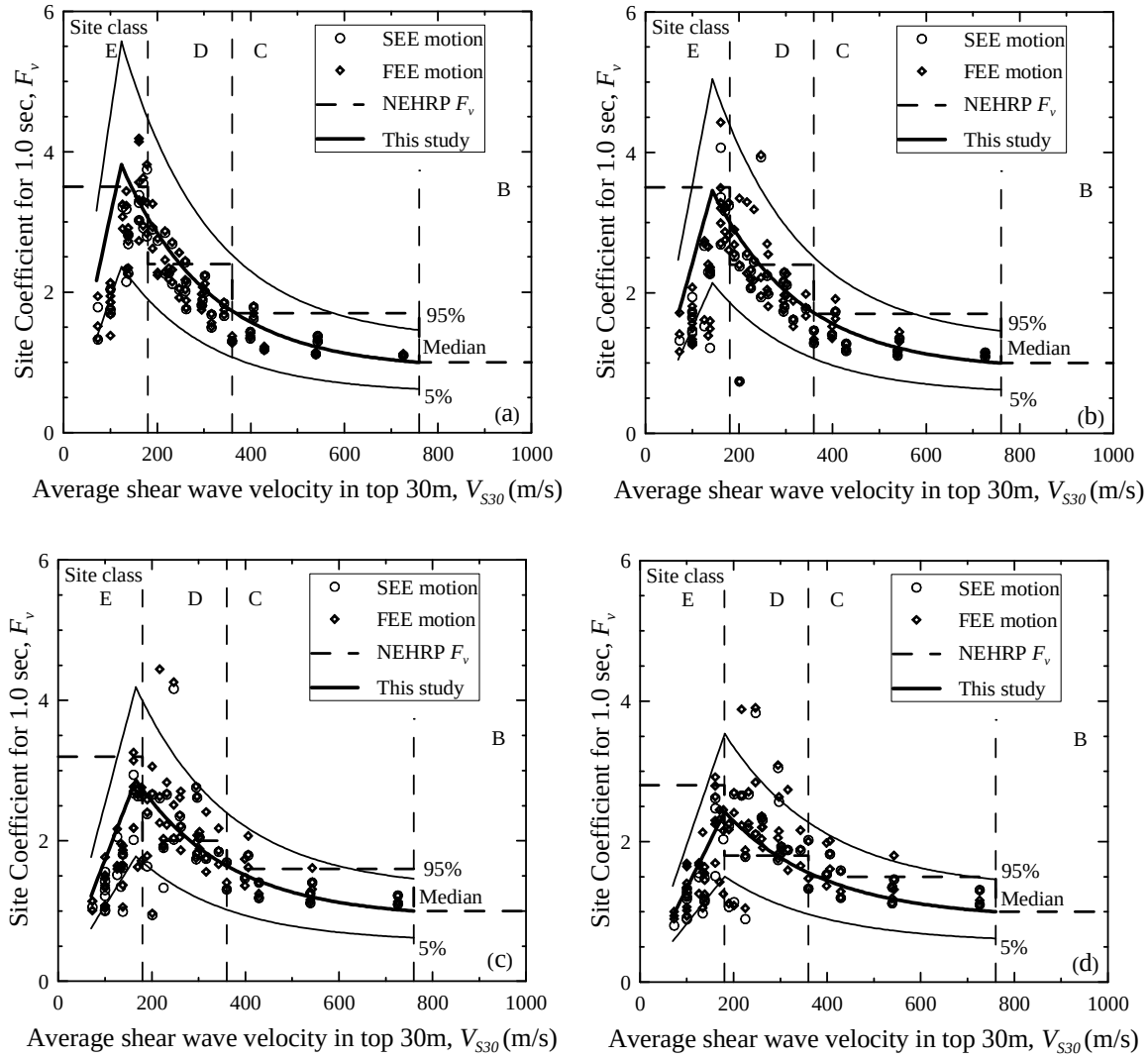

Figure E.4: Site coefficients for 1.0 s (long) spectral period with S_1 equal to (a) 0.05 g, (b) 0.10 g, (c) 0.20 g, and (d) 0.30 g for Savannah.

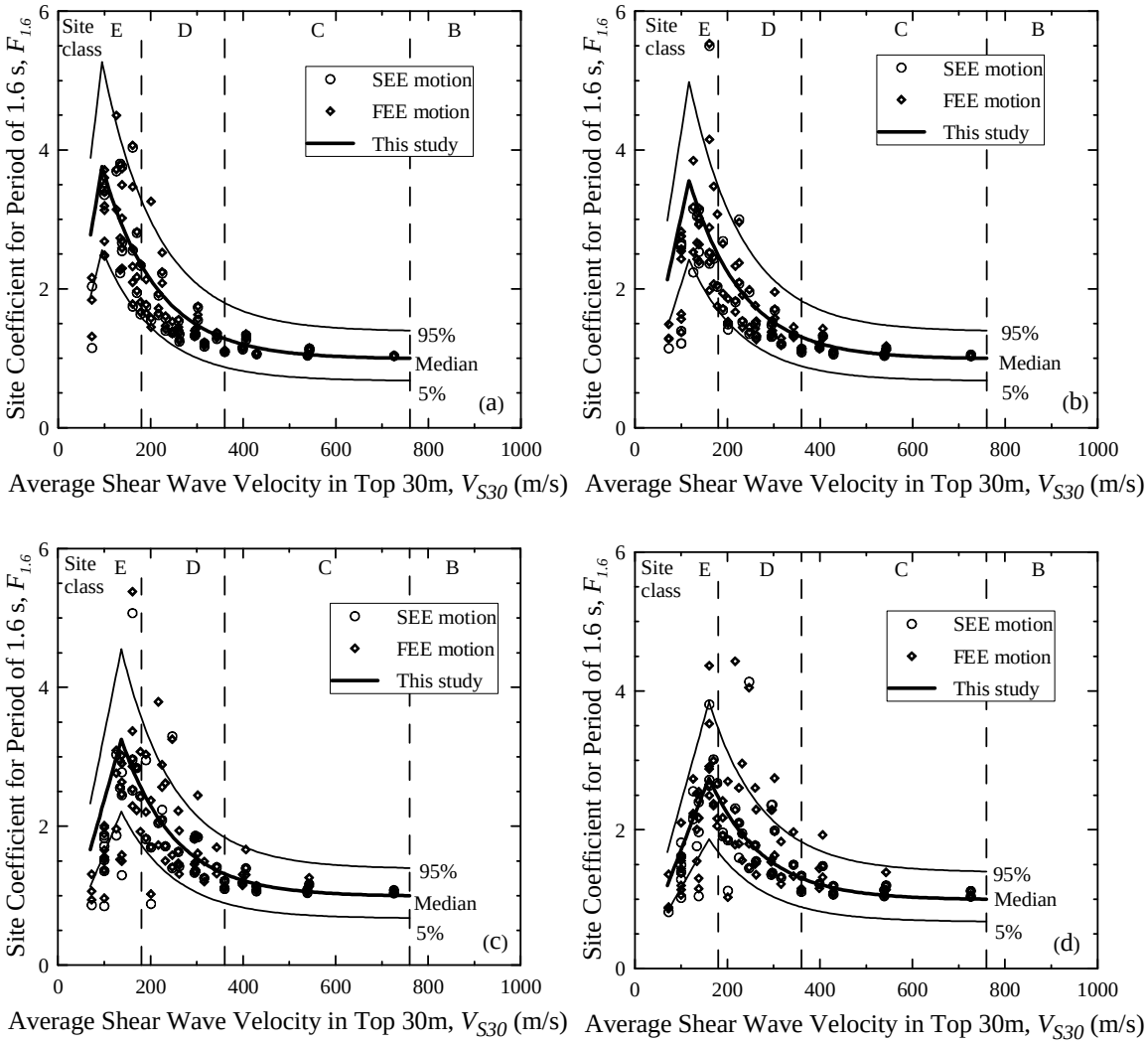

Figure E.5: Site coefficient for 1.6 s spectral period with $S_{1.6}$ equal to (a) 0.02 g, (b) 0.05 g, (c) 0.10 g, and (d) 0.20 g for Savannah.

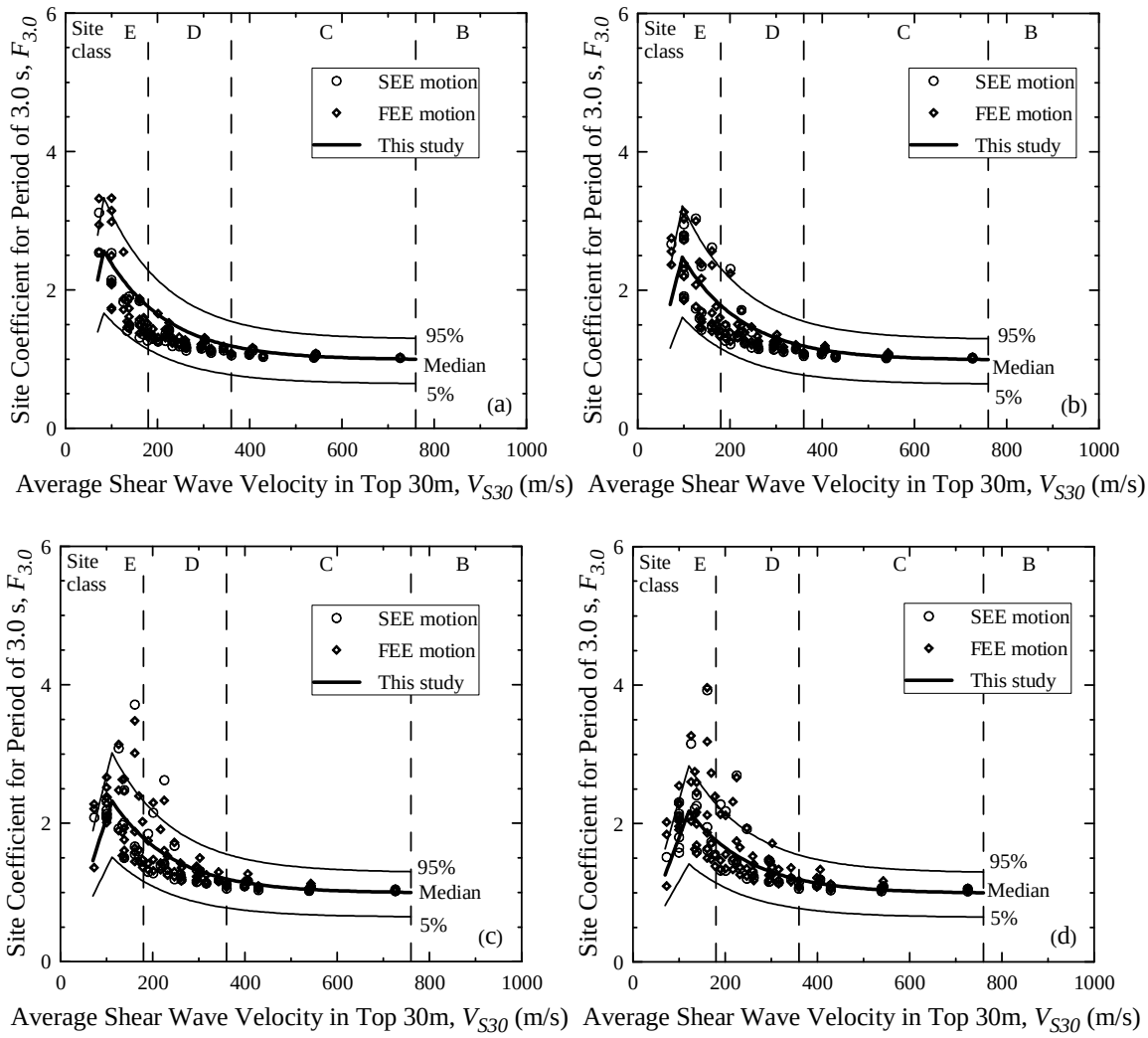

Figure E.6: Site coefficient for 3.0 s spectral period with $S_{3.0}$ equal to (a) 0.01 g, (b) 0.02 g, (c) 0.04 g, and (d) 0.06 g for Savannah.

APPENDIX F

SUMMARY OUTPUTS OF SITE RESPONSE ANALYSIS FOR FLORENCE

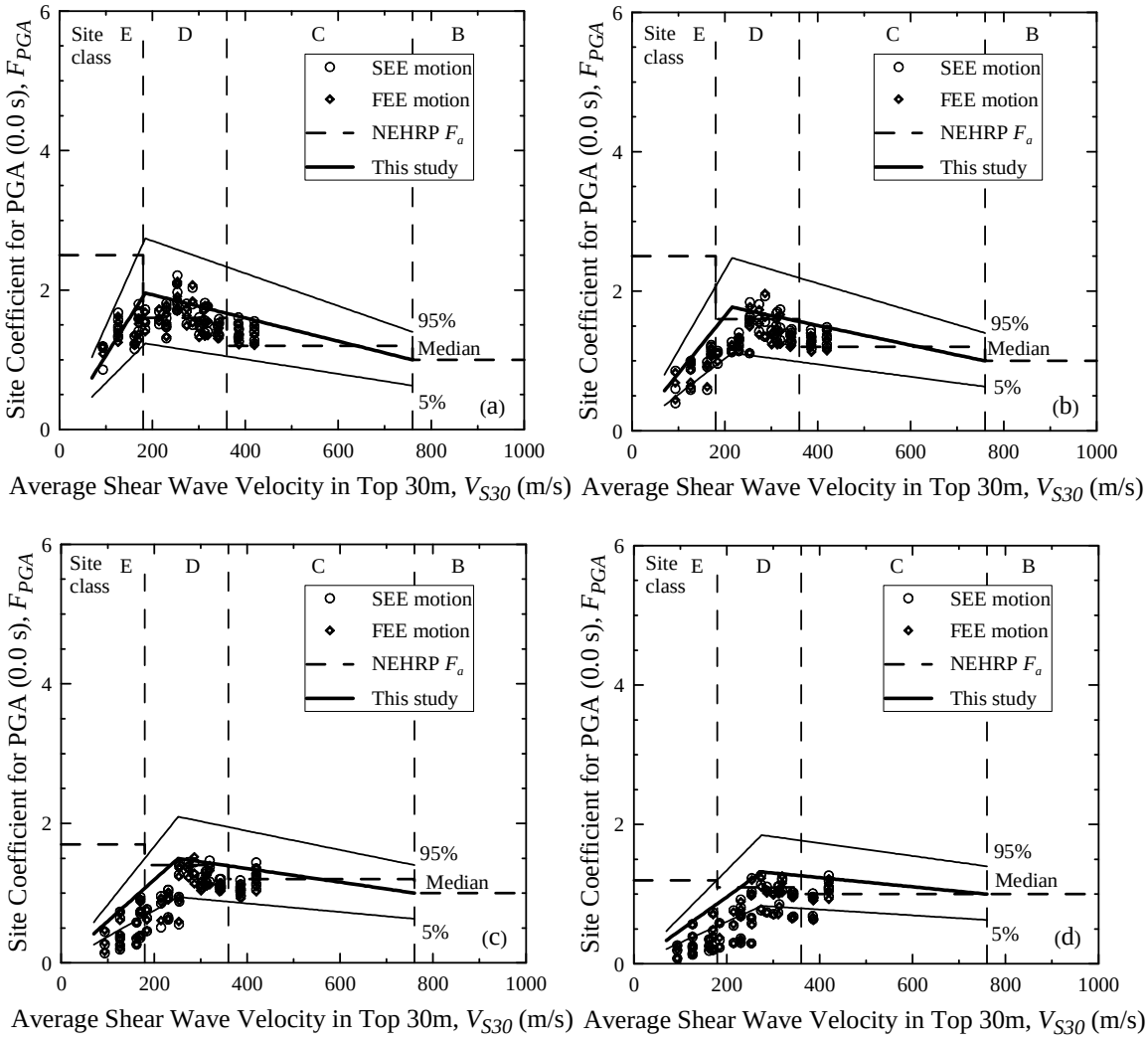

Figure F.1: Site coefficients for 0.0 s spectral period (free-field) with *PGA* equal to (a) 0.05 g, (b) 0.1 g, (c) 0.2 g, and (d) 0.3 g for Florence.

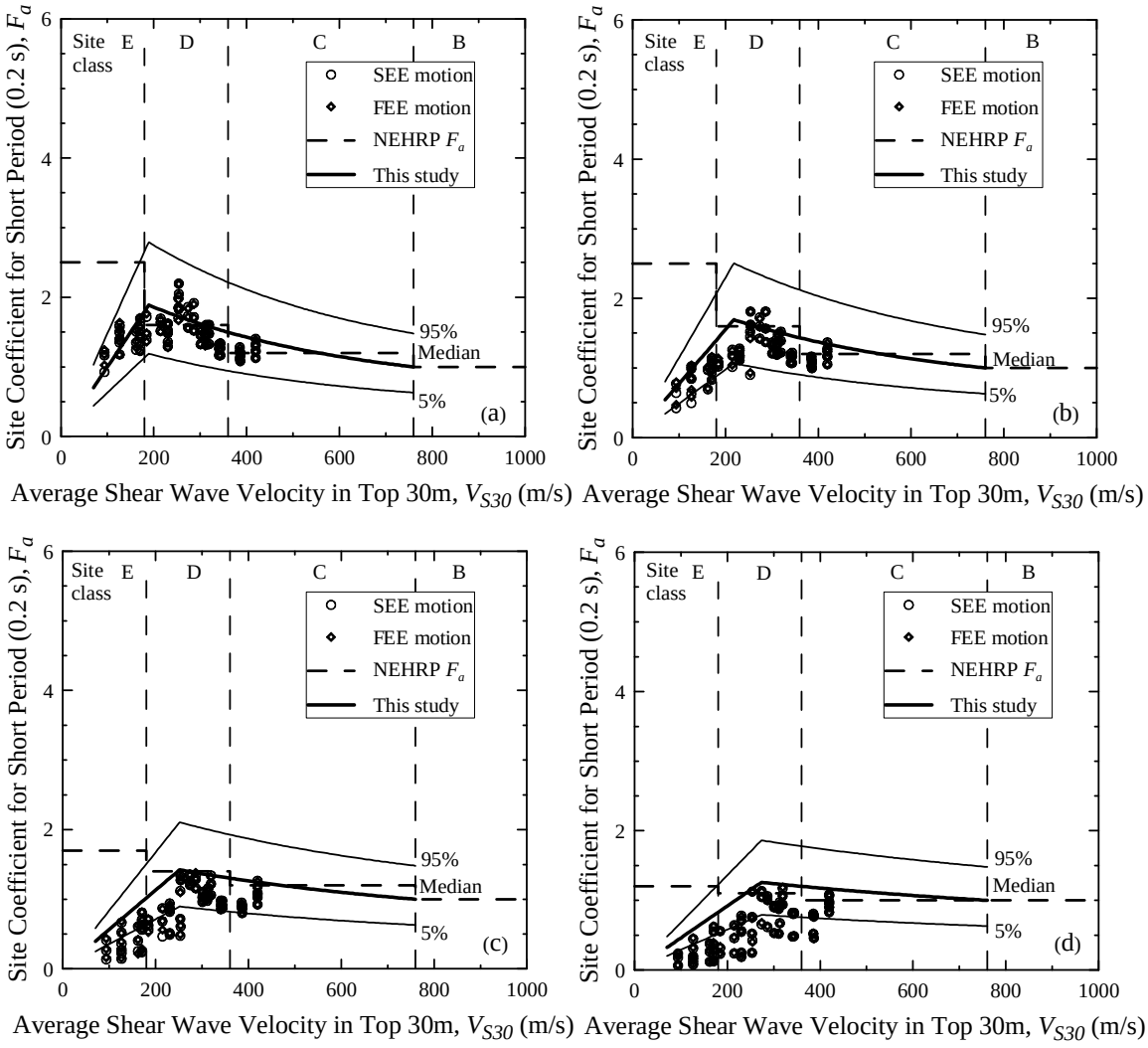

Figure F.2: Site coefficients for 0.2 s (short) spectral period with S_s equal to (a) 0.125 g, (b) 0.25 g, (c) 0.50 g, and (d) 0.75 g for Florence.

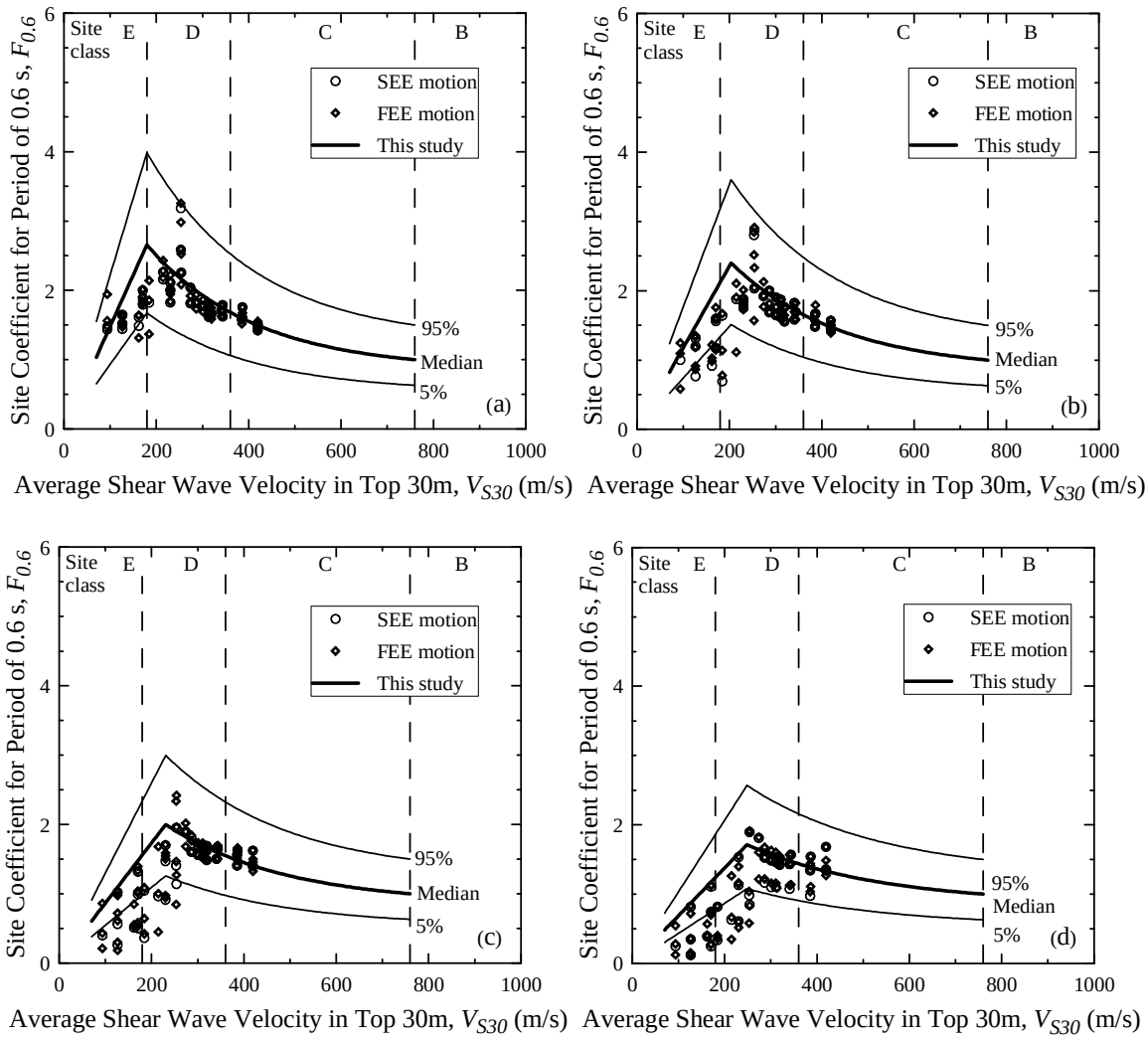

Figure F.3: Site coefficients for 0.6 s spectral period with $S_{0.6}$ equal to (a) 0.05 g, (b) 0.10g, (c) 0.20 g, and (d) 0.30 g for Florence.

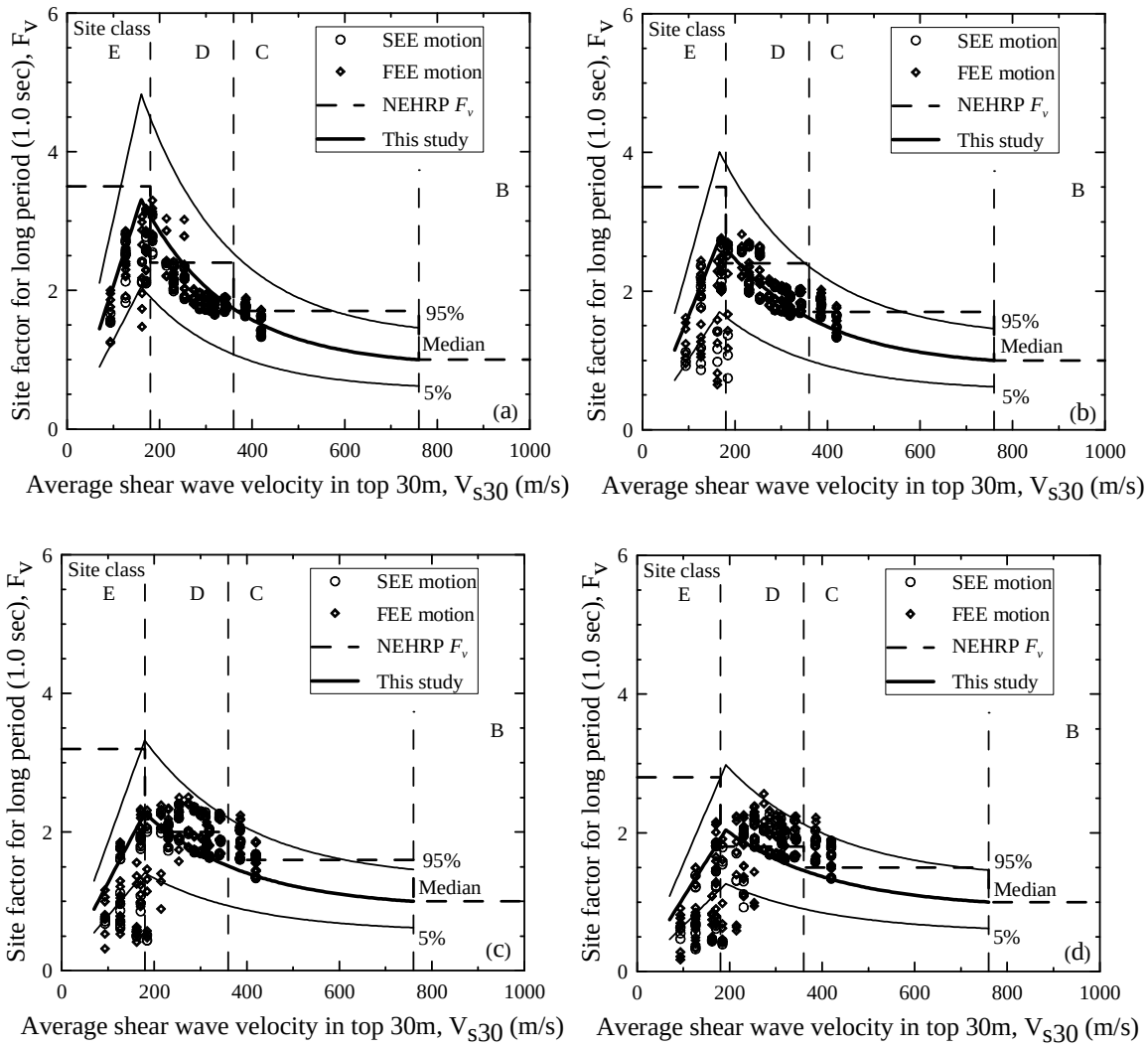

Figure F.3: Site coefficients for 1.0 s (long) spectral period with S_1 equal to (a) 0.05 g, (b) 0.10 g, (c) 0.20 g, and (d) 0.30 g for Florence.

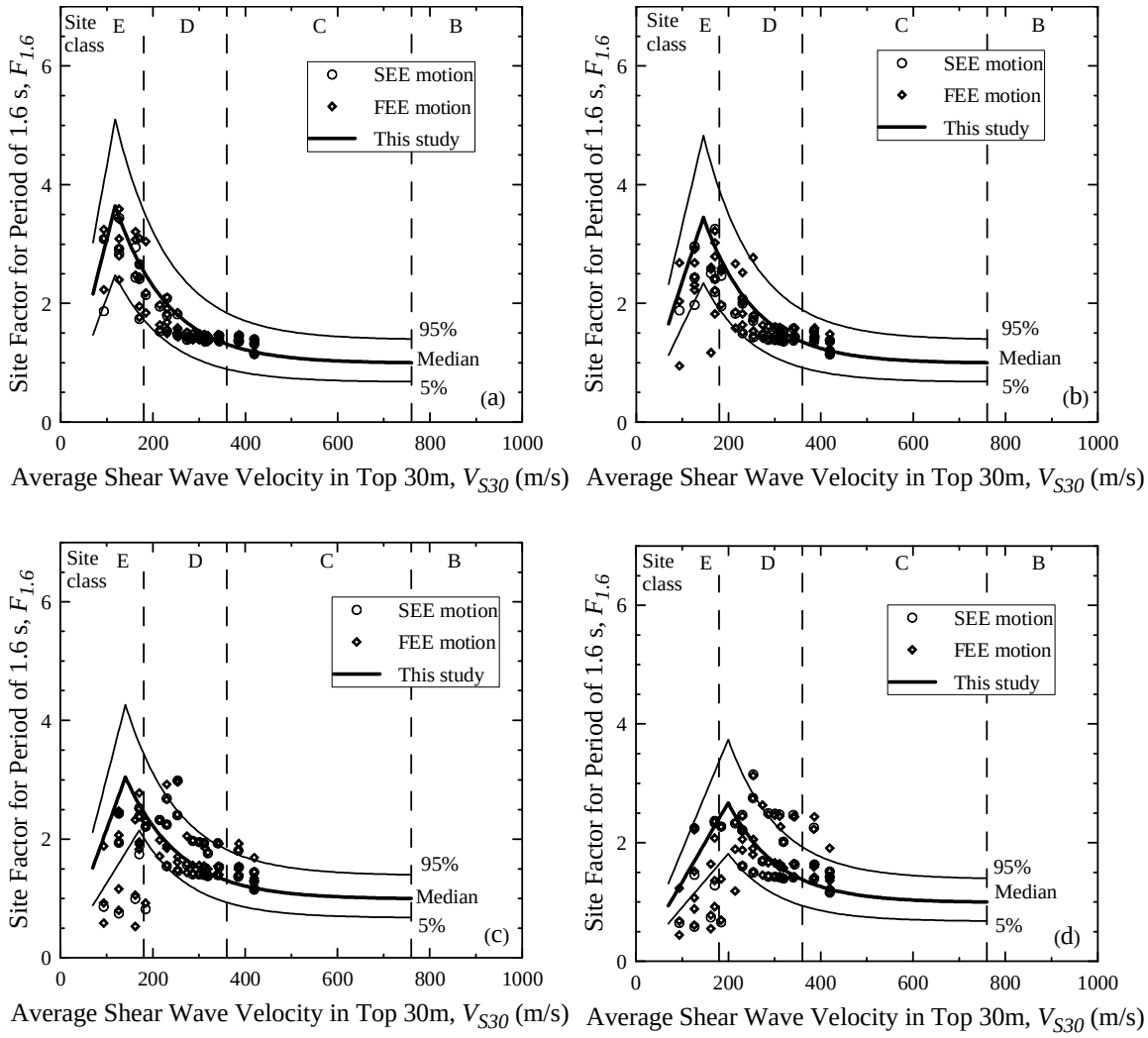

Figure F.5: Site coefficient for 1.6 s spectral period with $S_{1.6}$ equal to (a) 0.02 g, (b) 0.05 g, (c) 0.10 g, and (d) 0.20 g for Florence.

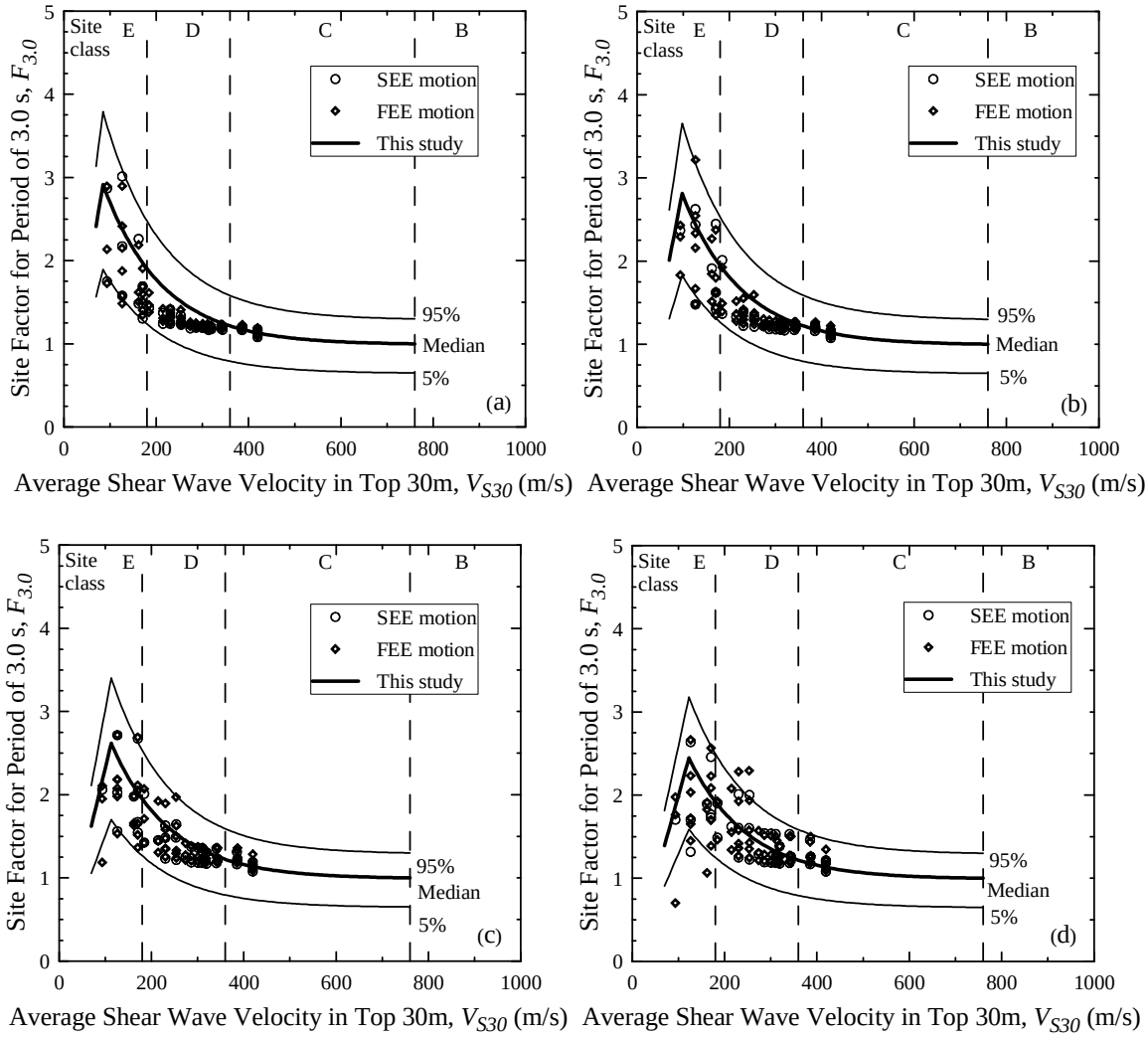

Figure E.6: Site coefficient for 3.0 s spectral period with $S_{3.0}$ equal to (a) 0.01 g, (b) 0.02 g, (c) 0.04 g, and (d) 0.06 g for Florence.

APPENDIX G

SUMMARY OUTPUTS OF SITE RESPONSE ANALYSIS FOR LAKE MARION

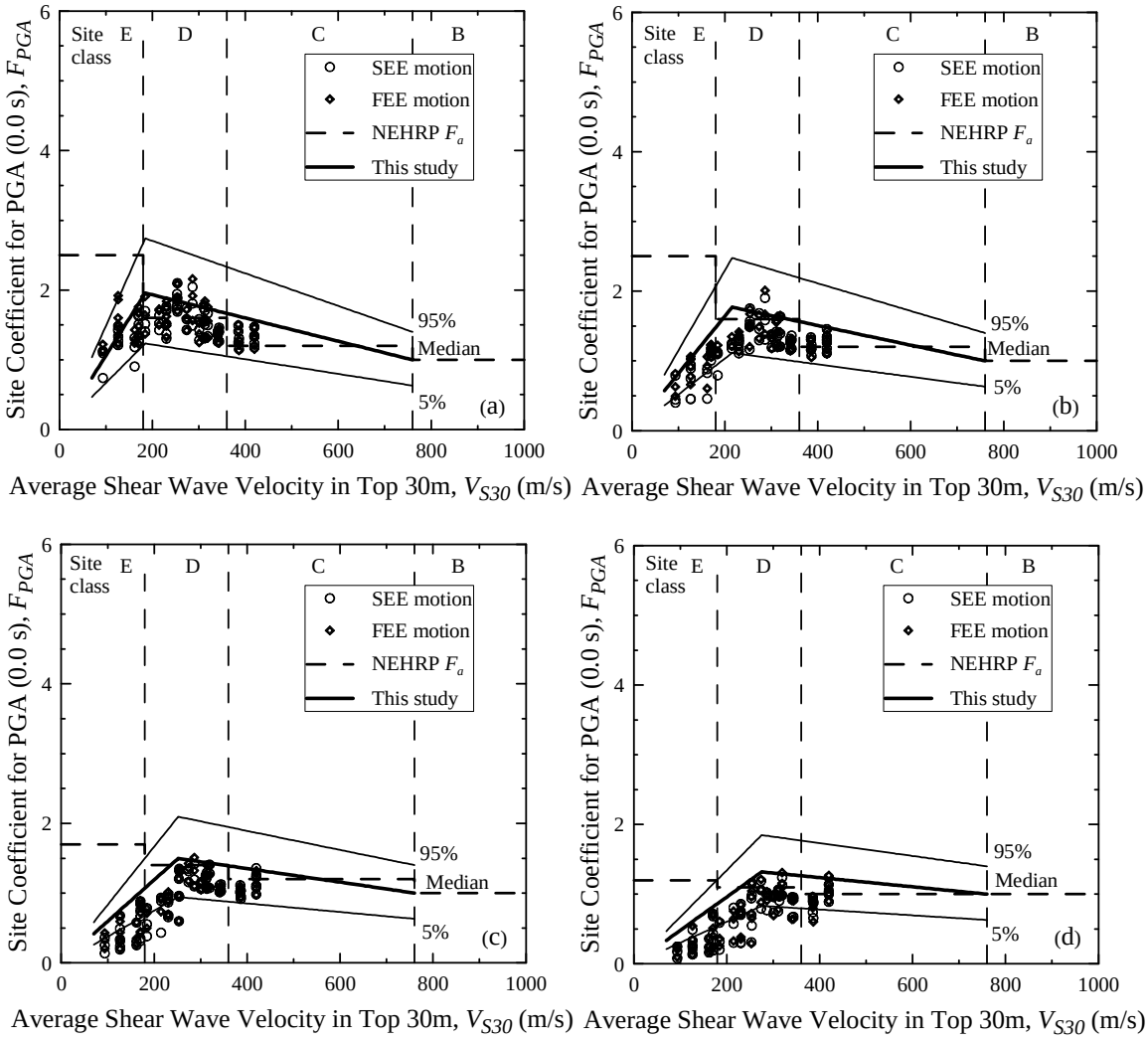

Figure G.1: Site coefficients for 0.0 s spectral period (free-field) with *PGA* equal to (a) 0.05 g, (b) 0.1 g, (c) 0.2 g, (d) 0.3 g, and (e) 0.4 g for Lake Marion.

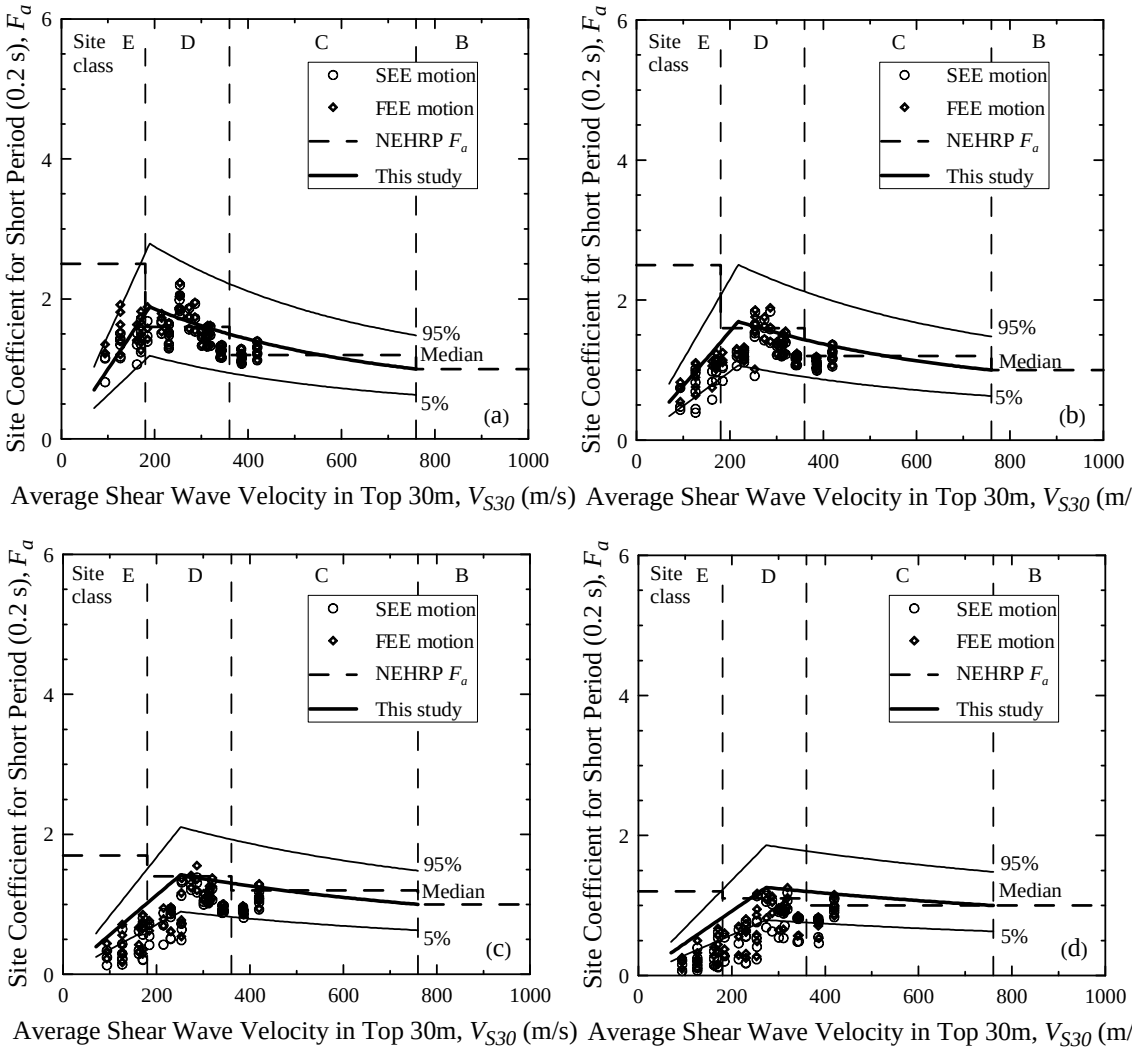

Figure G.2: Site coefficients for 0.2 s (short) spectral period with S_s equal to (a) 0.125 g, (b) 0.25 g, (c) 0.50 g, and (d) 0.75 g for Lake Marion.

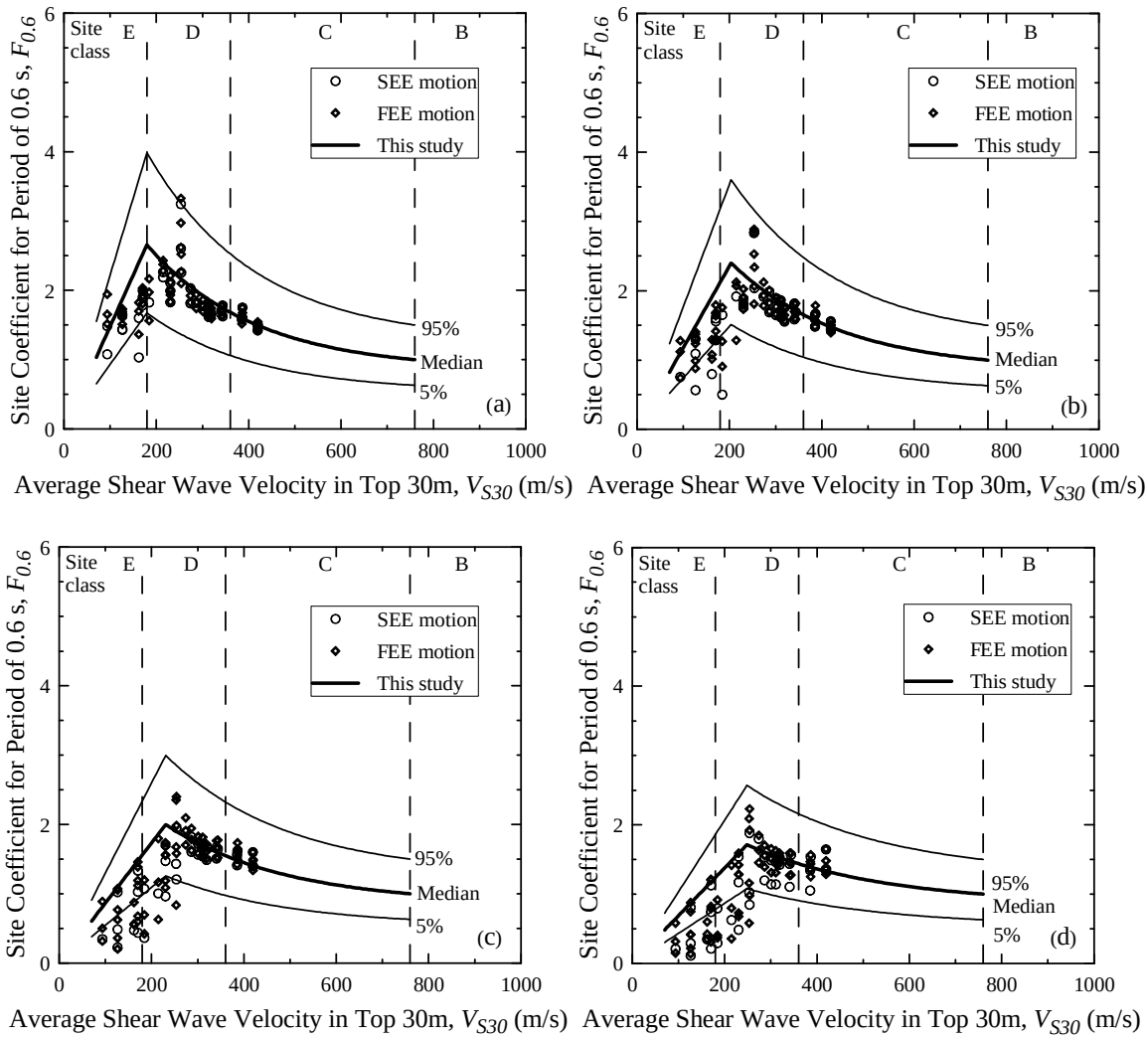

Figure G.3: Site coefficients for 0.6 s spectral period with $S_{0.6}$ equal to (a) 0.05 g, (b) 0.10g, (c) 0.20 g, and (d) 0.30 g for Lake Marion.

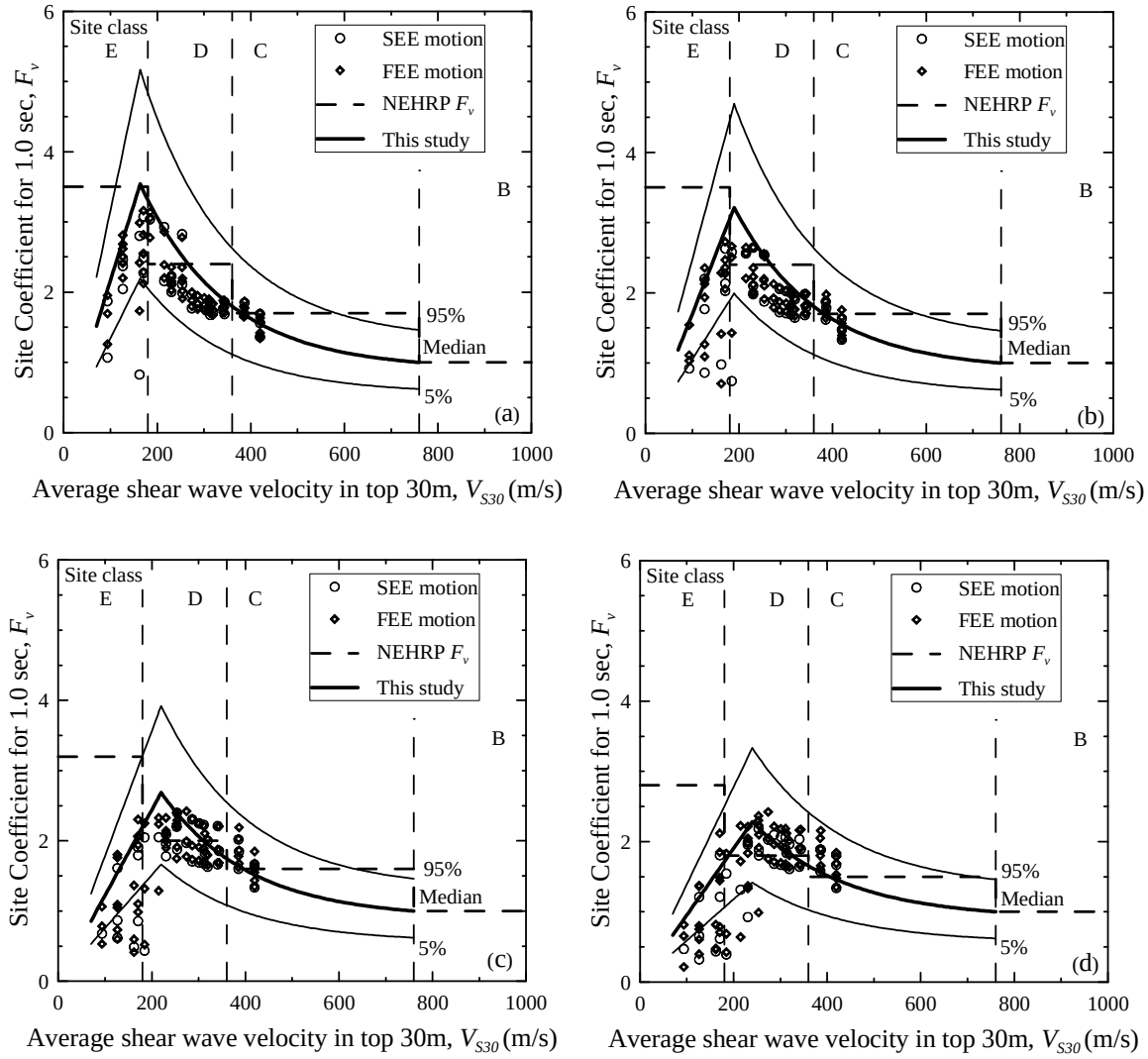

Figure G.4: Site coefficients for 1.0 s (long) spectral period with S_1 equal to (a) 0.05 g, (b) 0.10 g, (c) 0.20 g, and (d) 0.30 g for Lake Marion.

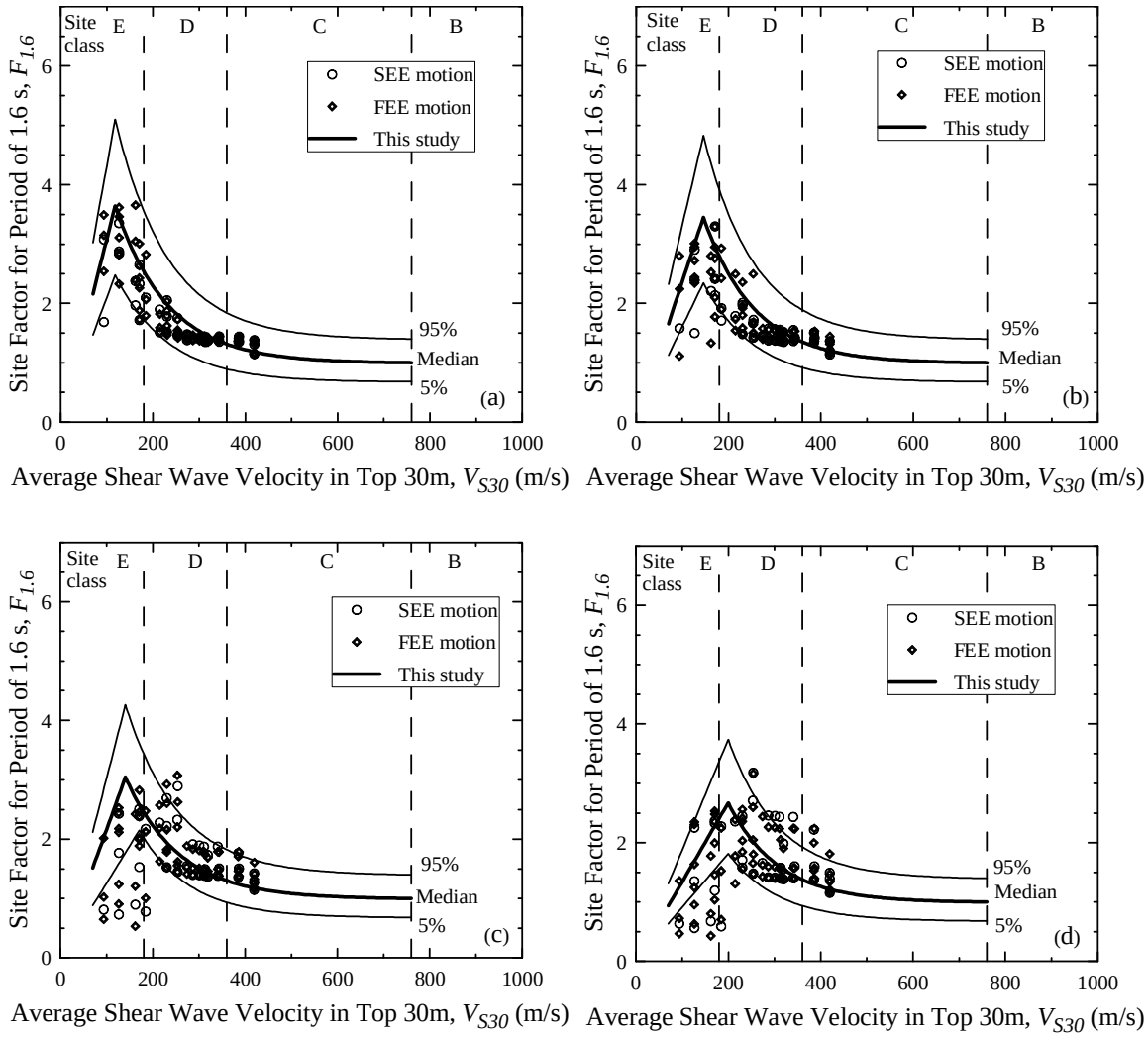

Figure G.5: Site coefficient for 1.6 s spectral period with $S_{1.6}$ equal to (a) 0.02 g, (b) 0.05 g, (c) 0.10 g, and (d) 0.20 g for Lake Marion.

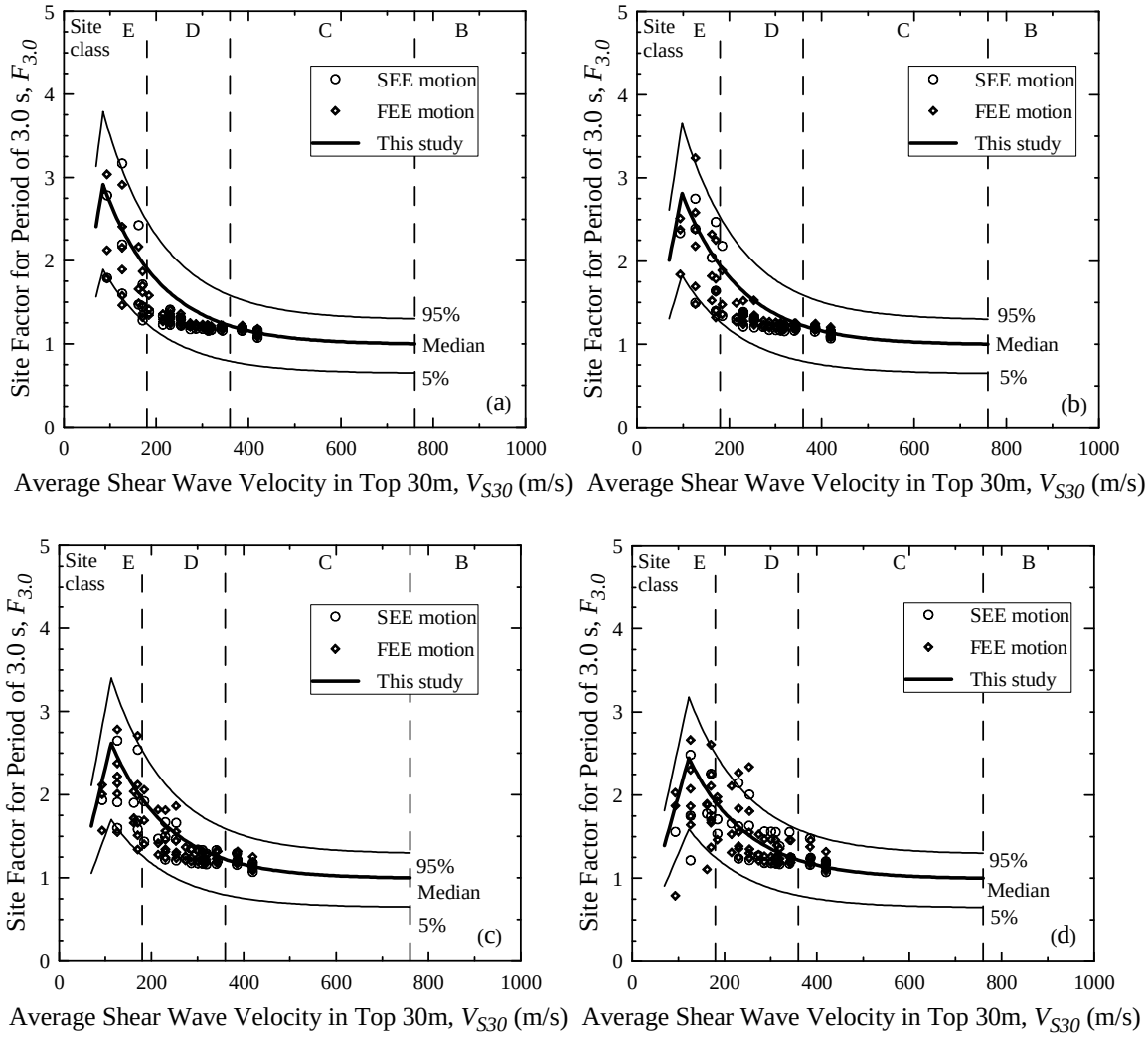

Figure G.6: Site coefficient for 3.0 s spectral period with $S_{3.0}$ equal to (a) 0.01 g, (b) 0.02 g, (c) 0.04 g, and (d) 0.06 g for Lake Marion.

APPENDIX H

SUMMARY OF INPUTS AND OUTPUTS OF SITE RESPONSE ANALYSIS FOR DIFFERENT B/C BOUNDARY FOR THE COLUMBIA AREA

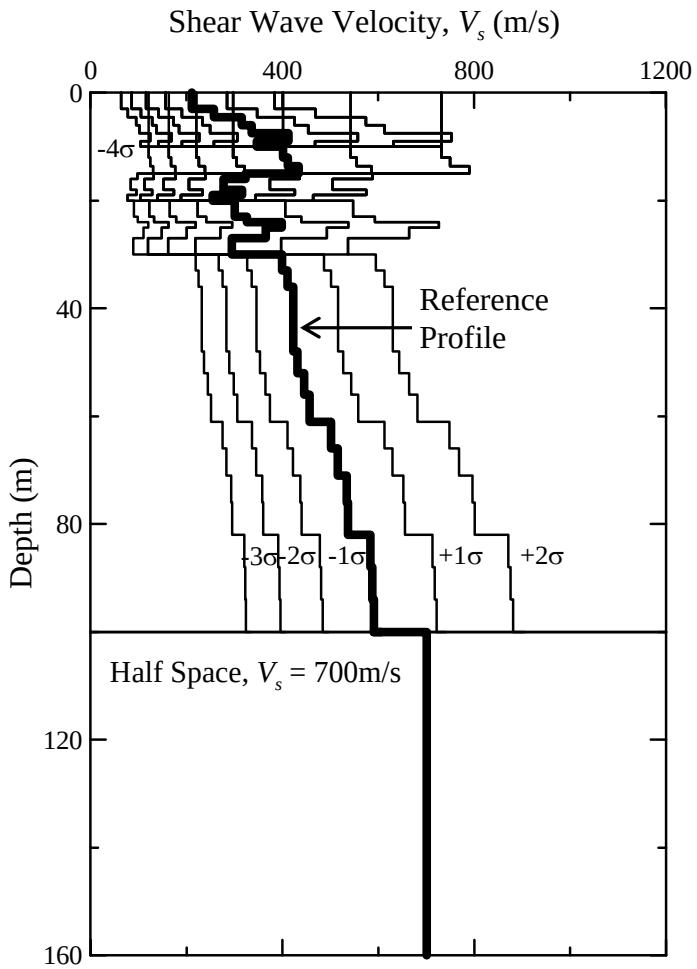

Figure H.1: Shear wave velocity profiles considered for Columbia-Florence-Lake Marion area with soft rock half space at depth = 100 m. The reference profile is compiled from Odum et al. (2003), Silva et al. (2003), Chapman et al. (2006) and Andrus et al. (2006), and the standard deviation values are based on Andrus et al. (2006).

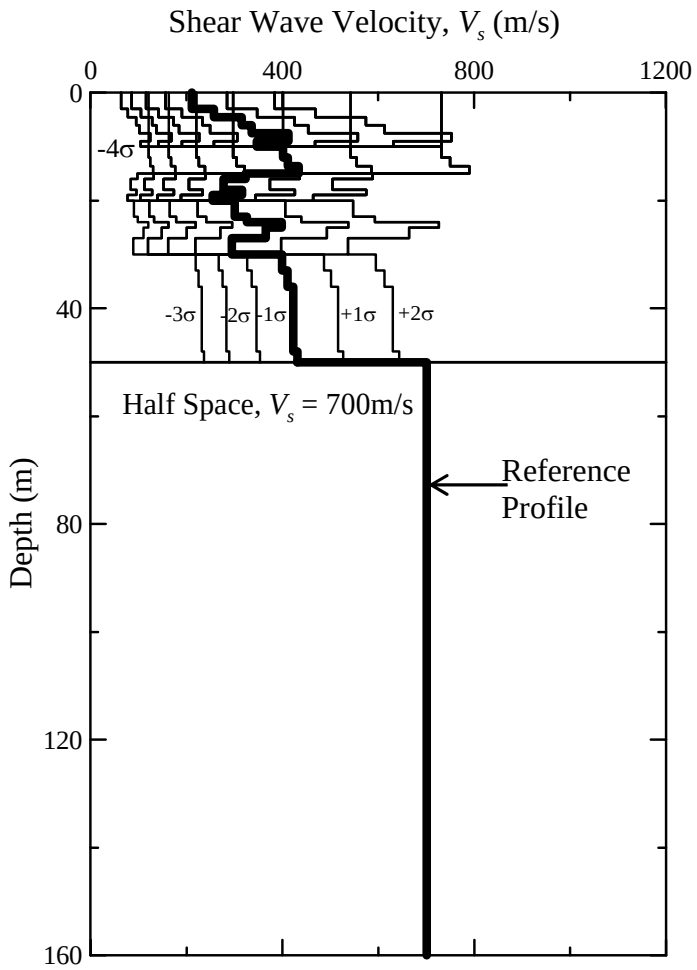

Figure H.2: Shear wave velocity profiles considered for Columbia-Florence-Lake Marion area with soft rock half space at depth = 50 m. The reference profile is compiled from Odum et al. (2003), Silva et al. (2003), Chapman et al. (2006) and Andrus et al. (2006), and the standard deviation values are based on Andrus et al. (2006).

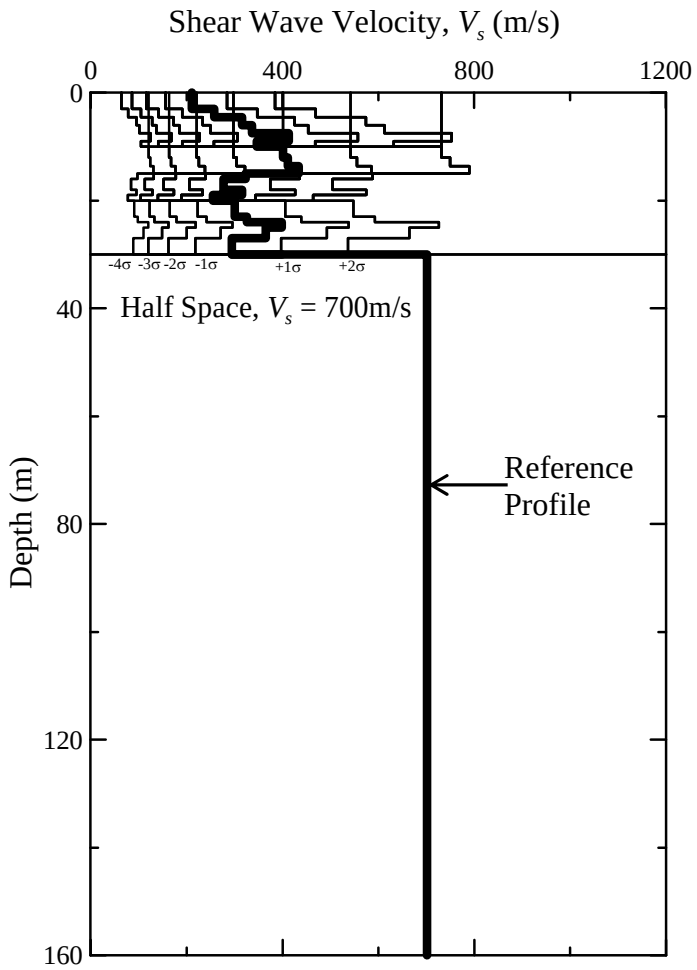

Figure H.3: Shear wave velocity profiles considered for Columbia-Florence-Lake Marion area with soft rock half space at depth = 30 m. The reference profile is compiled from Odum et al. (2003), Silva et al. (2003), Chapman et al. (2006) and Andrus et al. (2006), and the standard deviation values are based on Andrus et al. (2006).

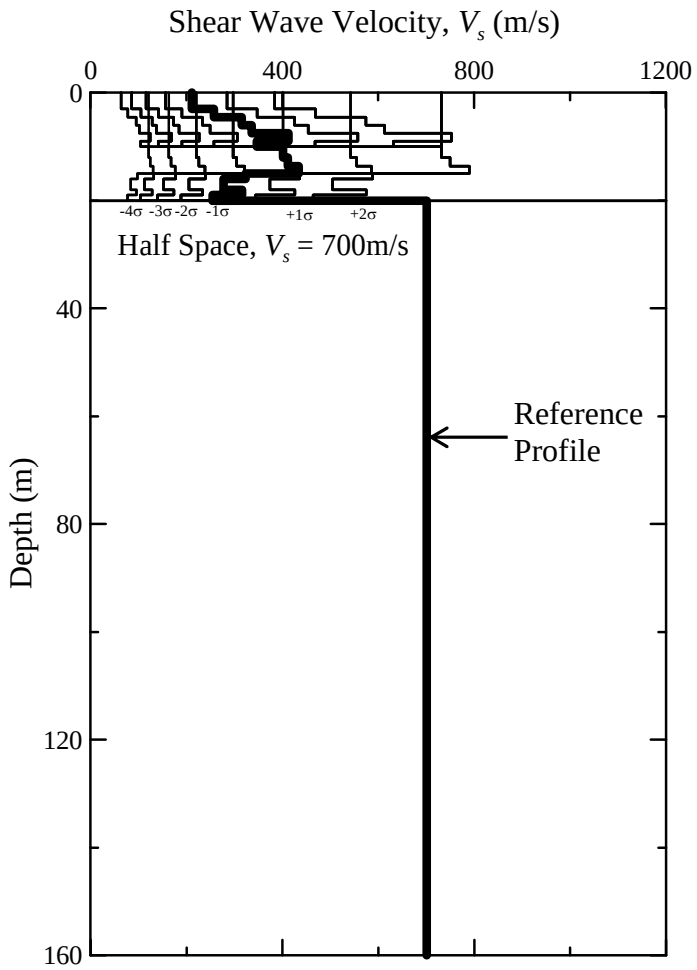

Figure H.4: Shear wave velocity profiles considered for Columbia-Florence-Lake Marion area with soft rock half space at depth = 20 m. The reference profile is compiled from Odum et al. (2003), Silva et al. (2003), Chapman et al. (2006) and Andrus et al. (2006), and the standard deviation values are based on Andrus et al. (2006).

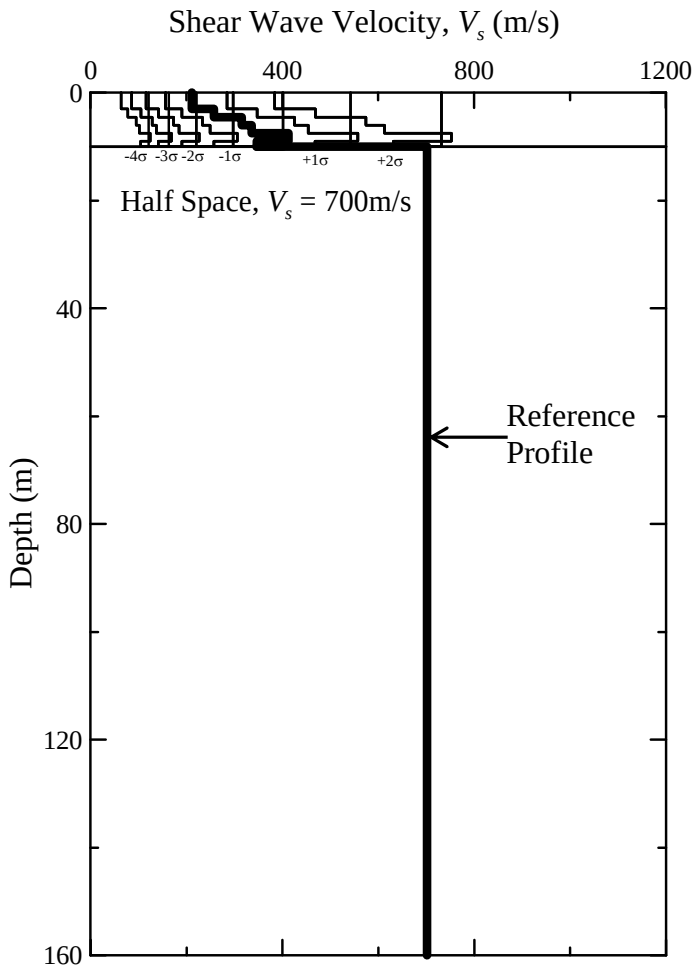

Figure H.5: Shear wave velocity profiles considered for Columbia-Florence-Lake Marion area with soft rock half space at depth = 10 m. The reference profile is compiled from Odum et al. (2003), Silva et al. (2003), Chapman et al. (2006) and Andrus et al. (2006), and the standard deviation values are based on Andrus et al. (2006).

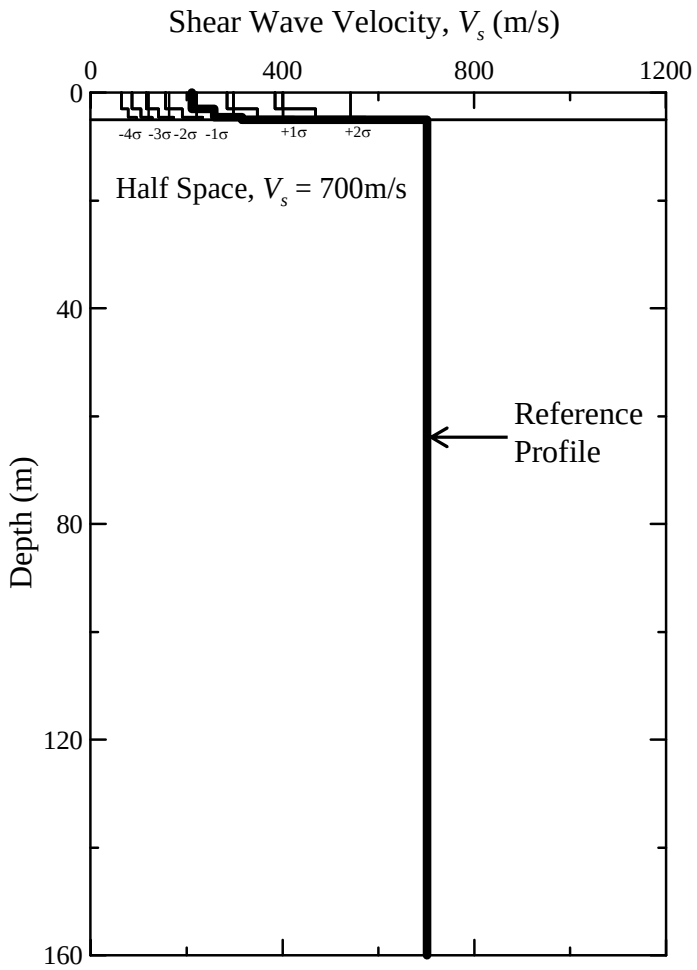

Figure H.6: Shear wave velocity profiles considered for Columbia-Florence-Lake Marion area with soft rock half space at depth = 5 m. The reference profile is compiled from Odum et al. (2003), Silva et al. (2003), Chapman et al. (2006) and Andrus et al. (2006), and the standard deviation values are based on Andrus et al. (2006).

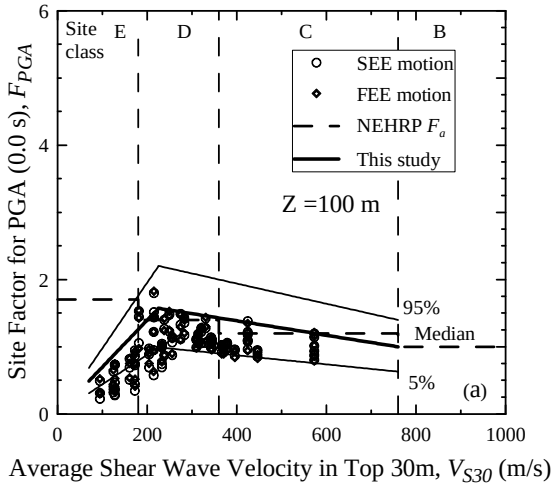
Site class
E
D
C
B
SEE motion
FEE motion
NEHRP F_a
This study
Z =100 m
95%
Median
5%
(a)
Site Factor for PGA (0.0 s), F_{PGA}
Average Shear Wave Velocity in Top 30m, V_{S30} (m/s)

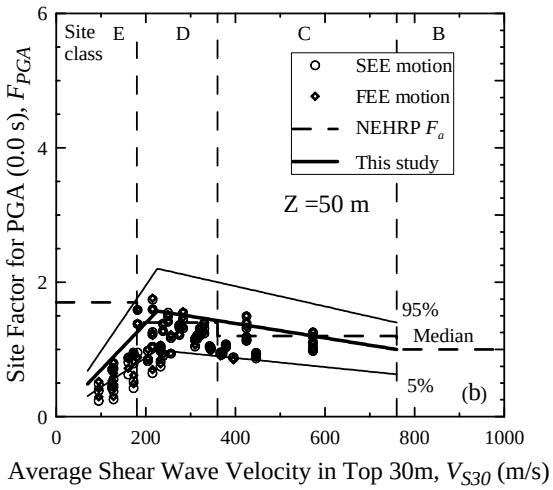
Site class
E
D
C
B
SEE motion
FEE motion
NEHRP F_a
This study
Z =50 m
95%
Median
5%
(b)
Site Factor for PGA (0.0 s), F_{PGA}
Average Shear Wave Velocity in Top 30m, V_{S30} (m/s)

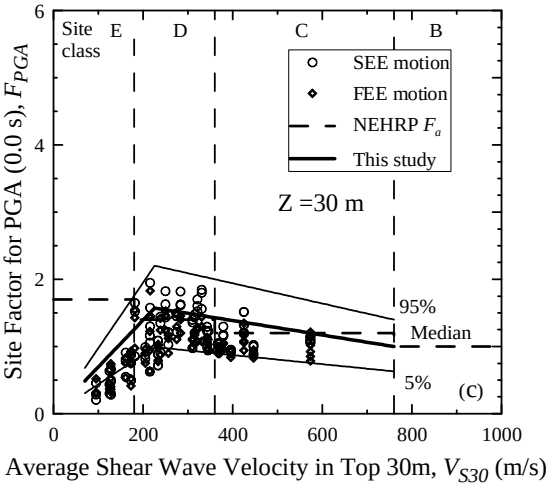
Site class
E
D
C
B
SEE motion
FEE motion
NEHRP F_a
This study
Z =30 m
95%
Median
5%
(c)
Site Factor for PGA (0.0 s), F_{PGA}
Average Shear Wave Velocity in Top 30m, V_{S30} (m/s)

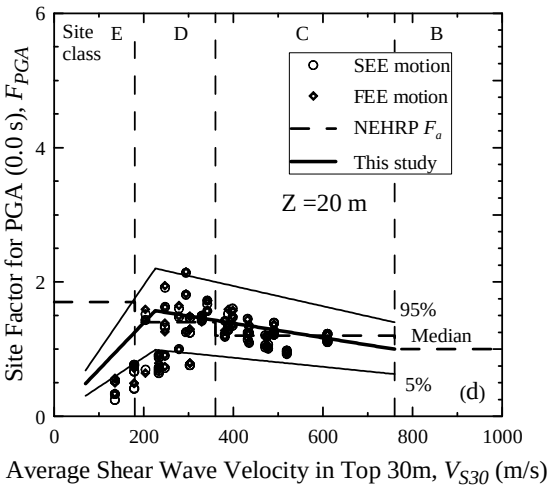
Site class
E
D
C
B
SEE motion
FEE motion
NEHRP F_a
This study
Z =20 m
95%
Median
5%
(d)
Site Factor for PGA (0.0 s), F_{PGA}
Average Shear Wave Velocity in Top 30m, V_{S30} (m/s)

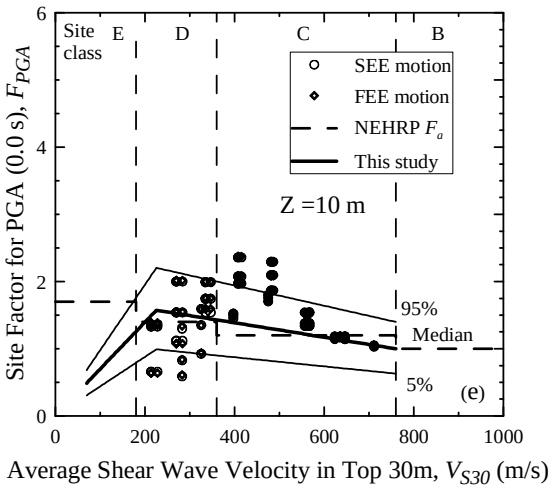
Site class
E
D
C
B
SEE motion
FEE motion
NEHRP F_a
This study
Z =10 m
95%
Median
5%
(e)
Site Factor for PGA (0.0 s), F_{PGA}
Average Shear Wave Velocity in Top 30m, V_{S30} (m/s)

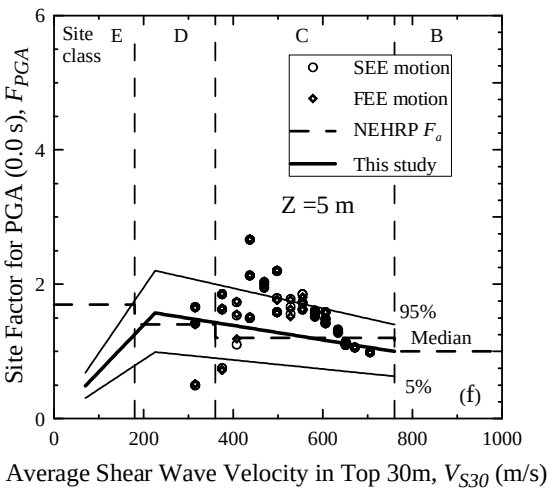
Site class
E
D
C
B
SEE motion
FEE motion
NEHRP F_a
This study
Z =5 m
95%
Median
5%
(f)
Site Factor for PGA (0.0 s), F_{PGA}
Average Shear Wave Velocity in Top 30m, V_{S30} (m/s)

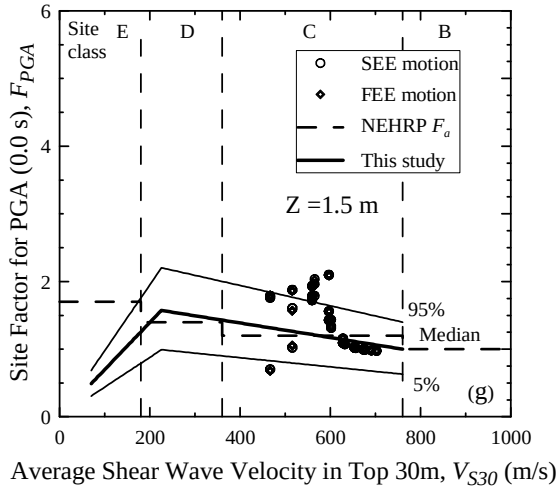

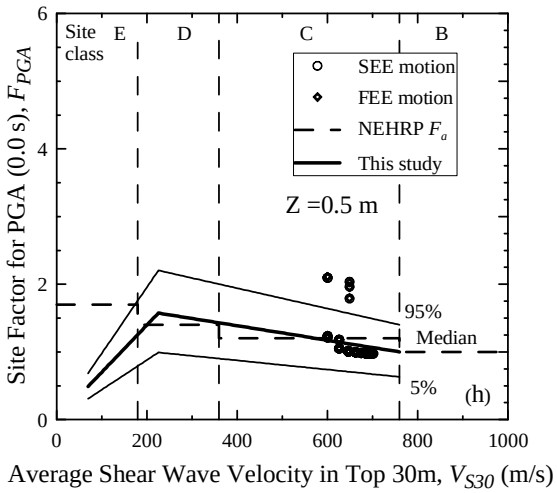

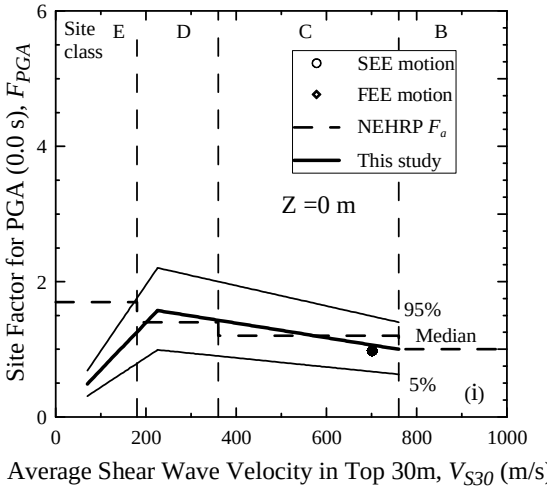

Figure H.7: Site coefficients for 0.0 s spectral period (free-field) with *PGA* equal to 0.2 g and soft rock half space at depth equal to (a) 100 m, (b) 50 m, (c) 30 m, (d) 20 m, (e) 10 m, (f) 5 m, (g) 1.5 m, (h) 0.5 m, and (i) 0.0 m based on V_s profiles shown in Figures C.2-C.7 for the Columbia area.

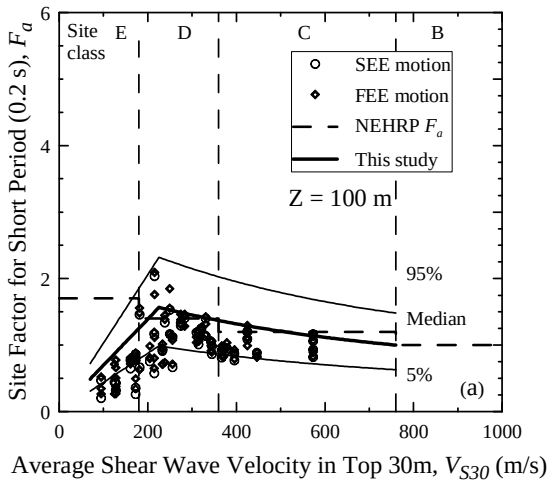
Site class
E
D
C
B
SEE motion
FEE motion
NEHRP F_a
This study
Z = 100 m
95%
Median
5%
(a)
Site Factor for Short Period (0.2 s), F_a
Average Shear Wave Velocity in Top 30m, V_{S30} (m/s)

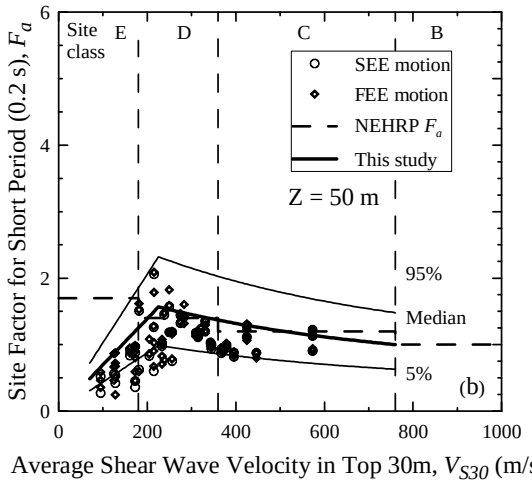
Site class
E
D
C
B
SEE motion
FEE motion
NEHRP F_a
This study
Z = 50 m
95%
Median
5%
(b)
Site Factor for Short Period (0.2 s), F_a
Average Shear Wave Velocity in Top 30m, V_{S30} (m/s)

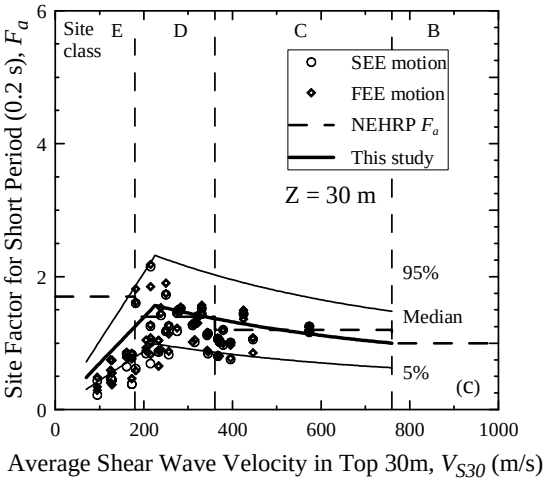
Site class
E
D
C
B
SEE motion
FEE motion
NEHRP F_a
This study
Z = 30 m
95%
Median
5%
(c)
Site Factor for Short Period (0.2 s), F_a
Average Shear Wave Velocity in Top 30m, V_{S30} (m/s)

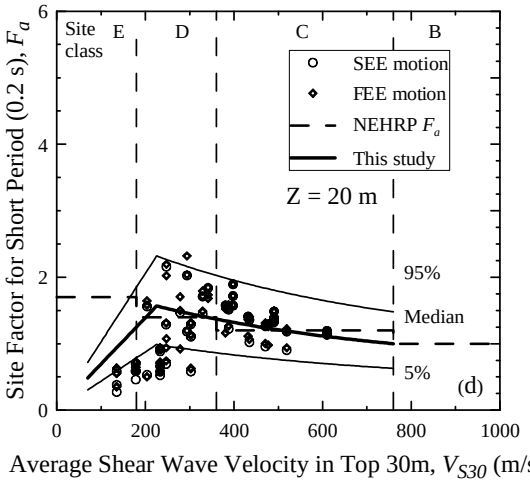
Site class
E
D
C
B
SEE motion
FEE motion
NEHRP F_a
This study
Z = 20 m
95%
Median
5%
(d)
Site Factor for Short Period (0.2 s), F_a
Average Shear Wave Velocity in Top 30m, V_{S30} (m/s)

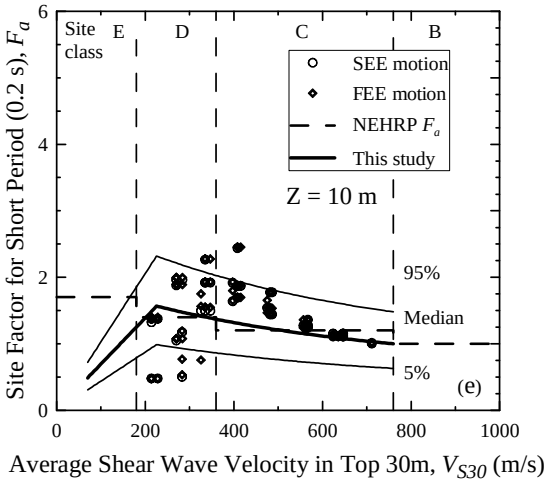
Site class
E
D
C
B
SEE motion
FEE motion
NEHRP F_a
This study
Z = 10 m
95%
Median
5%
(e)
Site Factor for Short Period (0.2 s), F_a
Average Shear Wave Velocity in Top 30m, V_{S30} (m/s)

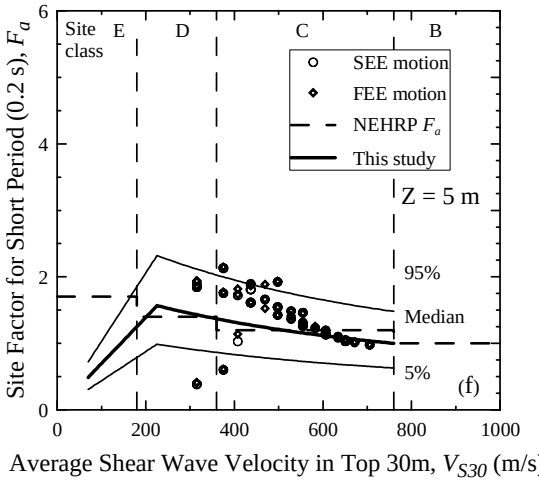
Site class
E
D
C
B
SEE motion
FEE motion
NEHRP F_a
This study
Z = 5 m
95%
Median
5%
(f)
Site Factor for Short Period (0.2 s), F_a
Average Shear Wave Velocity in Top 30m, V_{S30} (m/s)

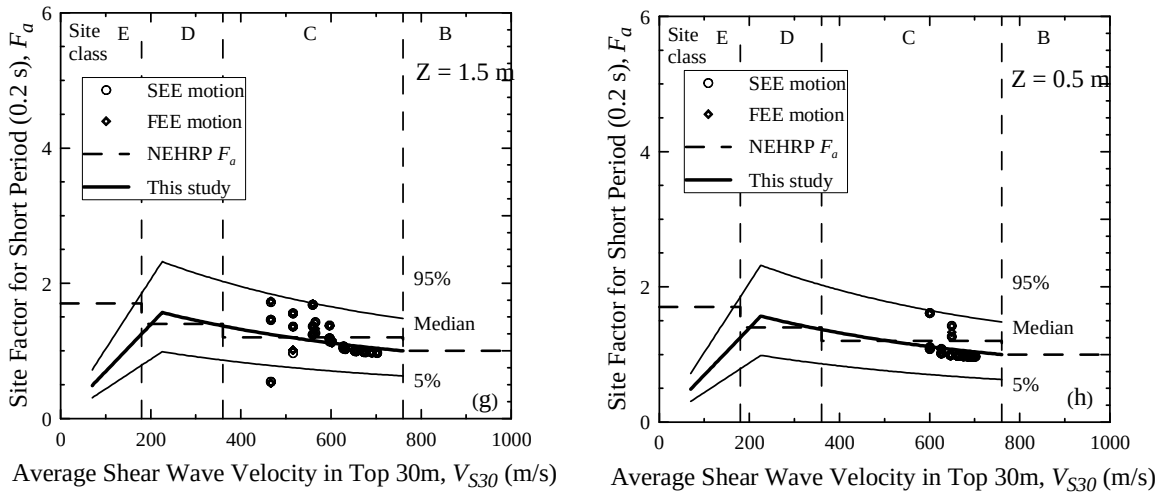

Figure H.8: Site coefficients for 0.2 s (short) spectral period with S_s equal to 0.5 g, and soft rock half space at depth equal to (a) 100 m, (b) 50 m, (c) 30 m, (d) 20 m, (e) 10 m, (f) 5 m, (g) 1.5 m, and (h) 0.5 m, based on V_s profiles shown in Figures C.2-C.7 for the Columbia area.

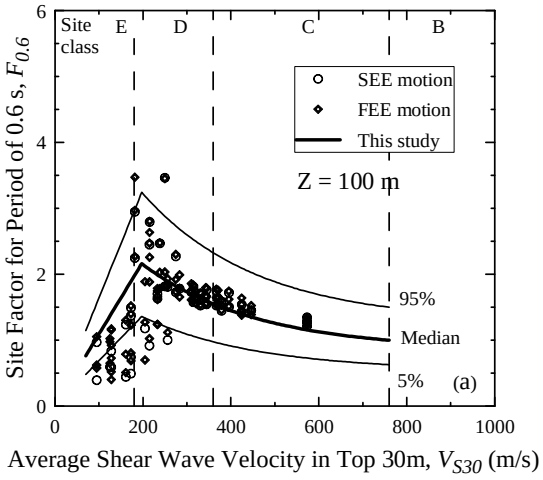
Site class
E
D
C
B
SEE motion
FEE motion
This study
Z = 100 m
95%
Median
5%
(a)
Site Factor for Period of 0.6 s, $F_{0.6}$
Average Shear Wave Velocity in Top 30m, V_{S30} (m/s)

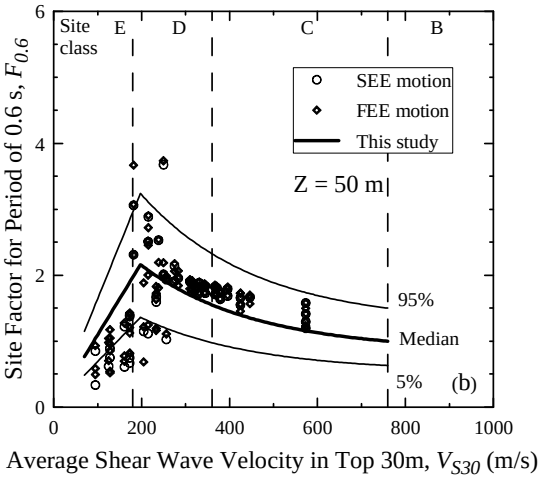
Site class
E
D
C
B
SEE motion
FEE motion
This study
Z = 50 m
95%
Median
5%
(b)
Site Factor for Period of 0.6 s, $F_{0.6}$
Average Shear Wave Velocity in Top 30m, V_{S30} (m/s)

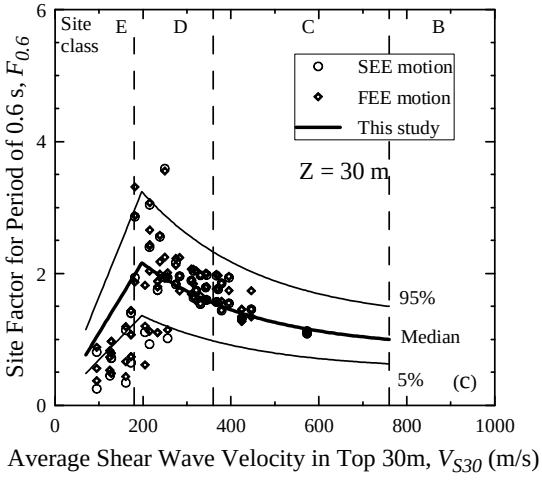
Site class
E
D
C
B
SEE motion
FEE motion
This study
Z = 30 m
95%
Median
5%
(c)
Site Factor for Period of 0.6 s, $F_{0.6}$
Average Shear Wave Velocity in Top 30m, V_{S30} (m/s)

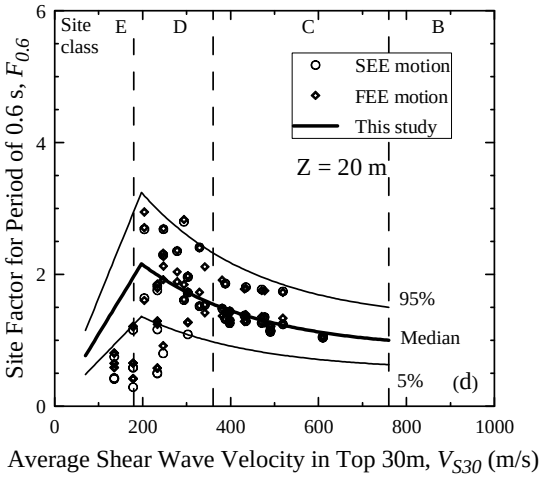
Site class
E
D
C
B
SEE motion
FEE motion
This study
Z = 20 m
95%
Median
5%
(d)
Site Factor for Period of 0.6 s, $F_{0.6}$
Average Shear Wave Velocity in Top 30m, V_{S30} (m/s)

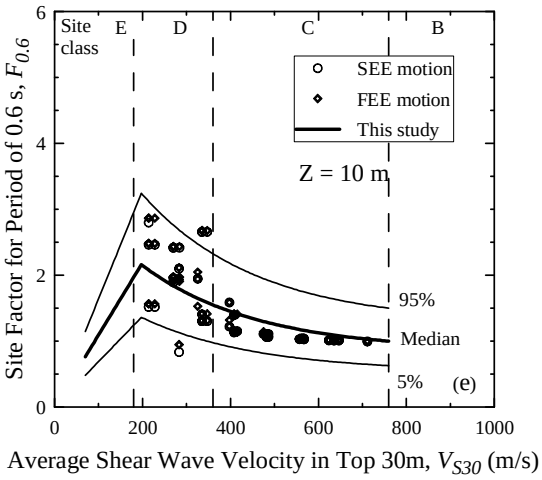
Site class
E
D
C
B
SEE motion
FEE motion
This study
Z = 10 m
95%
Median
5%
(e)
Site Factor for Period of 0.6 s, $F_{0.6}$
Average Shear Wave Velocity in Top 30m, V_{S30} (m/s)

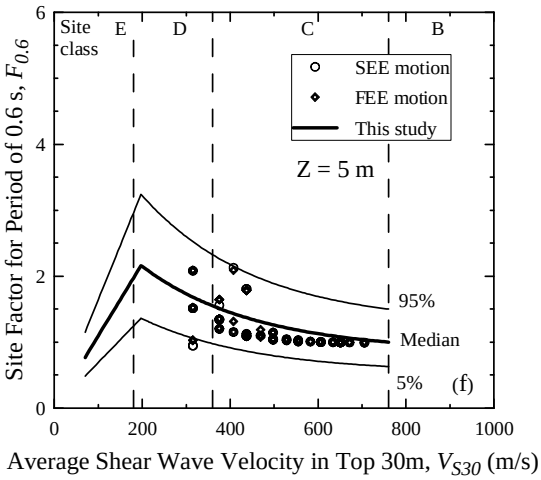
Site class
E
D
C
B
SEE motion
FEE motion
This study
Z = 5 m
95%
Median
5%
(f)
Site Factor for Period of 0.6 s, $F_{0.6}$
Average Shear Wave Velocity in Top 30m, V_{S30} (m/s)

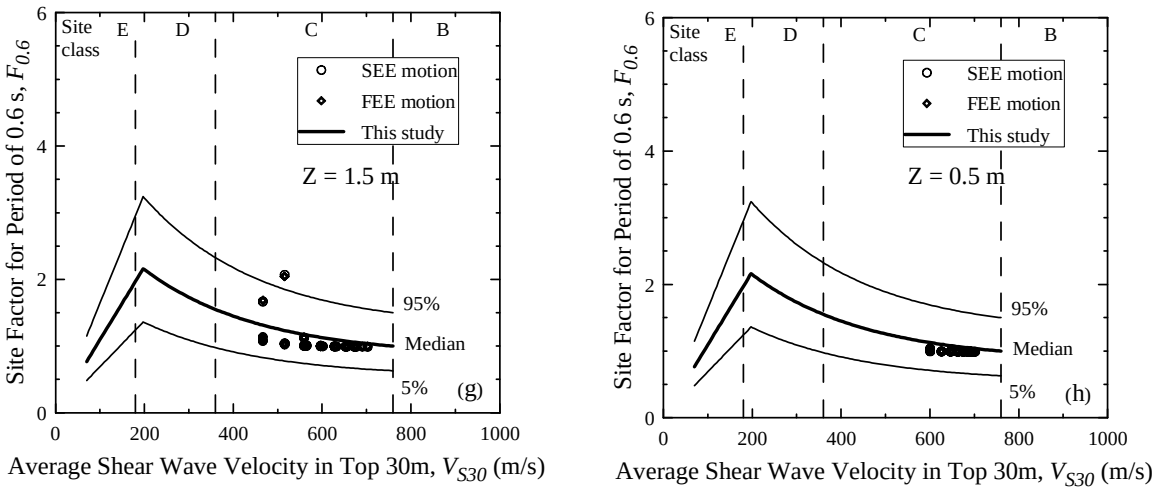

Figure H.9: Site coefficients for 0.6 s spectral period with $S_{0.6}$ equal to 0.2 g, and soft rock half space at depth equal to (a) 100 m, (b) 50 m, (c) 30 m, (d) 20 m, (e) 10 m, (f) 5 m, (g) 1.5 m, and (h) 0.5 m, based on V_s profiles shown in Figures C.2-C.7 for the Columbia area.

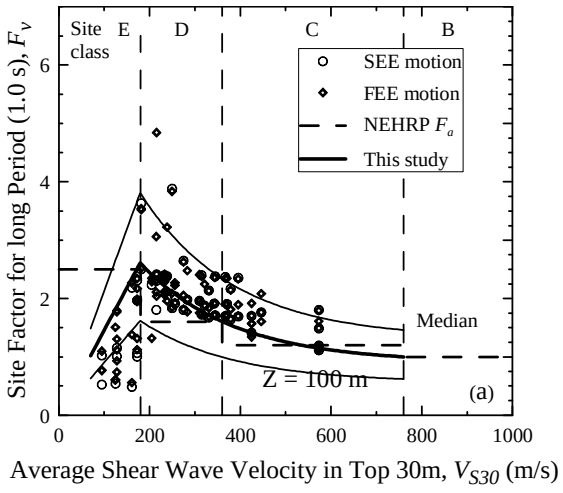
Site class
E
D
C
B
SEE motion
FEE motion
NEHRP F_a
This study
Median
Z = 100 m
(a)
Site Factor for long Period (1.0 s), F_v
Average Shear Wave Velocity in Top 30m, V_{S30} (m/s)

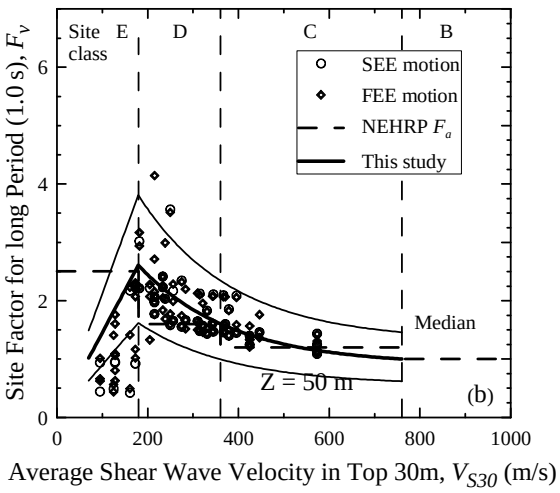
Site class
E
D
C
B
SEE motion
FEE motion
NEHRP F_a
This study
Median
Z = 50 m
(b)
Site Factor for long Period (1.0 s), F_v
Average Shear Wave Velocity in Top 30m, V_{S30} (m/s)

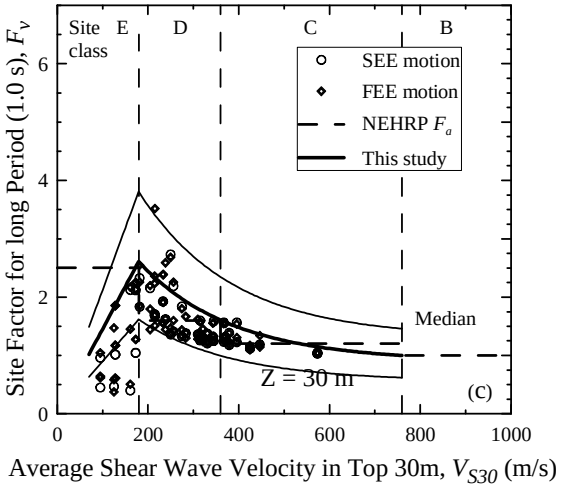
Site class
E
D
C
B
SEE motion
FEE motion
NEHRP F_a
This study
Median
Z = 30 m
(c)
Site Factor for long Period (1.0 s), F_v
Average Shear Wave Velocity in Top 30m, V_{S30} (m/s)

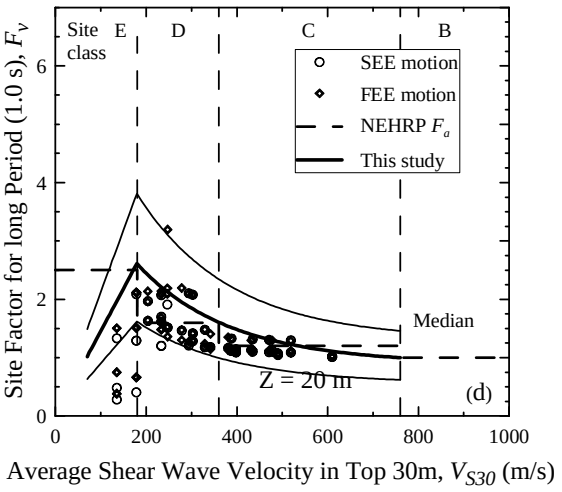
Site class
E
D
C
B
SEE motion
FEE motion
NEHRP F_a
This study
Median
Z = 20 m
(d)
Site Factor for long Period (1.0 s), F_v
Average Shear Wave Velocity in Top 30m, V_{S30} (m/s)

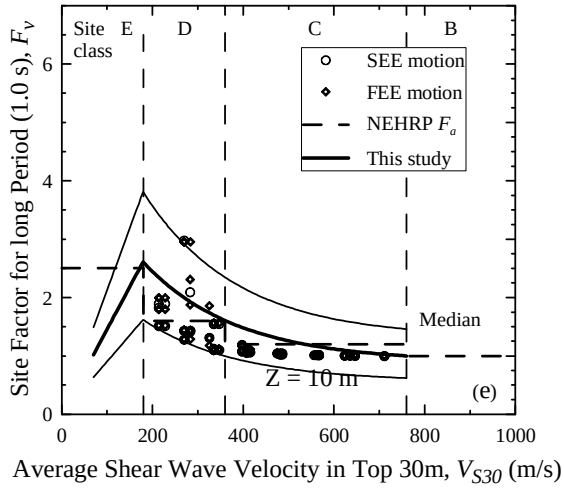
Site class
E
D
C
B
SEE motion
FEE motion
NEHRP F_a
This study
Median
Z = 10 m
(e)
Site Factor for long Period (1.0 s), F_v
Average Shear Wave Velocity in Top 30m, V_{S30} (m/s)

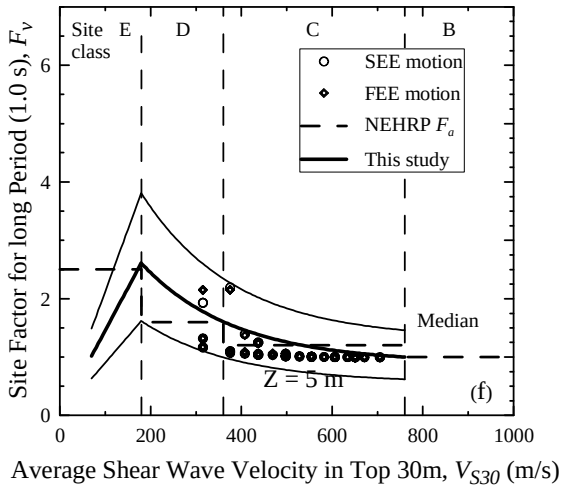
Site class
E
D
C
B
SEE motion
FEE motion
NEHRP F_a
This study
Median
Z = 5 m
(f)
Site Factor for long Period (1.0 s), F_v
Average Shear Wave Velocity in Top 30m, V_{S30} (m/s)

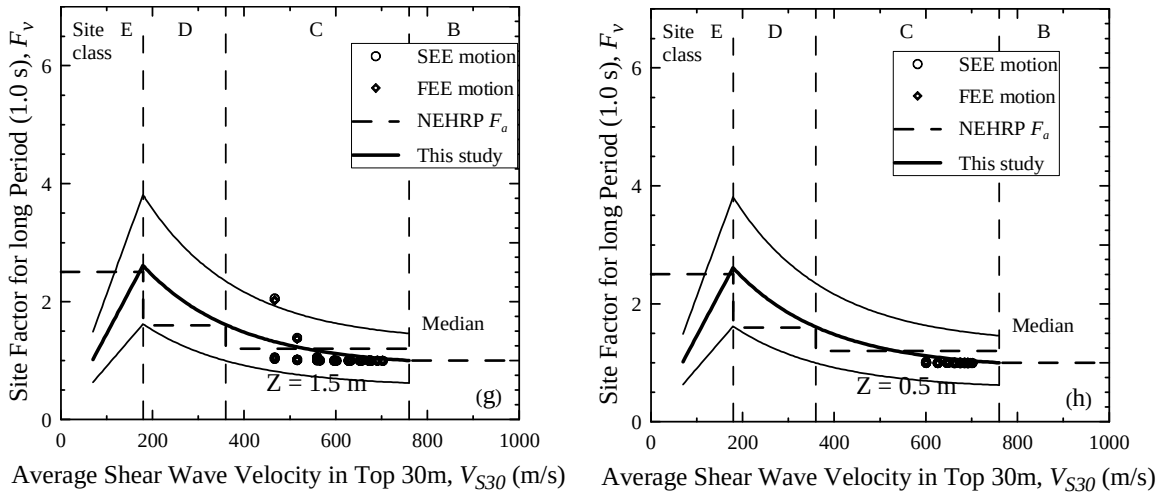

Figure H.10: Site coefficients for 1.0 s (long) spectral period with S_1 equal to 0.2 g, and soft rock half space at depth equal to (a) 100 m, (b) 50 m, (c) 30 m, (d) 20 m, (e) 10 m, (f) 5 m, (g) 1.5 m, and (h) 0.5 m, based on V_s profiles shown in Figures C.2-C.7 for the Columbia area.

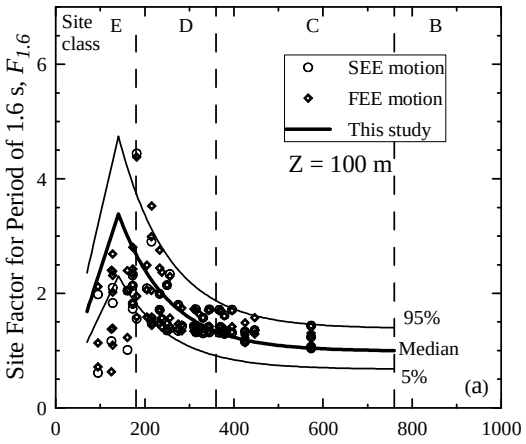
Site class
E
D
C
B
SEE motion
FEE motion
This study
Z = 100 m
95%
Median
5%
(a)
Site Factor for Period of 1.6 s, $F_{1.6}$
Average Shear Wave Velocity in Top 30m, V_{S30} (m/s)

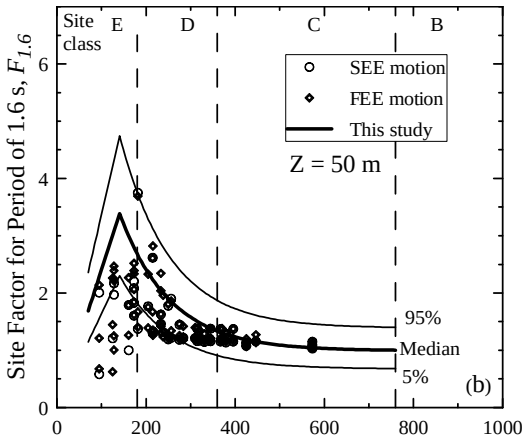
Site class
E
D
C
B
SEE motion
FEE motion
This study
Z = 50 m
95%
Median
5%
(b)
Site Factor for Period of 1.6 s, $F_{1.6}$
Average Shear Wave Velocity in Top 30m, V_{S30} (m/s)

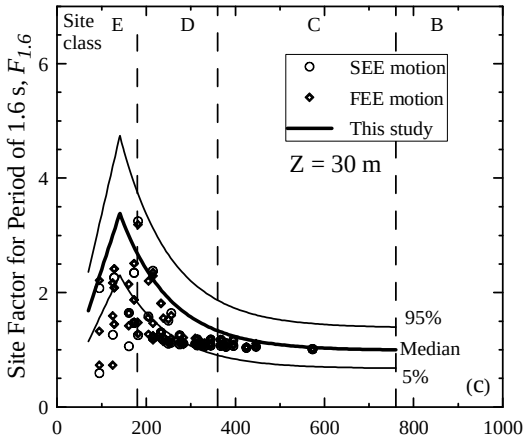
Site class
E
D
C
B
SEE motion
FEE motion
This study
Z = 30 m
95%
Median
5%
(c)
Site Factor for Period of 1.6 s, $F_{1.6}$
Average Shear Wave Velocity in Top 30m, V_{S30} (m/s)

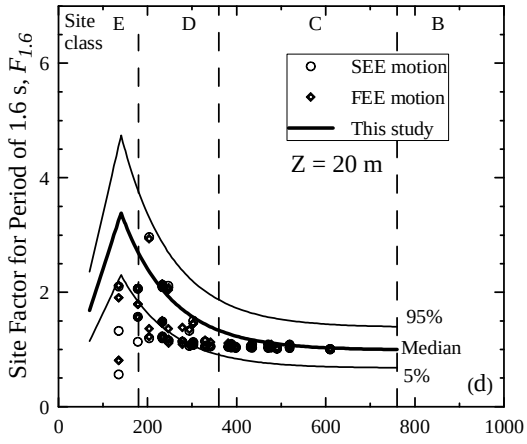
Site class
E
D
C
B
SEE motion
FEE motion
This study
Z = 20 m
95%
Median
5%
(d)
Site Factor for Period of 1.6 s, $F_{1.6}$
Average Shear Wave Velocity in Top 30m, V_{S30} (m/s)

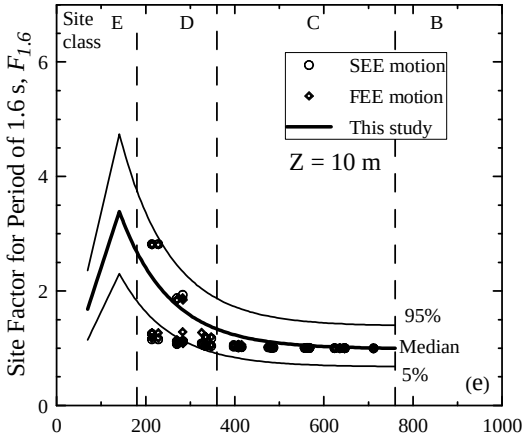
Site class
E
D
C
B
SEE motion
FEE motion
This study
Z = 10 m
95%
Median
5%
(e)
Site Factor for Period of 1.6 s, $F_{1.6}$
Average Shear Wave Velocity in Top 30m, V_{S30} (m/s)

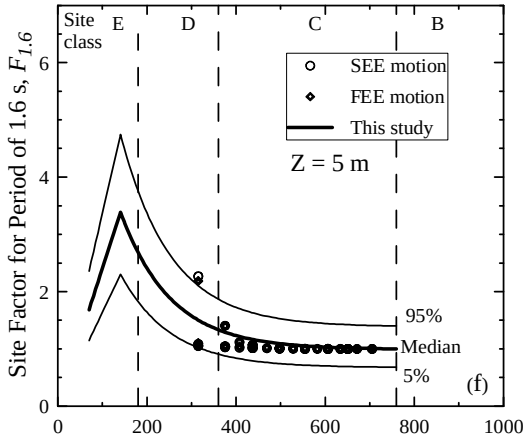
Site class
E
D
C
B
SEE motion
FEE motion
This study
Z = 5 m
95%
Median
5%
(f)
Site Factor for Period of 1.6 s, $F_{1.6}$
Average Shear Wave Velocity in Top 30m, V_{S30} (m/s)

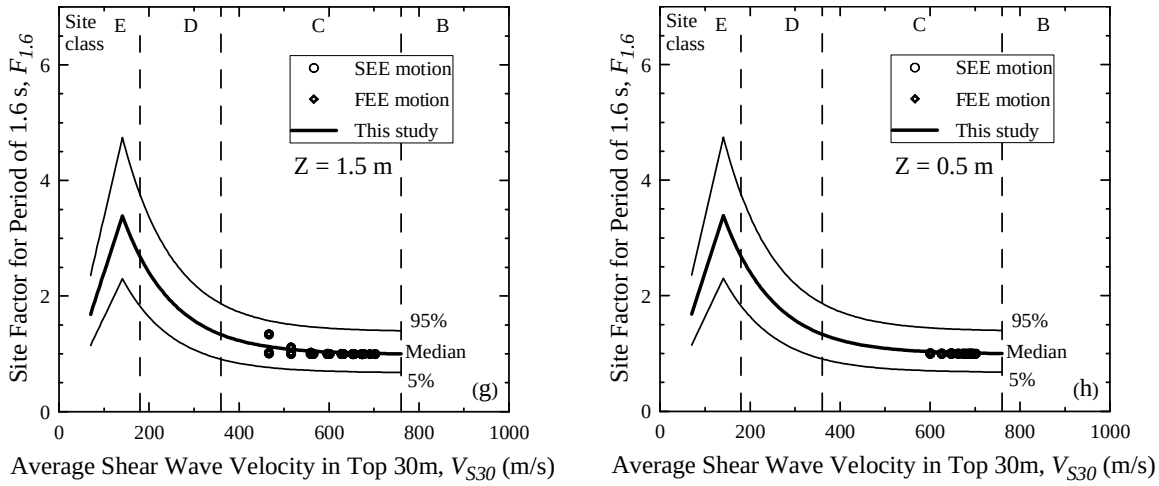

Figure H.11: Site coefficients for 1.6 s spectral period with $S_{1.6}$ equal to 0.1 g, and soft rock half space at depth equal to (a) 100 m, (b) 50 m, (c) 30 m, (d) 20 m, (e) 10 m, (f) 5 m, (g) 1.5 m, and (h) 0.5 m, based on V_s profiles shown in Figures C.2-C.7 for the Columbia area.

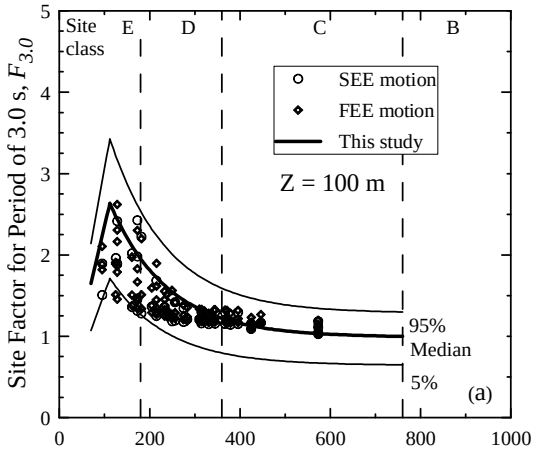
Site class
E
D
C
B
SEE motion
FEE motion
This study
Z = 100 m
95%
Median
5%
(a)
Site Factor for Period of 3.0 s, $F_{3.0}$
Average Shear Wave Velocity in Top 30m, V_{S30} (m/s)

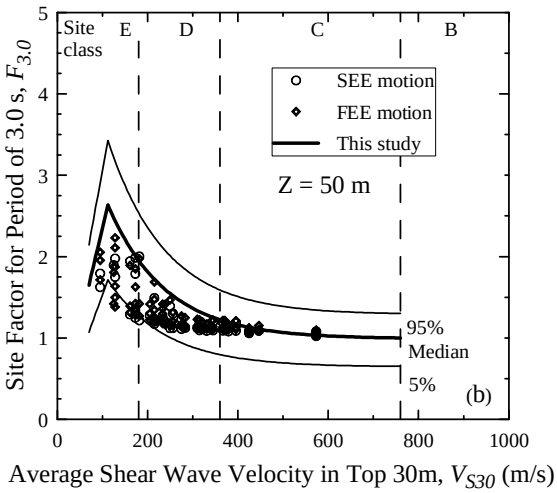
Site class
E
D
C
B
SEE motion
FEE motion
This study
Z = 50 m
95%
Median
5%
(b)
Site Factor for Period of 3.0 s, $F_{3.0}$
Average Shear Wave Velocity in Top 30m, V_{S30} (m/s)

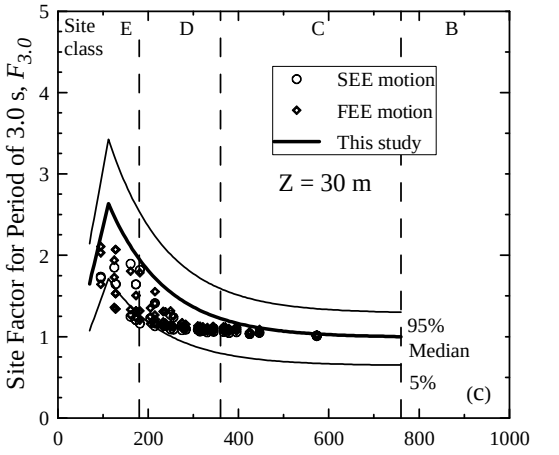
Site class
E
D
C
B
SEE motion
FEE motion
This study
Z = 30 m
95%
Median
5%
(c)
Site Factor for Period of 3.0 s, $F_{3.0}$
Average Shear Wave Velocity in Top 30m, V_{S30} (m/s)

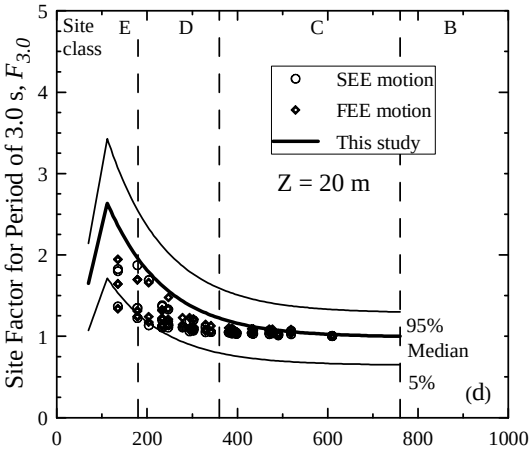
Site class
E
D
C
B
SEE motion
FEE motion
This study
Z = 20 m
95%
Median
5%
(d)
Site Factor for Period of 3.0 s, $F_{3.0}$
Average Shear Wave Velocity in Top 30m, V_{S30} (m/s)

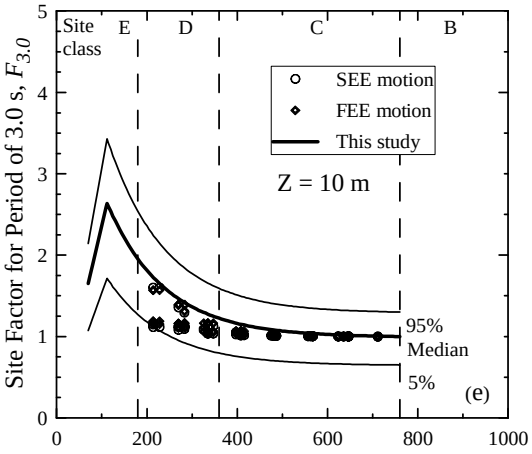
Site class
E
D
C
B
SEE motion
FEE motion
This study
Z = 10 m
95%
Median
5%
(e)
Site Factor for Period of 3.0 s, $F_{3.0}$
Average Shear Wave Velocity in Top 30m, V_{S30} (m/s)

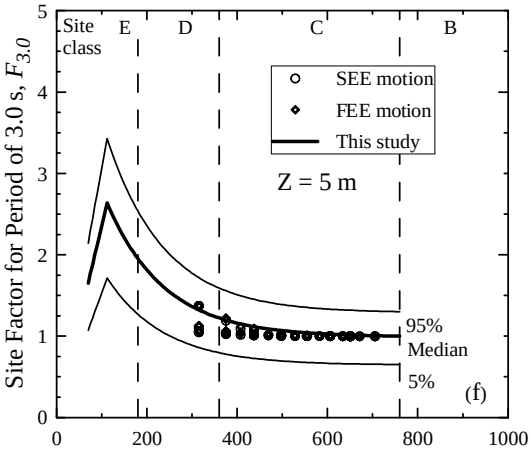
Site class
E
D
C
B
SEE motion
FEE motion
This study
Z = 5 m
95%
Median
5%
(f)
Site Factor for Period of 3.0 s, $F_{3.0}$
Average Shear Wave Velocity in Top 30m, V_{S30} (m/s)

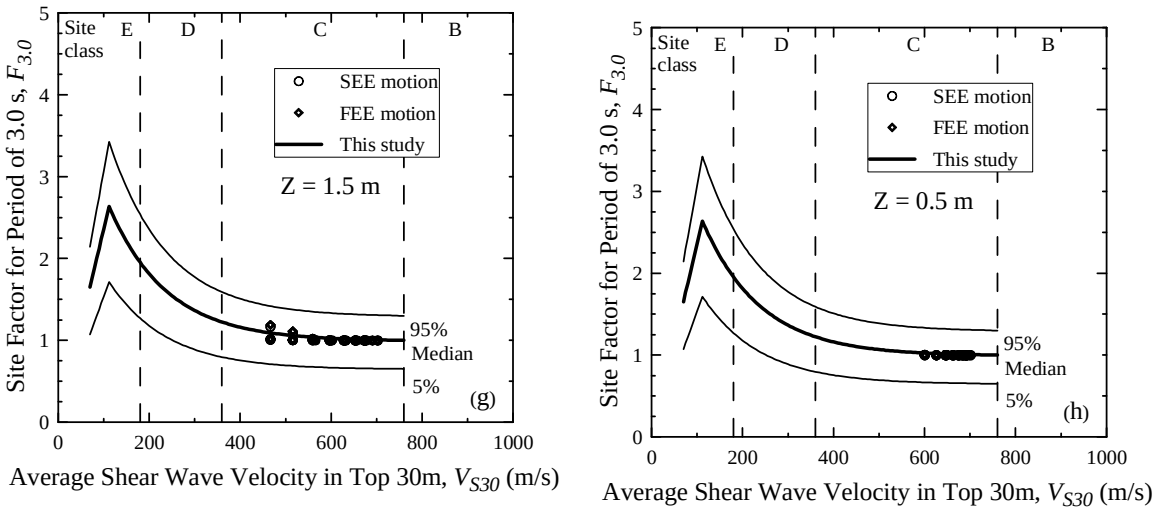

Figure H.12: Site coefficients for 3.0 s spectral period with $S_{3.0}$ equal to 0.04 g, and soft rock half space at depth equal to (a) 100 m, (b) 50 m, (c) 30 m, (d) 20 m, (e) 10 m, (f) 5 m, (g) 1.5 m, and (h) 0.5 m, based on V_s profiles shown in Figures C.2-C.7 for the Columbia area.

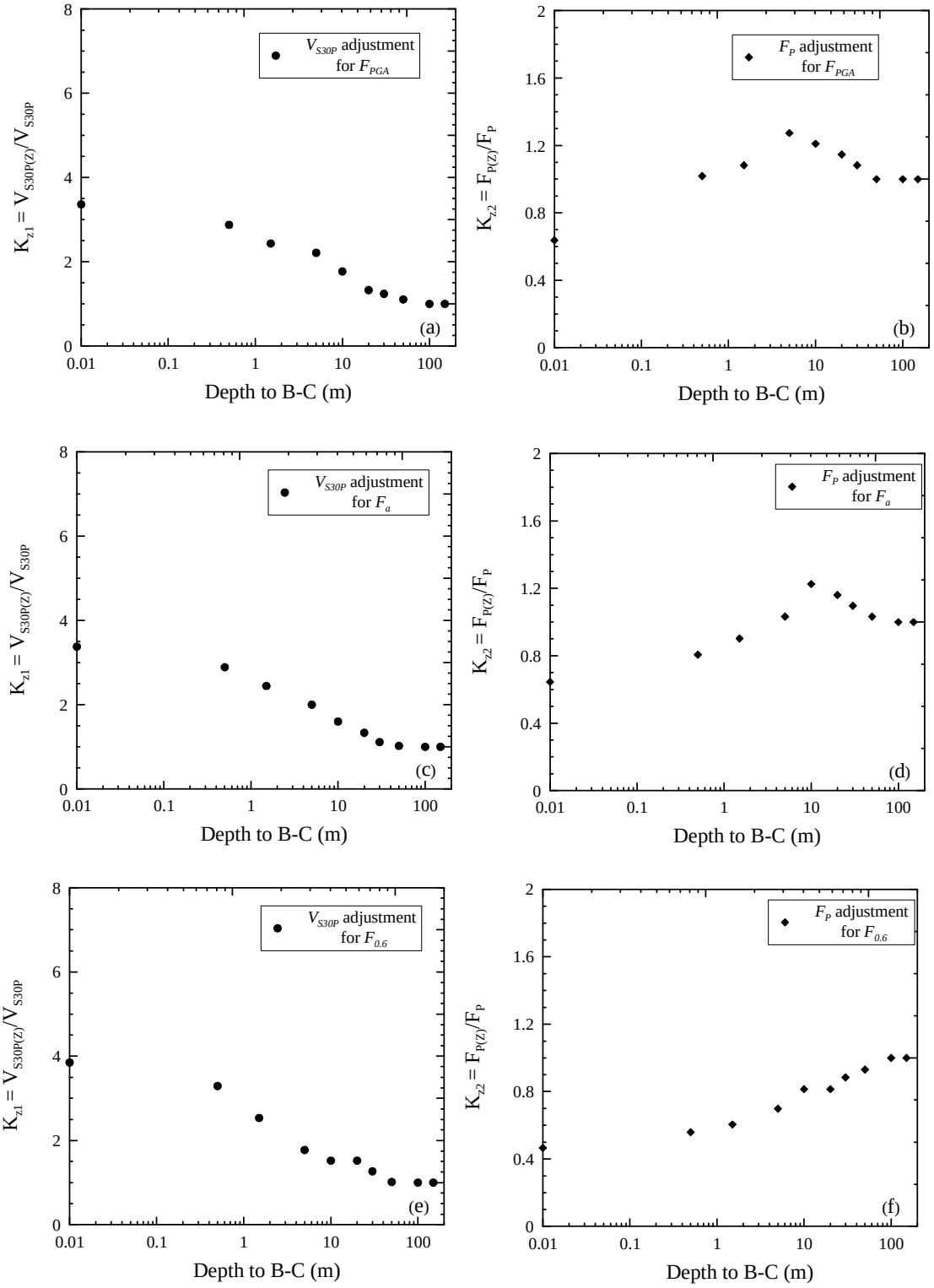

Figure H.13: Depth to B-C adjustment coefficients, K_{H1} and K_{H2}, for (a-b) F_{PGA}, (c-d) F_a, and (e-f) $F_{0.6}$.

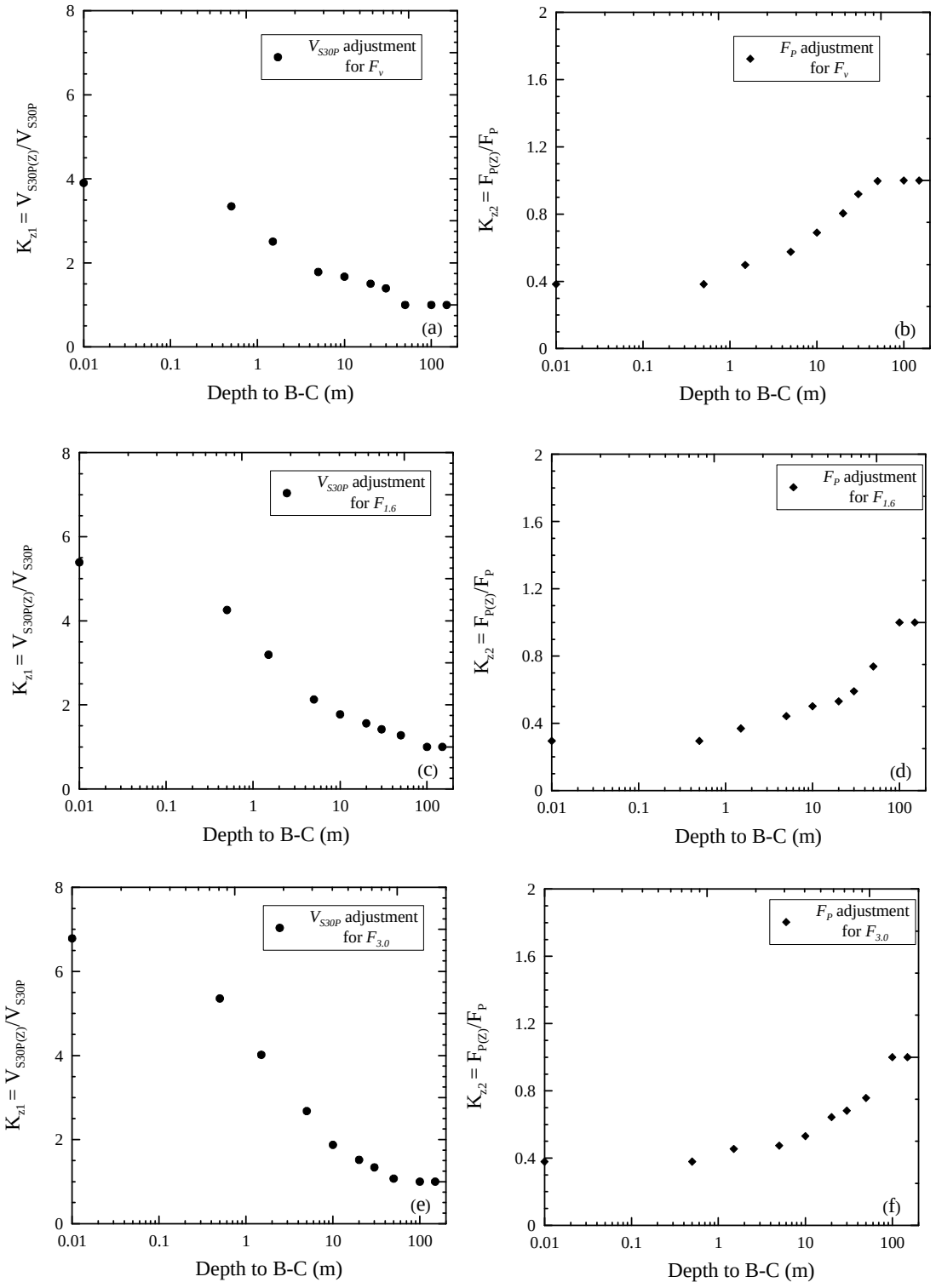

Figure H.14: Depth to B-C adjustment coefficients, K_{Z1} and K_{Z2}, for (a-b) F_v, (c-d) $F_{1.6}$, and (e-f) $F_{3.0.}$

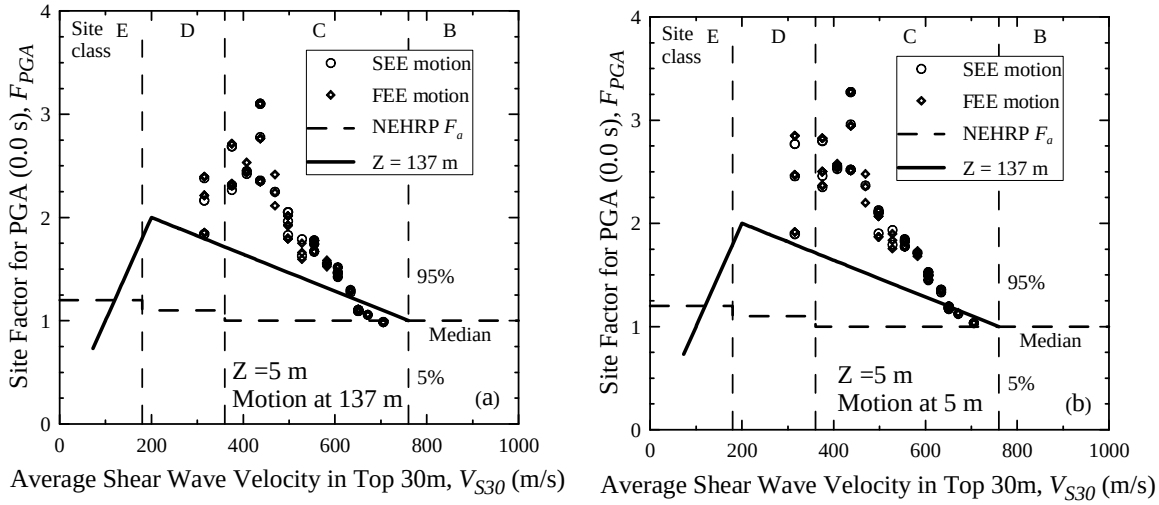

Figure H.15: Site coefficients for 0.0 s spectral period (free-field) with *PGA* equal to 0.05 g and soft rock half space at depth equal to 5 m, when motion is applied at a depth of (a) 137 m, and (b) 5 m.

APPENDIX I

EFFECT OF NORMALIZED PERIOD

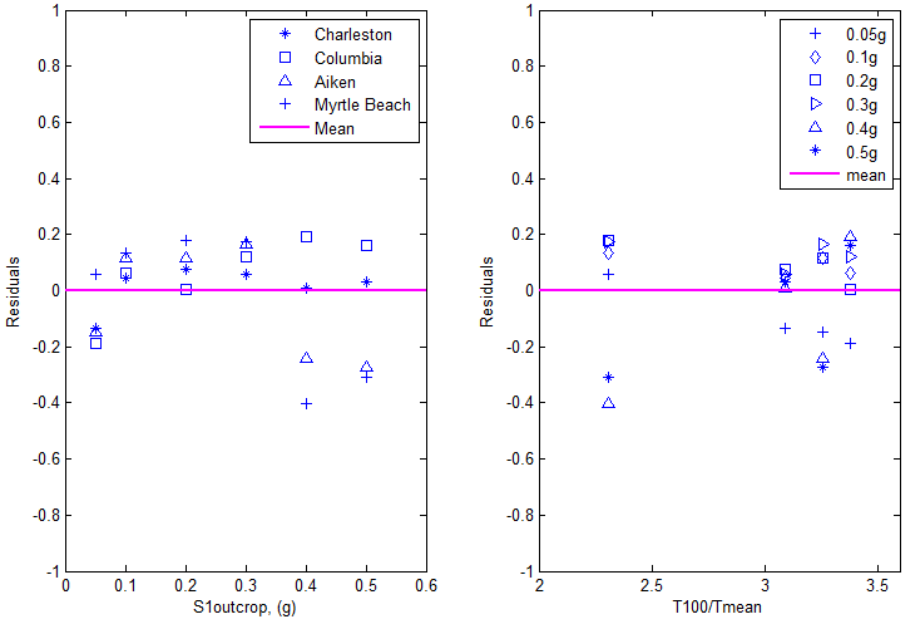

Figure I.1: Residuals of F_P for 0.0 s spectral period (free-field).

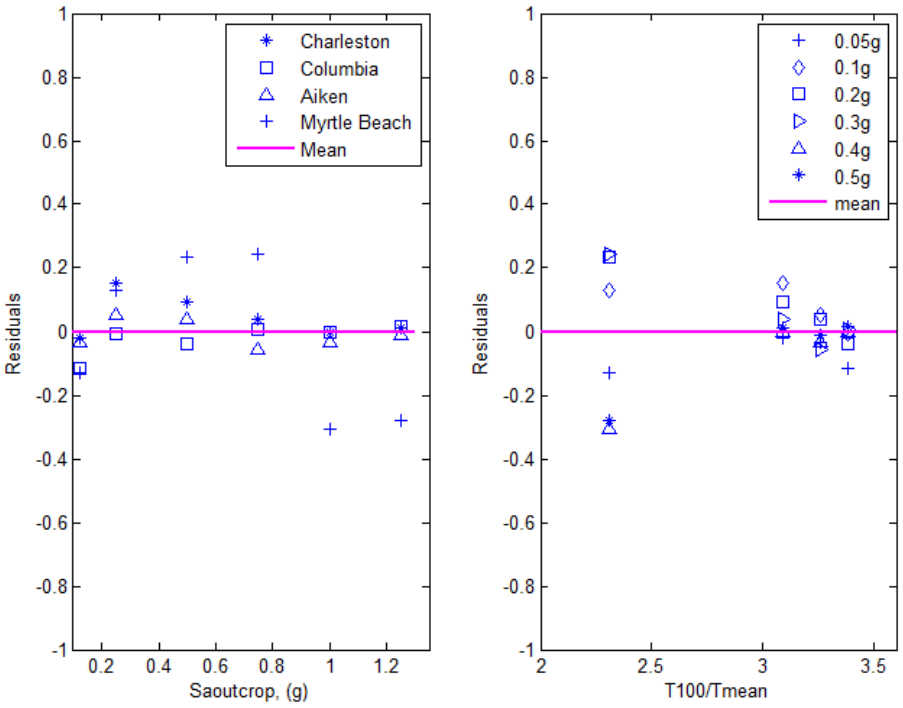

Figure I.2: Residuals of F_P for 0.2 s spectral period (short-period).

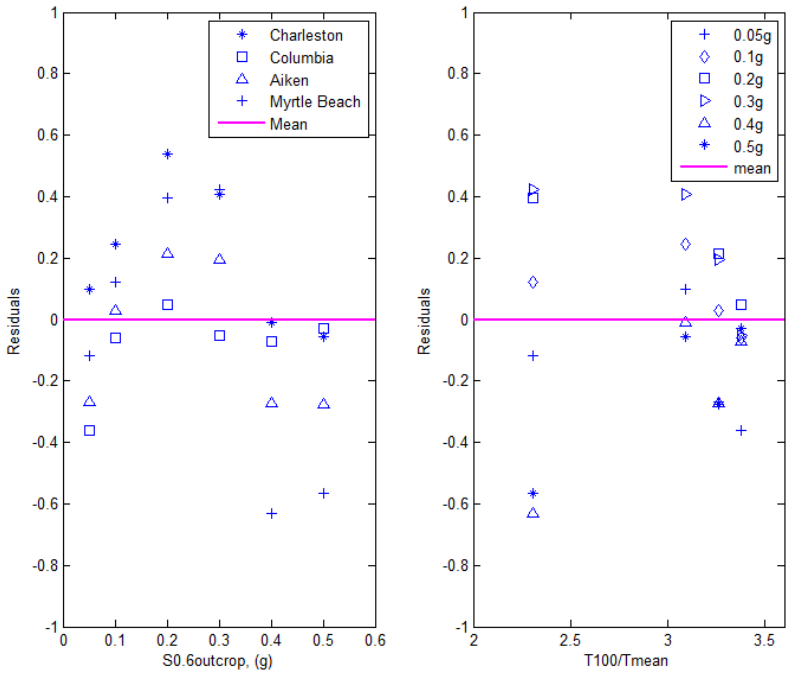

Figure I.3: Residuals of F_P for 0.6 s spectral period.

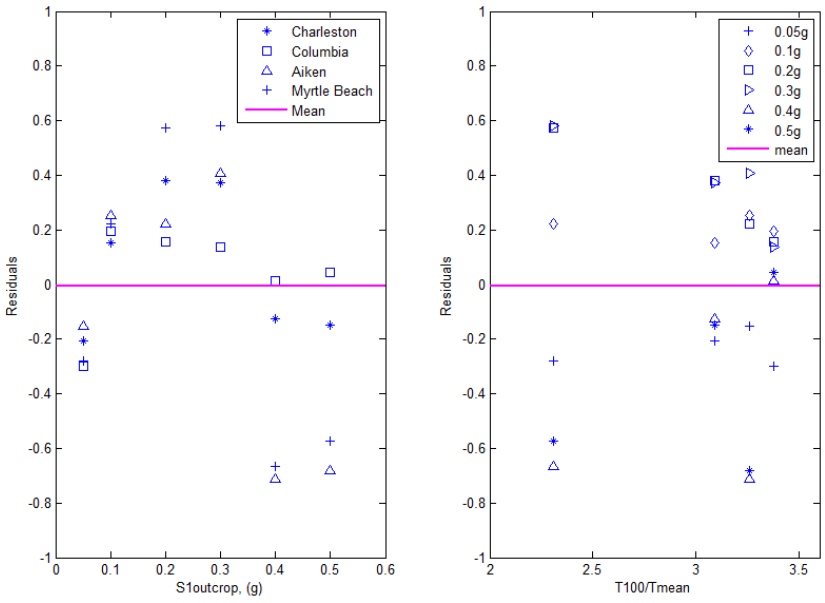

Figure I.4: Residuals of F_P for 1.0 s spectral period.

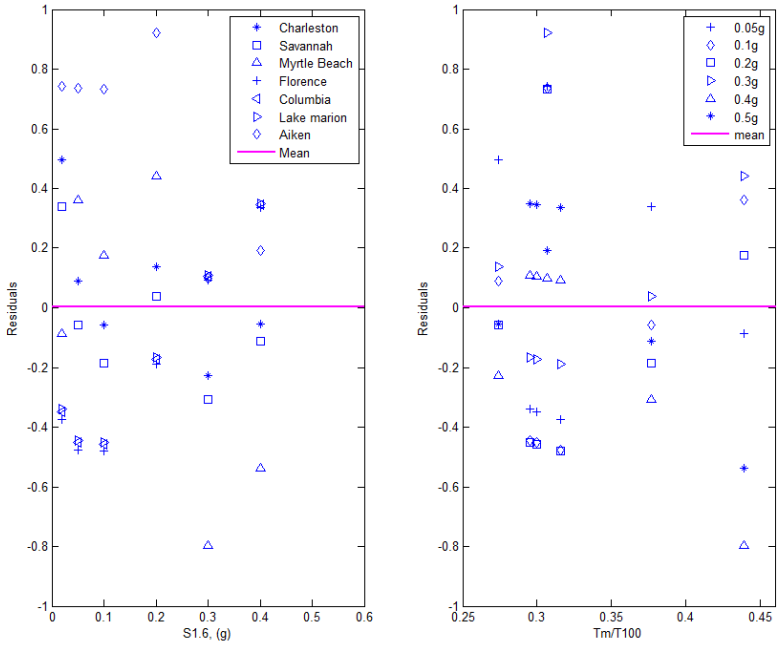

Figure I.5: Residuals of F_P for 1.6 s spectral period.

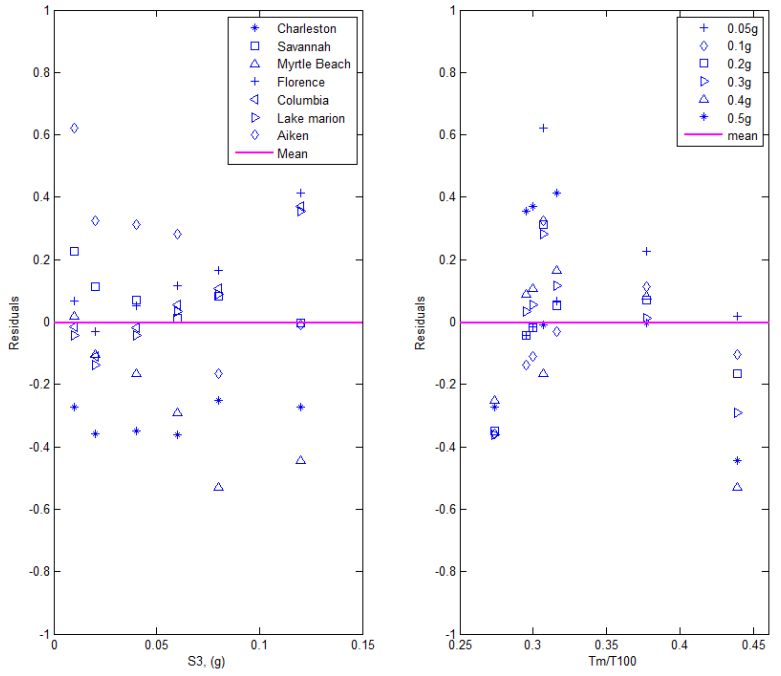

Figure I.6: Residuals of F_P for 3.0 s spectral period.

APPENDIX J

INFLUENCE OF MOMENT MAGNITUDE

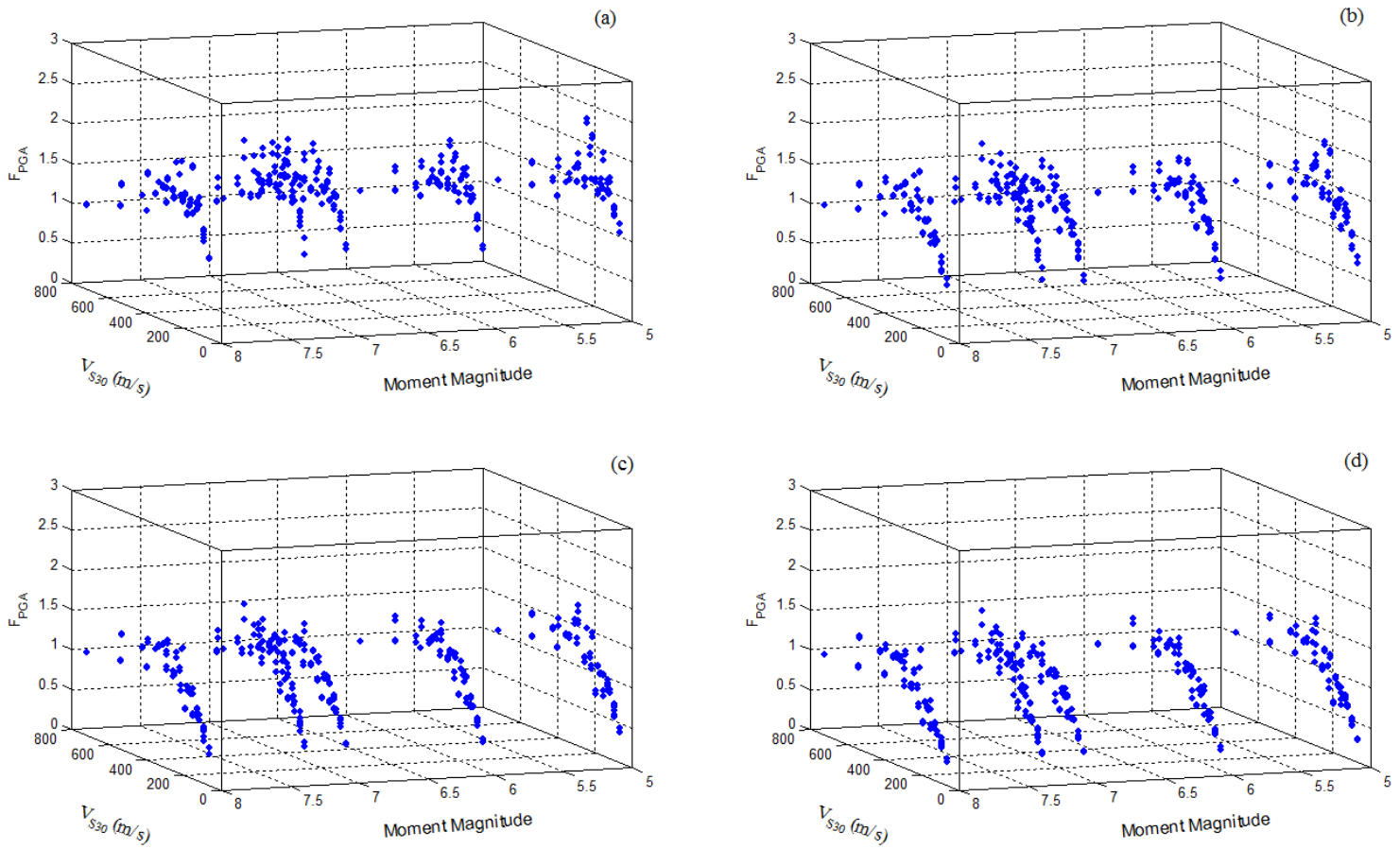

Figure J.1: F_{PGA} versus V_{S30} and moment magnitude with *PGA* equal to (a) 0.05 g, (b) 0.1 g, (c) 0.2 g, and (d) 0.3 g.

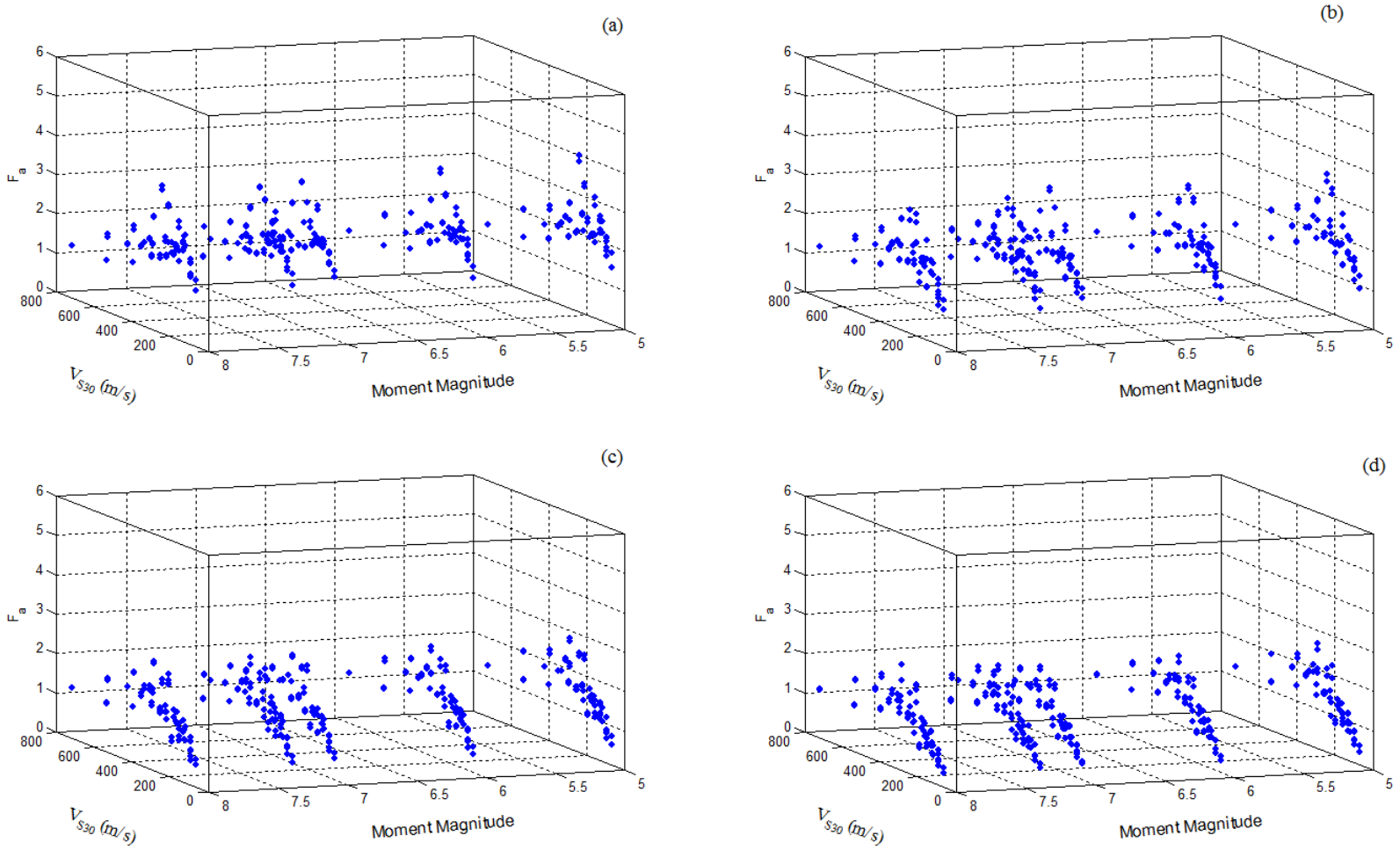

Figure J.2: F_a versus V_{S30} and moment magnitude with S_s equal to (a) 0.125 g, (b) 0.25 g, (c) 0.50 g, and (d) 0.75 g.

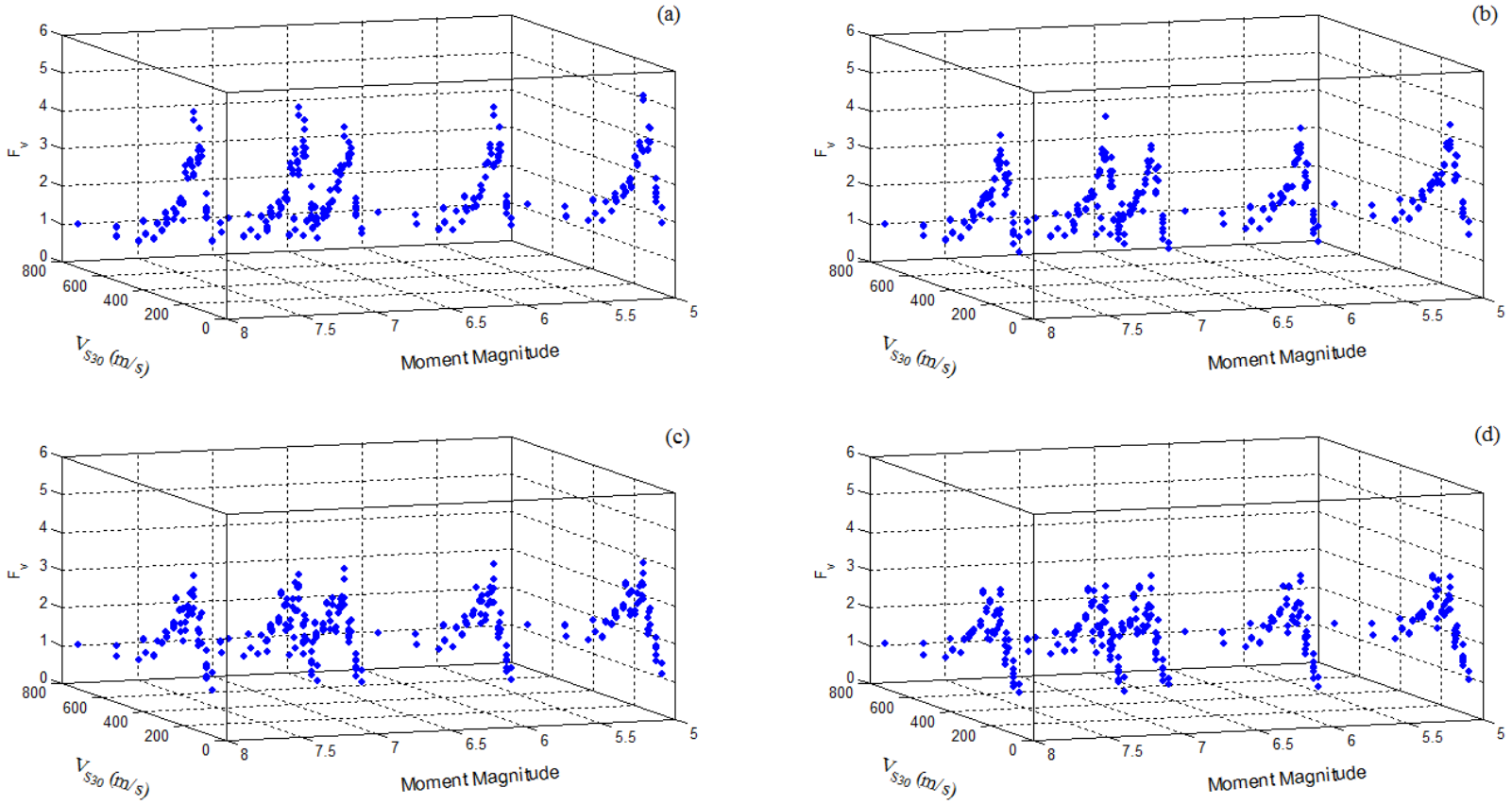

Figure J.3: F_v versus V_{S30} and moment magnitude with S_1 equal to (a) 0.05 g, (b) 0.1 g, (c) 0.2 g, and (d) 0.3 g.

REFERENCES

Aboye, S., Andrus, R. D., Ravichandran, N., Bhuiyan, A. and Harman, N., 2011. Site factors for estimating peak ground acceleration in Charleston, South Carolina, based on V_{S30}. *Proc., 4th IASPEI/IAEE International Symposium: Effects of Surface Geology on Seismic Motion*, University of California Santa Barbara, CA, August 23-26, http://esg4.eri.ucsb.edu/.

Aboye, S., Andrus, R. D., Ravichandran, N., Bhuiyan, A. and Harman, N., 2012. Development of a New Seismic Site Factor Model Based on Conditions in South Carolina, *Program and Abstracts of the 84th annual Meeting of the Seismological Society of America Eastern Section*, Virginia Polytechnic Institute and State University, Blacksburg, VA, October 28-30, *Seismological research Letters*, 84(1), page 148 (January/February 2013).

Aboye, S. A., Andrus, R. D., Ravichandran, N., Bhuiyan, A. H., and Harman, N. E., 2013a. Amplitude- and V_{S30}- based Seismic Site Factor Model for Myrtle Beach South Carolina, *Proc., 7th National Seismic Conference on Bridges and Highways*, *MCEER*, University of Buffalo, NY, May 20-22, Oakland, CA.

Aboye, S. A, Andrus, R. D., Ravichandran, N., Bhuiyan, A., and Harman, N., 2013b. Seismic Site Factors and Design Response Spectra Based on Conditions in Charleston, South Carolina." *Earthquake Spectra*, accepted for publication in June 2013 (in print).

Aboye, S., Andrus, R. D., Ravichandran, N., Bhuiyan, A., and Harman, N. Generalized Seismic Site Factor Model for the South Carolina Coastal Plain, submitted to the *Bull. Seism. Soc. Am.*, (to be submitted).

Abrahamson, N. A., and Silva, W. J., 1997. Empirical response spectral attenuation relations for shallow crustal earthquake, *Seism. Res. Lett.*, **68**(1), 94-127.

American Association of State Highway and Transportation Officials (AASHTO), 2011. *LRFD Bridge Design Specifications, AASHTO 2th Edition*, Washington, D.C, 286 p.

American Society of Civil Engineers (ASCE), 2010. *Minimum Design Loads for Buildings and Other Structures, ASCE standard 7-10*, Reston, VA, 650 p.

Andrus, R. D., Fairbanks, C. D., Zhang, J., Camp III, W. M., Casey, T. J., Cleary, T. J., and Wright, W. B., 2006. Shear-wave velocity and seismic response of near-surface sediments in Charleston, South Carolina, *Bull. Seism. Soc. Am.*, **96**(5), 1897-1914.

Archuleta, R. J., Seale, S. H., Sangas, P. V., Baker, L. M., and Swain, S. T., 1992. Garner Valley downhole array of accelerometers: instrumentation and preliminary data analysis, *Bull. Seism. Soc. Am.*, **82**(4), 1592–1621.

Atkinson, G. M., and Boore, D. M., 1995. Ground motion relations for eastern North America, *Bull. Seism. Soc. Am.*, **85**(1), 17-30.

Bachman, R. E., 1995. Case studies of Kobe earthquake damage; industrial, transportation and port facilities, *Proc., Structural engineers Association of California, 64th annual convention*, 41-53.

Baska, D. A., and Tang, A. K. K., 2011. A tale of two earthquakes and one city, *Geo-Strata*, GeoInstitute of ASCE, Reston, VA, **15**(5), 36, 38, 40-41.

Bhuiyan, M. H., Ravichandran, N., Andrus, R. D., and Aboye, S. A., 2013. Comparison of nonlinear one-dimensional and two-dimensional site response analysis tools for Charleston, SC. *Proc., 2013 Geo-Congress: Stability and Performance of Slopes and Embankments III, Geotechnical Special Publication No. 231*, ASCE, San Diego, CA, March 3-7, 1240-1249

Bollinger, G. A., 1977. Reinterpretation of the intensity data for the 1886 Charleston, South Carolina, earthquake, *Studies Related to the Charleston, South Carolina, Earthquake of 1886: A Preliminary Report, U.S.G.S. Prof. Paper 1028*, Reston, VA, D. W. Rankin (editor), 17-32.

Boore, D. M., Joyner, W. B., and Fumal, T. E., 1994. Estimation of response spectra and peak acceleration from western North American earthquakes: *An Interim Report, U.S.G.S. Open-File Report*, vol 2, Merlo Park, CA, 94-124.

Borcherdt, R. D., and Glassmoyer, G., 1992. On the characteristics of local geology and their influence on ground motions generated by the Loma Prieta earthquake in the San Francisco Bay region, California, *Bull. Seism. Soc. Am.*, **82(2), 603-641.**

Borcherdt, R. D., 1994. Estimates of site-dependent response spectra for design (methodology and justification), *Earthquake Spectra*, **10**(4), 617-653.

Borcherdt, R. D., 2002. Empirical evidence for site coefficients in building-code provisions, *Earthquake Spectra*, **18**(2), 189-218.

Building Seismic Safety Council (BSSC), 1995. NEHRP Recommended Provisions for Seismic Regulations for New Buildings (1994 edition), *Federal Emergency*

Management Agency, *FEMA* 222A/223A, Building Seismic Safety Council, Washington, D.C.

Building Seismic Safety Council (BSSC), 2010. NEHRP Recommended Provisions for Seismic Regulations for New Buildings and Other Structures (2009 edition), Fe*deral Emergency Management Agency, FEMA P-749*, Building Seismic Safety Council, Washington, D.C.

Chapman, M. C., 2006. User's guide to SCENARIO_PC and SCDOTSHAKE, Report to the South Carolina Department of Transportation, Columbia, SC.

Chapman, M. C., Martin, J. R., Olgun, C. G., and Beale, J. N., 2006. *Site-response models for Charleston, South Carolina and vicinity developed from shallow geotechnical investigations, Bull. Seism. Soc. Am.*, **96**(2), 467-489.

Chapman, M. C., and Talwani, P., 2002. Seismic hazard mapping for bridge and highway design, Report to the South Carolina Department of Transportation, Columbia, SC.

Choi, Y. and Stewart, J. P., 2005. Nonlinear site amplification as function of 30 m shear wave velocity, *Earthquake Spectra*, **21**(1), 1-30.

Côté, R. N., 2006. *City of Heroes: The Great Charleston Earthquake of 1886*, Corinthian Books, Mt. Pleasant, SC, 542 p.

Crouse, C. B., 2011. Effects of local geology on earthquake ground motions: from research to engineering practice and building codes, *4th IASPEI/IAEE International Symposium: Effects of Surface Geology on Seismic Motion*, University of California Santa Barbara, CA, August 23-26, http://esg4.eri.ucsb.edu/.

Crouse, C. B., and McGuire, J. W., 1996. Site response studies for purpose of revising NEHRP seismic provisions, *Earthquake Spectra*, **12**(3), 407-439.

Dobry, R., Martin, G. M., Parra, E., and Bhattacharya, A., 1994. Development of site-dependent ratios of elastic response spectra (RRS) and site categories for building seismic codes, *Proc. NCEER, SEAOC, BSSC Workshop on Site Response during Earthquakes and Seismic Code Provisions*, University of Southern California, Los Angeles, CA, November 18 - 20, 1992.

Dobry, R., Ramos, R., and Power, M. S., 1999. Site Factors and Site Categories in Seismic Codes, *Technical Report MCEER-99-0010*, 81 pp.

Dobry, R., Borcherdt, R. D., Crouse, C. B., Idriss, I. M. Joyner, W. B. Martin, G. R. Power, M. S. Rinne, E. E., and Seed R. B., 2000. New site coefficients and site classification system used in recent building seismic code provisions, *Earthquake Spectra*, **16**(1), 41-67.

Durá-Gómez, I., and Talwani, P., 2009. Finding faults in the Charleston area, South Carolina: 1. Seismological Data, *Seism. Res. Lett*., **80**(5), 883–900.

Dutton, C. E., 1889. The Charleston earthquake of August 31, 1886, *U.S.G.S.*, *Ninth Annual Report 1887-1888,* Washington, D.C., 203-528.

DuBar, J. R., 1987. Geology of the Dongola 7.5-Minute quadrangle, Horry and Marion Counties, South Carolina, South Carolina Geological Survey, 31(1), Columbia, SC, 15 p.

Fairbanks, C. D., Andrus, R. D., Camp III, W. M., and Wright, W. B., 2008. Dynamic periods and building damage at Charleston, South Carolina during the 1886 earthquake, *Earthquake Spectra*, **24**(4), 867-888.

Field, E. H., 2000. A modified ground motion attenuation relationship for southern California that accounts for detailed site classification and a basin depth effect, *Bull. Seism. Soc. Am.*, **90**(6), 209-221.

Gutenberg, B., 1931. Microseisms in North America, *Bull. Seism. Soc. Am.*, **21**(1), 1-24.

Harmsen, S. C., 1997. Determination of site amplification in the Los Angeles urban area from inversion of strong motion records, *Bull. Seism. Soc. Am.*, **87**(4), 866-887.

Hashash, Y. M. A., and Park, D., 2001. Non-linear one-dimensional seismic ground motion propagation in the Mississippi embayment. *Eng. Geology*, **62**(1–3), 185–206.

Heck, N. H., and Neumann, F., 1933. Destructive Earthquake Motions Measured for the First Time. *Engineering News Record*, 804-807.

Heidari, T, and Andrus R. D., 2010. Mapping liquefaction potential of aged soil deposits in Mount Pleasant, South Carolina. *Engineering Geology* **112**(1), 1-12.

Hwang, H. H. M., Lin, H., and Huo, J.-R., 1996. Site coefficients for design of buildings in eastern United States. *Soil Dynamics and Earthquake Engrg.*, **16** (1), 27–40.

Idriss, I. M., 1990. Response of soft soil sites during earthquake, *Proc. of H. Bolton Seed Memorial Symp.*, vol. 2, BiTechPublishers Ltd., Richmond, British Columbia, Canada, pp. 273–289.

International Codes Council, Inc. (ICC), 2012. *International Building Code (IBC)*, Falls Church, VA, 328 pp.

Johnston, A. C., 1996. Seismic moment assessment of earthquakes in stable continental regions, III. New Madrid 1811-1812, Charleston 1886 and Lisbon 1755. *Geophys. J. Int.*, **126**(2), 314–344.

Joyner, W. B. and Boore, D. M., 2000. Recent developments in earthquake ground motion estimation, *Proc. Sixth International Conference on Seismic Zonation,* Palm Springs, CA, November 12- 15.

Joyner, W. B., Fumal, T. E., and Glassmoyer, G., 1994. Empirical spectral response ratios for strong motion data from the 1989 Loma Prieta, California, earthquake, *Proc. NCEER, SEAOC, BSSC Workshop on Site Response during Earthquakes and Seismic Code Provisions*, University of Southern California, Los Angeles, CA, November 18 - 20, 1992.

Kramer, S. L., 1996. *Geotechnical Earthquake Engineering*, Prentice-Hall, Upper Saddle River, NJ, 653 pp.

Kramer, S. L., and Paulsen, S. B., 2004. Practical use of geotechnical site response models, *NSF/PEER Int. Workshop on Uncertainties in Nonlinear Soil Properties and their Impact on Modeling Dynamic Soil Response*, March 18-19, University of California, Berkeley, CA.

Lester, A. P., and Chapman, M. C., 2005. An examination of site response in Columbia, South Carolina, *Seism. Res. Lett.*, **76**(1), 118 p.

Lawson, A., 1908. The California Earthquake of April 18, 1906, *Report-Earthquake Investigation Commission,* Carnegie Institute of Washington, Washington, D.C., vol. 1, 434-435.

Martin, J. R., II, and Clough, G. W., 1994. Seismic parameters from liquefaction evidence. *J. Geotech. Eng.*, 120(8), 1345–1361.

Matasović, N., 1993. Seismic response of composite horizontally-layered soil deposits, *Ph.D. Dissertation*, Civil Engineering Department, University of California, Los Angeles, CA, 483 p.

Matasovic, N., and M. Vucetic 1993. Cyclic characterization of liquefiable sands. *J. of Geotech. Eng.*, **119**(11), 1805-1822.

Matasović, N., and *Ordóñez*, G. A., 2011. D-MOD2000: A Computer program for seismic response analysis of horizontally layered soil deposits, earthfill dams and solid waste landfills, user's manual, Geomotions, LLC, Lacey, WA, 172 pp., http://www.geomotions.com.

Maybin, A.H., III, and Nystrom, P.G., Jr., 1995. Generalized geologic map of South Carolina: South Carolina Department of Natural Resources, Geology Map 1.

McCartan, L., Lemon, E. M., and Weems, R. E., 1984. Geologic Map of the area between Charleston and Orangeburg, South Carolina, *U.S. Geol. Surv. Misc. Investigations Series Map I-1472*, Reston, VA.

Midorikawa, S., Matsuoka, M., and Sakugawa, K., 1994. Site effects on strong-motion records observed during the 1987 Chiba-Ken-Toho- Oki, Japan earthquake, *Proc., 9th Japan Earthq. Symp.*, vol. 3, Tokyo, Japan, pp. E085–E090.

Moses, C., 2002. Geologic mapping of the central portion of the Myrtle Beach 7.5-minute Quadrangle, *Proc., 37th South-Central Section and 52nd Southeastern Section GSA Joint Annual Meeting*, Memphis, March 12-13.

Odum, J. K., Williams, R. A., Stepheson, W. J., and Worley, D. M., 2003. Near-surface S-wave and P-wave seismic velocities of primary geological formations on the Piedmont and Atlantic Coastal Plain of South Carolina, US, *U.S.G.S., Reston, VA, Open-file Report 03-043,* 14 p.

Ordóñez, G. A., 2011. SHAKE2000: A computer program for the 1D analysis of geotechnical earthquake engineering problems, user's manual, Geomotions, LLC, Lacey, WA, 250 p.

Owens, J. P., 1989. Geologic map of the Cape Fear region, Florence 1° x 2° quadrangle and northern half of the Georgetown 1° x 2° quadrangle, North Carolina and South Carolina, 1:250,000, *Misc. Investigations Series, Map I-1948-A, U.S.G.S.*, Reston, VA.

Park, D., and Hashash, Y. M. A., 2004. Soil damping formulation in nonlinear time domain site response analysis, *Journal of Earthquake Engrg.,* **8**(2), 249-274.

Power, M. S., Mayes, R. L., and Friedland, I. M., 1998. National representation of seismic ground motion for new and existing highway facilities, *Proc., Sixth National Conference on Earthquake Engineering*, May 31-June 4, Seattle, WA, EERI.

Prowell, D. C., 1996. Geological map of the Savannah river site, Aiken, Allendale and Barnwell counties, South Carolina, *Misc. Field Studies Series, Map MF-2300, U.S.G.S.*, Reston, VA.

Pyke, R. M., 1979. Nonlinear models for irregular cyclic loadings, *Journal Geotech. Engrg. Div*., **105**(6), 715-726.

Rathje, E. M., Abrahamson, N.A., and Bray, J. D., 1998. Simplified frequency content estimates of earthquake ground motions, *Journal Geotech. and Geoenviron. Engrg*,

124(2), 150-159.

Rodriguez-Marek, A., Bray, J. D., and Abrahamson, N. A., 2001. An empirical geotechnical seismic site response procedure, *Earthquake Spectra*, **17**(1), 65-87.

Schnabel, P. B., Lysmer, J., and Seed, H. B., 1972. SHAKE: a computer program for earthquake response analysis of horizontally layered sites, *Report EERC 72-12*, University of California, Berkeley, CA.

Seed, H. B., and Idriss, I. M., 1969. Influence of soil conditions on ground motions during earthquakes, *Journal of the Soil Mechanics and Foundations Division, Proc., ASCE*, vol. **95**(1), 99-137.

Seed, H. B., Murarka, R., Lysmer, J., and Idriss, I.M., 1976. Relationships of the maximum acceleration, maximum velocity, distance from source and local site conditions for moderately strong earthquakes, *Bull. Seism. Soc. Am.*, **66**(4), 1323-1342.

Seed, H. B., and Idriss, I. M., 1982. Ground motions and Soil Liquefaction during earthquakes, *Earthquake Engineering Research Institute Report EERI-MNO*-5, 134 p.

Seed, H. B., Romo, M. P., Sun, J. i., Jaime, A., and Lysmer, J., 1988. The Mexico Earthquake of September 19, 1985, Relationships Between Soil Conditions and Earthquake Ground Motions, *Earthquake Spectra*, vol. **4**(4), 681-729.

Seed, R. B., Dickenson, S., and Mok, C. M., 1994. Site effects on strong shaking and seismic risk: recent developments and their impact on seismic design codes and practice, *Proc., ASCE Structures Congress XII*, vol. 1, Atlanta, GA, 573–578.

Seyhan, E., and Stewart, J. P., 2012. Site response in NEHRP provisions and NGA models, *Proc., GeoCongress 2012*, Oakland, CA, March 25-29, 359-379.

Silva, W., Darragh, R., Gregor, N., Martin, G., Abrahamson, N., and Kircher, C., 2000. Reassessment of site coefficients and near-fault factors for building code provisions, *NEHRP Program Report 98-HQ-GR-1010, U.S.G.S., Merlo Park, CA.*

Silva, W., Wang, I., Siegel, T., Gregor, N., Darragh, R. and Lee, R., 2003. Ground motion and liquefaction simulation of the 1886 Charleston, South Carolina, earthquake, *Bull. Seism. Soc. Am.,* **93** (6), 2717-2736.

Somerville, P.G., 2003. Magnitude scaling of near fault rupture directivity pulse. Earthquake, *Physics of the Earth and Planetary Interiors*, **137** (1), 201-213.

South Carolina Department of Transportation (SCDOT), 2008. *Geotechnical Design Manual. Version 1.0.* South Carolina Department of Transportation, Columbia, SC.

South Carolina Department of Natural Resources (SCDNR), 2005. *Generalized Geologic Map of South Carolina*, South Carolina Department of Natural Resources and South Carolina Geological Survey, Columbia, SC.

Steidl, J. H., 2000. Site response in southern California for probabilistic seismic hazard analysis, *Bull. Seism. Soc. Am*, **90**(6), 149-169.

Stewart, J. P., Chiou, S., Bray, J. D., Graves, R. W., Somerville, P. G., and Abrahamson, N. A., 2001. Ground Motion Evaluation Procedures for Performance-Based Design. *PEER Report 2001/09*, Pacific Earthquake Engineering Research Center, University of California, Berkeley, CA.

Stewart, J. P., Liu, A. H., and Choi, Y., 2003. Amplification factors for spectral acceleration in tectonically active regions, *Bull. Seism. Soc. Am.*, **93**(1), 332-352**.**

Talwani, P., and Schaeffer, W. T., 2001. Recurrence rates of large earthquakes in the South Carolina Coastal Plain based on paleoliquefaction data, *Journal Geophys. Res*., **106**(b4), 6621-6642.

Weems, R.E., and Lewis, W.C., 2002. Structural and tectonic setting of the Charleston, South Carolina, region: Evidence from the Tertiary stratigraphic record, *Geological Society of America Bulletin*, **114**(1), 24–42.

Weems, R.E., Lewis, W.C., and Chirico, P., 2011. Surficial geology of Charleston and parts of Berkeley, Dorchester, Colleton, and Georgetown Counties, South Carolina, *U.S.G.S., Reston, VA, Open-file Report,* Scale 1:1,000,000.

Wheeler, R. L., and Cramer, C. H., 2000. Preliminary estimate of the amplification of possible earthquake ground motion at a site in Charleston County, South Carolina, *U.S.G.S., Reston, VA, Open-file Report 00-048.*

Zhang J., Andrus, R. D., and Juang, C. H., 2005. Normalized shear modulus and material damping ratio relationships, *Journal Geotech. and Geoenviron. Engrg*, **131**(4), 453-464.

Zhang J., Andrus, R. D., and Juang, C. H., 2008. Model uncertainty in normalized shear modulus and damping relationships, *Journal Geotech. and Geoenviron. Engrg*, **134**(1), 24-36.